

Title	The role of renal afferent signalling in chronic intermittent hypoxia-induced sympathoexcitation and hypertension
Authors	AlMarabeh, Sara
Publication date	2021
Original Citation	AlMarabeh, S. Y. A. R. 2021. The role of renal afferent signalling in chronic intermittent hypoxia-induced sympathoexcitation and hypertension. PhD Thesis, University College Cork.
Type of publication	Doctoral thesis
Rights	© 2021, Sara Yousef Abdel Razaq AlMarabeh. - http://creativecommons.org/licenses/by-nc-nd/3.0/
Download date	2024-04-20 04:49:07
Item downloaded from	https://hdl.handle.net/10468/11341

Ollscoil na hÉireann, Corcaigh
National University of Ireland, Cork



**The role of renal afferent signalling in chronic
intermittent hypoxia-induced sympathoexcitation
and hypertension**

Thesis presented by

Sara Yousef Abdel Razaq AlMarabeh, BSc, MSc

Department of Physiology

For the degree of

Doctor of Philosophy

University College Cork

School of Medicine, Department of Physiology

Head of Department: Prof. Ken D. O'Halloran

Supervisors: Prof. Ken D. O'Halloran and Dr. Mohammed H. Abdulla

2021

Diatoms to Daphnia: Our Most Popular Microscope Images for November 2020

By Kerry Israel - 9 December, 2020



November's fan favorites were mainly very small samples with large personalities. From diatoms to Daphnia.

Image on left: Kidney section captured by Sara AlMarabeh on an Olympus BX53F with a DP72 camera.

<https://www.olympus-lifescience.com/en/discovery/top-images-november-2020/>

Table of contents

Declaration.....	x
List of Figures.....	xi
List of Tables	xiv
Acknowledgments	xvi
Abstract.....	xviii
 Chapter 1. Introduction: The role of renal afferent signalling in baroreflex regulation and sympathetic activity: Potential contribution to chronic intermittent hypoxia-induced hypertension	 1
List of Abbreviations.....	2
1.1. Chronic intermittent hypoxia as a model for obstructive sleep apnoea-induced hypertension	5
1.2. Baroreflex control of blood pressure	8
1.2.1. Anatomy and physiology of high-pressure baroreceptors	8
1.2.2. High-pressure baroreflex control of heart rate.....	10
1.2.3. High-pressure baroreflex control of RSNA	11
1.2.4. Altered baroreflex function in hypertension.....	12
1.2.5. Up to date evidence of high-pressure baroreflex changes in intermittent hypoxia.....	14
1.3. Low-pressure baroreflex.....	16
1.3.1. Anatomy and physiology of low-pressure baroreceptors	16
1.3.2. Altered low-pressure baroreflex function in hypertension	20
1.4. Renal sensory afferent nerves.....	22
1.4.1. Distribution and projection to brain.....	22
1.4.2. The physiological activity of renal afferent and efferent sensory nerves	23
1.4.3. Activation pathways of renal afferent sensory nerves	25

1.4.4.	Renal afferent nerves and hypertension.....	26
1.4.4.1.	Suppression of the inhibitory reno-renal reflex	27
1.4.4.2.	Activation of the excitatory reno-renal reflex	27
1.4.4.3.	Kidney inflammation, excitatory reno-renal reflex and baroreflex dysregulation	29
1.4.4.4.	A possible link between renal afferent nerves and CIH-induced hypertension: Role of inflammation and oxidative stress	30
1.5.	TRPV1 channels.....	33
1.5.1.	Location and activation pathways.....	33
1.5.2.	TRPV1: physiological role in the kidney	36
1.5.3.	The putative role of renal TRPV1 channels in hypertension.....	37
1.5.4.	TRPV1 receptors and hypoxia.....	41
1.6.	Renal kallikrein-kinin system.....	43
1.6.1.	Bradykinin formation and localisation	43
1.6.2.	Renal bradykinin receptors: location and transduction pathways	43
1.6.3.	Physiological role of bradykinin in the kidney	45
1.6.4.	The kallikrein-kinin system changes in hypertension.....	47
1.6.5.	The role of the kallikrein-kinin system in baroreflex regulation	50
1.6.6.	Kallikrein-kinin system during hypoxic injury.....	51
1.7.	Renal functional changes during hypoxia	55
1.7.1.	Effects of intermittent hypoxia on renal function.....	57
1.7.2.	Renal function alteration in acute hypoxia	60
1.7.3.	Renal functional changes in chronic hypoxia.....	65
1.8.	Knowledge gaps addressed in this project.....	68
1.9.	Thesis aims	70

Chapter 2. Methods.....72

List of Abbreviations.....	73
2.1. Animal model.....	74
2.2. Non-recovery surgical instrumentation.....	77

2.2.1. First cohort experimental protocol	80
2.2.1.1. Baroreflexes assessment	80
2.2.1.2. Measurement of Excretory Parameters	81
2.2.1.3. Validation of intra-renal infusion	84
2.2.1.4. Atrial natriuretic peptide (ANP) assay	84
2.2.1.5. Statistical analysis	85
2.2.2. Second cohort experimental protocol.....	88
2.2.2.1. Statistical analysis	89
2.2.3. Third cohort experimental protocol.....	90
2.2.3.1. Intra-renal pelvic infusions.....	90
2.2.3.2. Measurement of Excretory Parameters	93
2.2.3.3. Validation of concentrations of bradykinin and capsaicin	93
2.2.3.4. Possible desensitization of bradykinin receptors.....	94
2.2.3.5. Statistical analysis	94
2.3. Tissue preparation	96
2.4. Biochemical assays	98
2.4.1. TRPV1 ELISA	98
2.4.2. Bradykinin receptor 1 ELISA assay	98
2.4.3. Bradykinin receptor 2 ELISA assay	99
2.4.4. AOPP assay	99
2.4.5. NOX activity assay.....	100
2.4.6. SOD activity assay	101
2.4.7. Catalase activity assay.....	102
2.4.8. Renal inflammatory cytokines	102
2.5. Immunofluorescence	104
2.5.1. TRPV1 receptors	104
2.5.2. CGRP and NK1 receptor	104
2.5.3. Image analysis	105
2.6. Renal histopathological staining	107
2.6.1. Haematoxylin and eosin stain	107

2.6.2. Sirius red stain	108
2.6.3. Histological analysis	108
2.6.4. Statistical analysis	110

Chapter 3: Effect of chronic intermittent hypoxia on the high-pressure baroreflex control of heart rate and renal sympathetic nerve activity111

List of Abbreviations.....	112
3.1. Introduction	113
3.2. Results	115
3.2.1. General	115
3.2.2. Effect of CIH on baseline values of MAP, HR and RSNA.....	116
3.2.3. Effect of CIH on the high-pressure baroreflex	118
3.2.4. Effects of intra-renal TRPV1 blockade	122
3.2.5. Validation of intra-renal (cortico-medullary) cannulation	124
3.3. Discussion	125
3.3.1. Chronic intermittent hypoxia causes hypertension	125
3.3.2. High-pressure baroreflex control of HR.....	129
3.3.3. High-pressure baroreflex control of RSNA	131
3.3.4. Blockade of TRPV1 channels	133
3.4. Conclusion	135

Chapter 4: Effect of chronic intermittent hypoxia on renal sympatho-inhibition and renal functional responses to volume expansion before and after TRPV1 blockade136

List of abbreviations.....	137
4.1. Introduction	139
4.2. Results	142
4.2.1. Basal haemodynamic and renal excretory parameters before VE.....	142
4.2.2. Effect of CIH on the low-pressure baroreflex control of RSNA.....	145
4.2.3. RSNA response to VE during intra-renal TRPV1 blockade	145

4.2.4. Effect of CIH on renal excretory responses to VE.....	148
4.2.5. Renal excretory responses to VE during intra-renal TRPV1 blockade.....	148
4.2.6. Cardiovascular responses to VE.....	148
4.2.7. Content of TRPV1 in renal tissue	149
4.3. Discussion	151
4.3.1. Low-pressure baroreflex control of RSNA	151
4.3.2. Renal excretory responses to VE	153
4.3.3. Blockade of TRPV1 channels	158
4.4. Conclusion	161

Chapter 5: Molecular changes in kidney tissue exposed to chronic intermittent hypoxia 162

List of abbreviations.....	163
5.1. Introduction.....	165
5.2. Results.....	166
5.2.1. Renal histopathological assessment	166
5.2.2. Renal oxidative stress, inflammation and protein oxidation	167
5.2.3. Adjunct molecular analysis on renal tissue	168
5.3. Discussion	172
5.3.1 No evidence of kidney injury	172
5.3.2. Expression of other receptors in the renal pelvic wall	174
5.4. Conclusion	175

Chapter 6: Assessment of reno-renal reflex in rats exposed to chronic intermittent hypoxia 176

List of abbreviations.....	177
6.1. Introduction.....	179
6.2. Results.....	182
6.2.1. General	182

6.2.2. Effect of CIH on baseline values of MAP, HR, RSNA and kidney function	182
6.2.3. RSNA response to different concentrations of bradykinin	184
6.2.4. Effect of CIH on cardiovascular responses to the intra-pelvic infusion of bradykinin.....	185
6.2.5. Effect of CIH on RSNA responses to the intra-pelvic infusion of bradykinin	186
6.2.6. Effects of intra-pelvic blockade of bradykinin receptors	190
6.2.7. Effects of intra-pelvic infusion of bradykinin receptor blockers on cardiovascular responses induced by bradykinin	193
6.2.8. Effects of intra-pelvic infusion of bradykinin receptor blockers on RSNA responses induced by bradykinin	195
6.2.9. Possible desensitization of bradykinin receptors	195
6.2.10. Differences in cardiovascular and RSNA responses to intra-pelvic vs. intravenous infusion of bradykinin	196
6.2.11. Effect of CIH on cardiovascular and RSNA responses to the intra-pelvic infusion of capsaicin.....	197
6.2.12. Renal excretory responses to intra-pelvic infusion of bradykinin and capsaicin	200
6.2.13. Verification of the intra-renal pelvic route.....	201
6.2.14. Tissue content of bradykinin receptors type 1 and 2.....	203
6.3. Discussion	203
6.3.1. Responses of RSNA and heart rate to bradykinin.....	203
6.3.2. Responses of RSNA and HR to capsaicin.....	210
6.3.3. Effect of CIH on RSNA and cardiovascular responses to bradykinin	212
6.3.4. Effect of intra-renal pelvic infusion on kidney excretory function	216
6.4. Conclusion	220
Chapter 7: Summary and Conclusion.....	221
List of abbreviations.....	222
7.1. Summary	223

7.2. Limitations	230
7.3. Future studies and knowledge gaps.....	234
7.4. Conclusions	236
Appendix I	238
List of publications, conference abstracts and awards	255
References	257

Declaration

This is to certify that the work I am submitting is my own and has not been submitted for another degree, either at University College Cork or elsewhere. All external references and sources are clearly acknowledged and identified within the contents. I have read and understood the regulations of University College Cork concerning plagiarism.

Signed: Sara AlMarabeh

February, 2021

List of Figures

Chapter 1: Introduction

Figure 1. 1. Central and peripheral circuits of the baroreflex arc.	9
Figure 1. 2. Cardiopulmonary baroreflex arc.....	17
Figure 1. 3. Renal afferent and efferent sympathetic nerves.....	24
Figure 1. 4. A representation of possible pathways that enhance renal afferent nerve activity in a renal afferent nerve ending.....	26
Figure 1. 5. Interaction of TRPV1 with other receptors in the renal pelvic wall.....	36
Figure 1. 6. Suggested mechanisms of intermittent hypoxia-mediated renal functional changes.....	59
Figure 1. 7. Variable renal responses to acute hypoxia in different species in response to various hypoxic protocols.	64
Figure 1. 8. A schematic representation of a proposed mechanism of CIH-induced hypertension that was investigated in this project.....	71

Chapter 2: Methods

Figure 2. 1. Oxycycler system and oxygen profiles in two chambers operating simultaneously.	76
Figure 2. 2. Surgical instrumentation of non-recovery surgical experiments.....	79
Figure 2. 3. The design of the intra-renal pelvic cannula.....	80
Figure 2. 4. A schematic representation of the surgical protocol of the first cohort..	83
Figure 2.5. Logistic sigmoidal baroreflex function curve.....	88
Figure 2.6. A schematic representation of the surgical protocol of the second cohort.	89
Figure 2. 7. A schematic representation of the surgical protocol of the third cohort.	92
Figure 2.8. Formation and dismutation of superoxide radicals.....	101
Figure 2.9. The peroxidase activity of catalase enzyme.	102
Figure 2.10. Assessment of renal fibrosis.	109

Chapter 3: Effect of chronic intermittent hypoxia on the high-pressure baroreflex control of heart rate and renal sympathetic nerve activity

Figure 3. 1. Original recordings of cardiovascular parameters and RSNA in an anaesthetised rat.	116
Figure 3. 2. Original recordings illustrating high-pressure baroreflex control of RSNA in anaesthetised rats.	119
Figure 3. 3. High-pressure baroreflex control of RSNA.	120
Figure 3. 4. Correlations between baseline MAP and baroreflex parameters.	122
Figure 3. 5. Validation of intra-renal (cortico-medullary) infusion of TRPV1 blocker, capsaizepine.	125

Chapter 4: Effect of chronic intermittent hypoxia on renal sympatho-inhibition and renal functional responses to volume expansion before and after TRPV1 blockade

Figure 4. 1. Representative recordings of RSNA response to VE in anaesthetised rats.	145
Figure 4. 2. RSNA responses to VE.	146
Figure 4. 3. Cardiovascular and renal excretory responses to VE.	147
Figure 4. 4. TRPV1 immunofluorescence in the renal pelvic wall.	150

Chapter 5: Molecular changes in kidney tissue exposed to chronic intermittent hypoxia

Figure 5. 1. Renal histology.	167
Figure 5. 2. Immunofluorescence labelling of CGRP in the renal pelvic wall.	169
Figure 5. 3. Immunofluorescence of NK1 in the renal pelvic wall.	170
Figure 5. 4. CGRP and NK1 immunofluorescence in renal pelvic wall.	171

Chapter 6: Assessment of reno-renal reflex in rats exposed to chronic intermittent hypoxia

Figure 6. 1. Original recordings of cardiovascular parameters and RSNA in an anaesthetised rat from surgical cohort 3.	184
Figure 6. 2. Dose-response curve of bradykinin.	185
Figure 6. 3. Cardiovascular and RSNA responses to the intra-pelvic infusion of bradykinin.	187
Figure 6. 4. Area under the curve (AUC) analysis for the cardiovascular and RSNA responses to the infusion of bradykinin.	189

Figure 6. 5. Original recordings illustrating cardiovascular and RSNA responses to bradykinin.	190
Figure 6. 6. Cardiovascular and RSNA responses to the intra-pelvic infusion of bradykinin receptor blockers with and without bradykinin.	192
Figure 6. 7. Area under the curve (AUC) analysis for the cardiovascular and RSNA responses to bradykinin during the blockade of bradykinin receptors.....	194
Figure 6. 8. MAP and RSNA responses to the intra-pelvic infusion of repetitive concentrations of bradykinin.....	196
Figure 6. 9. Cardiovascular and RSNA responses to the intra-pelvic infusion of capsaicin.	198
Figure 6. 10. Original recordings illustrating cardiovascular and RSNA responses to capsaicin.	199
Figure 6. 11. Validation of the patency of urine drainage from renal pelvic wall. ...	202
Figure 6. 12. Tissue content of bradykinin receptors in sham and CIH-exposed rats.	203

Appendix I

Figure 8.1. High-pressure baroreflex control of RSNA and HR using the five-parameter model.....	245
Figure 8. 2. Body weights recorded during 14 days of CIH and normoxia (sham) exposure.	247
Figure 8.3. RSNA-MAP baroreflex curves of a sham and a CIH-exposed rat from cohort 1 and 2.....	252
Figure 8. 4. Haematocrit changes during VE.....	253
Figure 8. 5. Immunofluorescence of CGRP and NK1 in a cross section of ureter obtained from a sham rat.....	254

List of Tables

Chapter 3: Effect of chronic intermittent hypoxia on the high-pressure baroreflex control of heart rate and renal sympathetic nerve activity

Table 3. 1. Baseline cardiovascular and RSNA parameters in sham and CIH-exposed rats.	118
Table 3. 2. High-pressure baroreflex parameters during intra-renal infusion of saline in sham and CIH-exposed rats (cohort 1 and cohort 2).	121
Table 3. 3. Baseline MAP, HR and RSNA in sham and CIH-exposed rats (cohort 2).	123
Table 3. 4. High-pressure baroreflex parameters during intra-renal infusion of capsaizepine in sham and CIH-exposed rats (cohort 2).	124

Chapter 4: Effect of chronic intermittent hypoxia on renal sympatho-inhibition and renal functional responses to volume expansion before and after TRPV1 blockade

Table 4. 1. Baseline renal excretory parameters in sham and CIH-exposed rats.	143
Table 4. 2. MAP, HR and RSNA before and during VE challenges in sham and CIH-exposed rats.	144

Chapter 5: Molecular changes in kidney tissue exposed to chronic intermittent hypoxia

Table 5. 1. Biomarker concentrations in kidney tissue homogenates of sham and CIH-exposed rats.	168
--	-----

Chapter 6: Assessment of reno-renal reflex in rats exposed to chronic intermittent hypoxia

Table 6.1. Baseline parameters in sham and CIH-exposed rats (cohort 3).	183
Table 6.2. Area under the curve analysis of RSNA responses to the intra-pelvic infusion of bradykinin, blockers of bradykinin receptors and capsaicin.	191
Table 6.3. Comparison between intra-pelvic and intravenous infusion of 150 μ M bradykinin.	197

Table 6.4. Renal excretory responses to intra-renal pelvic infusion of bradykinin and capsaicin.	200
---	-----

Appendix I

Table 8. 1. Oxidative stress and inflammatory biomarkers (↑, an increase; ↓, a decrease) in animals exposed to different protocols of CIH.	239
Table 8.2. High-pressure baroreflex parameters of RSNA and HR in sham and CIH-exposed rats of cohort 1.	246
Table 8. 3. Body weight gain parameters during 14 days of CIH and normoxia (sham) exposure.	248
Table 8. 4. Haematocrit and blood gases analysis of surgical cohort 1 and cohort 2.	249
Table 8. 5. Haematocrit and blood gases analysis of surgical cohort 3.	250
Table 8. 6. A comparison of basal cardiovascular parameters and RSNA between sham and CIH-exposed rats of cohort 1 and 2.	251

Acknowledgments

First, I would like to thank my PhD supervisors Prof. Ken O'Halloran and Dr. Mohammed Abdulla for the opportunity to do my training under your supervision, for the opportunity to choose between many projects and take on this project. Mohammed, thank you for the invaluable advice all along the way, the invaluable time you gave, your continuous mentorship, your limitless support even at the hardest times and for the infinite, non-stop teaching you gave. I am looking forward to building up on this experience and working together in the future. Ken, thank you for being accommodating when I contacted you. Your guidance during my PhD has taught me an awful lot, both professionally and personally, and I thank you for the opportunity to complete my PhD training with you. Dr. Eric Lucking, thank you for your continuous and generous support, starting from my first day at the first project meeting and continuing even after I submitted the thesis. Thank you for the positivity that you always gave and for your tolerance at all times.

I would like to thank my thesis examination committee, Dr. Carolyn Barrett (University of Auckland), Dr. Vincent Healy (UCC) and the independent chair Prof. Catriona O'Driscoll (UCC). Special thanks to the postgraduate review committee, Dr. Vincent Healy and Dr. John Mackrill, for your kindness and advice. Thank you to all academic and technical staff of the Department of Physiology for your assistance and Dr. Greg Jasioneck for the support, advice and contribution to this research project. I would like to thank the administrative office staff, Nora, Nicola and Jackie for being continuously accommodating from day one. Thank you especially to Jay Radford for being my friend and for the kindness and for the support at all times. Thank you to all BSU staff and technicians for my training during the studies. I am grateful for all the help that you provided, which was invaluable.

I would like to thank Dr. Julie O' Neill and Mr. Jeremy Cavers for your support and for your great ideas and your hard work in this project. Thank you to Dr. Fiona McDonald and Ms. Suzanne Crotty for your training and your continuous inputs and advice. Thank you to Dr. Kieran Rea for your kind facilitation in the APC.

To all my friends, in Ireland, home and abroad, thank you for the positivity and the encouragement. To all previous and current postgraduates, thank you for your peer support, advice, and for the best wishes. I wish you the best success in your life and

career. I would like to thank Cork, which is now a piece of my heart, for the lovely experience and the warm reception (and the warm weather indeed!).

I am very grateful to the University of Jordan (JU) for funding my PhD and to the staff members, especially my previous mentors during my masters at School of Pharmacy of JU for their support and encouragement.

To my parents, Yousef and Haya, and siblings, Tamara, Ala'a and Mohammed, for all the support, love and encouragement that you gave during this journey and all the years before; I dedicate this thesis to you.

Abstract

Introduction: Sensory inputs from the kidney induce sympatho-excitation, and are integrated in brainstem regions receiving protective sensory inputs from high- and low-pressure baroreceptors. Blunted baroreflex control of renal sympathetic nerve activity (RSNA) was revealed in hypertension models that involve renal inflammation. Suppression of inflammation restored the normal baroreflex control of RSNA in some of these models, suggesting that renal inflammation impairs baroreflex control of blood pressure through the disruption of renal afferent nerve signalling. Renal oxidative stress and inflammation are evident following exposure to chronic intermittent hypoxia (CIH) in addition to blunted baroreflex control of heart rate. However, little information is available about the baroreflex control of RSNA. In addition, because kidney injury disrupts renal afferent nerve signalling, changes in the reno-renal reflex control of sympathetic outflow may occur following exposure to CIH. Therefore, understanding the stage at which baroreflexes and the reno-renal reflex are altered is required to explore the mechanisms that contribute to the early CIH-induced sympathetic hyperactivity and the onset of hypertension.

Methods: Following exposure to CIH or normoxia, baroreflexes were examined under anaesthesia. Kidney excretory function was measured during the assessment of low-pressure baroreflex by volume expansion (VE). Baroreflexes were assessed before and after blockade of renal TRPV1 channels. Moreover, to investigate if the excitatory reno-renal reflex contributes to sympathetic over-activity in CIH, renal afferent nerves located in the renal pelvic wall were chemically stimulated by bradykinin and capsaicin, or inhibited by bradykinin receptor type 1 (BK1R) and/or 2 (BK2R) blockers, and cardiovascular and RSNA responses were measured. Renal histology, inflammation and oxidative stress biomarkers were assessed.

Results: CIH-exposed rats were hypertensive with elevated RSNA, with no evidence of glomerular hypertrophy or renal inflammation and oxidative stress. Water and sodium excretion were increased following CIH exposure. However, diuresis and natriuresis during VE were attenuated in CIH-exposed rats despite preservation of the progressive decrease in RSNA during VE, suggesting that altered kidney excretory function in CIH was independent of neural control. The increase in atrial natriuretic

peptide during VE was attenuated in CIH. Assessment of the high-pressure baroreflex revealed decreased slope in CIH-exposed rats with substantial hypertension, but not when hypertension was modest. Diuresis and natriuresis during VE were enhanced in CIH-exposed and sham rats following the intra-renal blockade of TRPV1 channels, suggesting a role for renal TRPV1 in the control of renal excretory function. However, TRPV1 protein expression in the kidney was unchanged and TRPV1 activation by intra-renal pelvic infusion of capsaicin induced a similar sympatho-excitation in sham and CIH-exposed rats. Moreover, sympatho-excitation during intra-renal pelvic infusion of bradykinin was suppressed in CIH-exposed rats. This was associated with 53% decreased expression of BK2R in the renal pelvic wall of CIH-exposed rats compared with sham rats. Inhibition of renal bradykinin receptors did not affect cardiovascular parameters or RSNA in sham and CIH-exposed rats.

Conclusion: Our findings show no evidence of an excitatory reno-renal reflex driving sympathetic hyperactivity and the onset of hypertension in CIH. This was revealed by the absence of renal pathology despite the presence of a hypertensive phenotype. Moreover, the findings indicate suppressed rather than exacerbated sympatho-excitation in CIH-exposed rats in response to bradykinin. In addition, the baroreflex control of RSNA was maintained in CIH-exposed rats with modest hypertension, indicating that blunted baroreflex control is not obligatory for the onset of hypertension in CIH. Overall, renal injury appears to develop after the progressive elevation of blood pressure, although it may also develop in circumstances of exposure to severe CIH, suggesting that chronic kidney disease, frequently observed concomitant with obstructive sleep apnoea (OSA), may be mitigated if OSA is controlled at an early stage.

Chapter 1. Introduction: The role of renal afferent signalling in baroreflex regulation and sympathetic activity: Potential contribution to chronic intermittent hypoxia-induced hypertension

List of Abbreviations

ACEI	Angiotensin-converting enzyme inhibitors
ADH	Antidiuretic hormone
AKI	Acute kidney injury
Ang II	Angiotensin II
ANP	Atrial natriuretic peptide
ARNA	Afferent renal nerve activity
AT1	Angiotensin II receptor type 1
AT2	Angiotensin II receptor type 2
BK1R	Bradykinin receptors type 1
BK2R	Bradykinin receptors type 2
CGRP	Calcitonin gene-related peptide
CIH	Chronic intermittent hypoxia
CKD	Chronic kidney disease
COX	Cyclooxygenase
CPZ	Capsaizepine
CVLM	Caudal ventrolateral medulla
DOCA	Deoxycorticosterone acetate
ECM	Extracellular matrix
ENaC	Endothelial sodium channels
ERK	Extracellular signal-regulated kinase
ERSNA	Efferent renal sympathetic nerve activity
ET-1	Endothelin-1
ET-A	Endothelin receptor type A
ET-B	Endothelin receptor type B
FiO ₂	Fraction of oxygen inspired
GFR	Glomerular filtration rate
H ₂ O ₂	Hydrogen peroxide
HIF	Hypoxia inducible factor
HO-1	Heme oxygenase-1
ICV	Intra-cerebral ventricular
IH	Intermittent hypoxia

IL-1 β	Interleukin-1 beta
IL-4, 6, 10	Interleukin-4, 6, 10
IP3	Inositol triphosphate
JNK	c-Jun N-terminal kinase
LOX	Lipoxygenase
LPS	Lipopolysaccharides
LSNA	Lumbar sympathetic nerve activity
MAP	Mean arterial blood pressure
MAPK	Mitogen-activated protein kinase
MCP-1	Monocyte chemoattractant protein-1
NE	Norepinephrine
NEP	Neutral Endopeptidase
NF- κ B	Nuclear factor kappa B
NK1	Neurokinin 1 receptor
NO	Nitric oxide
eNOS	Endothelial nitric oxide synthase
NOX	NADPH oxidase
NTS	Nucleus tractus solitarius
O ₂ ⁻	Superoxide
OSA	Obstructive sleep apnoea
PG	Prostaglandin
PKA	Phosphokinase A
PKC	Phosphokinase C
PLC	Phospholipase C
PVN	Paraventricular nucleus
RAAS	Renin-angiotensin-aldosterone system
RBF	Renal blood flow
ROS	Reactive oxygen species
RPP	Renal perfusion pressure
RSNA	Renal sympathetic nerve activity
RVC	Renal vascular conductance
RVLM	Rostral ventrolateral medulla
RVR	Renal vascular resistance

SFO	Subfornical organ
SHR	Spontaneous hypertensive rat
sLTF	Sensory long-term facilitation
SNA	Sympathetic nerve activity
SNS	Sympathetic nervous system
SOD	Superoxide dismutase
SON	Supraoptic nucleus
SP	Substance P
TGF- β	Transforming growth factor- beta
TNF- α	Tumour necrosis factor- alpha
TRPV1	Transient receptor potential cation channel subfamily V member 1

1.1. Chronic intermittent hypoxia as a model for obstructive sleep apnoea-induced hypertension

Individuals with sleep apnoea experience periodic interruption of ventilation during sleep epochs accompanied by arterial hypoxaemia, hypercapnia and sleep fragmentation. Recurrent apnoeas (pauses in breathing) can arise from occlusions of the upper airway giving rise to obstructive sleep apnoea (OSA) or periodic suppression of central respiratory drive causing central sleep apnoea (150, 281). During apnoea, hypoxaemia stimulates arterial chemoreceptors in the carotid bodies, which transduce afferent signals to hindbrain regions primarily to nucleus tractus solitarius (NTS) which are then conveyed to the rostral ventrolateral medulla (RVLM), nucleus ambiguus and dorsal and ventral respiratory groups located in the medulla oblongata (91). Central integration of these afferent inputs enhances sympathetic discharge to peripheral organs (221). Reflex sympatho-excitation increases cardiac output, which facilitates oxygen supply to essential organs. Individuals with OSA experience nocturnal hypertension (159). Hypertension accompanied by elevated sympathetic nervous activity persists even during normal oxygenation giving rise to diurnal hypertension (248, 318, 376). Indeed, OSA is an independent risk factor for hypertension and is associated with high incidence of cardiovascular co-morbidities such as ischaemic heart disease, heart failure, arrhythmia and angina (119, 177, 317). Clinical trials addressing the relationship between OSA and hypertension estimate that 30-70% of individuals with OSA are hypertensive (12). The combined evidence points to a strong causal relationship between OSA and hypertension.

Exposure to recurrent intermittent hypoxia (IH) of varying severity and duration is considered the primary stimulus causing autonomic dysregulation in OSA. Furthermore, experimental animal models of IH consistently demonstrate persistent increases in arterial blood pressure (74, 98, 217, 226, 258, 273, 318, 392, 415). Indeed, animal models of chronic IH (CIH) are widely used in the study of pathophysiological processes associated with sleep apnoea. Exposure of animals to IH increases sympathetic outflow as evidenced by observations of IH-induced increases in muscle, renal, and splanchnic sympathetic nerve activity and increased vascular tone (251, 269, 324, 332). Ganglion blockade results in a greater reduction of blood pressure in CIH-exposed animals compared with controls, which highlights that sympatho-

excitation is the primary cause of high blood pressure in this model (416). This was revealed by increased catecholamine release from the adrenal medulla, the major end organ of the SNS (279). Duration of exposure to CIH has a major impact on blood pressure, which correlates with elevated sympathetic activity and increased levels of catecholamine. For a given duration, increased hypoxia intensity or increased number of hypoxia cycles also correlate with increased blood pressure (15).

Exposure to CIH of mild severity (9 cycles/hr) for 3 days resulted in enhanced basal sensory activity of carotid bodies during normoxic breathing phase (i.e. during wakefulness) that reached its maximum following 10 days of exposure (271). Meanwhile, elevated blood pressure was shown after 5 days of exposure to a severe protocol of CIH (48 cycles/hr), indicating that augmented firing of carotid bodies are involved in the initiation of hypertension (202). Consistent with this, selective ablation of carotid bodies prevented blood pressure elevation and catecholamine release from the adrenal medulla (279). Meanwhile, decreased cardiac baroreflex sensitivity was revealed after 17 days of exposure to the same CIH protocol (202). Furthermore, three days of exposure to a severe protocol of CIH (30 cycles/hr) was associated with increased level of endothelial injury biomarkers (342), suggesting endothelial dysfunction to occur during the early phase of CIH-induced hypertension. In addition, decreased renal oxygen tension was shown after 14 days of exposure to a moderate protocol of CIH (12 cycles/hr) (258). Exposure to 3 weeks of CIH was associated with central neural inflammation (263), while upregulation of central N-methyl-D-aspartate receptors and enhanced neuronal excitability were shown after 7 days of exposure to CIH (73). Overall, this indicates that a variety of CIH protocols utilizing different hypoxic durations and intensities evoke different mechanisms associated with the development and maintenance of hypertension, which are related to IH itself and indirectly related to sympathetic hyperactivity (15).

Similar to ischemia-reperfusion, during the reoxygenation phase of IH, reactive oxygen species (ROS) are produced (280). ROS are detected in the carotid bodies following exposure to CIH and are associated with augmented firing of carotid bodies and enhanced respiratory drive (282, 283). Moreover, increased ROS generation following exposure to IH was revealed centrally and in the adrenal medulla, causing increased levels of plasma catecholamine and increased sensitivity of adrenal medulla to hypoxia (283). Consistent with this, the administration of a superoxide dismutase

(SOD) mimetic prevented blood pressure elevation and abolished the enhanced activity of carotid bodies (282). The cellular mechanism involved in ROS generation during exposure to IH is related to the inhibition of the mitochondrial complex I of the electron transport chain and the upregulation of NADPH oxidase (NOX), mainly NOX2 (283). Additionally, exposure to IH was shown to be associated with an increase in the expression of hypoxia-inducible factor (HIF)-1 and a decrease in the expression of HIF-2, where HIF-1 encodes the transcription of oxidative enzymes and HIF-2 regulates the expression of anti-oxidants (316). HIF is composed of hypoxia sensitive α subunit and constitutively expressed β subunit. Proline hydroxylases require aerobic conditions to hydroxylate HIF-1 α subunit and degrade HIF heterodimers (316). Therefore, exposure to IH stabilizes HIF-1 while HIF-2 degradation is enhanced through the activation of calpain proteases (316). This imbalance in HIF-1/HIF-2 ratio eventually lead to oxidative dysregulation, NOX activation, loss of SOD and ROS generation. In support of this, a mouse model of partial HIF-2 $\alpha^{+/-}$ deficiency had augmented activity of carotid bodies and breathing instability in addition to decreased expression of SOD (316). This was normalized when HIF-2 $\alpha^{+/-}$ mice were treated with a superoxide scavenger. Meanwhile, mice with partial HIF-1 $\alpha^{+/-}$ deficiency that were exposed to IH had no increased levels of ROS and catecholamine, and the basal activity of carotid bodies was not augmented (274). Overall, pathophysiological changes induced by IH are related to oxidative stress and the generation of ROS. This is mainly caused by the stabilisation of HIF-1 followed with the upregulation of NOX, in conjunction with the degradation of HIF-2 followed with decreased expression of SOD (316).

1.2. Baroreflex control of blood pressure

Under physiological conditions, short-term changes in blood pressure stimulate mechanoreceptors known as high- and low-pressure baroreceptors (163, 260). In response to an increase in blood pressure, sensory inputs from both class of receptors are integrated in the NTS in the dorsal medulla of the brainstem, with resultant inhibition of the sympathetic nervous outflow and activation of the parasympathetic nervous system to restore blood pressure to normal (10).

1.2.1. Anatomy and physiology of high-pressure baroreceptors

High-pressure baroreceptors are stretch-sensitive receptors classified, according to their location, into aortic baroreceptors (in the tunica adventitia of the aortic arch) and carotid sinus baroreceptors, which are found in the wall of a dilation in the internal carotid artery superior to the carotid bifurcation (162). They are also classified based on nerve fibre myelination as type 1 (A-fibres) and type 2 (C-fibres) baroreceptors. These receptors stimulate a feedback mechanism that buffers short-term fluctuations of arterial blood pressure (55, 162, 350). Type 1 receptors, but not type 2 receptors, are involved in the acute resetting mediated by the fast conducting A-fibres (350). Meanwhile, some studies have highlighted a significant role for high-pressure baroreflex in the long-term regulation of blood pressure (291, 350).

Changes in mean arterial pressure (MAP) and/or pulse pressure causes an alteration in transmural pressure and dimensional change in the arterial wall (162). Consequently, baroreceptors send afferent information to the brainstem through the glossopharyngeal nerve originating from carotid sinus nerve and/or through the vagus nerve from the aortic arch. Inputs are transmitted to the NTS of the dorsal medulla, which acts as a relay centre of the baroreflex arc and sends inputs to the paraventricular nucleus (PVN), which is one of the sites of renal afferent nerve projections. Neurons of the NTS send inputs to other regions responsible for autonomic nervous system and cardiovascular regulation, including the caudal ventrolateral medulla (CVLM) and subsequently, the RVLM; both involve preganglionic sympathetic neurons. The NTS is also connected to the nucleus ambiguus, which comprises parasympathetic preganglionic neurons that synapse with postganglionic parasympathetic nerves to the

heart (Figure 1.1). Afferent discharges from the baroreceptors to the NTS cause reciprocal changes in sympathetic and parasympathetic outputs to maintain stable blood pressure (162, 291).

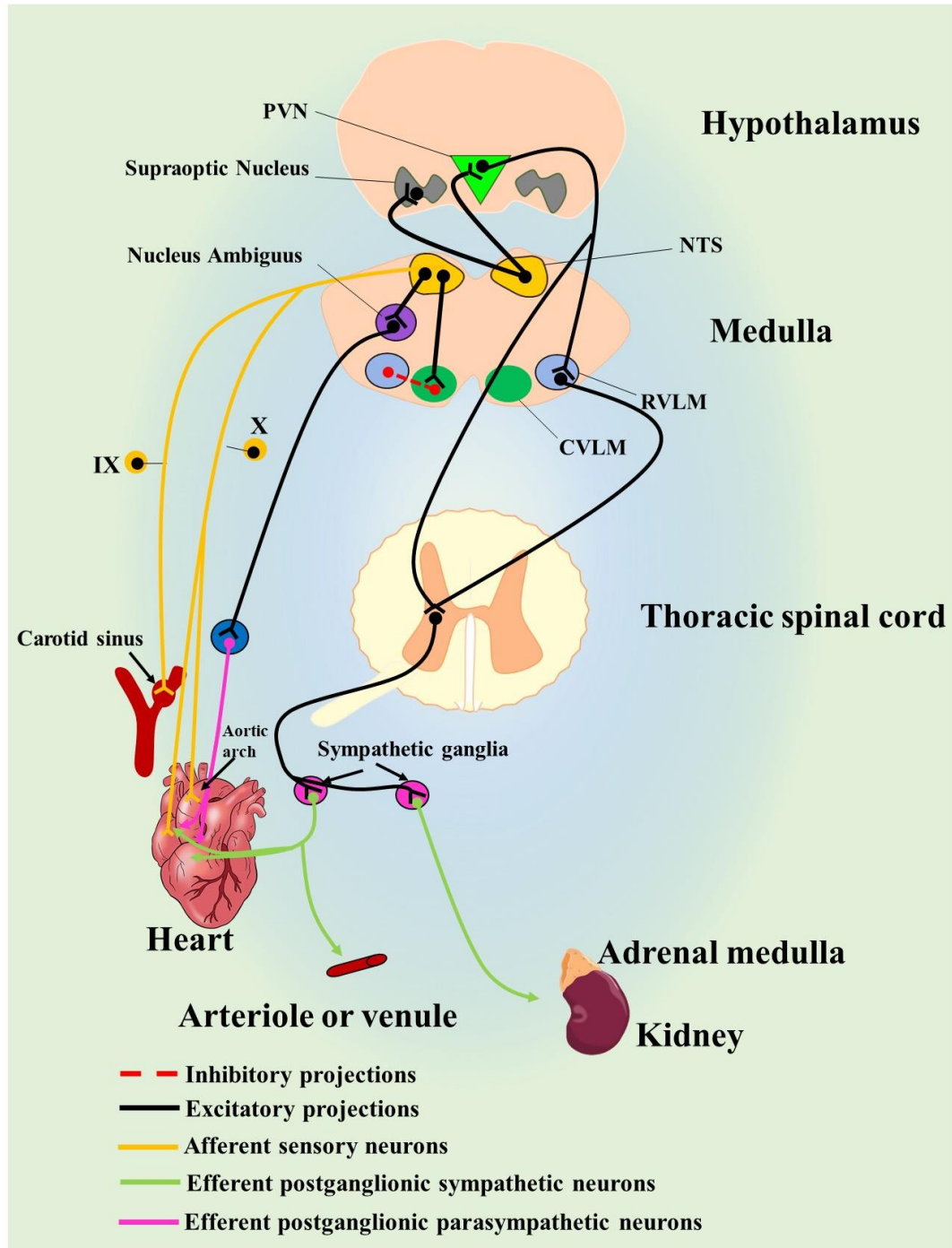


Figure 1. 1. Central and peripheral circuits of the baroreflex arc. Figure illustrates afferent signals arising from carotid sinus and aortic arch baroreceptors. Signals are transmitted through the glossopharyngeal nerve (IX) and vagus nerve (X) to medullary regions followed by modulation of efferent outputs (sympathetic and parasympathetic) to different organs. NTS, nucleus tractus solitarius; RVLM, rostral ventrolateral medulla; CVLM, caudal ventrolateral medulla. Figure was modified and re-drawn (162).

1.2.2. High-pressure baroreflex control of heart rate

An increase in blood pressure activates the baroreflex feedback mechanism, which causes an increase in the efferent preganglionic parasympathetic discharge. This is followed by an increase in the firing of vagal nerve innervating the sinoatrial node. This is accompanied by an activation of the CVLM neurons and an inhibition of the RVLM neurons, which decreases the activity of pre-sympathetic neurons projecting to the spinal cord (Figure 1.1). It is worth mentioning that the heart rate response to vagus nerve firing (latency period of 200-600ms) is quicker than its response to the sympathetic outflow (latency period of 2-3s). This is due to the variability of the adrenergic and cholinergic postsynaptic mechanisms involved (162). However, response of heart rate to baroreflex-mediated alterations in the sympathetic and parasympathetic arms of the autonomic nervous system is likely different to responses seen in other organs. This has been reported in previous studies where the RSNA response to high-pressure baroreflex is notably different from heart rate response in the same physiological model as in exercise (243), or pathophysiological models, such as in renal wrap Grollman and two-kidney one-clip hypertension models (133, 363). In rats, an increase in the maximum gain of the RSNA baroreflex was observed during exercise. However, no change in the baroreflex gain of heart rate was observed (243). In renal wrap Grollman hypertension, baroreflex regulation of RSNA after development of hypertension was maintained, but the baroreflex sensitivity of heart rate was decreased (363). Moreover, in rabbits, a renal hypertension model exhibited attenuated baroreflex regulation of heart rate and a normal baroreflex regulation of lumbar sympathetic nerve activity (LSNA) (363). There are different reasons for the differential baroreflex regulation between the kidney and the heart. For example, heart rate results from compound changes in the parasympathetic and the sympathetic neuronal activities. Meanwhile, the kidney is mainly controlled by the sympathetic nervous system (SNS) with no evidence of parasympathetic innervation. On the other hand, in the two-kidney one-clip model in rabbits, cardiac sympathetic nerve activity (CSNA) was measured instead of heart rate during baroreflex function assessment. However, the CSNA response to baroreflex was comparable to control animals, while an increase in the baroreflex gain of RSNA was observed (133). This suggests differential responses of sympathetic nerves in hypertension, which could be due to

dissimilar alteration of interpretation of afferent baroreflex inputs and/or alteration in descending medullary neurons accompanied with regional variability in the delivery of sympathetic signals. In support of this notion, it was shown that the PVN, a region involved in the integration of baroreceptor afferent information, has a greater influence on RSNA compared with CSNA in normal and heart failure sheep (294). Nevertheless, the vagal parasympathetic segment of the baroreflex loop is overlooked in the literature.

1.2.3. High-pressure baroreflex control of RSNA

The implication of baroreflex regulation of RSNA and renal function in long-term blood pressure control has been illustrated previously in the literature (26). Most of the prior investigations show the importance of high-pressure baroreceptors in moment-to-moment regulation of SNA and blood pressure, while being of less significance in long-term regulation (350). This suggestion was based on reports that showed rapid re-setting of the arterial baroreflex during sustained blood pressure elevation, but no alteration in blood pressure following sinoatrial denervation (67). This was opposed however by a study conducted by Thrasher et al. (351), where baroreceptors in the aortic arch and one carotid sinus were denervated while baroreceptors in the other carotid sinus were left intact. The intact baroreceptors were activated using a common carotid artery ligation procedure, which caused an increase in the arterial blood pressure over 7 days after ligation. This was accompanied by an increase in heart rate, renin levels, and a decrease in sodium excretion, indicating an increase in RSNA. These physiological alterations were restored to normal after the removal of the ligation, suggesting no baroreflex resetting. Alternatively, a sustained decrease in RSNA has been reported for 7 days in rabbits with Ang II-induced hypertension (26). It was found that in the presence of unilateral renal denervation, Ang II infusion increased sodium excretion from the innervated kidney compared with the denervated one, suggesting a sustained reduction in RSNA (220). However, following denervation of the baroreceptors, sodium excretion decreased from the innervated kidney during Ang II infusion, indicating that RSNA decrease and sodium excretion increase, before sinoaortic denervation, were baroreflex-mediated. Besides, the RSNA baroreflex did not reset during the 7 days of Ang II infusion despite sustained blood pressure elevation and heart rate baroreflex resetting (26). This

provides further evidence about differences in the baroreflex-mediated organ responses, but it also indicates that the high-pressure baroreflex has a significant long-term effect on RSNA and blood pressure regulation. The dispute about the role of the baroreflex in short-term vs. long-term blood pressure regulation has gained significant attention supported by multiple commentaries on this topic (79, 328, 350). Moreover, the utilisation of renal denervation as a promising treatment for resistant hypertension in humans, provides evidence of the importance of baroreflex control of RSNA in long-term regulation of blood pressure (158, 197, 376).

1.2.4. Altered baroreflex function in hypertension

Inadequate control of SNA destabilizes blood pressure and causes poor cardiovascular outcomes. Baroreflex function parameters that are usually studied in experimental models include midpoint pressure (A3) and sensitivity (A2) or maximum gain. The midpoint pressure reflects the operating pressure at which baroreceptors have the highest capability to buffer blood pressure fluctuations. A change in the operating pressure range and/or a change in threshold pressure over a range of change in holding pressure is called resetting of baroreceptors. The latter occurs when the operating point moves away from the centre of the baroreflex curve and closer to threshold pressure, at a site of reduced sensitivity. Resetting allows the baroreflex to control blood pressure efficiently at higher levels of blood pressure caused by the sustained elevation of arterial blood pressure (296). This maintains reflex inhibition of RSNA at the new resting levels of arterial blood pressure. If the baroreflex does not reset after sustained elevation of blood pressure, RSNA and heart rate responses remain at the lower plateau of the curve with lessened control of RSNA or heart rate during arterial blood pressure fluctuation around the new operating pressure (363). Resetting can occur at a peripheral level due to increased threshold pressure of baroreceptors; thus, decreased sensitivity to a defined stimulus. In addition, central resetting can be associated with neuro-hormonal mechanisms such as increased levels of Ang II, or enhanced afferent peripheral inputs that causes altered coupling between afferent signals and efferent nerves activities (53). Indeed, blunted baroreflex mechanism is associated with long-term elevation of resting SNA, which eventually leads to hypertension (132). In many hypertensive disease models, differential alterations of baroreflex control of SNA was

observed (133, 354, 363). For example, in the renal wrap hypertension model, an attenuation of heart rate baroreflex with normal RSNA and LSNA baroreflexes was illustrated, in addition to a resetting of the midpoint pressure at which the baroreceptors operate (363).

Alteration in the baroreflex mechanism is associated with peripheral modulation in receptor function and/or alterations in the central loop. The latter includes alteration of the medullary centres receiving afferent information from baroreceptors, and modulation of efferent medullary sympathetic pathways going to peripheral organs. However, mechanisms involved in peripheral or central changes in the baroreflex arc could differ among hypertensive disease models. These mechanisms involve hormonal and/or structural changes that develop during hypertension such as Ang II, renin and aldosterone. Moreover, kidney injury, through a reno-renal reflex mechanism, causes blunted baroreflex control through excessive sympathetic over-activity, which eventually leads to blood pressure elevation (6).

In the two-kidney one-clip model in rabbits, resetting of heart rate and RSNA baroreflexes was observed after 3 and 6 weeks of kidney clipping along with a decline in baroreflex sensitivity after 3 weeks. However, after 6 weeks, RSNA baroreflex sensitivity was restored to sham levels with continued attenuation of heart rate baroreflex (133). This suggests that the RSNA baroreflex is sensitive to hormonal changes that happen in the beginning of hypertension, such as angiotensin, which lessen at a later stage of the disease. Meanwhile, after 6 weeks, structural changes begin such as cardiac and vascular hypertrophy, which could be related to blunted heart rate baroreflex. Conversely, the same model in sheep exhibited increased sensitivity of the RSNA baroreflex along with no change in the baroreflex control of CSNA and heart rate after 3 weeks of clipping (354). This is similar to the Ang II-induced hypertension model during which RSNA decreases after 7 days of Ang II infusion, but increases after a longer duration of Ang II infusion or by combining another stressor such as high-sodium diet (26, 124). Ang II has been described as a sympatho-excitatory mediator that acts on different central regions such as PVN, area postrema, subfornical organ (SFO) and the A5 region of the pons (124). In fact, administration of a low dose of Ang II with high-sodium diet resulted in upward shift in the RSNA response to blood pressure increase i.e. augmented excitatory RSNA. Moreover, high-sodium diet was associated with resetting of baroreflex control of

RSNA after 21 days of Ang II administration. However, the increase in RSNA occurred at later stage of the study and after hypertension was established (124). In addition, high-sodium diet and Ang II infusion alone was not associated with an increase in blood pressure or RSNA over the 7 day period (124). Therefore, it might be that the increase in RSNA in this model is a consequence of the development of hypertension and endogenous Ang II release rather than a cause of it. In addition, blood pressure elevation at later stages of the disease evoke renal damage, which in turn can activate renal afferent nerves and contribute to increased RSNA activity.

1.2.5. Up to date evidence of high-pressure baroreflex changes in intermittent hypoxia

In one study of the effects of exposure to CIH, it was shown that elevated ROS centrally was associated with a decrease in nitric oxide (NO) levels in the brain, mainly the PVN (390). The injection of a NO donor into the PVN decreased blood pressure and RSNA following exposure to CIH (142). It was shown that the enhanced baroreflex sensitivity mediated by the central activation of angiotensin II type 2 (AT2) receptors was reversed by NO blockade (4). Similarly, central inhibition of angiotensin II type 1 (AT1) receptors resulted in increased sensitivity of RSNA and heart rate baroreflexes. This increase in the baroreflex sensitivity was reversed when NO production was inhibited (4). The injection of apocynin into the RVLM attenuated the pressor response caused by Ang II, suggesting that ROS generation is associated with Ang II-AT1 receptor dependent mechanism (240). Of note, it was shown that the generation of central ROS is regulated by an increase in the activity of NOX and uncoupling of nitric oxide synthase (NOS), both were revealed following exposure to CIH (22, 240). Oxygen free radicals bind to NO to produce highly toxic peroxynitrite anions, causing protein nitration and DNA damage (265). In addition, CIH exposure is associated with decreased expression of neuronal NOS in the PVN and SFO regions (142). Normally, NO controls the responsiveness of arterial and cardiopulmonary baroreflexes to blood pressure changes (4, 5). Indeed, impaired baroreflex control of heart rate was reported in CIH-exposed rats after 17 days of exposure to IH (202). On the other hand, exposure to IH for 7 days was associated with a resetting of RSNA baroreflex with no changes in baroreflex gain (392). This is consistent with a previous

IH study that illustrated increased expression of pro-inflammatory cytokines in some brain regions, but not in the RVLM and NTS, after 7 days of exposure to CIH (330). However, longer exposure to CIH was associated with inflammation in the NTS and RVLM, which might underpin blunted baroreflex control of heart rate observed during the later stages of CIH (202, 263). Bilateral carotid body ablation restored the mid-point operating pressure to levels similar to sham rats; however, blunted baroreflex gain of heart rate was not restored (74). This suggests the presence of other aberrant afferent inputs to the NTS in CIH models contributing to blunted baroreflexes. In contrast, ten days of exposure to IH (6% O₂ for 40 seconds every 9 minutes) in juvenile male rats was enough to cause hypertension and enhance the sensitivity of the sympathetic and parasympathetic baroreflex regulation of blood pressure (416). Moreover, Moraes et al. (246) reported increased gain of the high-pressure baroreflex during expiration using the *in situ* rat preparation after 10 days of exposure to IH. This was associated with CIH-mediated respiratory modulation and enhanced inhibitory responses of RVLM presympathetic neuronal activity. In patients with OSA and hypertension, an impaired baroreflex response to hypotension induced by sodium nitroprusside was reported. Interestingly, this was observed even when blood pressure is within the normal range (49), suggesting that derangements are present before the onset of hypertension in OSA. Viewed together, a full understanding of high-pressure baroreflex changes in CIH-exposed animals has not yet been achieved and there is still a scarcity of studies that have examined baroreflex control of RSNA in CIH-exposed animals.

1.3. Low-pressure baroreflex

1.3.1. Anatomy and physiology of low-pressure baroreceptors

Cardiac and pulmonary receptors are described in the literature as a united population known as cardiopulmonary receptors or low-pressure baroreceptors although there is evidence that each induce particular response patterns (110). Atrial receptors mainly located in the left atrium, monitor blood volume changes and initiate a reflex mechanism to change urine volume, thereby regulating body fluid homeostasis (129). The receptors present as unencapsulated nerve endings and are classified into type A receptors that are activated during atrial contraction, type B receptors that are stimulated during atrial filling, and intermediate receptors with both A and B activities (129). Studies point toward afferent inputs from the left side of the heart as the major sensors for the cardiopulmonary reflex (110). Cardiac receptors are innervated by myelinated and non-myelinated afferent fibres that travel through the vagus nerve carrying afferent impulses to the NTS to regulate sympathetic outflow. From the NTS, signals travel to the hypothalamus, mainly to the supraoptic nucleus (SON) and PVN to regulate antidiuretic hormone (ADH) secretion (Figure 1.2). There is evidence of some afferent nerves that travel through sympathetic rami and are activated by mechanical (pressure or volume) and chemical stimuli (129).

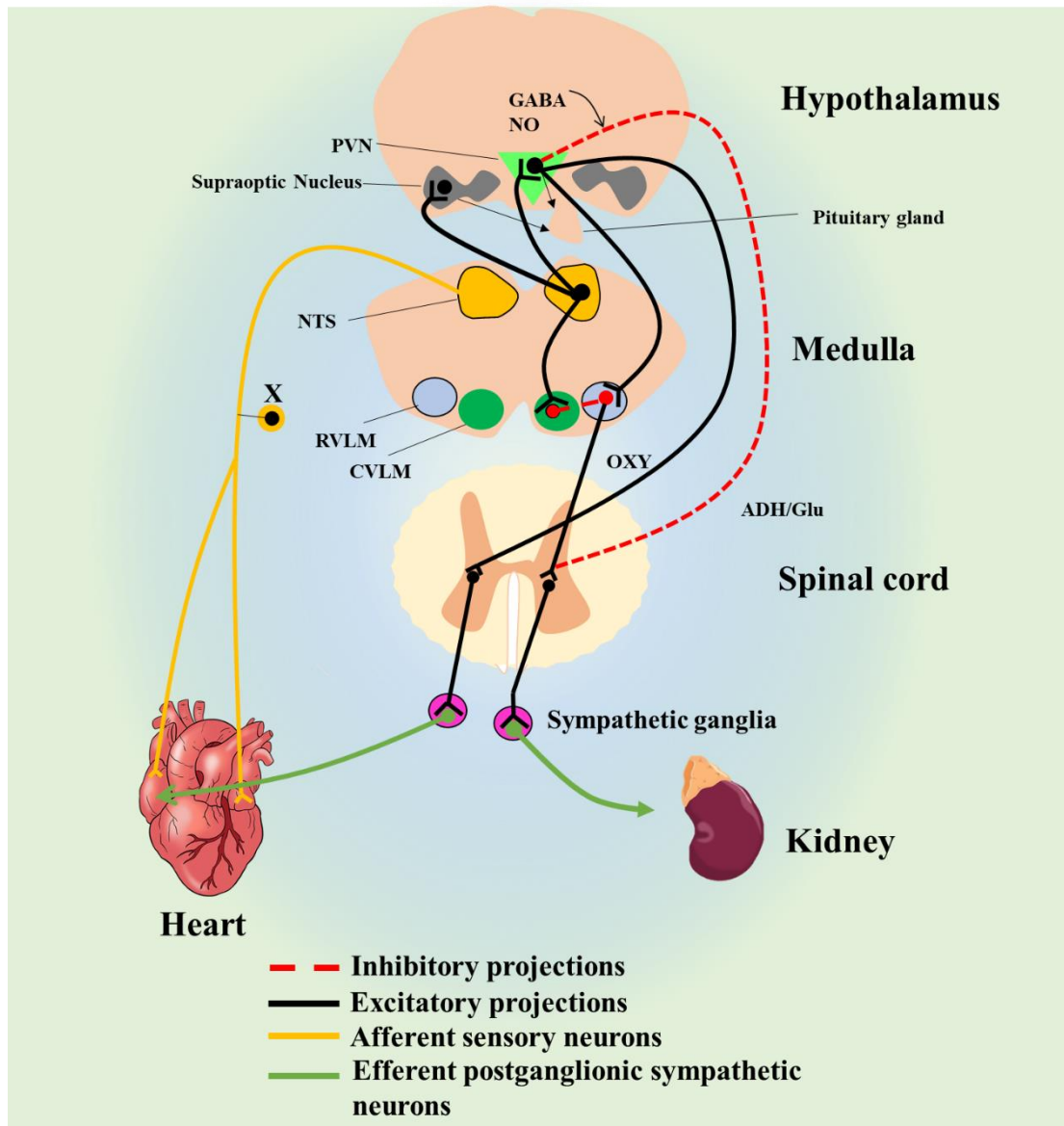


Figure 1. 2. Cardiopulmonary baroreflex arc. Afferent sensory signals travel from different cardiac regions to the NTS followed by their projection to higher brain centres within the hypothalamus. This modulates efferent sympathetic outflow to different organs and antidiuretic hormone release from the pituitary gland. Activation of cardiopulmonary receptors inhibits preganglionic renal sympathetic neurons and activates preganglionic cardiac sympathetic neurons through different projection pathways. NTS, nucleus tractus solitarius; RVLM, rostral ventrolateral medulla; CVLM, caudal ventrolateral medulla; PVN, paraventricular nucleus; NO, nitric oxide; OXY, oxytocin pathway; ADH/GLU, antidiuretic hormone/glutamate pathway.

An increase in blood volume increases atrial pressure and activates atrial receptors. This triggers a negative-feedback loop that causes a decrease in ADH hormone secretion and RSNA. This eventually causes an increase in urine flow and restoration of blood volume. In contrast, this reflex includes an increase in CSNA with no changes

in LSNA (63, 156). Interestingly, the increase in heart rate (known as the Bainbridge effect) reported in the literature was not accompanied by an increase in cardiac contractility or changes in peripheral vascular resistance except for the renal vasculature, where an increase in renal blood flow was observed (129). Therefore, the SNS responds to cardiac afferent inputs in a non-uniform fashion, which is due to discrete pathways within the hypothalamus that differentially regulate the activity of renal and cardiac sympathetic preganglionic nerves (63). The PVN is the central command site that regulates the RSNA response within the reflex arc of the cardiopulmonary receptors. Destruction of PVN neurons significantly attenuates the RSNA response to saline overload (63). PVN ADH/glutamate neurons projecting to the spinal cord elicit an excitatory effect on renal preganglionic sympathetic nerves. ADH nerves are inhibited by GABA interneurons within the PVN. This central network was found to be dependent on NO, as inhibition of NO synthase attenuates RSNA sympatho-inhibition mediated by the volume reflex. There is also a group of ADH/glutamate neurons travelling from the PVN to the RVLM that regulates sympathetic outflow through vasomotor nerves (63). Interruption of cardiac afferent inputs by pericardial lidocaine or by bilateral vagotomy totally abolished the renal sympatho-inhibitory response to volume expansion. Importantly, lidocaine eliminated sensory inputs from the heart, not the lungs, which indicates that pulmonary receptors do not contribute to the renal sympatho-inhibitory response (245). On the other hand, CSNA is mainly regulated by the PVN oxytocin pathway projecting to the spinal cord, which influences preganglionic cardiac sympathetic nerves. The cardiac arm of the volume reflex is independent of ADH or GABA (63).

Multiple physiological conditions can activate intra-thoracic mechanoreceptors such as positive- and negative-pressure breathing. Positive-pressure breathing causes a decrease in intra-thoracic blood volume, which eventually causes a reflex increase in plasma ADH and a decrease in urine volume (110). In contrast, negative-pressure breathing was associated with an increase in intra-thoracic blood volume, an increase in urine volume and a decrease in ADH secretion (110). This suggests that renal function alterations and ADH secretion were reflex-regulated by intra-thoracic mechanoreceptors including cardiac receptors. However, other cardiovascular and haemodynamic changes occur during positive- and negative-pressure breathing that could mediate renal responses. For example, a decrease in arterial blood pressure and

an increase in central venous pressure were reported during positive-pressure breathing. In addition, bilateral cervical vagotomy did not abolish completely the increase in ADH secretion and the decrease in water diuresis that had happened during positive-pressure breathing in rats and dogs (110). Thus, the putative presence of mechanisms other than the cardiac volume reflex that might be attributed to reflex alterations in renal function and plasma ADH levels cannot be excluded.

Other studies that involved balloon inflation at different regions of the left side of the heart supported the presence of a cardiac receptor-mediated reflex. These studies include balloon inflation in the left atrium near the mitral valve or at the junction of the pulmonary vein and the atrium, or at the left and right atrial appendages. In relation to that, an increase in diuresis and a decrease in plasma ADH was reported during atrial balloon distension (110). Balloon inflation in the left atrium was associated with haemodynamic changes such as an increase in heart rate, which mediates, at least partly and in conjugation with ADH, the diuretic response. In addition, infusion of pitressin (ADH analogue) caused attenuation but not elimination of the diuretic response. Interestingly, damaging the appendages of the left and right atria eliminated the renal response to balloon inflation, which suggests that the response is mediated by stretching of these appendages. Mechanical distension of the right atrial appendages was associated with an increase in urine flow. This suggests that right atrial receptors in addition to the left atrial receptors can influence renal function (110). Importantly, however, pressures or forces used in balloon inflation do not necessarily reflect physiological pressure changes.

Atrial distension was shown to be associated with sodium excretion, which also can be mediated by a decrease in RSNA, an inhibition of the renin-angiotensin-aldosterone system (RAAS), and an increase in the release of atrial natriuretic peptide (ANP) (109). ANP is stored in atrial granules as an inactive pro-hormone and its release is stimulated by cardiac stretch. It plays a physiological role in renal sodium excretion acting on ANP-A receptors that exist on renal tubules (378). It boosts natriuresis and diuresis through different mechanisms that include the decrease of aldosterone secretion and the inhibition of apical sodium channels and the basolateral Na^+/K^+ ATPase pump in the inner medullary collecting duct. There is evidence that ANP inhibits Ang II-induced release of ADH from the posterior pituitary gland (378). Moreover, ANP increases glomerular filtration rate (GFR) through afferent arteriolar

vasodilation, the inhibition of renin release and the relaxation of the contractile mesangial cells. Indeed, the administration of atrial tissue extracts to anaesthetised rats was associated with natriuresis and diuresis (109). Moreover, volume expansion in anaesthetised rats resulted in diuresis and natriuresis concomitant with increased plasma levels of ANP (308). The prevention of ANP increase during saline overload in anaesthetised rats abolished renal diuretic and natriuretic responses (308). However, in dogs, cardiac denervation during volume expansion eliminated the natriuretic effect despite a fourfold increase in the plasma levels of atrial peptides (111). Overall, volume expansion studies suggest that ANP contributes to diuresis and natriuresis observed during the stimulation of the cardiopulmonary reflex.

1.3.2. Altered low-pressure baroreflex function in hypertension

There is less focus on low-pressure baroreflex control of blood pressure in hypertension compared with the high-pressure baroreflex. Blunted cardiopulmonary reflex is observed in many hypertensive disorders that involve cardiac hypertrophy, such as renovascular hypertension and aortic stenosis (107). Interestingly, normotensive athletes with thickened heart walls also showed a decreased response to cardiopulmonary reflex stimulation (107). In spontaneously hypertensive rats (SHR), acute volume expansion caused a 25% decrease in RSNA compared with a 45% decrease in control rats. In addition, these SHR rats had a blunted bradycardic response to chemical stimulation of the cardiopulmonary receptors and higher left ventricular to body weight ratio (357). It is therefore suggested that distension of the left atrium due to hypertrophy in these rats resets the cardiopulmonary receptors.

Studies on obese rats and in the cisplatin-induced renal injury model showed blunted RSNA response to volume expansion accompanied by decreased diuresis and natriuresis (3, 120, 169). However, unilateral and or bilateral denervation of the kidney in these rats restored the normal baroreflex and kidney function response to volume expansion (120, 168). In relation to that, elevation of renal transforming growth factor beta (TGF-1 β) in cisplatin-induced renal failure animals, and tumour necrosis factor- α (TNF- α) and interleukin 6 (IL-6) in kidneys harvested from obese rats was also reported (120, 170). Therefore, immunosuppression using tacrolimus restored the blunted RSNA baroreflex response of either obese or cisplatin-induced renal failure

rats (2, 170). In this regard, it is proposed that kidney inflammation activates afferent renal nerves which cause a reflex sympatho-excitation and the attenuation of the low-pressure baroreflex function.

Studies in humans showed that increased venous return due to leg raising in athletes was associated with attenuated cardiopulmonary reflex function as demonstrated by a lesser decrease in forearm vascular resistance and plasma norepinephrine (NE) compared with controls (107). Similar findings were reported in response to a decrease in venous return by lower body negative pressure in athletes (107). Moreover, mild-to-moderate hypertensive individuals showed slightly decreased forearm vascular resistance in response to leg raising, while it was markedly attenuated in patients with more severe hypertension and cardiac hypertrophy (232). The vasoconstrictor response to cold pressor test was similar in athletes vs. controls, and in patients with mild-to-moderate hypertension vs. patients with severe hypertension and cardiac hypertrophy. Therefore, it was suggested that impaired cardiopulmonary reflex is associated with changes in the neural arc of the loop rather than diminished effector sensitivity (107, 232). Overall, the cardiopulmonary reflex might be maintained in the beginning of hypertension and impaired as cardiac structural changes develop (232). This suggests that blunted cardiopulmonary reflex is not a cause of hypertension rather it is a consequence of it, and it increases sympathetic activity and contributes to a vicious cycle of hypertension. Interestingly, in one study, normotensive individuals with OSA showed increased left ventricular wall thickness and left atrial size compared with normotensives individuals with no OSA (86). However, the cardiopulmonary reflex has not been studied in CIH-induced hypertension.

1.4. Renal sensory afferent nerves

1.4.1. Distribution and projection to brain

Renal sensory receptors are present as free nerve endings in the kidney that project to thoracolumbar region of dorsal root ganglia primarily from T12 to L3 (372). Afferent fibres synapse with interneurons within the ipsilateral dorsal horn in laminae I and laminae III to V. They project to brain sites including NTS, RVLM, SFO and PVN (151).

The location of the renal sensory nerve fibres has been identified using highly specific wheat germ agglutinin horseradish peroxidase nerve tracing (237). Immunohistochemistry has also been implemented to explore renal sensory nerves by tracking calcitonin gene-related peptide (CGRP) and substance P (SP) as specific neurotransmitters of sensory neurons (115, 179, 186, 247). In the kidney, the sensory fibres travel parallel to the renal vein, renal artery and ureter entering the kidney at the hilus. The nerve endings of these sensory fibres are predominantly found in the ureter and the muscular layer of the renal pelvic wall with some located in the uroepithelial layer of the renal pelvis (237). This is evidenced by the presence of SP in the space between the muscular layer and the epithelial cells of renal pelvic wall (96) indicating the presence of sensory nerves in the renal pelvis. Similarly, CGRP was identified in the renal pelvic wall in previous studies in rat and sheep (37, 101) and was utilised to examine the validity of renal denervation in these studies. Marfurt and Echtenkamp (237) identified renal afferent nerves in the renal cortex by labelling these fibres with wheat germ agglutinin-horseradish peroxidase. However, labelling was not detected in the renal medulla or papilla. Immuno-labelling by the same group indicated the presence of afferent fibres in the interlobular and arcuate arteries. Some of these afferent sensory fibres were stimulated when the renal artery and renal vein were obstructed (36, 389). Similarly, an elevation in renal venous pressure resulted in an increase in urinary sodium excretion and urine flow. This response was not attenuated when lidocaine, a local anaesthetic, was injected into the renal pelvis (195), providing evidence for the presence of sensory nerves in the renal vein separate from those present in the renal pelvis. In rats, around 76% of afferent nerves are unmyelinated slowly conducting axons while some 19% are thin myelinated and only 5% are rapidly

conducting myelinated fibres (176). In general, sensory nerve endings in the kidney are of two types: mechanoreceptors and chemoreceptors (338).

The mechanoreceptors are sensitive to stretch induced by volume expansion, capsaicin or any stimulus that increases SP and CGRP formation. However, a group of renal sensory nerves were found to be responsive to ischaemia due to renal artery occlusion or due to cyanide, but not to pelvic pressure elevation (298). These sensory nerves that were sensitive to ischaemia, were not activated by mechanical stretch and were therefore referred to as chemoreceptors, which are classified to R1 and R2 receptors. R1 chemoreceptors are silent under resting conditions and are innervated by the non-myelinated slow conducting nerve fibres, which elicit action potentials of long duration when activated (298). In contrast, R2 chemoreceptors are active in the resting state and are slowly-adapting insofar as their firing continues 15-20 minutes after death. They are activated by renal ischaemia and by backflow of hypertonic or hyperosmotic urine (118, 297). Studies pointed toward a role for chemoreceptors in initiating an excitatory reno-renal reflex, which contributes to sympatho-excitation and blood pressure elevation (44, 118, 298). To distinguish the role of mechanoreceptors from that of chemoreceptors, an increase in renal pelvic pressure over a physiological range (2.5–10 mmHg) was utilised to activate the mechanoreceptors while a solution of 450mM NaCl was used to stimulate the chemoreceptors (189, 364). However, there is still a scarcity in the literature of studies that differentiate between mechanoreceptors and chemoreceptors in terms of structure and function.

1.4.2. The physiological activity of renal afferent and efferent sensory nerves

Efferent nerves travelling into the kidneys are sympathetic in nature and are mainly located in the corticomedullary region and to a lesser extent, in the renal pelvic wall. The renal efferent nerves are intertwined with afferent nerves in the same nerve fibre bundle (178, 186). Efferent sympathetic stimulation increases NE release, which binds to α_1 and α_2 adrenoreceptors in the renal pelvic wall (186). NE stimulates renin release followed by RAAS activation, which results in increased renal sodium and water reabsorption (126). This causes an increase in ureter and renal pelvic pressure that activates mechanosensitive receptors through the opening of transient receptor

potential cation channel subfamily V member 1 (TRPV1) and release of SP and CGRP, which in turn enhances afferent renal nerve activity (ARNA). Renal afferent nerve stimulation provides a negative feedback mechanism that causes reflex natriuresis and diuresis i.e. a fall in efferent renal sympathetic nerve activity (ERSNA) (180). This is known as the inhibitory reno-renal reflex, which protects against sympathetic over-activity and blood pressure elevation (Figure 1.3).

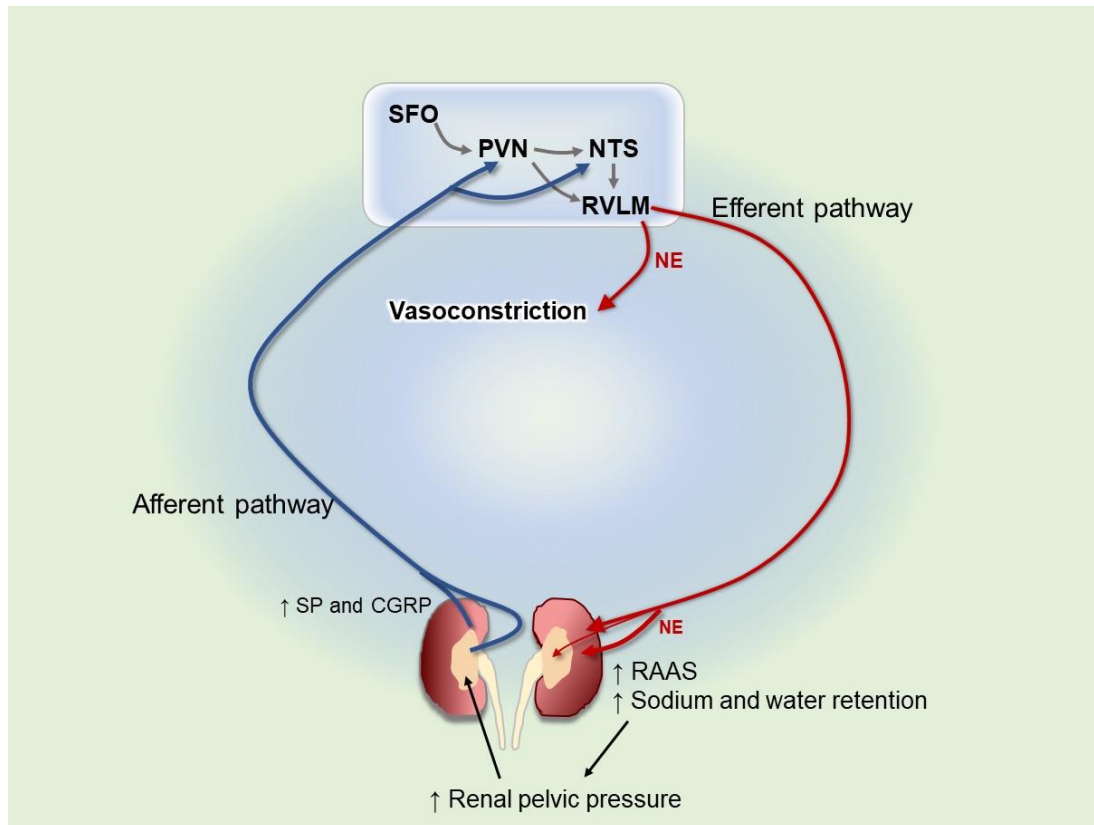


Figure 1. 3. Renal afferent and efferent sympathetic nerves. Blue lines represent afferent signals and red lines represent efferent sympathetic discharge. Afferent signals, mediated by the release of substance P (SP) and calcitonin gene-related peptide (CGRP), are integrated in the paraventricular nucleus (PVN) and nucleus tractus solitarius (NTS) to activate the rostral ventrolateral medulla (RVLM), increasing sympathetic nerve activity to different organs including the kidneys. An increase in efferent renal sympathetic nerve activity enhances the release of norepinephrine (NE) and activates the renin-angiotensin-aldosterone system (RAAS). This decreases sodium and water excretion and increases renal pelvic pressure, causing stimulation of the mechanoreceptors of the afferent pathway (15).

SP natriuretic and diuretic response is associated with two mechanisms. First, SP activates an inhibitory reno-renal reflex to decrease sympathetic outflow, thus, increasing water and sodium excretion. Second, SP induces pelvic contractions that facilitate urine movement into the bladder (182). The role of CGRP in renal sensory

nerve endings is not extensively studied, but there is convincing evidence that CGRP stimulates renal afferent nerves and increases renal sodium excretion (114, 115, 385). Of high interest, the effect of CGRP and SP together on ARNA is greater than the effect of each neuropeptide alone. In addition, CGRP infusion into the pelvis causes a greater increase in ARNA induced by an increase in renal pelvic pressure (116). Although neurokinin 1 (NK1) receptor antagonism blocks CGRP-mediated effect on ARNA, CGRP receptor blockade was not associated with a similar effect on SP-mediated activation of afferent renal nerves (116). Therefore, it was suggested that CGRP action is mediated via a mechanism which involves inhibition of SP metabolism, thus, augmenting SP-mediated activation of ARNA.

On the other hand, previous studies have shown that the intra-renal infusion of ischaemic mediators such as adenosine or backflow of urine into the renal pelvis, causes reflex sympatho-excitation and a decrease in sodium and water excretion (59, 161). Moreover, the infusion of hypoxic blood into the kidney induces reflex sympatho-excitation, which was greatly attenuated by the inhibition of adenosine and bradykinin synthesis (18). This is known as the excitatory reno-renal reflex which was frequently observed in different models of hypertension. Receptors involved in the activation of the excitatory reno-renal reflex are not clearly illustrated. However, it was shown that the infusion of bradykinin and capsaicin into the kidney induces contralateral renal sympatho-excitation (101, 391, 397), indicating that renal bradykinin receptors and TRPV1 channels are involved in the excitatory reno-renal reflex. Studies of hypertension and the excitatory reno-renal reflex are described in section 1.4.4.2.

1.4.3. Activation pathways of renal afferent sensory nerves

Signalling pathways involved in sensory mechanoreceptor activation have been extensively studied by Kopp et al. (180) employing pharmacological agents and direct recording of renal afferent nerve signals in rats. Activation pathways of mechanoreceptors are via two main routes: NK1 activation by SP and/or stimulation of TRPV1 as illustrated in Figure 1.4. These pathways result in the release of SP and CGRP, primary neurotransmitters for ARNA and/or increase intracellular calcium with subsequent depolarization through TRPV1 channels. Some signalling pathways

require the presence of cyclooxygenase (COX) enzyme and prostaglandins (PGs) as previously reported (194). The pathway involves PGE2 binding to its receptors resulting in the activation of the cAMP/PKA signalling cascade and this ultimately causes SP and CGRP production (185). Detailed information is provided in sections 1.5 and 1.6 regarding TRPV1 and bradykinin receptors.

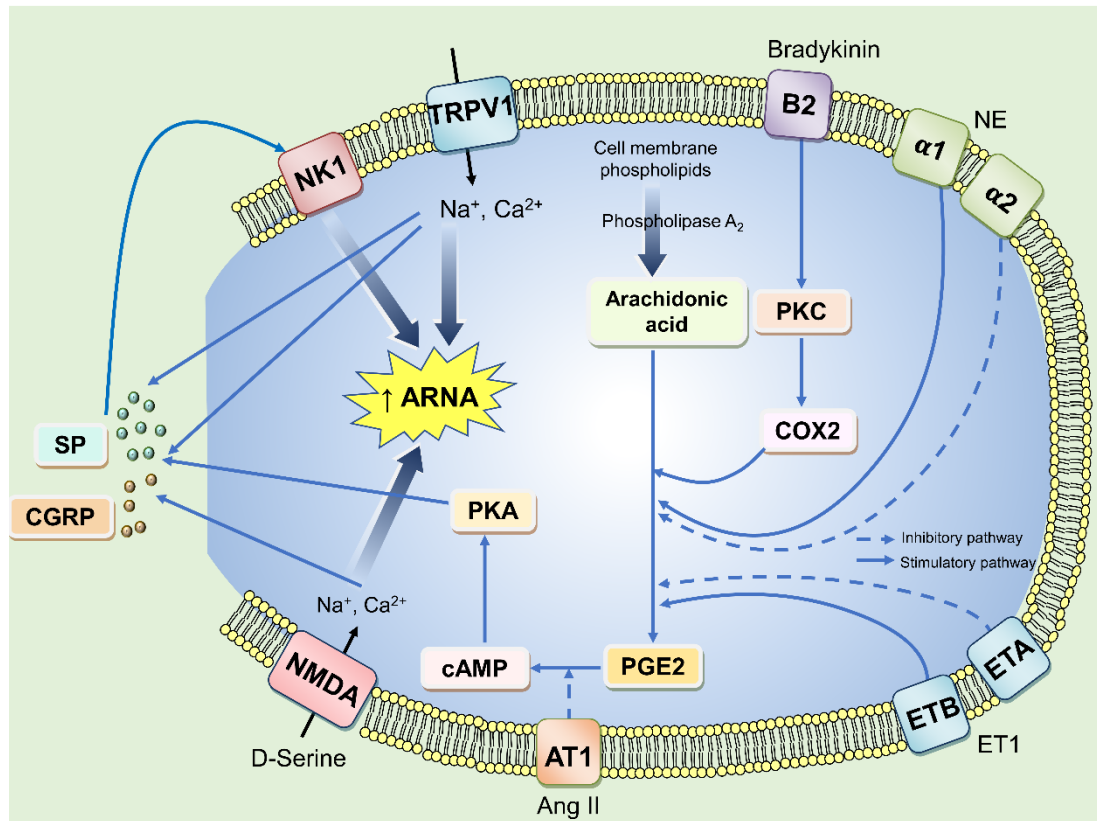


Figure 1. 4. A representation of possible pathways that enhance renal afferent nerve activity in a renal afferent nerve ending. B2, Bradykinin receptor type 2; PKC, protein kinase C; NE, norepinephrine; ET1, endothelin 1; ETA and ETB, endothelin receptor type A and type B; PKA, phosphokinase A; SP, substance P; CGRP, calcitonin gene related peptide; NK1, neurokinin receptor 1; TRPV1, Transient receptor potential cation channel; NMDA, N-methyl-D-aspartate receptors; ARNA, afferent renal nerve activity. Solid lines represent excitatory pathways and dashed lines represent inhibitory pathways. Chronic intermittent hypoxia may evoke aberrant renal afferent signalling contributing to hypertension through action on one or more of the above signalling mechanisms (15).

1.4.4. Renal afferent nerves and hypertension

Renal afferent nerve hyperactivity is associated with derangement of reno-renal reflex control, contributing to blood pressure elevation by suppression of the pre-mentioned inhibitory reflex and/or activation of an excitatory reno-renal reflex (180).

Sympathetic over-activity, and sodium and water retention associated with high blood pressure was reported in different models of hypertension such as the two-kidney one-clip Goldblatt model (198), SHR (149), high fat diet-induced hypertension (169), and CIH-induced hypertension (320, 416). In the CIH model for example, a neurogenic mechanism is activated early in the disease process and is dependent on increased sympathetic tone (318). It is not known, however, if renal afferent signalling has a contributory role in mediating increased sympathetic nerve activity in CIH and OSA.

1.4.4.1. Suppression of the inhibitory reno-renal reflex

In the SHR, elevation of peripheral sympathetic nerve activity is eliminated when the injured kidney is denervated (182), with almost a 50% decrease in blood pressure observed 10 minutes after denervation. In addition, renal denervation is associated with a decrease in renal cortical NE levels (104). Therefore, it has been suggested that part of the decrease in blood pressure following renal denervation is due to a reduction in NE release from the postganglionic efferent nerves. It is also suggested that the decrease in blood pressure following denervation is due to interruption of renal afferent neuronal signalling. Janssen et al. (149) utilised selective renal afferent nerve denervation to demonstrate the significant influence of renal afferents on SNS activity and baroreflex sensitivity in SHR. Renal afferent denervation in the latter study did not elicit a blood pressure lowering effect, and had no effect on urine volume or sodium excretion. Relevant to these findings, an increase in renal pelvic pressure or an intra-renal pelvic injection of bradykinin, neither caused an increase in ARNA, nor an increase in SP release (182, 190). Moreover, there was a decreased responsiveness of NK1 receptors to SP in SHR (182). These studies collectively provide evidence for suppression of the inhibitory reno-renal reflex in the SHR, which contributes to sympathetic over-stimulation in this model.

1.4.4.2. Activation of the excitatory reno-renal reflex

Activation of the excitatory reflex is proposed to play a major role in renovascular hypertension and hypertension associated with chronic kidney disease (46, 149, 169, 383). In the two-kidney, one-clip model of hypertension, the clipped kidney undergoes ischaemic damage compared with the non-clipped kidney. While renal denervation of

the non-clipped kidney caused a decrease in sodium excretion, renal denervation of the clipped kidney resulted in an increase in ipsilateral and contralateral sodium excretion along with a fall in contralateral ERSNA (181). Likewise, dorsal rhizotomy followed by clipping of the renal artery resulted in a significant partial decrease in blood pressure in the one-kidney, one-clip model. However, contralateral dorsal rhizotomy of the nephrectomised kidney did not cause any change in blood pressure (383). This confirms the presence of excitatory afferent signals from the clipped kidney due to ischaemic insult. Furthermore, previous studies suggested that ischaemia induces adenosine release, which in turn stimulates afferent nerves (18, 212). Therefore, based on these studies, it was suggested that adenosine, in addition to bradykinin and prostaglandin E2, which are mediators released during ischaemia, are associated with the activation of renal chemoreceptors (18).

The effect of renal deafferentation was also studied in the 5/6 nephrectomy model and was shown to attenuate hypertension and decrease NE turnover in the brain (46). Moreover, renal afferent denervation decreased forebrain Ang II, AT1 receptors, c-fos in RVLM and tyrosine hydroxylase levels. Similarly, at the level of the kidney, macrophage count, fibrosis markers and NOX expression were reduced following denervation (48). In deoxycorticosterone acetate (DOCA) hypertensive rats, renal denervation decreased arterial blood pressure by 50% together with a decrease in plasma NE. Interestingly, the same effect was observed after selective afferent denervation using capsaicin. Importantly, renal afferent denervation was performed prior to DOCA initiation, which supports a key role for afferent nerves in the development of hypertension in this model (101). Based on these studies, it is possible that blood pressure reduction is attributed to an interruption of renal afferents, in addition to the effect of removal of efferent nerves to the kidneys.

Ischaemia-reperfusion injury is another disease model associated with elevated blood pressure and heart rate. In this model, oxidative stress and inflammatory cytokines are elevated in the systemic circulation, SFO, hippocampus, corpus callosum and cerebral cortex. Overexpression of NOX2 and NOX4 in the kidney, SFO and hippocampus was reported in this model (47, 155, 326). In a renal ischaemia-reperfusion injury model, deafferentation by intra-renal capsaicin decreased blood pressure, and renal and central oxidative and inflammatory mediators (47). Ma et al. (229) reported an impaired release of SP and downregulation of NK1 receptors in the post-ischaemic

kidney. In the latter study, selective stimulation of mechanoreceptors by an increase in intra-pelvic pressure impaired renal excretory function. It can be suggested from the above studies that ischaemia as characterized by increased NOX, activates chemoreceptors in the kidney, which contribute to the enhanced sympathetic activity seen in hypertension.

1.4.4.3. Kidney inflammation, excitatory reno-renal reflex and baroreflex dysregulation

Baroreflex regulation of blood pressure is impaired in several models of hypertension including some animal models of CIH (202, 392). Indeed, failure of the baroreflex mechanism is associated with long-term elevation of resting SNA (132). In different models of hypertension, it was reported that impairment of the normal baroreflex mechanism is secondary to afferent renal nerve activation (6). Kidney injury, through reno-renal reflex mechanisms, causes a blunted baroreflex through excessive sympathetic over-activity, which eventually leads to blood pressure elevation.

As mentioned above, studies of cisplatin-induced renal injury and a high-fat diet model of obesity in rats demonstrated that it is the excitatory reno-renal reflex that is dominant in these models, responsible for blunted baroreflex control of blood pressure (168, 170). The dysregulation of the baroreflex in cisplatin or high-fat diet models is attributed to renal inflammation that initiates excitatory afferent neural signals, a suggestion supported by the increase in renal and systemic inflammatory cytokines such as TNF- α and IL-6 (170). Treatment of rats in both models by tacrolimus, an anti-inflammatory agent, restored the low- and high-pressure baroreflex, in addition to decreased renal tissue levels of TNF- α and IL-6 in these rats (2, 170). Together, the involvement of inflammation and renal nerves in mediating the derangement of the baroreflex control of blood pressure in these studies was evident when bilateral renal denervation and/or the administration of an anti-inflammatory agent restored the sensitivity of low- and high-pressure baroreflexes to changes in blood volume and blood pressure, respectively.

1.4.4.4. A possible link between renal afferent nerves and CIH-induced hypertension: Role of inflammation and oxidative stress

OSA is a known inflammatory disease that activates inflammatory signalling molecules in the systemic circulation and kidney tissue. This can cause renal fibrosis and apoptosis as indicated by studies of CIH-exposed animals (11, 223, 382). Chronic kidney disease is often diagnosed in patients with OSA. Therefore, molecular mechanisms underlying OSA-induced kidney damage are currently of interest. Inflammation plays a major role in the pathogenesis of CIH-induced hypertension as reported by a number of studies (9, 146, 224, 342). In addition, in response to oxidative stress, HIF-1 stimulates the translocation of nuclear factor kappa B (NF- κ B), which increases the expression of genes that encode TNF α , interleukin 1 β (IL-1 β) and IL-6 (76, 146, 263). Chronic treatment of CIH-exposed carotid bodies with ibuprofen in a previous study decreased cytokine levels and attenuated the enhanced ventilatory response to hypoxia, and prevented the development of hypertension (76). An anti-inflammatory treatment was associated with a decrease in c-fos levels in the NTS indicating a role for cytokines in neurogenic hypertension in agreement with a number of previous reports (76, 154, 321, 336). However, ibuprofen failed to decrease 3-nitrotyrosine levels and did not impede the augmented sensitivity of the carotid bodies to hypoxia (76). Meanwhile, anti-oxidant treatment abolished enhanced responsiveness of peripheral chemoreceptors and the ventilatory response to hypoxia along with a decrease in cytokine levels in carotid bodies (76). Thus, it is likely that inflammation and increased cytokine levels are secondary to oxidative stress in the vasculature associated with exposure to CIH. Similar increases in inflammatory and oxidative stress markers were reported in the kidneys of CIH-exposed animals as shown by a number of studies in the literature (Appendix 1, Table 8.1) (224, 330, 382, 409).

Based on previous studies, it appears that exposure to CIH induces a temporal response such that short-term or mild IH initiates an early renal response during which cellular defence anti-oxidative mechanisms are activated to elicit a compensatory response (Table 1.4). However, long-term or severe IH induces inflammation, apoptosis and a decrease in the levels of antioxidant enzymes and anti-inflammatory cytokines (de-compensatory response) (80, 164, 224, 277, 380, 382). Although some studies reported compensatory responses for up to 3 weeks of exposure to IH, other studies

reported renal morphological damage and attenuation of antioxidant enzymes after just 2 weeks of exposure to more frequent cycles of IH (277). Moreover, short-term IH exposure (3 days) was sufficient to induce lipid peroxidation, release of adhesion molecules and fibrogenetic factors (342). This indicates that IH might induce early renal changes as indicated by lipid peroxidation and activation of endothelial dysfunction markers (277, 342).

Furthermore, exposure to IH for 28 days and for 8 weeks was accompanied by HIF-1 upregulation in renal tissue (164, 224). HIF-1 α expression was also observed in NTS and RVLM after exposure to CIH (273). HIF-1 upregulation is a ROS-dependent process mediated by NOX. NOX4 is located in renal pelvic wall (216), and NOX4 overexpression in the kidney was reported after exposure to CIH accompanied by a decrease in SOD levels (223). It has been shown that renal denervation and antioxidant treatment significantly decrease renal oxidative stress and blood pressure in CIH models (164, 224, 384). In addition, treating CIH-exposed rats with N-acetyl cysteine restored renal tissue SOD levels and decreased RSNA and blood pressure (223). This proposes a clear link between oxidative stress and renal nerves contributing to sympatho-excitation and hypertension. Additionally, metallothionein knockout mice exhibited renal fibrosis after 3 weeks of exposure to IH, but 8 weeks of exposure was needed to induce fibrosis in wild-type mice (380). Moreover, SOD was downregulated while NOX2 was upregulated in the NTS and RVLM after 10 days of exposure to IH (273). When viewed together, these findings highlight an important interaction between oxidative stress and sympatho-excitation either at the level of the peripheral organs (carotid bodies and kidneys) and/or within the higher control centres.

TRPV1 is sensitised by hydrogen peroxide (H₂O₂) administration leading to SP release in renal mechanoreceptors. The impact of H₂O₂ on TRPV1 is inhibited by catalase. Of interest, renal NOX4 is upregulated after exposure to CIH and is co-localized with TRPV1 receptors in renal sensory nerve endings. (216). Likewise, it was shown that ROS mediates TRPV1 signalling in peripheral sensory nerves and in carotid bodies (174, 218). Increased ROS in carotid bodies was due to HIF-1-mediated NOX2 upregulation and it was associated with enhanced sympatho-excitatory response to hypoxia. (200). These studies led to the one of hypotheses of this thesis, that early changes in renal oxidative and/or inflammatory signalling sensitizes renal TRPV1

receptors and contributes to afferent renal nerve hyperactivity, similar to the role of TRPV1 in sensitizing the carotid bodies following exposure to CIH (235), contributing to CIH-induced hypertension.

1.5. TRPV1 channels

1.5.1. Location and activation pathways

TRP (Transient receptor potential) channels are polypeptides composed of six helices with intracellular C- and N-terminals. Subunits join each other to form a tetramer and the functional channel is composed of a non-selective cationic permeable pore. TRPV1 channels are predominant in nociceptors in addition to trigeminal and nodose ganglia (160). They are also distributed throughout the tubules of the renal cortex, outer medulla and juxtaglomerular apparatus. In addition, TRPV1-positive sensory nerves were identified in renal pelvic wall and in the ureter (96).

TRPV1 channels are more selective to Ca^{2+} and Mg^{2+} compared with Na^+ . In addition to mechano-stimulation, they are also activated by heat ($>43^\circ$) and acidic pH (<5.9), relevant to inflammation or ischaemia (160, 211). Endogenous activators of TRPV1 channels are mainly arachidonic acid metabolite derivatives known as endovanilloids such as anandamide, in addition to lipoxygenase (LOX) products, which are subdivided into endocannabinoids and eicosanoids (160, 211). The most commonly used exogenous activator of TRPV1 channels is capsaicin. Resiniferatoxin is another TRPV1 agonist with markedly greater potency than capsaicin (211). Of note, agonist binding was found to induce allosteric changes and to lower the rate binding energy required for other agonists (144). Accordingly, protons enhance the binding of capsaicin to TRPV1 channels which increases TRPV1 response current to protons and temperature.

Furthermore, TRPV1 activity is mediated by the phosphorylation of kinases, such as phosphokinase A (PKA), PKC, calcium calmodulin-kinase II and Src kinase (211). Inflammatory mediators such as prostaglandins activate PKA, which sensitizes the TRPV1 response to capsaicin and temperature. Similarly, other inflammatory mediators such as bradykinin activates, via its binding to bradykinin type 2 (BK2R) receptors, PKC which phosphorylates TRPV1 (211, 276). This lowers the threshold required to evoke TRPV1 response when stimulated by heat, protons or capsaicin (340). However, continuous activation of PKA, PKC or intracellular calcium causes desensitisation of TRPV1 (187, 211, 234).

It was shown that local inflammation of peripheral sensory neurons stimulates BK2R to phosphorylate TRPV1 channels by a $\text{G}_{q/11}$ dependent mechanism (337). In

nociceptive receptors, bradykinin stimulates phospholipase C (PLC), which activates phosphatidylinositol 4, 5-bisphosphate to release inositol triphosphate (IP₃) and diacylglycerol. IP₃ in turn enhances the release of intracellular calcium and depolarizes sensory neurons (51). Bradykinin, through PLA₂, releases arachidonic acid which is a precursor for LOX products that are endogenous agonists for TRPV1 (187). Therefore, BK₂R activation of sensory neurons might partially be mediated by TRPV1 channels or by stimulating the release of intracellular calcium. As in nociceptive neurons, it is expected that a cross talk exists between BK₂R and TRPV1 channels in the renal sensory afferent neurons of the renal pelvic wall. Figures 1.4 and 1.5 illustrate the mechanisms of TRPV1 activation of renal afferent nerve endings whether direct via increasing intracellular calcium or indirect by stimulating the release of CGRP and SP neurotransmitters, the latter of which acts on NK1 receptors and stimulates ARNA.

It has been suggested that TRPV1-mediated modulation of the reno-renal reflex either due to capsaicin or resiniferatoxin binding to TRPV1 can be abolished when an NK1 receptor antagonist was injected into the renal pelvis (385). However, CGRP receptor blockade did not eliminate capsaicin-mediated activation of renal afferent sensory nerves. On the other hand, TRPV1 blockade in the renal pelvis by capsiazepine (CPZ) abolished CGRP-mediated stimulation of ARNA (385). There is evidence that capsaicin activation of renal afferent nerves occurs through PLC, which is the main second messenger for CGRP receptors. Therefore, it is suggested that PLC inhibition is responsible for the elimination of CGRP receptor-dependent effect on ARNA following TRPV1 blockade (385). However, it is also plausible that CGRP might mediate part of the TRPV1 effect on renal afferent sensory nerves, as CGRP has been shown to decrease SP metabolism (116).

An increase in the efferent RSNA causes the release of NE and the activation of the RAAS, which causes a decrease in sodium and water excretion. The release of NE is often accompanied with increased release of endothelin-1 (ET-1) that induces vasoconstriction, leading to decreased blood flow to the kidney and decreased GFR (188). Endothelin type A (ET-A) receptors are found in the smooth muscle cells of the renal pelvis and ET-B receptors are located near to unmyelinated schwann cells of renal sensory nerve fibers in the renal pelvic wall (188). ET-1 binds to endothelin type B (ET-B) receptors located in the renal pelvic wall which increases ARNA and

facilitates the inhibitory reno-renal reflex to induce sodium and water excretion (188). On the other hand, it has been shown that rats fed with low sodium diet had increased expression of ET-A receptors in the renal pelvic wall (183). The binding of ET-1 with ET-A receptors inhibits PGE₂-mediated activation of ARNA and suppresses the inhibitory reno-renal reflex, causing sodium and water retention (183). TRPV1 receptors was found to mediate ET-B receptor-induced activation of afferent renal nerves and diuresis and natriuresis that follow the infusion of ET-1 into the renal pelvis. ET-B blockade did not affect capsaicin-induced activation of ARNA (386). Furthermore, ET-A receptor-mediated suppression of ARNA in wild-type mice disappeared in TRPV1^{-/-} mice, indicating a cross talk between ET-A and TRPV1 receptors (386). Interestingly, infusion of a PKC inhibitor into the renal pelvis suppresses ET-B receptors-mediated sensory nerves activation but did not affect capsaicin-mediated activation of these nerves (386). Enhancement and suppression of ARNA were associated with a corresponding increase and decrease of the release of SP and CGRP, respectively. Together, there is considerable evidence that TRPV1 channels have a central role in mediating renal afferent nerves activity directly or as part of other receptor signalling pathways, making TRPV1 a possible candidate in the modulation of the reno-renal reflex (Figure 1.5).

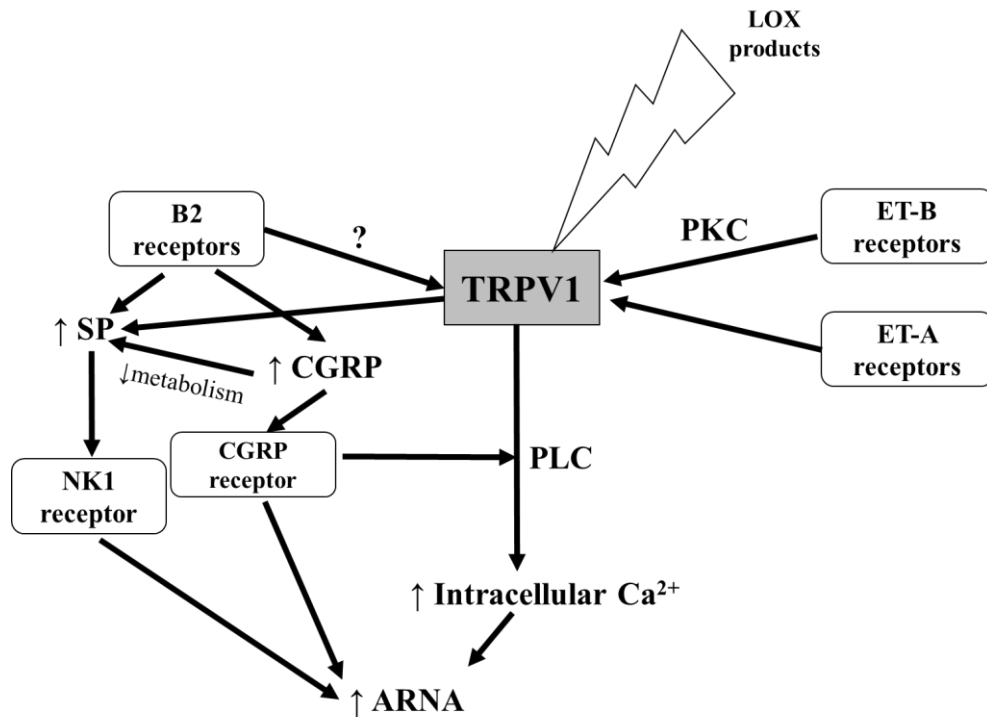


Figure 1. 5. Interaction of TRPV1 with other receptors in the renal pelvic wall. TRPV1 plays a central role in mediating afferent renal nerve activity (ARNA). Putative cross talk between bradykinin type 2 (B2) receptors and TRPV1 is evident in peripheral sensory neurons (276), but is yet to be confirmed in the renal sensory mechanism. LOX, lipooxygenase; PKC, phosphokinase C; ET-A, endothelin receptor type A; ET-B, endothelin receptor type B; TRPV1, transient receptor potential cation channel member 1; PLC, phospholipase C; SP, substance P; CGRP, calcitonin gene-related peptide; NK1, neurokinin 1 receptor.

1.5.2. TRPV1: physiological role in the kidney

In renal pelvic wall, TRPV1 channels function as baroreceptors that regulate the release of neuropeptides including SP and CGRP in response to stretch (414). Unilateral TRPV1 activation stimulates an ipsilateral and contralateral inhibitory renorenal reflex, which causes an increase in sodium and water excretion (386, 413). The latter was blocked following ipsilateral TRPV1 blockade and ipsilateral renal denervation (96, 413). Enhanced ARNA induced by an increase in renal pelvic pressure was abolished following NK1 receptor blockade, but not CGRP receptor antagonism (191).

Due to the wide distribution of TRPV1 channels in different parts of the kidney, they play a significant role in modulating renal haemodynamic function. Studies in the

literature point towards a role for TRPV1 channels in endothelium-dependent vasorelaxation and therefore their protective effect on different organs (57, 411). In the kidney, TRPV1 activation causes an increase in GFR, natriuresis and diuresis. Following increased perfusion pressure by phenylephrine injection, TRPV1 activation resulted in an attenuated perfusion pressure and increased GFR, mediated by decreased renal vascular resistance (210). The latter indicates that TRPV1 channels cause larger vasodilation in afferent compared with efferent arterioles. It was also reported that TRPV1 activation increases the absolute but not fractional sodium excretion so receptor activation does not alter proximal tubular sodium reabsorption (412). Importantly, the effect of TRPV1 activation on GFR and water/sodium excretion was completely abolished after the infusion of SP and CGRP receptor blockers Spantide II and CGRP₈₋₃₇, which indicates a major role for SP and CGRP in TRPV1-mediated vasodilation (210).

Further evidence of TRPV1-mediated vasorelaxation was proposed by Zygmunt et al. (418) who showed that vanilloid receptors located within the perivascular sensory neurons mediate vasodilation induced by anandamide *ex vivo* in small mesenteric arteries and hepatic arteries isolated from the rat. The application of CPZ abolished anandamide and capsaicin-mediated vasodilation, which was associated with suppression of CGRP release. Furthermore, CGRP receptor antagonism blunted the vasodilator effect of anandamide. Conversely, pre-treatment with a high dose of capsaicin, sufficient to desensitise vanilloid receptors, did not alter vasodilation produced by exogenous CGRP administration (418). Similar findings were reported by Ralevic et al. (290) who studied the vasodilator effect of methanandamide on rat mesenteric arterial bed and small mesenteric arteries. In the latter, pre-treatment with high dose capsaicin or CPZ or CGRP antagonism blocked the methanandamide-dependent vasodilation effect.

1.5.3. The putative role of renal TRPV1 channels in hypertension

Several studies have investigated the role of renal TRPV1 receptors in sympathetic modulation and hypertension, with reports showing variable effects of TRPV1 receptor activation and suppression on the SNS, and therefore blood pressure regulation. Kopp et al. (192), Zhu et al. (413), Feng et al. (96) and Ditting et al. (82)

reported renal sympatho-inhibition without significant changes in blood pressure in response to intra-renal pelvic or intra-renal arterial infusion of an agonist dose of capsaicin. This was associated with contralateral increase in sodium and water excretion. The effect of intra-renal pelvic infusion of capsaicin on RSNA and kidney function was abolished by an infusion of CPZ (82). In contrast, Ye et al. (397) showed clear evidence of a role for renal TRPV1 receptors in mediating an excitatory reno-renal reflex and high blood pressure. Intra-renal infusion of an agonist dose of capsaicin caused an increase in blood pressure and contralateral RSNA, and increased c-fos labelling in the PVN. This excitatory effect was abolished by intra-renal infusion of CPZ and by the denervation of the same kidney, pre-infused with capsaicin (287, 397). Interestingly, intra-renal infusion of an agonist dose of capsaicin caused an increase in superoxide production in the PVN (287). Tempol, N-acetyl cysteine and apocynin (an NOX inhibitor) applied to the PVN before intra-renal infusion of capsaicin caused a decrease in basal RSNA and blood pressure, and prevented the intra-renal capsaicin-mediated sympatho-excitatory response. On the other hand, the administration of an Ang II receptor blocker or the inhibition of the release of Ang II in the PVN abolished the excitatory effect of intra-renal capsaicin and reduced superoxide production in the PVN (287). This suggests that renal TRPV1 activation is associated with sympatho-excitation and can contribute to blood pressure elevation through the Ang II-AT-1 receptor-NADPH oxidase-ROS production pathway in the PVN. This is similar to the sympatho-excitatory effect of capsaicin mediated via the adipose afferent reflex (70). In this regard, capsaicin injected into white adipose tissue caused an increase in c-fos in the posterior region of the PVN and SON (70).

In the cisplatin-induced renal failure model, intra-renal infusion of CPZ restored the blunted high-pressure baroreflex control of RSNA to normal. Moreover, the blunted renal sympatho-inhibitory response to volume expansion during low-pressure baroreflex stimulation was normalized following blockade of renal TRPV1 channels by CPZ (1). This points to a contributing role of TRPV1 in the sympathetic hyperactivity in hypertension disease models that involve kidney inflammation and injury. These findings are in agreement with a previous study on two-kidney, one-clip renovascular hypertension model (261). In the latter, activation of renal afferent nerves caused an increase in blood pressure, with concomitant increased lumbar, splanchnic and renal SNA. Application of a high dose of capsaicin on the renal artery was

associated with complete elimination of TRPV1 as revealed by immunofluorescence and a significant reduction in blood pressure after clipping of the kidney (261). On the contrary, another study using the same experimental model in mice showed that a low amount of capsaicin in the diet for 6 weeks significantly decreases blood pressure (313). Administration of L-NAME, NO synthase inhibitor, abolished the blood pressure lowering effect of systematic administration of capsaicin. Moreover, dietary capsaicin has been associated with upregulation of phosphorylated endothelial NO synthase (eNOS). This indicates that the blood pressure lowering effect of capsaicin in renovascular hypertension was partly mediated by a NO-vasorelaxation effect through TRPV1 channels. Thus, one can propose that the activation of kidney TRPV1 receptors activates SNS distinctively from other sites activated by systematic administration of capsaicin, which cause a lowering of blood pressure, as shown in the two-kidney, one-clip model. Meanwhile, dietary capsaicin in sham rats was associated with a similar increase in eNOS phosphorylation, but with no alteration in blood pressure levels (313). Therefore, in sham rats fed with capsaicin, blood pressure was not altered because capsaicin activates SNS through TRPV1 receptors which compensates for the blood pressure decrease that occurs in response to vasodilation. On the other hand, in the two-kidney, one-clipped mouse model, the basal SNA is greater than shams, and diet mixed with capsaicin did not cause further activation of sympathetic nerves, which resulted in a decrease in blood pressure mediated by NO synthase-mediated vasodilation. Therefore, it is suggested that capsaicin mediates dual effects: a blood pressure lowering effect through TRPV1/NO synthase pathway producing an effect on the vasculature (313); and a sympatho-excitatory effect through TRPV1 receptors in other sites, such as carotid bodies, kidneys and adipose tissue (70, 307, 397).

Protective effects of TRPV1 activation on the cardiovascular system have been also reported and characterised by lowering of blood pressure, an improvement in cardiac and renal function following ischaemic injury (57, 360, 401, 411). In the DOCA-salt hypertension model, glomerulosclerosis, glomerular hypertrophy, tubular proliferation and tubulointerstitial fibrosis were more severe in TRPV1^{-/-} mice compared with wild-type mice (368). Furthermore, renal macrophage infiltration and 8-isoprostane levels in urine (a marker of oxidative stress) were significantly less in DOCA-salt-treated wild-type mice compared with DOCA-salt-treated TRPV1^{-/-} mice,

which suggest anti-inflammatory and anti-oxidative properties of TRPV1 (368). Of interest, TRPV1 were highly expressed in DOCA-salt-treated mice, which suggests that TRPV1 upregulation in this model is adaptive and may limit renal injury (368). This is supported by a previous report that showed TRPV1 upregulation in renal cortex, medulla and mesenteric arteries following high sodium intake in Dahl salt-resistant rats (369). In contrast, TRPV1 expression was greatly reduced following high-sodium diet in Dahl salt-sensitive rats (369). Down regulation of CGRP was also revealed in dorsal root ganglion of Dahl salt-sensitive rats, but not in Dahl salt-resistant rats, both groups fed with high-sodium diet (369). Therefore, it is suggested that attenuated blood pressure elevation observed in Dahl salt-resistant rats is partly attributed to the protective effect elicited by the increased expression of TRPV1. In addition, however, the salt-induced blood pressure elevation in Dahl salt-sensitive rats is partly due to an impairment in the sensory autonomic mechanism, which involves TRPV1 in the kidney. This notion is further supported by studies involving intravenous capsaicin administration which caused a greater lowering of blood pressure in Dahl salt-resistant rats compared with Dahl salt-sensitive rats both fed with high sodium-diet (369). Similarly, intra-pelvic infusion of capsaicin was associated with lesser activation of afferent renal nerves accompanied with lower release of SP and CGRP in Dahl salt-sensitive rats following high-sodium diet, which was followed by impaired contralateral diuresis and natriuresis (387). Therefore, in salt-sensitive models, protective regulatory mechanisms against renal injury are lost due to TRPV1 downregulation, which contributes to blood pressure elevation in a mechanism that involves suppression of the sympatho-inhibitory reno-renal reflex. These results are consistent with previous findings obtained after high-salt diet in rats with renal ischaemia-reperfusion injury. In this regard, subcutaneous administration of a low dose of capsaicin prior to ischaemia was associated with a significant decrease in blood pressure, oxidative stress markers and inflammatory cytokines, accompanied with an upregulation in renal TRPV1 (401, 402). This was also associated with an increase in ARNA and CGRP release while RSNA was decreased, along with an improvement in kidney function. Additionally, high dose of subcutaneous capsaicin prior to ischaemia, was associated with down-regulation of TRPV1 in the kidney and a decrease in ARNA, in addition to deterioration in renal and cardiovascular parameters following high-sodium diet (402). Systemic administration of capsaicin 30 minutes prior to ischaemia-reperfusion injury attenuated serum creatinine levels, tubular injury and

decreased inflammatory macrophages. However, CPZ treatment did not alter kidney injury or function in the ischaemia-reperfusion model (57). Altogether, TRPV1 channels modulate SNS activity and blood pressure regulation. There is a dual role however, and the modulation can be excitatory or inhibitory and thus, detrimental or protective to kidney function, such that the influence of TRPV1 channels remains controversial.

1.5.4. TRPV1 receptors and hypoxia

Recent evidence has shown that TRPV1 contributes to afferent-mediated sympatho-excitation in carotid bodies and NTS following intermittent hypoxia (175, 307). Exposure to CIH increases spontaneous postsynaptic excitatory currents in the NTS and decreases tractus solitarii evoked postsynaptic excitatory firing, which alter the synaptic activity between afferent neurons and second level neurons of the NTS. Interestingly, synaptic transmission changes elicited by exposure to CIH in wild-type mice were absent in TRPV1^{-/-} mice. Furthermore, the application of CPZ to NTS slices harvested from CIH-exposed mice reduced the enhanced spontaneous and asynchronous postsynaptic excitatory activity (175). The mechanism by which TRPV1 mediates CIH-induced enhanced NTS synaptic transmission is still unknown. It was suggested that exposure to CIH activates calcium/calmodulin-protein kinase II which phosphorylates TRPV1 channels. In addition, it is proposed that inflammation, observed during and after exposure to CIH, activates LOX that produces endovanilloid by-products, which are endogenous agonists for TRPV1 channels (175). The latter explanation has been supported by *in vitro* studies conducted on HEK293T cells in which exposure to 3% O₂ increased the amplitude of TRPV1 currents with no reported changes in TRPV1 protein expression, indicating the possibility that hypoxia increases the production of TRPV1 activators (172). It is also suggested that hypoxia might induce TRPV1 membranous translocation, a phenomenon that was reported in rat pulmonary artery smooth muscle cells exposed *ex vivo* to 1% O₂ for 48 hours (266). In addition, hypoxia-mediated activation of TRPV1 was inhibited by CPZ and tiron, a ROS scavenger that is membrane permeable (172). This suggests that ROS increases the activity of TRPV1 channels through an intracellular pathway. In HEK293T cells, desensitization of TRPV1 channels was reduced under hypoxic and high glucose

conditions (304). In this regard, hypoxia alone caused a greater reduction in TRPV1 desensitization compared with high glucose conditions (304).

On the other hand, TRPV1 activation and subsequent release of intracellular calcium cause ROS production which leads to mitochondrial depolarization and DNA damage (343). It was also found that challenging H9C2 rat cardiac myoblasts with hypoxia and reoxygenation increased apoptosis. Capsaicin treatment further decreased cell viability, which was later attenuated when TRPV1 was blocked by CPZ. Of interest, after ischaemia-reperfusion injury (40 minutes of no flow in Langendorff heart preparation followed by 30 reperfusion) and during concomitant inhibition of CGRP, TRPV1^{-/-} mice had improved cardiac function compared with wild-type mice (343). This suggests that TRPV1 activation produces detrimental consequences through calcium release, whereas it can elicit cardio-protective effects through the release of SP and CGRP as reported in other studies of ischaemia-reperfusion injury (360).

Exposure to acute intermittent hypoxia supplemented with bouts of hypercapnia causes sensory long-term facilitation (sLTF) of the carotid bodies i.e. increased basal firing of carotid bodies in addition to their exacerbated responsiveness to acute challenges such as hypoxia. This is mediated by P2X2/3 and TRPV1 receptors located at the postsynaptic afferent nerve fibres through a mechanism that is dependent on PKC phosphorylation (307). It has been shown that TRPV1 blockade causes 50% attenuation in carotid body sLTF (307). Similarly, TRPV1 located in renal sensory nerve endings might mediate enhanced firing of afferent renal nerves in the CIH model of hypertension (15). In support of this possibility, immunofluorescence confirmed co-localisation of TRPV1 channels with NOX4 in renal pelvic wall (216). Molecular analysis showed that NOX4 stimulates the release of hydrogen peroxide (H₂O₂) which activates TRPV1 to increase calcium entry and/or to enhance the release of SP and CGRP, with resultant activation of renal afferent nerves. In further support of this potential mechanism, H₂O₂ perfusion to the renal pelvis was associated with increased ARNA, an effect that was inhibited by CPZ and catalase infusion (216). On the basis of the above evidence, hypoxia can induce changes in TRPV1 activity which can alter SNA, blood pressure and induce pathophysiological changes at the tissue level.

1.6. Renal kallikrein-kinin system

1.6.1. Bradykinin formation and localisation

Kallikrein-kinin systems are either composed of high molecular weight kininogens and found only in liver tissue or low molecular weight kininogens, found in a variety of cells (309). Kinins are biologically active peptides that result from the hydrolysis of kininogens by a kallikrein enzyme from serine proteases family. In the kidney, kinins are formed within groups of cells at the terminal part of the distal nephron: collecting duct cells and connecting tubule cells (117, 309). At this site, kininogen is stored in the collecting duct cells and when the kallikrein enzyme is released from the connecting tubule cells, it converts kininogen to the kinins: bradykinin, lys-bradykinin and met-lys-bradykinin at the luminal and basolateral sides of the collecting duct. Bradykinin is formed either directly from kininogen by kallikrein or from lys-bradykinin by aminopeptidase. Inactive kininogen represents 10% of human urinary protein (1.6-6.2 mg/L, respectively) and presents at a higher amount in renal medulla (2.4 mg/g protein) (113, 117). Kinins are degraded to inactive metabolites mainly by neutral endopeptidases (NEP) or angiotensin converting enzyme (kininase II). They are also converted by kininase I (carboxypeptidases) to Arg⁹-bradykinin and des-Arg¹⁰-lys-bradykinin, which are both bradykinin receptor type 1 (BK1R) agonists (276, 309). The kallikrein-kinin system is also found in the cerebral cortex, hypothalamus, thalamus and choroid plexus (335).

1.6.2. Renal bradykinin receptors: location and transduction pathways

There are two types of bradykinin receptors: bradykinin receptors type 2 (BK2R) that are constitutively expressed and mediate the majority of physiological functions of bradykinin and BK1R that are absent in healthy conditions and are activated by kininase II hydrolysis products of bradykinin. Nevertheless, BK1R mRNA expression is rapidly stimulated in response to inflammation (367). Inflammatory cytokines including IL-6, TNF- α , IL-1 β and growth factors trigger BK1R expression and augments its effects (117, 335). In addition, the BK1R gene activates the transcription sequences of NF- κ B and activation protein-1 factor (335). BK1R mRNA expression is also stimulated by lipopolysaccharides (LPS) especially in the efferent arterioles, thin ascending and descending loop of Henle and distal tubules (117). In addition,

observations from functional studies indicate the localisation of BK1R in the afferent arterioles and mesangial cells (309). In response to inflammation, BK1R are also expressed in neurons, microglia and astrocytes of the spinal cord and the brain, which illustrate their role in neuroinflammation. Of interest, there is weak homology (~36%) between BK1R and BK2R, and high variability regarding BK1R between humans and rodents (335).

Different methods were used to determine the location of BK2R in the kidney, such as the binding of micro-labelled bradykinin to nephron dissected segments, immunohistochemistry and RT-PCR (117). It was reported that BK2R are located in proximal tubules, thick ascending loop of Henle and connecting tubule cells. They are also located in the cortical and outer medullary collecting ducts and in the afferent arterioles. In relation to that, BK2R were identified using RT-PCR in the distal tubules. Moreover, BK2R were detected in the interstitial space of the renal medulla. BK1R and BK2R have been also localised in renal afferent sensory nerve endings and the lamina propria of the renal pelvic wall (151).

Bradykinin is a well-known physiological pro-inflammatory mediator involved in pain sensation and inflammatory responses. Therefore, bradykinin receptors are also found in nociceptive small unmyelinated and thinly myelinated sensory fibres and nerve cell bodies of dorsal root ganglia, trigeminal ganglia and nerve terminations in the superficial parts of the spinal cord. They are also located in cardiac afferent fibres and stellate ganglia (339).

Studies showed that both BK2R and BK1R are G-protein coupled receptors with seven transmembraneous helices. In the kidney, the BK2R transduction pathway is coupled to G α q and G α i subunits, which stimulate PLC, PLA2, PLD and PKC intracellular pathways (113, 117, 309). PLC activates second messengers such as diacylglycerol and IP3 which stimulate the release of intracellular calcium. Moreover, PKC phosphorylation activates sodium entry in distal nephron in addition to phosphatidyl inositol-mediated intracellular calcium stores mobilisation (105, 117). Cytosolic calcium in turn activates the release of prostaglandins, c-AMP/PKA-mediated inhibition of potassium efflux, in addition to an increase in SP and CGRP release (105). In a similar pathway in nociceptive nerve terminals, BK2R activation inhibits potassium efflux and causes nerve ending depolarization (105). BK2R, through PLA2

activation, increases the formation of arachidonic acid, which is a precursor for prostaglandin synthesis (105). Meanwhile, in renal sensory afferent nerve endings, the identified BK2R signalling pathway involves PKC-mediated activation of prostaglandins formation, which in turn activates the cAMP/PKA pathway and enhances the release of SP and CGRP (15, 187), as shown in Figure 1.4. Overall, bradykinin binding to BK2R directly activates ion channels causing depolarization and/or induces the release of neuropeptides that act on other receptors such as NK1 receptor causing the activation of sensory nerve endings.

For BK1R, there is a lack of information about its transduction pathway as it is not highly expressed under normal conditions. However, BK1R are G α_q and G α_i coupled receptors which activate PLC and stimulates IP3 and diacylglycerol to increase intracellular calcium (335). In addition, it is suggested that the BK1R transduction pathway involves P38 mitogen-activated protein kinase (MAPK) activation and extracellular signal-regulated kinase (ERK) phosphorylation (276, 335). Previous studies have shown that BK2R are desensitized following acute stimulation by bradykinin, which is due to receptor internalisation and ligand-receptor dissociation i.e. decreased binding affinity. However, there is no evidence of BK1R desensitisation after activation, rather than reports showing their upregulation in the presence of an agonist through the activation of NF- κ B (105, 335).

1.6.3. Physiological role of bradykinin in the kidney

Endogenous bradykinin activates the renal mechanosensory afferent nerves through BK2R-mediated SP release. This is associated with a decrease in ipsilateral and contralateral RSNA i.e. an inhibitory reno-renal reflex (137, 180). In addition, bradykinin, through BK2R, enhances diuresis and natriuresis independent of the reno-renal reflex by a glomerular-mediated action and a direct effect on the tubule (309). Furthermore, bradykinin stimulates the release of PGE2 from the collecting ducts, which results in inhibition of sodium reabsorption (117). It was also reported that bradykinin, through BK2R, inhibits sodium chloride reabsorption in the thick ascending limb of loop of Henle by cytochrome P450 and cyclooxygenase-2 (COX2)-dependent mechanism (309). Indeed, BK2R are co-localised with COX2 as demonstrated by immunohistochemistry (305). Interestingly, infusion of bradykinin

into the renal medulla was associated with enhanced diuresis and natriuresis, an effect that was abolished after NO synthesis blockade (244). This effect of bradykinin is partially mediated by a reduction in ADH-enhanced water permeability and sodium reabsorption in the collecting ducts. In support of this notion, it was shown, using Fab fragments of antibodies, that a decrease in kallikrein activity by 80% and kinin release by 77% were associated with a 30% decrease in diuresis and 20-40% decrease in natriuresis, without alteration in blood pressure. This was confirmed by enhanced water and chloride reabsorption in the collecting ducts after the administration of HOE140, a selective BK2R antagonist (117). Of note, an increase in sodium intake was associated with an increase in urinary bradykinin levels, leading to inhibition of endothelial sodium channels (ENaC) in the distal tubules (231). In a transgenic rat model of excess bradykinin in the proximal tubules, RAAS alteration was observed, in addition to a decrease in mRNA expression of ADH A1 receptors and a decrease in ENaC expression in the distal nephron (27). RAAS changes involved increased Ang II levels and decreased plasma concentration of renin.

Bradykinin, through BK2R, results in vasodilation in the afferent and efferent arterioles and vasa recta. However, there is also contraction of the glomerular mesangium leading to a decrease in filtration surface area and glomerular filtration coefficient. Therefore, bradykinin enhances diuresis but without changing GFR (309). In rabbits and rats, bradykinin's vasodilator effect on afferent arterioles was found to be mediated by prostaglandins. In addition, bradykinin causes a dose-dependent vasodilation in the efferent arterioles mediated by cytochrome P450 in rabbits (299). Bradykinin at high concentration however can cause vasoconstriction that was found to be related to thromboxane. As previously mentioned, BK1R are not detected in tissues under healthy conditions, which indicates their minor physiological role. Nonetheless, results from isolated perfused rat kidneys showed increased renal vascular resistance in response to a BK1R agonist infusion. In rabbits, "BK1R-mediated" vasoconstriction was abolished by HOE140, a BK2R antagonist. Conversely, activation of BK1R and BK2R in anaesthetised dogs resulted in an increase in renal blood flow (309). These conflicting results could be due to different roles of BK1R and BK2R in different species.

Bradykinin triggers variable effects on the reno-renal reflex depending on the route of administration. Intra-renal bradykinin elevates RSNA, decreases natriuresis and

diuresis in the contralateral kidney with an immediate increase in heart rate, blood pressure and vascular resistance. This effect was abolished by renal denervation or by ganglionic blockade (3, 29, 329). However, intravenous injection of the same dose of bradykinin did not induce any significant changes in blood pressure or heart rate (101), but it produced mesenteric vasodilation (329). Moreover, intra-pelvic infusion of bradykinin was associated with the activation of afferent renal sensory nerves that stimulate an inhibitory reno-renal reflex and a contralateral natriuresis (190). Contrariwise, bradykinin infusion into the renal artery was associated with enhanced firing of ADH cells in SON, increased plasma ADH levels, and increased blood pressure and vascular resistance (101, 391). The sympatho-excitatory effect was abolished after the denervation of the kidney that was infused by bradykinin, strongly suggesting an excitatory reflex resulted from bradykinin activation of sensory afferent renal nerves (151, 391).

1.6.4. The kallikrein-kinin system changes in hypertension

BK1R and BK2R activation contributes to many physiological and pathophysiological elements of cardiovascular dysfunction. Both receptors mediate inflammatory responses as BK2R are involved in the acute phase of inflammation and BK1R are involved in the chronic inflammatory phase (335). Decreased levels of kallikrein was observed in hypertensive individuals (309). In addition, kininogen deficient rats, BK2R^{-/-} deficient mice and control mice subjected to BK2R blockade, each exhibited salt-sensitive hypertension (244). Intra-renal infusion of a BK2R blocker increased blood pressure in rats with normal sodium intake (353). Moreover, transgenic mice with overexpression of BK2R were hypotensive and BK2R blockade restored their blood pressure back to normal (244). Therefore, considerable evidence related to the protective role of kallikrein-kinin system, in particular through BK2R signalling, has been proposed.

One of the protective mechanisms of BK2R is linked to the pressure natriuretic response to elevation in arterial blood pressure. When blood pressure increases, it induces preglomerular vasoconstriction as part of the autoregulatory mechanism. This induces shear stress and the release of endothelial humoral factors such as kinins and NO. Subsequently, bradykinin increases medullary and papillary blood flow (both lack

autoregulation), which causes pressure natriuresis. Bradykinin-mediated increase in papillary blood flow is dependent on NO production, rather than PGE₂. This was further confirmed by the effects of HOE140, a BK₂R antagonist, on lowering basal and pressure-induced increase in nitrate/nitrite urinary excretion (353).

Bradykinin through BK₂R decreases the expression of extracellular matrix (ECM) protein by increasing the activity of plasminogen and metalloproteinase 2 (310), which explains bradykinin-mediated decrease in cardiac and tubulointerstitial fibrosis. The latter has been observed in BK₂R^{-/-} deficient mice that exhibited exaggerated interstitial fibrosis after unilateral ureteral obstruction. Transgenic mice with overexpressed kallikrein gene had attenuated interstitial fibrosis in this model, which was blocked after BK₂R inhibition (310). In general, ureteral obstruction is associated with increased mRNA expression of many fibrotic proteins and the differences between B₂^{-/-} receptor deficient and B₂ overexpressed mice were related to changes in collagen III and IV expression (310).

Importantly, suppression of the inhibitory reno-renal reflex mediated by impaired ARNA was observed in SHR. Kopp et al. (190) illustrated that suppressed ARNA is related to attenuated bradykinin. Intra-renal pelvic bradykinin that activates renal sensory nerve endings in control rats, failed to increase ARNA in SHR. Similarly, intra-renal pelvic infusion of 4β-phorbol 12,13-dibutyrate, a PKC activator, did not increase ARNA in SHR (190). Therefore, impaired inhibitory reno-renal reflexes in the SHR can be due to attenuated PKC activity that is necessary for mediating bradykinin effects.

Increased expression of BK₁R was observed in different disease models involving kidney injury. BK₁R antagonism elicited a protective role in obstructive nephropathy, LPS-induced renal inflammation and glomerulonephritis (286). It has also been shown that BK₁R disrupt blood brain barrier integrity and sustain arterial hypertension in SHR and Ang II-induced hypertension models (335). Intracerebroventricular (ICV) injection of Sar[D-Phe⁸]-desArg⁹-BK, a BK₁R agonist, increases arterial blood pressure in normotensive and SHR, whereas a decrease in blood pressure and heart rate was observed after its blockade in SHR (90). Furthermore, BK₁R antagonism in SHR was associated with a decrease in left ventricular hypertrophy and improvement in the ejection fraction. This was also associated with maintained mitochondrial

structure that is known to be disrupted in the SHR model (77). Enhanced activity of ERK1/2 and c-Jun N-terminal kinases (JNK) in SHR cardiovascular tissues was attenuated after BK1R antagonism (77). Conversely, in the two-kidney, one-clip model in BK2R^{-/-} mice, BK1R induced opposing effects in response to antagonism such as an increase in blood pressure, in addition to a decrease in blood pressure after their stimulation. It was suggested that BK1R overexpression in the clipped kidney of BK2R^{-/-} mice exhibits BK2R-like haemodynamic changes (88).

In Ang II-induced hypertension, BK1R inhibition abolishes inflammatory cytokines and the expression of oxidative stress biomarkers. Furthermore, it was found that AT1 and BK1R form heterodimers in hypertensive individuals. This suggests a cross talk between BK1R and RAAS. Therefore, as AT1 receptor activation by Ang II mediates neuroinflammation in hypertension, it is suggested that BK1R are also involved in the pathogenesis of neuroinflammatory features of hypertension (335). Indeed, BK1R are upregulated in the hypothalamus of SHR and DOCA-induced hypertension models, as well as in the spinal cord and brain of Ang II-induced hypertensive rats, and in the PVN of hypertensive mice expressing pro-inflammatory cytokines. Moreover, BK1R inhibition attenuates blood pressure and neuroinflammation observed in salt-sensitive hypertension (335). It has also been shown that BK1R activation enhances inducible NO synthase and induces superoxide production by NADPH oxidase (335). NO interaction with superoxide produces peroxynitrite anions that cause nitrosative stress, inflammation and DNA damage (335). Of interest, these pathological features were detected in kidneys harvested from CIH-exposed rats (224). BK1R receptor activation induces neutrophil degranulation, leukocyte migration and the release of matrix metalloproteinase 9 through ERK1/2 and P38-MAPK pathway (335). MAPK enhanced phosphorylation of ERK1/2 and P38 apoptotic pathways were also detected in renal tissues after exposing mice to 3 days of CIH (342, 380). BK1R inhibition was associated with a decrease in proteinuria, renal inflammation (CCL2 and CCL7 chemokines), CD4⁺ T cells, renal macrophages and attenuation of blood pressure in lupus nephritis and obstructive nephropathy. In addition, BK1R antagonism was also associated with a decrease in renal fibrosis in obstructive nephropathy and a reduction in renal inflammation in LPS, cisplatin models and ischaemia-reperfusion injury (286). Of importance, BK1R antagonism decreased blood pressure in glucose-fed rats, which was accompanied by decreased superoxide levels in the renal medulla (78).

Therefore, there is conclusive evidence that BK1R expression and/or activation are involved in the pathogenesis of hypertension.

1.6.5. The role of the kallikrein-kinin system in baroreflex regulation

Intra-renal bradykinin infusion disrupts the autonomic control of blood pressure, resulting in decreased high-pressure baroreflex sensitivity. Moreover, it was associated with 13% decrease in RSNA sympatho-inhibitory response to volume expansion compared with 58% RSNA sympatho-inhibition following intra-renal infusion of saline (167). Furthermore, intra-renal bradykinin was associated with increased contralateral ERNSA and decreased diuresis and natriuresis (28). Renal stenosis in addition to 50% decrease in renal blood flow was associated with R2 chemoreceptor stimulation, which caused a decrease in baroreflex sensitivity and a reflex increase in vascular resistance i.e. renal sympatho-excitatory reflex (230). In addition, systemic administration of aprotinin, an inhibitor of tissue kallikrein, caused 33% decrease in vascular resistance, which suggests partial contribution of kinins in the chemoreceptor-mediated renal pressor reflex (230). In support of these findings, Abdulla et al. (3) investigated the role of renal bradykinin receptors in the modulation of the baroreflex in a cisplatin-induced renal failure model. In renal failure rats, blockade of BK2R, but not BK1R, markedly restored arterial baroreflex regulation of RSNA and heart rate to near control levels. In addition, BK1R blockade enhanced the RSNA sympatho-inhibitory response to volume expansion (3). Unexpectedly, BK1R blockade blunted RSNA sympatho-inhibitory response to volume expansion in control rats. In contrast with the aforementioned results, impaired baroreflex control of heart rate has been reported in transgenic mice lacking BK2R (244). Nevertheless, the renal kallikrein-kinin system potentiates the excitatory reno-renal reflex observed in some hypertension disease models that involve kidney injury, which have been shown to impair baroreflex homeostasis. However, there is insufficient evidence regarding the subtype of bradykinin receptors involved in the excitatory vs. inhibitory reno-renal reflexes, and this requires further investigation.

Together, these studies support the presence of an excitatory reno-renal reflex that is activated with contributions from a number of receptors such as TRPV1 and bradykinin. As in CIH-induced hypertension, inflammatory mediators such as TNF- α

and IL-6 were found to be highly expressed in the kidney in several models of renal injury and hypertension which showed BK1R upregulation (131, 224, 333, 335, 382). This points to a possible role of these mediators in initiating a sympatho-excitatory response leading to impaired blood pressure homeostasis.

1.6.6. Kallikrein-kinin system during hypoxic injury

Individuals exposed to acute hypoxia (10% O₂ and 12% O₂) showed an increase in renal blood flow, with no changes in GFR or plasma and urine bradykinin concentration (17). In relation to that, the action of kinins on BK1 and BK2 receptors exhibited both protective and deleterious effects during ischaemia-reperfusion injury. Wang et al. (367) reported pathological changes in the kidney in response to 45 minutes of renal ischaemia followed by reperfusion. BK2R^{-/-} mice in this study had higher serum creatinine concentration 24 hours following ischaemia-reperfusion compared with wild-type mice. However, serum creatinine was lower in mice lacking BK1R at 4, 24, 48 and 120 hours following injury. Furthermore, BK1R antagonism pre-treatment in wild-type mice elicited a similar decrease in serum creatinine as in BK1R^{-/-} deficient mice. In support of the functional improvement associated with BK1 receptor antagonism, BK1R^{-/-} mice exhibited an increase in mRNA expression of anti-apoptotic Bcl-2 and an attenuation of gene expression of Bad and caspase-3, which are apoptotic factors. Moreover, following ischaemia-reperfusion, in BK1R^{-/-} mice and wild-type with BK1R antagonism, increased mRNA expression of anti-inflammatory mediators (IL-4, IL-10 and GATA-3) and decreased pro-inflammatory mediators including IL-1 β and T-bet transcription factor were observed (367). BK1R inhibition was also associated with increased heme oxygenase-1 (HO-1) and decreased expression of monocyte chemoattractant protein-1 (MCP-1) (367). This highlights the deleterious consequences of BK1R activation in hypoxic injury. In another study of renal ischaemia-reperfusion injury, BK2R^{-/-} mice showed decreased serum creatinine compared with wild-type mice. This was associated with a decrease in TNF- α , ROS, apoptosis and MCP-1 expression (367). However, the elimination of BK1R and BK2R together elicited greater pathological deterioration. Kakoki et al. (153) reported exaggerated renal ischaemia-reperfusion injury in BK1R^{-/-} /BK2R^{-/-} mice compared with BK2R^{-/-} mice. This was associated with low NO production as reflected by lower

plasma nitrite/nitrate ratio in BK1R^{-/-}/BK2R^{-/-} mice compared with BK2R^{-/-} mice and wild-type mice (153). Moreover, tubular damage, growth factors (TGF- β 1, CTGF and endothelin-1) and 8-hydroxy-2'-deoxyguanosine were higher after ischaemia-reperfusion injury in the BK1R^{-/-}/BK2R^{-/-} mice compared with either BK2R^{-/-} or wild-type mice (153).

The findings from the above studies explain the superior effect of angiotensin-converting enzyme inhibitors (ACEI) as anti-hypertensive agents compared with Ang II receptor blockers, because ACEI inhibit Ang II and decrease the degradation of bradykinin, which induces vasodilation through endothelial NO release (153). Bradykinin through BK2R induces relaxation of rat, dog and mouse carotid arteries and causes vasodilation in the middle cerebral arteries and coronary arteries (352). The protective role of BK2R was also revealed after myocardial ischaemic injury, as BK2R were upregulated at the zone between scar tissue and healthy myocytes (352). In addition, hypoxia (5% O₂) exposure of rat cardiac microvascular endothelial cells and cultured human coronary artery endothelial cells was associated with increased mRNA expression of BK2R, which suggests a role for BK2R in mediating hypoxia-induced angiogenesis (352). Similarly, neuronal ischaemia-reperfusion injury was also associated with enhanced activation of inflammasomes, which causes cleavage of caspase-1 that converts IL-1 β and interleukin-18 (IL-18) to their active form. This was accompanied by increased inflammatory cytokines and brain inflammation (347). These pathological consequences were decreased by bradykinin pre-treatment acting on BK2R, which were upregulated in response to ischaemia-reperfusion injury. Accordingly, HOE140, BK2R blocker, attenuated the neuroprotective effect elicited by bradykinin. In addition, bradykinin activation of BK2R was associated with a decrease in the percentage of apoptotic neurons that are triggered by hypoxia-reperfusion injury (347). In primary cortical neuronal cultures, hypoxia-reoxygenation treatment was also associated with increased levels of gasdermin D (GSDMD) substrate of caspases by two-fold. Generation of the active form of GSDMD by activated caspase-1 induces apoptosis, which was suppressed by bradykinin pre-treatment of neuronal cultured cells (347). Hypoxic-reperfusion injury induced by the obstruction of middle cerebral arteries, was associated with an increase in miR-200c expression and a decrease in syntaxin 1A. BK2R antagonism worsened brain function and increased miR-200c expression (348).

Post-conditioning is a protective phase following ischaemia that is defined by repeated cycles of obstruction and reperfusion. This phase involves the activation of many transduction pathways that include kinins-mediated activation of NO, c-GMP and mitochondrial K⁺ ATP channels, which induce ROS release (275). BK2R blockade during the reperfusion phase of isolated rat heart eliminated post-conditioning protection. This was also observed in response to antagonism of NO, PKG, mitochondrial K⁺ ATP channels and ROS scavengers such as N-acetylcysteine and 2-mercapto-propionylglycine. Intermittent injection of diazoxide (activates K⁺ ATP channels) and bradykinin enhanced post conditioning protection (275). Importantly, exposure to chronic hypoxia (10% O₂) for two weeks decreased kallikrein in renal tissue, which was associated with sodium retention. This elevates oxygen demand and worsens kidney hypoxia; thus, exacerbates hypertension. Therefore, it is unknown whether decreased kallikrein contributes to kidney hypoxia initiation or it occurs as a consequence of hypoxia, or both (362). Overall, hypoxia is associated with changes in kallikrein-kinin system that might involve BK2R or BK1R. BK2R can mediate a protective compensatory pathway through vasodilation and increased medullary blood flow whilst renal bradykinin can cause sympatho-excitation through the activation of renal sensor nerve endings. It is also suggested that BK1R activation plays a part in the pathological consequences of hypoxic injury. However, further studies are required to confirm the exact role of BK1R.

Results from a previous study suggest that bradykinin acting through carotid bodies can induce a vasopressor response. Intra-carotid injection of bradykinin causes a biphasic effect; an early depressor phase, which was associated with decreased blood pressure and heart rate and a later pressor phase during which blood pressure and SNA were significantly elevated but with no change in heart rate. Interestingly, denervation of the carotid bodies abolished the pressor effect and exacerbated the early depressor effect (346). A similar biphasic response was also observed after ICV injection of bradykinin. Intra-carotid and/or ICV injection of indomethacin attenuated the pressor response of ICV-injected bradykinin (346). Similarly, intra-carotid infusion of arachidonic acid decreased the depressor effect and augmented the pressor response. This suggests that the bradykinin pressor reflex is dependent on PGE₂ synthesis (346). Notwithstanding that the bradykinin pressor reflex is mediated by the carotid bodies, the possible role of bradykinin receptors in carotid body activation during hypoxia was

not studied. Exposure to CIH induces the expression of inflammatory cytokines and profibrotic factors that are involved in the upregulation of BK1R (15). In addition, in renal tissue after exposure to different protocols of CIH, transduction signalling pathways of bradykinin receptors are activated such as MAPK and P38 pathways, peroxynitrite release and enhanced superoxide (382). However, the influence of exposure to CIH on renal expression and function of bradykinin receptors involved in the reno-renal reflex mechanism is yet to be determined.

1.7. Renal functional changes during hypoxia

Under normal conditions, the kidneys are supplied with 25% of the cardiac output. This makes blood and oxygen supply to the kidney greater than oxygen demand. The cortex receives high blood perfusion (~20% of cardiac output), which brings cortical PO_2 levels to 50-60 mmHg. In contrast, the renal medulla is perfused with as little as 10-15% of the total blood supplied to the kidney such that PO_2 is relatively low at 10-20 mmHg (327). It is known that the renal medulla is highly vulnerable to hypoxic damage due to low blood supply, lack of auto-regulatory mechanisms in deep regions and the arteriovenous shunt of vasa recta (66, 327). Kidney PO_2 remains preserved in response to decreased renal blood flow (RBF) within the physiological range (up to 30%). Preserved kidney oxygen tension is due to afferent arteriolar dilation and a decrease in filtered sodium load corresponding to the decrease in GFR, which maintains relatively constant oxygen supply to demand ratio (8). Meanwhile, another study has shown that cortical PO_2 was preserved when RBF was decreased by $\pm 30\%$ as a result of stenosis and during the infusion of vasoactive agents. This was not conjugated with reduced medullary PO_2 . It was strongly proposed that the preserved PO_2 levels in the cortex is related to decreased preglomerular oxygen shunt from arteries to veins when RBF is decreased (92, 108, 205). Specific preservation of PO_2 in the renal cortex during decreased renal blood flow was not conjugated with changes in the cortical oxygen consumption while medullary PO_2 was reduced. It was strongly proposed that preserved PO_2 levels in the cortex is related to decreased preglomerular oxygen shunt from arteries to veins (205). Beyond these limits, hypoxia develops and the production of superoxide ($O_2^{\cdot -}$) and H_2O_2 is enhanced, which play a major role in regulating renal medullary blood flow and sodium excretion (66). It was also reported that superoxide radicals activate $Na^+/K^+/2Cl^-$ co-transporters and through the PKC- α pathway, they increase sodium reabsorption within the medullary thick ascending limb of the loop of Henle. Oxygen radicals produced from NOX, through NO suppression, enhance Na^+/K^+ ATPase activity in the renal medulla. Subsequently, oxygen demand is increased due to enhanced active reabsorption of sodium. Moreover, oxygen radicals produced from the mitochondria enhance phosphorylation of MAPK and increases the expression of COX-2. The latter activates cAMP/PKA pathway in renal afferent nerve endings as a part of the reno-renal reflex mechanism (Figure 1.4) (66, 180).

It was shown that renal medullary blood flow is decreased after 3 weeks of hypertension in SHR and in Dahl salt-sensitive rats (66). Intra-medullary but not systemic infusion of captopril, an ACEI, enhanced renal medullary blood flow by 40% and attenuated blood pressure by 50% (222). Indeed, renal medullary infusion of tiron ($\text{O}_2^{\cdot -}$ scavenger) increased renal medullary blood flow and enhanced sodium excretion. In addition, intra-medullary infusion of diethyldithiocarbamate (SOD inhibitor) reduced blood flow to the medulla and caused an anti-natriuretic effect (66). Interestingly, the latter was associated with the development of hypertension, which was abolished by intra-medullary infusion of catalase and tempol (SOD mimetic) (66). Moreover, apocynin (NOX inhibitor) infusion to the renal medulla attenuated salt-induced hypertension by 50% in salt-sensitive rats (349). Thus, it was suggested that $\text{O}_2^{\cdot -}$ and H_2O_2 play a synergistic role in reducing renal medullary blood flow and increasing sodium retention, contributing to the development and/or exacerbation of hypertension. Interestingly, a number of studies in the literature reported, using different hypoxia protocols, renal oxidative stress, accumulation of ROS and kidney injury (80, 224, 277, 342, 381).

Furthermore, hypoxia is considered a mutual feature in acute kidney injury (AKI) and chronic kidney disease (CKD) (14). Ischaemic damage of the interstitium i.e. tubulointerstitial fibrosis, which is known as a cause and consequence of hypoxia, is a common feature in end-stage renal disease (262). In addition, epidemiological studies have shown a strong correlation between OSA and CKD (14, 215). An increased risk of hypertension by 46% has been reported in subjects that have sleep-related oxygen saturation of less than 90% (14). On the other hand, increased filtration fraction and glomerular hypertrophy, a precursor for CKD, were detected in OSA patients (11). This is related to increased RSNA and enhanced renal RAAS. In relation to that, it was found that continuous positive airway pressure reverses the increase in glomerular pressure and the decrease in filtration fraction in OSA patients (403). Interestingly, however, altitudes of 159 m and higher showed a negative association with CKD prevalence, which suggests that renal changes might differ between intermittent and chronic hypoxia conditions (106). Other than OSA, several disease models such as renovascular hypertension, polycystic kidney disease and remnant kidney models reported a decline in kidney function concomitant with local renal hypoxia (8, 262, 327). However, the temporal contribution of hypoxia to the

development and progression of kidney malfunction is not fully established as most of these studies undertake assessments at just one time interval of the disease stage. This necessitates further studies to look at the time course of the disease process and add to our understanding of the effects of hypoxia on kidney functions.

1.7.1. Effects of intermittent hypoxia on renal function

Active transport in the medullary thick ascending limb of the loop of Henle is higher than in proximal tubules, with greater Na^+/K^+ ATPase activity. Accordingly, the thick ascending limb consumes 50% more energy per mg of tissue protein compared with proximal tubules (327). Thus, the oxygenation state of the kidney is profoundly controlled by a balance between sodium transport and oxygen supply on the one hand, and between sodium transport and oxygen consumption on the other hand. Disruption of this balance leads to a decline in renal PO_2 , a phenomenon that has been observed in a rat model of CIH (258). O'Neill et al (258) reported no change in diuresis and natriuresis in rats exposed to CIH (6.5% O_2 , 12 cycles/hr, 8 hr/day, 14 days). A decrease in RBF and GFR was reported along with an increase in renal vascular resistance (RVR) (258). This was accompanied by a fall in tissue NO levels, moderate proteinuria and an increase in kidney injury marker-1. Of note, another study using a different protocol of CIH (10% O_2 , 20 cycles/hr, 10 days) has shown increased cortical expression of adenosine type 2 receptors. Activation of these receptors causes efferent arteriolar vasodilation, which can explain decreased GFR in this model (173). Using the latter protocol, a decrease in RBF was detected in addition to a decrease in SOD1 expression and an increase in IL-6 in the renal cortex (355). Importantly, the decline in GFR that was associated with a decrease in sodium load, was not associated with a reduction in oxygen consumption. Therefore, a shift in the linear relationship between transported sodium and oxygen consumption was observed, which indicates that for any amount of sodium reabsorbed, there is a higher oxygen consumption indicating a decrease in the efficiency of renal sodium transport mechanism. The altered balance could be due to lowering in NO bioavailability, as NO competes with oxygen for mitochondrial respiration leading to decreased oxygen consumption (258, 327). However, the type of NOS involved is unknown, but uncoupling of eNOS in response to a different CIH protocol has been reported (22). As a result, decreased cortical PO_2

was observed following exposure to CIH, but interestingly medullary PO₂ was normal (258), suggesting greater susceptibility in cortex compared with medulla in the CIH model. In another study, CIH-exposed rats had increased tissue IFN- γ and increased haematocrit level which indicates increased production of erythropoietin by HIF-1 α (258). Similarly, a more severe protocol of CIH (20 cycles/hr, 5% O₂, 8 hr/day, 6 weeks) was associated with a decline in GFR and an increase in plasma creatinine (303). The latter suggests that intermittent hypoxia damaged medullary tubular epithelial cells and disrupted the integrity of the tight junction with a resultant back leak of creatinine into the bloodstream. Moreover, CKD rats that were exposed to the same CIH protocol had exacerbated hypertension. Medullary expression of HO-1, a gene that is regulated by Nrf2, was greater after exposure to CIH compared with the CKD group breathing normal air (303). It is well-known that HO-1 decreases the expression of vasodilatory enzymes. Therefore, the additive effect of CIH in terms of decreased ET-1 expression, suppressed NO bioavailability and increased expression of HO-1, augments endothelial dysfunction, which leads to further kidney hypoxia and hypertension in CKD animals. Overall, the current evidence shows that exposure to CIH induces renal hypoxia and kidney damage mainly through endothelial dysfunction in addition to the potential for tubular-dependent modulation as tubular transport efficiency is decreased (Figure 1.6). The possible role of renal nerves in mediating the reduction in RBF and GFR following exposure to CIH has not been studied. In addition, it is not determined whether renal alterations observed in CIH-induced hypertension are due to hypoxia per se or secondary to blood pressure elevation. Friederich-Persson et al. (103) showed an a decrease in renal PO₂ and proteinuria in the absence of other confounding variables such as hypertension or diabetes, after systemic administration of 2,4-dinitrophenol, a mitochondrial uncoupler to oxidative phosphorylation that increases oxygen consumption. Moreover, renal hypoxia was revealed 3 days after the initiation of type 1 diabetes mellitus lasting 15 days before the emergence of albuminuria (262). This suggests that renal hypoxia might precede and cause kidney injury.

Patients with AKI who had cardiopulmonary bypass exhibited a fall in GFR and sodium reabsorption with no decrease in oxygen consumption, which also indicates a decrease in transport efficiency that led to renal hypoxia (262). Similarly, in the SHR model of hypertension, a decrease in RBF and a decline in sodium transport efficiency

(decreased transported sodium/oxygen consumption ratio) was observed (373). These changes occur despite the fact that CIH-exposed rats showed higher blood PO₂ and lower PCO₂, which arises due to long-term facilitation of breathing and persistent hyperventilation (258). A previous study has shown that forced breathing of normal air alters renal function and enhances diuresis and natriuresis (68). Therefore, further studies are needed to consider the complex effects of hypoxia on kidney function independent of renal functional fluctuations that are mediated by intrathoracic pressure changes or the suppressing effect that lowered PCO₂ has on central chemoreceptors and SNA.

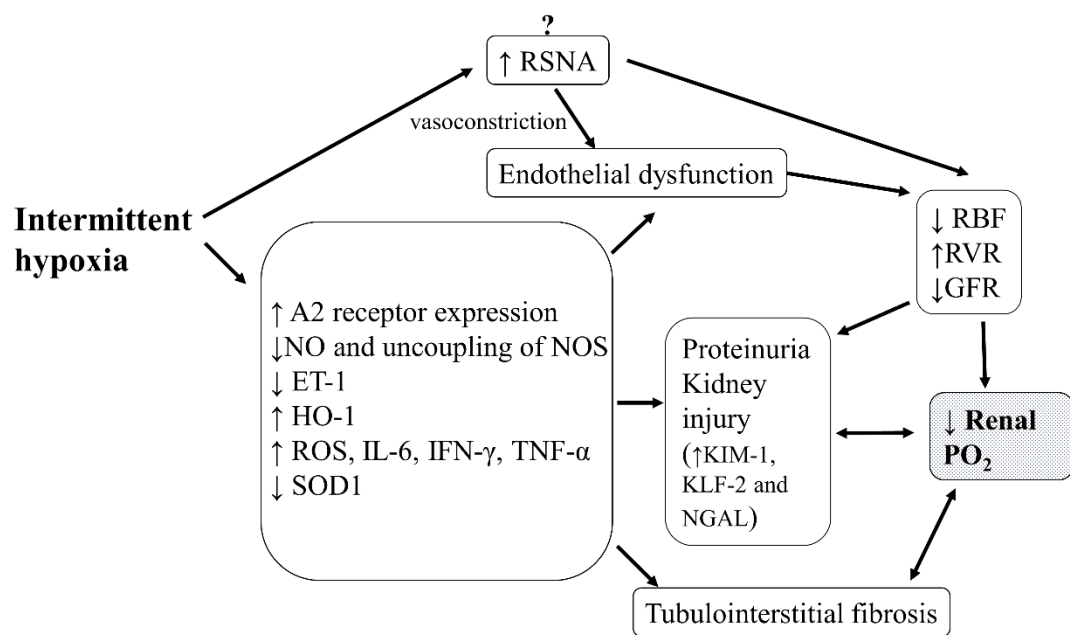


Figure 1. 6. Suggested mechanisms of intermittent hypoxia-mediated renal functional changes. There is scarcity in studies that investigated kidney function in response to intermittent hypoxia. The available data suggest that endothelial dysfunction as a result of intermittent hypoxia causes renal functional changes. “?”, increased renal sympathetic nerve activity (RSNA) is another possible mechanism for the decline in glomerular filtration rate (GFR), which is yet unknown. A2 receptor, adenosine type 2 receptor; NO, nitric oxide; NOS, nitric oxide synthase; ET-1, endothelin-1; HO-1, heme oxygenase-1; ROS, reactive oxygen species; SOD, superoxide dismutase; KIM-1, kidney injury marker-1; KLF-2, Krüppel-Like Factor-1; NGAL; Neutrophil gelatinase-associated Lipocalin; RBF, renal blood flow; RVR, renal vascular resistance.

1.7.2. Renal function alteration in acute hypoxia

Previous studies have shown that exposure to acute hypoxia induces inconsistent changes in renal function, due to species differences and type of anaesthesia used. Moreover, the hypoxic ventilatory response can interfere with renal responses, which are modulated when mechanical ventilation is utilized (254). Furthermore, respiratory and cardiovascular changes during hypoxia further modulate renal function. Nevertheless, similar species exhibited variable renal function responses to acute hypoxia, which could be related to different hypoxia protocols with different severity levels of hypoxia and exposure i.e. systemic exposure vs. isolated organ exposure of the kidneys or carotid bodies (Figure 1.7).

Acute exposure to hypoxia (12.5% O₂ for 30 minutes) in conscious rats was associated with alterations in cardiovascular parameters (a decrease in blood pressure and an increase in heart rate), respiratory modulation (hyperventilation with consequential changes in blood PO₂ and PCO₂) and renal functional changes (decreased GFR and electrolyte retention) (31). These changes were also associated with a decrease in RBF (31, 366). It was suggested that the decreased GFR is responsible for decreased water excretion and decreased sodium load and therefore less sodium excretion. The decrease in blood pressure in the mentioned study (31) could be due to hyperventilation-induced hypocapnia, as a previous study showed no changes in blood pressure during exposure to isocapnic or hypercapnic hypoxia (366). However, exposure to hypercapnic hypoxia (8% O₂ with 6% CO₂ for 30 minutes) in conscious rats and dogs was associated with a similar decrease in RBF to that observed in poikilocapnic hypoxia (366). Therefore, in hypercapnic hypoxia, an increase in RVR was observed which was due to the decrease in RBF along with a relatively maintained blood pressure.

In a similar acute poikilocapnic hypoxia exposure (12.5% O₂ for 30 minutes) in anaesthetised rats, a decrease in GFR was reported along with 50-65% decrease in urine and sodium excretion. In contrast to conscious rats, this was associated with increased RBF and renal vascular conductance (RVC) (254). It is proposed that differences between conscious and anaesthetised rats could be due to a greater increase in SNA in response to chemoreceptor stimulation in the conscious state, with higher activation of certain brain areas that cause a decrease in RBF, which overcomes the

auto regulatory mechanisms. Meanwhile, respiratory modulation in response to acute hypoxia was similar in anaesthetised and conscious rats (254). The decrease in GFR and renal perfusion pressure (RPP) along with an increase in RVC indicates the presence of a vasodilatory mechanism on efferent, but not afferent arterioles. Adenosine is released in response to systematic ischaemia which can trigger vasodilation on the efferent arterioles through A₂ receptors and vasoconstriction on the afferent arterioles through A₁ receptors (334). Similar to conscious rats, the decrease in GFR could be responsible for the retention in water and sodium excretion i.e. decreased pressure diuresis. Interestingly, when the same hypoxia protocol was repeated after occluding the abdominal aorta distal to the renal artery, no changes in diuresis and natriuresis were observed in response to acute hypoxia despite a PO₂ decline to 40-45 mmHg (254). This was related to stabilisation of blood pressure and RPP during occlusion. This provides evidence that the anti-diuretic and anti-natriuretic effects were caused by the hypoxia-dependent decrease in RPP. Moreover, sustained RPP improves O₂ supply to deeper regions of the kidney and therefore reduces the release of adenosine, which normally activates sodium-bicarbonate co-transporter causing sodium reabsorption (254). Indeed, other mechanisms mediated by the occlusion of abdominal aorta can contribute to kidney function alterations such as renin release, a decrease in baroreflex control of RSNA and the maintenance of adequate blood supply to carotid bodies; thus, decreasing their activity. The authors of the mentioned study excluded the possibility of altered ADH release because the PO₂ level required to alter ADH secretion is less than the lowest PO₂ level that was reached during the hypoxia protocol (254). Following renal denervation, acute hypoxia exhibited a similar decrease in urine and sodium excretion, which indicates that alterations in renal function were not mediated by changes in RSNA. However, renal denervation caused an increase in basal diuresis and natriuresis in addition to lower basal GFR (254).

A study using a similar protocol (12% O₂ for 20 minutes) in anaesthetised rats showed a 2.8 fold elevation in systemic renin activity (252). Nonetheless, it was illustrated that Ang II did not contribute to hypoxia-mediated anti-diuresis and anti-natriuresis, as losartan (Ang II receptor blocker) did not alter the magnitude of urine and sodium excretion during hypoxia. Maintenance of RPP by aortic occlusion decreased the anti-diuretic and anti-natriuretic effects of hypoxia. This provides further evidence that

RPP contributes partially to hypoxia-mediated alterations in renal function and its decrease stimulates renin release, but not vice versa.

In another study of acute hypoxia exposure in conscious rats (16.5% O₂ for 4 hours) followed by measurement of kidney function under anaesthesia, GFR and RBF were increased with a tendency towards increased water and sodium excretion. The decrease in RVR indicates afferent vasodilation supported by elevated plasma and cortical NO bioavailability (258). However, these parameters were measured under anaesthesia during whilst animals were breathing normal air.

Previous studies showed enhanced diuresis and natriuresis in response to acute hypoxia in conscious dogs, but the opposite was observed in anaesthetised dogs (40, 365). Perfusion of the kidney with venous blood for 20 minutes in anaesthetised dogs was associated with 22% increase in renal plasma flow and 10% decrease in creatinine clearance; thus, increased RVR. However, there was a gradual increase in urine volume and sodium excretion in 6 out of 8 experiments and a significant increase in potassium excretion in 4 out of 8 dogs (314). Enhanced sodium excretion despite a decreased GFR was suggested to be related to impaired tubular electrolyte reabsorption. The increase in water excretion in response to hypoxia was attributed to either a decrease in ADH or another mechanism that impairs water reabsorption in the distal convoluted tubules. This is similar to observations from a hypoxia study in humans with blood PO₂ of 50 mmHg (33, 314), where an increase in water and electrolyte secretion was seen despite decreased GFR. The increase in renal plasma flow in dogs was attributed to the possible release of adenine metabolites that mediate vasodilation. In relation to this, it was reported that anaesthetised dogs breathing 9 to 14% O₂ exhibited increased urine volume, while exposure to 5 to 7% O₂ was associated with water retention (314). Similarly, experiments at high altitude of 5,486 m in dogs showed increased renal plasma flow, whereas the opposite was observed at higher altitude of 7,315 m, indicating that severity of hypoxia might induce different modulation of kidney excretory function (165).

Direct stimulation of carotid bodies in anaesthetised dogs by venous blood (PO₂ ~27.4 mmHg) was associated with an increase in blood pressure, and decreases in heart rate, RBF, GFR and filtration fraction, in addition to a decrease in water and absolute, but not fractional, sodium excretion (157). In the latter study, the carotid bodies were

isolated so there was no effect of perfusion on the brain. Moreover, dogs were artificially ventilated, their skeletal muscles were paralyzed and vagosympathetic nerves were sectioned to eliminate any effects from the cardiopulmonary or intrathoracic receptors on kidney function (157).

The role of renal nerves in hypoxia-induced renal functional changes is still unclear. It has been shown that renal denervation is associated with increased baseline water and sodium excretion, but it does not change the anti-diuretic and the anti-natriuretic response to acute hypoxia in rats (254). However, renal denervation abolished the decrease in RBF, GFR and water excretion resulted from direct stimulation of carotid bodies with hypoxic venous blood in anaesthetised dogs with intact nerves (157). Interestingly, ablation of renal nerves reversed the inhibitory effect of hypoxic carotid bodies on sodium excretion which resulted in enhanced natriuresis compared with sham-exposed dogs, suggesting that enhanced natriuresis is mediated by humoral factors (157). Indeed, renal excretory changes in response to hypoxic venous blood were abolished after destruction of the carotid bodies (157).

Acute hypoxia in humans (12% O₂) was associated with enhanced diuresis and natriuresis (344). Similar observations were reported in some other studies on mammals, whereas some other experiments have shown no changes in renal function (31, 254, 344). It has been suggested that natriuresis is related to direct hypoxic stimulation of the chemoreceptors, although exposure of isolated kidneys to hypoxia in animal studies was associated with diuresis and natriuresis (314). A positive correlation has been reported in humans between diuresis and natriuresis and the isocapnic hypoxic ventilatory response i.e. increased minute ventilation (344). Therefore, the induced natriuresis in hypoxia could be due to the activation of intra-thoracic stretch receptors. Importantly, voluntary forced breathing of normal air for 45 minutes was associated with an enhanced diuresis of similar magnitude to that observed during breathing 6% CO₂ or 10% O₂ (68). In addition, during hypoxia, a decrease in PCO₂ induces respiratory alkalosis; thus, increasing bicarbonate and sodium excretion. However, bicarbonate excretion per se did not show any correlation with the hypoxic ventilatory response, while sodium-bicarbonate excretion showed an exponential rather than a linear relationship (344). This indicates that there is a higher sodium excretion for a given amount of bicarbonate excretion. Therefore, it is less likely that hyperventilation or bicarbonate excretion are predominantly responsible for

the natriuretic response during hypoxia. It is relevant to consider that hypocapnia decreases the activity of central chemoreceptors, which modulates hypoxic ventilatory responses that mediate renal excretory responses. Of note, no changes were detected in plasma ANP, aldosterone, angiotensin and renin, and no correlation has been found between measures of renal function and plasma levels of aforementioned humoral factors (344). Interestingly, since renal excretory responses were enhanced and it is well-known that RSNA is increased during hypoxia, it is apparent that the mechanism driving diuresis and natriuresis during hypoxia overrides the anti-diuretic and anti-natriuretic effects of RSNA.

It is not yet determined if the earlier change in renal function is sodium or water excretion. Currie et al (68) in this regard suggested that water precedes solute excretion. During normal breathing, drinking 500 ml of water in control experiments was associated with enhanced diuresis accompanied with natriuresis. Moreover, only during the initial phase of the diuretic response, was an increase in sodium excretion observed, but subsequently, urine flow continued to rise with no further increase or with a decrease in sodium excretion (68). Figure 1.7 summarizes renal functional responses to different acute hypoxia experiments in different species.

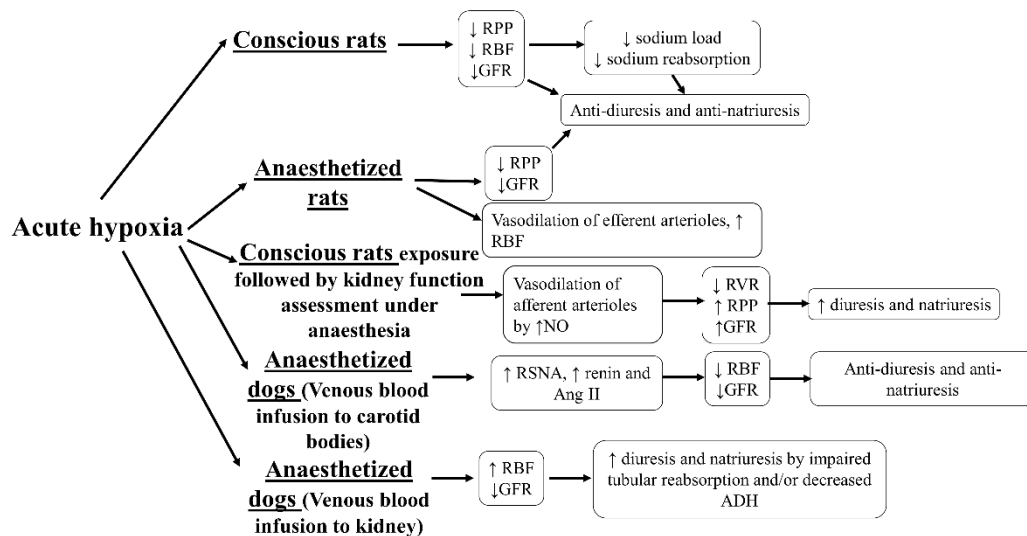


Figure 1. 7. Variable renal responses to acute hypoxia in different species in response to various hypoxic protocols. RPP, renal perfusion pressure; RBF, renal blood flow; GFR, glomerular filtration rate; RVR, renal vascular resistance; NO, nitric oxide; RSNA, renal sympathetic nerve activity; ADH, anti-diuretic hormone.

1.7.3. Renal functional changes in chronic hypoxia

Exposure of rats to short term sustained hypoxia, equivalent to 7,620 m, for one day was not associated with changes in kidney function, but with histological damage of the renal epithelial cells (58). After 3 and 7 days of exposure, kidney function deteriorated gradually with the maximum significant increase in plasma creatinine and blood urea nitrogen observed after 7 days, which were associated with more severe epithelial tubular damage and tubulointerstitial collagen deposition. However, prolonged hypoxia exposure for 3 to 5 weeks (12% O₂) elicited increased blood pressure and RVC, but no change in RBF or GFR (253), when were measured during 20 minutes of animals breathing normal air under anaesthesia. Diuresis and natriuresis were enhanced during normal air breathing following exposure to chronic hypoxia with increased right atrial pressure. It was suggested that pressure diuresis was mediated by increased RPP, as aortic occlusion eliminated the enhanced diuresis and natriuresis (253). Increased RPP increases interstitial hydrostatic pressure and subsequently decreases sodium reabsorption. Chronic hypoxia-exposed rats had 40% increase in urinary cGMP, which reflects increased ANP activity. However, it has been shown that ANP infusion into the control rats that elevates plasma levels of ANP to values similar to chronic hypoxia-exposed rats, did not cause diuresis and natriuresis. Chronic hypoxia-exposed rats had normal blood pressure and a normal O₂ content in response to acute hypoxia (12% O₂), compared with decreased blood pressure in control rats in response to acute hypoxia. In addition, chronic hypoxia-exposed rats had no changes in renal function in response to acute hypoxia, which differed to the finding of sodium and water retention in control rats (253). Similarly, renin activity in chronic hypoxia-exposed rats was not elevated to the same level as control rats breathing 12% O₂ (253). Therefore, it is suggested that increased ANP in chronic-hypoxia exposed rats, which was below the levels required to induce diuresis and natriuresis, can inhibit RAAS-mediated anti-diuretic and anti-natriuretic effects during acute hypoxia which were observed in control rats.

Furthermore, *in vivo* studies have reported increased plasma level of ANP in response to hypoxia in different species, as reviewed by Arjamaa et al. (16). Exposure to chronic hypoxia was associated with an increase in plasma [ANP] in rats with normal and right ventricular hypertrophy. During normoxia, [ANP] decreased to control levels despite the hypertrophied myocardium. Similarly, in the Langendorff preparation of the

isolated rodent heart, hypoxia caused a significant increase in [ANP] although ventricular pressure was constant (16). Other studies on sleeping seal pups showed that plasma [ANP] increases during the apnoea phase and returns to basal levels when breathing is restored to normal (16, 405). Therefore, it is hypothesised that blood volume and flow changes during the cycle of filling and emptying of the heart represent a weak signal to induce natriuretic peptide release. Instead, a large physiological stimulus is needed to induce natriuretic peptide secretion such as lowered oxygen tension. It is also suggested that hypoxia through HIF activation induces the transcription of natriuretic peptides (16). ANP induces a fluid shift from the blood to the interstitial space during hypoxia in addition to its diuretic and natriuretic effect and this causes a decrease in plasma volume leading to haemoconcentration (16, 378). This in turn increases oxygen carrying capacity and transport to the peripheral tissues.

In humans, chronic hypoxia was shown to have variable effects on renal function, which are dependent on the balance between RAAS and ANP activity. Some individuals subjected to high altitude showed enhanced diuresis with no changes in sodium excretion while others showed signs of acute mountain sickness with water and sodium retention (140, 253). Short-term exposure to high altitude is associated with hyperventilation and respiratory alkalosis (203). Increased plasma [ANP] correlated with the early diuretic response in high altitude. In hypobaric chambers of 4,559 m, ANP levels were unchanged and it was increased in hypobaric chambers of 6,000 m. However, it was decreased in chambers of 8,848 m (112). Enhanced diuresis was also associated with a decrease in ADH levels. Meanwhile, volunteers who developed acute mountain sickness has increased ADH levels which correlated with the severity of acute mountain sickness (219). In addition, decreased renal sensitivity to ADH after two days of high altitude was reported along with an increase in osmotic threshold required to induce ADH secretion (112). Moreover, high altitude was associated with decreased renin and aldosterone which were restored nearly to basal sea levels after 10 days of acclimatisation, reflecting normalisation of the diuretic response at a later stage (112). Increased urinary endothelin-1 levels was also observed at high-altitude concomitant with enhanced diuresis. The administration of an endothelin-1 blocker inhibited the enhanced diuretic response (112). Adrenomedullin decreases renin and aldosterone levels in addition to a decrease in RSNA (112). It was

shown that the urinary levels of adrenomedullin increases in correlation with low to moderate and high altitude (128). Nevertheless, after prolonged exposure to high altitude, water and sodium excretion rates were restored. It was also found that high altitude residents have low RBF, but preserved GFR and filtration fraction in addition to glomerular hypertrophy (112). However, studies at high altitude are confounded by the presence of other stressors. Importantly, there is a non-linear relationship between hypoxia and diuresis as fraction of inspired oxygen (FiO_2) higher than 0.16 was associated with no diuresis while FiO_2 of 0.12-0.16 resulted in a significant diuretic response. Sodium and water retention were observed with FiO_2 of less than 0.12 (112).

1.8. Knowledge gaps addressed in this project

Kidney hypoxia and the modulation of reno-renal reflex induces changes in sodium and water excretion which contribute to progression of hypertension and CKD. Chronic and acute hypoxia studies have shown major changes in renal haemodynamics that led to changes in renal excretory function evidenced by water and electrolytes retention or enhanced diuresis and natriuresis. However, studies of intermittent hypoxia have focused on the structural changes of the kidney and oxidative stress biomarkers with a scarcity of information on sodium and water excretion (9, 277, 342, 409). Furthermore, established structural changes of the kidney and clinical manifestations of CKD was shown in studies of severe CIH (9, 408, 409). Therefore, it is still unknown whether renal pathophysiological changes occur in response to hypoxia itself at an early stage of the disease or are developed at a later stage due to hypertension and/or hypoxia. Similarly, it is not yet established if kidney excretory function is changed early in response to CIH or modulated secondary to severe oxidative stress and inflammation, the latter arising subsequent to hypertension and sympathetic over-activity.

Denervation of the kidney during oxidative stress or injury was associated with the restoration of the normal baroreflex control (6, 169), providing evidence of the presence of afferent signals originating from diseased kidneys causing impaired baroreflex. Indeed, impaired baroreflex control of blood pressure contributes to the development and exacerbation of hypertension in different models (133, 168, 169, 363). Renal inflammation and/or oxidative stress is indirectly linked to the impaired baroreflex control, in a mechanism that is dependent on the activation of renal afferent nerves (2, 6, 170). Moreover, the activity and the expression of receptors involved in afferent renal neural activity such as TRPV1 and bradykinin receptors have been altered in the presence of hypoxia or inflammation (172, 335). In this regard, previous studies have shown early renal changes in CIH presented by the elevation of endothelial dysfunction biomarkers (342, 380), changes in oxidative signalling and inflammatory cytokines profiles (Appendix I, Table 8.1). Accordingly, blunted baroreflex control of heart rate was evident in CIH (62, 74). However, there is little information available on high-pressure baroreflex control of RSNA despite many reports that showed heightened renal, splanchnic and lumbar SNA in CIH (280, 324).

Moreover, low-pressure baroreflex control of RSNA, represented by the evaluation of the response to fluid overload, was not studied in CIH, although it was impaired in other hypertension models (3, 169) that involve renal structural changes similar to the ones observed in CIH. Impaired baroreflex control of heart rate was shown in studies utilising long durations of CIH exposure (62, 74). Therefore, it remains to be determined whether baroreflex dysfunction is one of the mechanisms that contribute to the onset of hypertension, or develops at an advanced stage as a consequence of hypertension, reflecting the role of the baroreflex mechanism in blood pressure elevation in OSA. On the other hand, selective removal of ARNA attenuated hypertension in some disease models, indicating an excitatory reno-renal reflex contributing to hypertension (24). This is also related to oxidative stress and inflammation that can alter the activity and/or the expression of receptors involved in afferent neuronal signalling (172, 335). Meanwhile, in other models such as SHR, suppression of ARNA in response to the increased renal pelvic pressure (181) and to the intra-renal pelvic infusion of bradykinin was shown (190). However, whether CIH is associated with suppressed reno-renal reflex, as in SHR (182, 190), or elevated excitatory reno-renal reflex, as in kidney-clipped models (18), remains unexplored. Furthermore, the direct effect of renal afferent nerve activation on blood pressure and RSNA in CIH was not previously studied.

1.9. Thesis aims

The primary aim of this project was to examine whether renal afferent nerves contribute to sympathetic over-activity and baroreflex dysregulation in CIH-induced hypertension (Figure 1.8). First, since there is considerable evidence that aberrant afferent outputs from kidneys interfere with the baroreflex function in hypertension, we sought to assess the high- and low-pressure baroreflex control of heart rate and RSNA after 14 days of exposure to a relatively moderate CIH protocol. This model is associated with modest pathological changes, yet it is sufficient to induce hypertension; thus, it mimics mild-to-moderate OSA at an early stage, providing an opportunity to determine whether baroreflex dysregulation contributes to the onset or progression of CIH-induced hypertension. For this purpose, experiments were conducted to study baroreflex control of RSNA and heart rate, and to investigate if RSNA sympatho-inhibition and renal functional responses to volume expansion are affected by exposure to CIH. Thereafter, we hypothesized that afferent renal nerve hyperactivity is responsible for the anticipated dysregulation of the baroreflex control of blood pressure. Therefore, studies were designed to interfere with one of the receptors involved in afferent renal neural signalling, TRPV1 channels. As such, we assessed high- and low-pressure baroreflexes after TRPV1 blockade using intra-renal capsaizepine infusion. We also investigated if moderate CIH exposure, reflecting an early stage of OSA, is associated with histopathological changes, inflammation and oxidative stress in renal tissue.

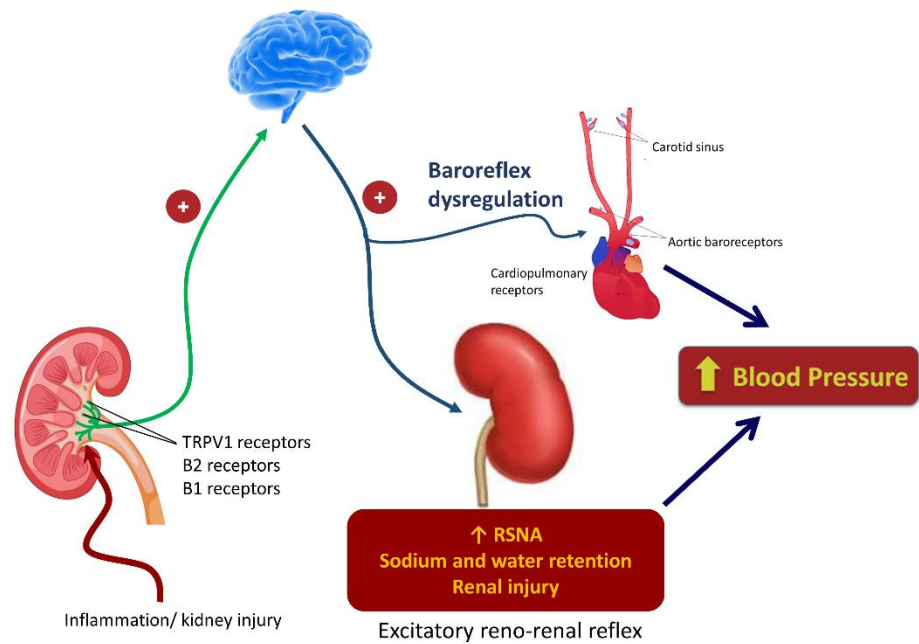


Figure 1. 8. A schematic representation of a proposed mechanism of CIH-induced hypertension that was investigated in this project. We hypothesized that renal afferent nerve hyperactivity, through reflex sympatho-excitation, causes baroreflex dysregulation. This results in hypertension, alterations in kidney function and renal injury.

Second, we aimed to explore if exposure to CIH is associated with alteration in the reno-renal reflex, by studying the direct impact of the activation of reno-renal reflex on cardiovascular and renal parameters. We focused on bradykinin receptors and TRPV1 channels located in the renal pelvic wall, which are part of the signalling pathway of sensory renal nerve endings. For this purpose, three doses of bradykinin were infused in random order into the renal pelvis of anaesthetised rats and this was repeated following the intra-renal pelvic blockade of bradykinin receptor type 1 and 2. At the end of the protocol, we infused capsaicin into the renal pelvis to activate TRPV1-expressing renal sensory nerve endings. During infusions, blood pressure, heart rate, and contralateral RSNA and kidney function were measured. We also studied the molecular expression of TRPV1, NK1 and bradykinin receptors in the renal pelvic wall, where most of the renal afferent nerve endings are localised.

Chapter 2. Methods

List of Abbreviations

ANP	Atrial natriuretic peptide
AOPP	Advanced oxidation protein products
CGRP	Calcitonin gene-related peptide
CIH	Chronic intermittent hypoxia
CPZ	Capsaizepine
DBP	Diastolic blood pressure
EGTA	Egtazic acid
ELISA	Enzyme-linked immunosorbent assay
GFR	Glomerular filtration rate
H ₂ O ₂	Hydrogen peroxide
HR	Heart rate
HRP	Horseradish peroxidase
IL-1 β	Interleukin-1 beta
MAP	Mean arterial blood pressure
NADPH	Nicotinamide adenine dinucleotide phosphate
NK1	Neurokinin 1 receptor
NOX	NADPH oxidase
NTB	Nitro blue tetrazolium
O ₂ ⁻	Superoxide
PE	Phenylephrine
RSNA	Renal sympathetic nerve activity
SBP	Systolic blood pressure
SNP	Sodium nitroprusside
SOD	Superoxide dismutase
TNF- α	Tumour necrosis factor- alpha
TRPV1	Transient receptor potential cation channel subfamily V member 1
UF	Urine flow rate
VE	Volume expansion

2.1. Animal model

Eight-week old male Wistar rats were purchased from Envigo (Bicester, UK) and were housed in our institution's animal facility as age-matched pairs in standard cages. All animals were housed under 12-hour light: 12-hour dark cycle receiving *ad libitum* water and standard chow (Teklad, 18% protein rodent diet, Madison, Wisconsin, USA). All experimental procedures were conducted under authorization from the Health Products Regulatory Authority [AE19130/P073] in accordance with European Union directive (2010/63/EU) with prior ethical approval from University College Cork (AEEC 2018/002).

Rats were randomly divided into two groups: CIH and sham (control). Rats of the CIH group were placed in commercial environmental chambers attached to a computer-controlled gas delivery system (Oxycycler™, Biospherix, NY, USA), which delivered programmed hypoxia/re-oxygenation cycles, servo-controlled with feedback from an oxygen sensor within each chamber. CIH rats were exposed to hypoxia cycles for 14 days as follows: during the hypoxia phase, O₂ concentration was reduced to 6±0.5% within 90 sec by infusing N₂ into the chamber. This was followed by an immediate infusion of pure oxygen into the chamber to elevate the O₂ concentration to near normal levels (21±2%). The normoxia phase of each cycle was maintained for 210 sec. This cycle was repeated every 5 minutes (i.e. 12 cycles per hour) for 8 hrs during the lights on period, the diurnal sleep period of the animals (Figure 2.1). The sham group was housed in the same room and rats were exposed to ambient air (~21% O₂) for 14 days. Both groups had free access to food and water *ad libitum* during exposures. On day 15, rats were prepared surgically under anaesthesia, for the assessment of high- and low-pressure baroreflexes, or the assessment of the reno-renal reflex. The experimental protocol was conducted in three successive cohort studies that involved 72 rats in total [first cohort (n=10 sham and n=10 CIH); second cohort (n=13 sham and n=10 CIH); third cohort (n=15 sham and n=14 CIH)]. One CIH-exposed rat from the first cohort died during surgery under anaesthesia before baseline measurements were recorded. Three sham rats from the second cohort did not produce a logistic sigmoidal fit during baroreflex assessment, and so they were excluded, but baseline parameters were included in the analysis. In the third cohort, baseline readings obtained at the beginning of the surgical protocol were excluded for one CIH

rat due to bleeding that had happened during arterial cannulation, and in one sham rat because the animal had difficulty in breathing due to mucus secretions before reaching an adequate level of anaesthesia to carry out tracheotomy. Moreover, in the third cohort, data were excluded from four CIH rats and three sham rats either due to poor or no RSNA recording, or due to difficulty in the cannulation of the renal pelvis. In addition, results of the reno-renal reflex were excluded from another sham rat due to a malfunction that had happened in the heating pad necessary to maintain body temperature during anaesthesia, when the rat's temperature dropped, which theoretically can affect the expression of receptors such as TRPV1, which were a focus of the study.

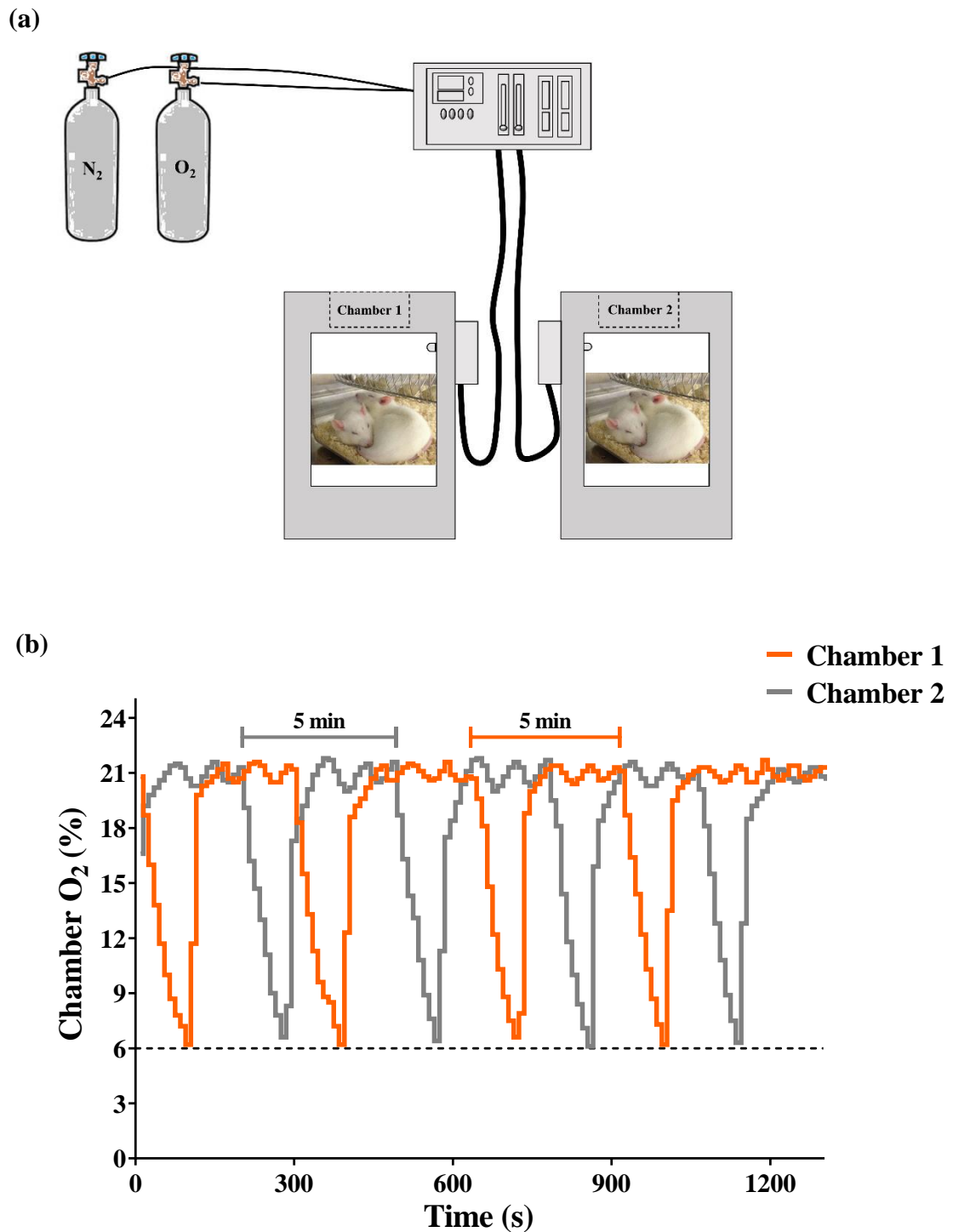


Figure 2. 1. Oxycycler system and oxygen profiles in two chambers operating simultaneously. A pair of rats was placed in each hypoxia chamber while two chambers were operating at any time point of the study as shown in the upper panel (a). The bottom panel is a snapshot of oxygen profile in one of the hypoxia studies (b). During hypoxia, O₂ concentration was reduced to 6% within 90 secs followed by a normoxia phase that lasted for 210 secs.

2.2. Non-recovery surgical instrumentation

CIH-exposed (n=34) and sham rats (n=38) were anaesthetized by intra-peritoneal injection of a mixture of urethane (416 mg/kg, Sigma-Aldrich, St. Louis, MO, USA), α -chloralose (27 mg/kg, Sigma-Aldrich) and sodium pentobarbitone (33 mg/kg, Euthatal (200 mg/ml), Merial animal health Ltd, UK). Adequacy of depth of anaesthesia was checked by the loss of reflex responses to paw and tail pinch and loss of the blinking reflex. Anaesthesia was maintained during the surgery using a maintenance dose of a mixture of urethane (62 mg/kg) and α -chloralose (4 mg/kg) given as intravenous bolus injection. Animals were placed on a temperature-controlled heating pad to maintain body temperature at 37°C (Harvard Apparatus, Cambridge, UK). Airway patency was facilitated by tracheotomy (PE240, Portex, Kent, UK). A cannula (PE25 attached to PE50) containing heparinized saline (4 U/ml) and connected to a fluid-filled pressure transducer (ADInstruments, Hastings, UK), was inserted into the right femoral artery to measure arterial blood pressure (MAP) and heart rate (HR) throughout the experiment. The pressure transducer was connected to a quad-bridge amplifier (ADInstruments, Hastings, UK) that recorded pulsatile blood pressure, which was used to generate MAP, systolic blood pressure (SBP), diastolic blood pressure (DBP) and HR using LabChart 7 software (ADInstruments, Oxford, UK). The right femoral vein was cannulated (PE50) to infuse FITC-inulin (10 mg/kg/hr, tdB consultancy, Uppsala, Sweden) continuously over the duration of the experiment (258). The urinary bladder was cannulated (PE240) to collect urine samples in the cohort 1 study (Figure 2.2).

Before commencing the next step in the surgical procedures and to exclude the effect of retroperitoneal access on baseline recordings, blood pressure was recorded for 2 minutes ~4-5 minutes after femoral artery cannulation and compared between the groups, in essence to confirm the hypertensive phenotype in CIH-exposed rats.

In the first cohort study, CIH-exposed (n=9) and sham animals (n=10) were then placed prone on their right side and the left kidney was exposed by a subcostal retroperitoneal flank incision. A cannula (PE10) was inserted into the rostral part of the left kidney at 3.5-4.5 mm depth, to reach the cortico-medullary region of the kidney (3) and was fixed in place using superglue (Ethyl cyanoacrylate and poly(methyl methacrylate)). This cannula was connected to a 25 μ l micro-syringe (Hamilton, USA)

placed on a micro-infusion pump (Figure 2.2, KD Scientific, Linton Instruments, Norfolk, UK) to infuse saline or capsaizepine (CPZ, 5 μ g/ml, Sigma-Aldrich, St. Louis, MO, USA) at 17 μ l/min. In the second cohort study, CIH-exposed (n=10) and sham rats (n=10) were placed prone on their left side to expose the right kidney, which was cannulated using a similar approach to that used in the first cohort. The insertion of the intra-renal cannula to target renal pelvic wall was validated as described in section 2.2.1.3.

In the third cohort, CIH-exposed (n=10) and sham rats (n=11) were placed on their left side to make a subcostal right retroperitoneal incision to expose the right kidney. A custom-made cannula (OD 0.5 mm, ID 0.25 mm, World Precision Instruments, Florida, USA) was then placed inside a PE50 cannula (Figure 2.3) and both were inserted into the proximal part of the ureter to cannulate the renal pelvis of the right kidney. The smaller internal cannula was connected to a 25 μ l micro-syringe placed on a Hamilton micro-infusion pump to infuse saline over the duration of the experiment at 20 μ l/min. The outside PE50 cannula facilitated perfusate and urine drainage during the experiment. This double luminal cannula was also used to infuse different doses of bradykinin, bradykinin receptor antagonists and capsaicin into the right renal pelvis. Following renal pelvic cannulation in rats of cohort 3, the right retroperitoneal incision was sutured (4-0 Vicryl Rapide, polyglactin 910, Ethicon®, Johnson & Johnson Medical Ltd, Scotland, UK) and rats were then placed on their opposite flank to make a left retroperitoneal incision to expose the left kidney. Then, a PE25 cannula was inserted into the left ureter to collect urine samples from the contralateral left kidney during the experiment.

In all cohorts, using a dissecting microscope, the renal nerve bundle running between the renal artery and vein of the left kidney was dissected from surrounding tissues and held placed on a bipolar multi-stranded stainless-steel electrode (Medwire, NY, USA). The nerve bundle was sealed over the recording electrode using silicone glue (Klasse 4 dental, Augsburg, Germany). Nerve recording of renal sympathetic nerve activity (RSNA) was performed using a high impedance head stage attached to an amplifier (NeuroAMP EX®, ADInstruments, UK) connected to a PowerLab data acquisition system (Figure 2.2). Signals were amplified (x100,000), filtered (high-pass filter 100 Hz and low pass filter of 2 kHz) and sampled at 1kHz and recorded on LabChart. Raw RSNA signal was rectified and then integrated using a time decay constant of 0.09s

Integrated RSNA ($\mu\text{V.s}$) values were averaged every second and then followed with the appropriate calculations to analyse baroreflexes and the reno-renal reflex.

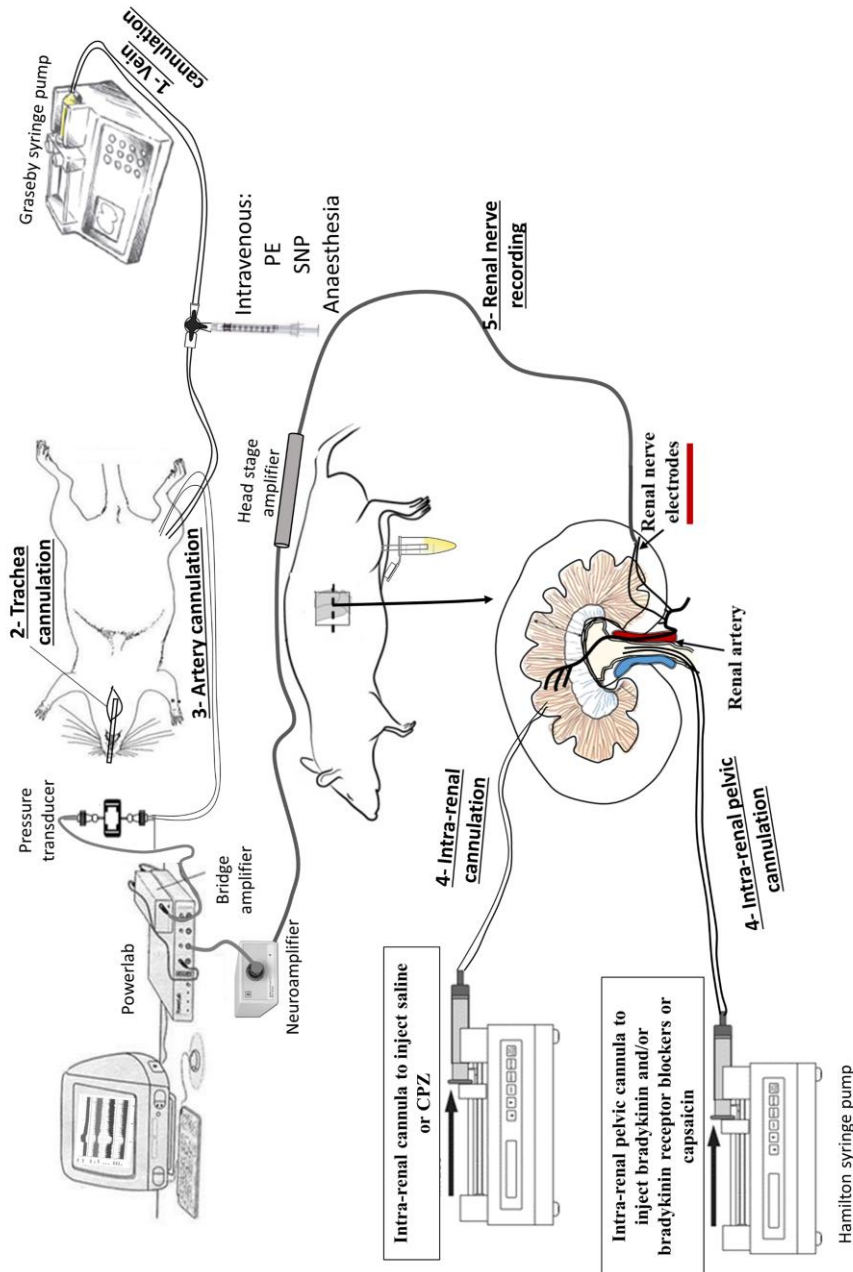


Figure 2. 2. Surgical instrumentation of non-recovery surgical experiments. Steps are numbered based on first to last cannula inserted into the rat. The first step was vein cannulation necessary to infuse intravenous anaesthesia following the intraperitoneal induction dose of anaesthesia. This was followed by tracheotomy to facilitate breathing and to minimise the consequences of anaesthesia-induced fluid accumulation on breathing. Then, the femoral artery was cannulated to measure basal blood pressure and heart rate. After ~8 minutes basal measurement, retroperitoneal incisions were carried out to insert an intra-renal cannula (cohort 1 and 2) or an intra-renal pelvic cannula (cohort 3), and to hold a branch of the renal nerve on the recording electrodes. PE, phenylephrine; SNP, sodium nitroprusside; CPZ, capsaizepine.

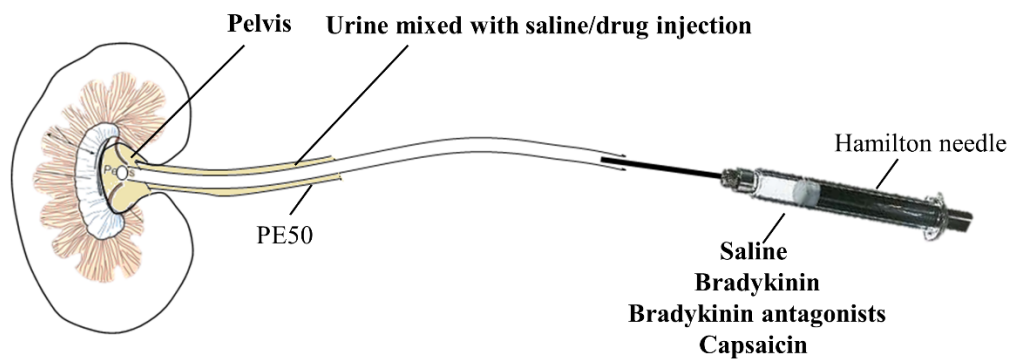


Figure 2. 3. The design of the intra-renal pelvic cannula. In cohort 3, drugs were infused through the renal pelvis without the obstruction of urine drainage. For this purpose, a double lumen cannula was custom-made, composed of an inner cannula that can easily move through an outer PE50 cannula. Both cannulas were inserted through the proximal part of the ureter until both reached the pelvic wall. The end of the inner cannula protruded 0.2 mm beyond the outer PE50 cannula, and the length of the PE50 cannula was 9 cm. The other end of the inner cannula was connected to a Hamilton syringe mounted on a Hamilton syringe pump, which was used to infuse saline during the experiment or drugs during experimental protocols. The space between the inner cannula and the end of the PE50 cannula inside the renal pelvis allows the flow of urine from pelvis to the other end of the PE50 cannula, which is opened to the atmospheric pressure. This allowed patent urine flow without increasing the pressure inside the renal pelvis during infusion.

2.2.1. First cohort experimental protocol

2.2.1.1. Baroreflexes assessment

The experimental protocol of the first cohort study is described in Figure 2.4. After surgical instrumentation, a stabilization period of one hour was allowed and baseline MAP, HR and RSNA was recorded for two minutes. Intravenous inulin (FITC-inulin in saline, 10 mg/kg/hr) infusion started at the beginning of the stabilization period and continued throughout the whole surgical protocol. After intra-renal infusion of saline (17 μ l/min, saline (control) phase) to the left kidney for 30 minutes, phenylephrine (PE, 50 μ g/ml, 0.2 ml) and sodium nitroprusside (SNP, 50 μ g/ml, 0.2 ml) were infused intravenously to increase and decrease blood pressure respectively, allowing the subsequent generation of high-pressure baroreflex curves. A volume expansion (VE) phase (saline phase) was then performed, which was followed by a 90-minute recovery period. This phase was called ‘saline phase’ because it was conducted during intra-

renal infusion of saline into the left kidney. Then, intra-renal infusion was switched from saline to CPZ and was sustained (17 $\mu\text{l}/\text{min}$) for 30 minutes. Then, a second VE phase (CPZ, drug phase) was performed. Saline and CPZ infusion into the left kidney was maintained at 17 $\mu\text{l}/\text{min}$ during VE trials.

Each VE trial involved inulin infusion (FITC-inulin in saline, 10 mg/kg) for 30 minutes via the femoral vein at 0.25 ml/min/100g body weight using a syringe pump (Graseby syringe pump 8100, Dublin, Ireland). Each VE trial period was followed by 30 minutes of recovery during which saline infusion through the intravenous line was stopped, but with continuous intra-renal infusion of saline or CPZ. The animals were euthanized at the end of the experiment by an overdose of anaesthetic (mixture of 80 g/kg urethane and 55 mg/kg α -chloralose) given intravenously. RSNA reaches its maximum level during euthanasia due to the sudden precipitous drop of blood pressure. This was followed by a complete disappearance of RSNA peaks and this part of the recording was used to measure background noise, which was subtracted from all recordings.

2.2.1.2. Measurement of Excretory Parameters

Blood samples (P1, P2 and P3 samples, Figure 2.3) of $\sim 400\ \mu\text{l}$ were collected and centrifuged at 10,956 g for 1 minute and the plasma was removed and stored at -20° for further analysis of inulin and/or sodium concentration. To minimize any change in haematocrit, the blood cells that remained after centrifugation were suspended in an equivalent volume of saline and returned to the animal via the arterial line. Further blood samples (at P1 and P3) were taken from the femoral artery to measure sodium concentration using an I-STAT system (Abbott Laboratories, Abbott Park, IL, USA). Two urine samples were collected over 10- and 20-minute periods, respectively (U1 and U2), during intra-renal infusion of saline or CPZ. In addition, a third urine sample was collected over the first 10 minutes of VE (U_{VE1}) and then every 5 minutes until the end of the 30-minute VE trial period (U_{VE2} , U_{VE3} , U_{VE4} and U_{VE5}). An additional urine sample was collected during the recovery period i.e. 30 minutes after the end of the VE trial (Figure 2.4).

Urine flow (UF), glomerular filtration rate (GFR), and absolute and fractional Na^{+} excretion were measured at baseline (U1 and U2) and at different time points during

the VE trial (U_{VE1} , U_{VE2} , U_{VE3} , U_{VE4} and U_{VE5}). Urine volume was measured gravimetrically and UF was calculated as: $UF = U_v/t$; U_v is urine volume, t is time of urine collection. GFR was measured as a function of FITC-inulin clearance and calculated using the formula: $GFR = ([U_{in}]U_v)/[P_{in}]$; $[U_{in}]$ is urine concentration of FITC-inulin, $[P_{in}]$ is plasma concentration of FITC-inulin. FITC-fluorescence was measured in urine and plasma samples using a fluorometric microplate reader (Wallac victor² 1420 multilabel counter, Perkin Elmer, MA, USA). Urinary Na^+ concentration was measured using flame photometry (M410, Sherwood Scientific, Cambridge, UK). Plasma Na^+ concentration at P2 was determined using flame photometry. However, plasma Na^+ concentration (P1 and P3) was measured immediately upon sample collection during surgery using the i-STAT system (Abbott Point of Care Inc, IL, USA). The latter samples were not drawn for analysis using flame photometry to minimize the volume of blood withdrawn and haematocrit change; the amount of blood sample required for i-STAT analysis did not exceed 70 μ l. Absolute Na^+ excretion was calculated using the formula: $[UNa^+].UF$; $[UNa^+]$ is urinary Na^+ concentration. Fractional Na^+ excretion was calculated using the equation: Na^+ clearance/GFR.100% where Na^+ clearance = $([UNa^+]U_v)/[PNa^+]$; $[PNa^+]$ is plasma Na^+ concentration.

It is worth mentioning that blood samples were not collected during VE to avoid fluctuations in the blood pressure and RSNA during VE challenge and to minimize any significant change in haematocrit after multiple blood collections. Therefore, inulin concentration in blood samples of P2 was used to calculate GFR values at baseline and at 10 minutes of the VE phase (U_{VE1}). Inulin concentration of P3 was used to calculate GFR values at 25 and 30 minutes of the VE phase (U_{VE4} and U_{VE5}). Meanwhile, GFR values at 15 and 20 minutes of VE (U_{VE2} and U_{VE3}) were calculated using average inulin concentrations obtained from P2 and P3 blood samples. A similar strategy of plasma samples was used in the calculation of absolute and fractional sodium excretion during each VE phase.

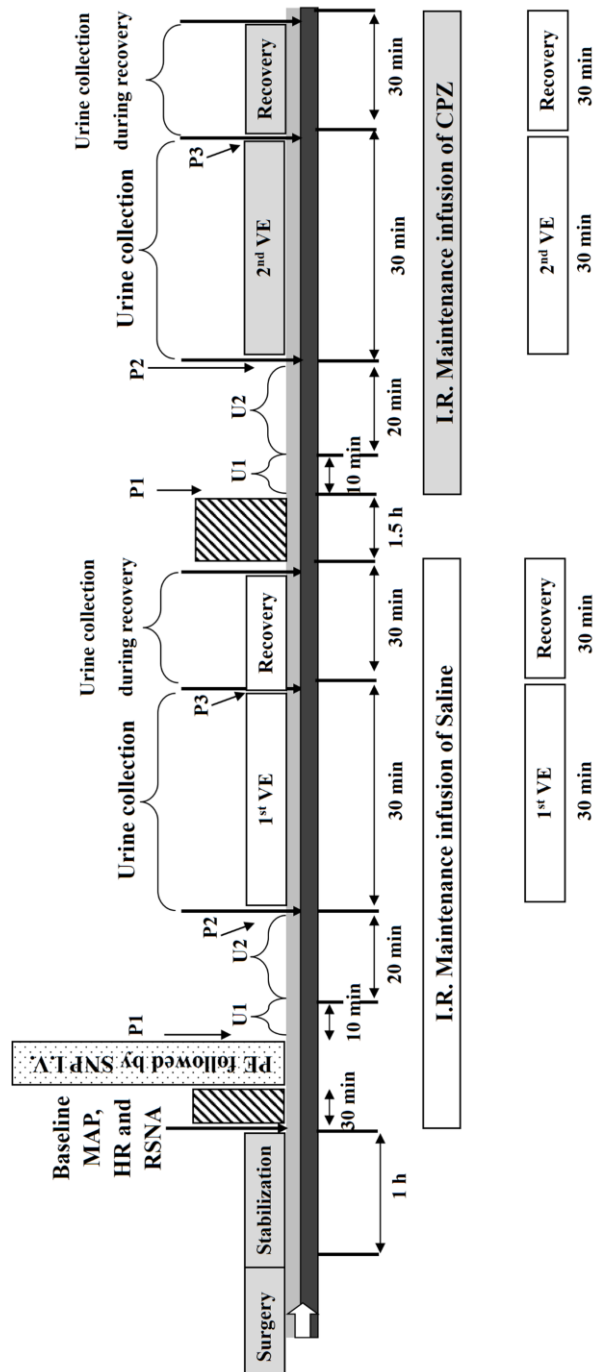


Figure 2. 4. A schematic representation of the surgical protocol of the first cohort. Following a one-hour stabilization period, baseline cardiovascular and RSNA were determined. After intra-renal infusion of saline to the left kidney for 30 minutes, phenylephrine and sodium nitroprusside were infused intravenously to elicit high-pressure baroreflex responses. The first volume expansion (VE) trial (saline phase) was then performed. For the second phase, intra-renal infusion of CPZ was initiated for 30 minutes into the left kidney and a second VE trial was performed (CPZ phase). Two urine samples (U1 and U2) were collected during baseline before each VE trial. The “Urine collection” phase represents the collection of a urine sample 10 minutes after the start of the VE trial followed by subsequent collection of urine samples every 5 minutes until the end of the VE challenge. Arterial blood was sampled for plasma (P2 and P3). Each VE trial was accompanied by infusion of inulin for 30 minutes after the end of the VE challenge. Arterial blood was sampled for plasma (P2 and P3). Each recovery during which continuous intra-renal infusion of saline or CPZ was maintained. P, plasma sample; VE, volume expansion; I.R., intra-renal; CPZ, capsaizepine; PE, phenylephrine; SNP, sodium nitroprusside.

2.2.1.3. Validation of intra-renal infusion

The purpose of this experiment was to confirm that CPZ infused through the intra-renal cannula reached renal pelvic wall, where most renal afferent nerves are located (180). Therefore, the same surgical experimental protocol was carried out on three untreated 10 week old Wistar rats. Following the end of the first VE phase (saline phase), Lissamine green stain (George T. Gurr. Limited, London, UK) was infused through the intra-renal cannula of the left kidney for 30 minutes instead of CPZ. Then, rats were euthanized by an overdose of anaesthesia (mixture of 80 g/kg urethane and 55 mg/kg α -chloralose) and the left kidney was frozen in optimal cutting compound and stored at -80° .

Kidneys were cross-sectioned (cryostat, Leica Biosystems, Wetzlar, Germany) from the middle region (containing the pelvic wall) in 30 μ m sections. The middle portion of the kidney was approximately divided to top, middle and bottom parts. One of every 5 sections was placed on polysine glass slides and using a random number generator, two sections from each region were imaged using Olympus BX53 upright microscope (Tokyo, Japan). A series of multiple images were captured using a 4X magnification lens and were digitally-stitched together using the real-time panoramic imaging option of CellSense software to create a full image of each kidney section. Areas stained with Lissamine green dye were visualized using the bright field filter of the microscope.

2.2.1.4. Atrial natriuretic peptide (ANP) assay

ANP was quantified in plasma samples at baseline (P2) and at the end of VE (P3) of the saline phase in sham (n=7) and CIH-exposed (n=7) groups using a quantitative sandwich ELISA kit (My BioSource, San Diego, CA, USA) as per the manufacturer's instructions. The kit is based on an interaction between ANP and horseradish peroxidase (HRP) detection antibody. The protocol involves the addition of chromogen solution A composed of hydrogen peroxide (H_2O_2) to each well to assist the interaction between HRP and chromogen solution B that is composed of tetramethylbenzidine substrate. The latter forms a blue complex which is converted into yellow solution after the addition of an acidic stop solution. Samples/standards and HRP-conjugated antibody were omitted from blank wells and replaced with buffer solution. Optical density was measured at 450 nm using a microplate

spectrophotometer (SpectraMax® M3, molecular devices, California, USA). Average optical density of blank wells was subtracted from average optical density of standards and samples wells. A standard curve was constructed with a cubic fitting between standards concentration and corresponding average of duplicate optical density readings.

During VE, the increase in plasma volume dilutes humoral factors within the systemic circulation despite their increased levels. Therefore, to account for the dilution factor of VE, ANP concentrations obtained from the kit were normalized by estimating plasma volume to calculate ANP amounts at baseline and at the end of the VE phase. Estimated plasma volume was calculated using the formula: *plasma volume estimate* = *GFR (body weight) (100/20)*, as 20% of the plasma volume passing through the glomerulus is filtered. GFR value at baseline was used to estimate plasma volume before the initiation of VE. GFR obtained at 30 minutes of VE was used to calculate plasma volume at the end of VE phase. The ANP amount at the end of VE (P3) was subtracted from the corresponding baseline (P2) amount to calculate delta (Δ) change in ANP during VE in each group.

2.2.1.5. Statistical analysis

Data in tables and within text are presented as mean \pm SD. Line figures are shown as mean \pm SE. Baseline MAP and HR were recorded for 2 minutes after arterial cannulation i.e. before retroperitoneal incisions were performed to expose the kidneys. The parameters in addition to RSNA were also recorded for 2 minutes after the stabilization period and were compared between groups using independent sample *t*-tests. Baseline RSNA was normalized using the maximum RSNA value recorded at the time of euthanasia, and is expressed as RSNA (% of max). Additional baseline values were recorded for 2 minutes before intra-renal infusion of saline/CPZ and for 30 minutes throughout infusion. Baseline values over a 2-minute period were averaged and compared between groups before and after the infusion of saline or CPZ using repeated-measures two-way ANOVA. To compare the changes in HR and MAP during VE, the last two minutes of each VE trial were averaged and compared with baseline values before VE. Values were compared between groups and at different time points during saline and CPZ phases using repeated-measures two-way ANOVA.

Renal sympatho-inhibitory response to VE was expressed as % of baseline (baseline=100%) and as RSNA (% of max), and was analysed using repeated-measures two-way ANOVA followed by a Bonferroni *post hoc* test to test for differences over time. The area under the curve (AUC) of RSNA % decrease vs. time was calculated for the VE trial period (without the recovery period) using the trapezoidal rule (358). Independent sample *t*-test and paired *t*-test were used for comparisons of AUC within and between groups during first and second VE trials with $P<0.0125$ taken as significant taking into consideration correction for multiple comparisons.

Baseline values for UF, GFR, and absolute and fractional Na^+ excretion at U1 and U2 were averaged and compared between CIH and sham groups and across trials, i.e. first vs. second VE using repeated-measures two-way ANOVA. During VE, the change in functional parameters over time in response to VE was analysed using repeated-measures two-way ANOVA followed by a Bonferroni *post hoc* test to indicate differences between groups at different time points. Similar to RSNA, the AUC of each functional parameter response was calculated and compared between groups and between the saline VE phase and CPZ VE phase using independent sample *t*-test and paired *t*-test, with $P<0.0125$ taken as significant, accounting for multiple comparisons.

High pressure baroreflex function curves were fitted according to a four-parameter logistic sigmoidal function equation that shows the relationship between MAP and RSNA or HR $[y=A1/(1+\exp(A2(x-A3)))+A4]$ where y is the RSNA or HR; $A1$, response range over which baroreceptors operate; $A2$, gain (curvature) coefficient; $A3$, mid-point blood pressure; $A4$, minimum response of RSNA or HR (166). During the infusion of PE and SNP, integrated RSNA were averaged per second and then divided on basal RSNA, which was calculated as an average of 2 minutes, to obtain RSNA (% of baseline). This was followed by the calculation of the average of RSNA (% of baseline) during a period of 5 mmHg change in MAP. Using the four-parameter equation, baroreflex parameters were calculated for each rat. Baroreflex parameters obtained from each rat were then used to construct the baroreflex curve for each exposure group by the calculation of RSNA (% of baseline) at fixed points of MAP using the four-parameter equation. The baroreflex function curve parameters (Figure 2.5) were compared between groups of the first cohort study using independent sample *t*-test and significance was taken at $P<0.05$. In addition, the relationship between MAP

and RSNA/HR during the assessment of the high pressure baroreflex was fitted using a five-parameter logistic sigmoidal equation $[y=A1/(1+f_x.\exp(A2(A3-x))+(1-f_x).\exp(A5(A3-x)))+A4]$ where $f_x=[1/(1+\exp(-\bar{c}(A3-x)))]$ and $\bar{c}=2(A2.A5)/(A2+A5)$ (214, 302). The meanings of the parameters are identical to the four-parameter equation where y is the RSNA or HR; $A1$, response range over which baroreceptors operate; $A3$, mid-point blood pressure; $A4$, minimum response of RSNA/HR. This equation describes the gain (curvature) coefficient as a function of two parameters, $A2$ and $A5$, estimating the gain of the upper and lower parts of the curvature, when the curve is asymmetrical. The four- and the five-parameter models merge when $A2$ and $A5$ are close to each other, enabling the curve to be symmetrical (302). Therefore, we used parameters obtained from the five-parameter model to calculate the index of asymmetry of RSNA/HR-MAP baroreflex curves (Appendix, Figure 8.1), $[\text{index of asymmetry}=2(A2-A5)/(A2+A5)]$. The index of asymmetry was analysed in CIH-exposed and sham rats using one-sample t -test to test if the mean asymmetry index is not different from zero. As shown in Figure 8.1 in appendix I, the mean asymmetry index of HR and RSNA baroreflex curves was not significantly different from zero in CIH-exposed and sham rats. It was shown that if there is no evidence of asymmetry, five-parameter equation is substituted by the four-parameter equation (302). Therefore, the analysis of the high pressure baroreflex was carried out using the four-parameter equation during the study.

Comparisons of baseline and Δ change in ANP between sham and CIH groups were performed using independent sample t -test and Mann-Whitney test. Significance was taken at $P<0.05$.

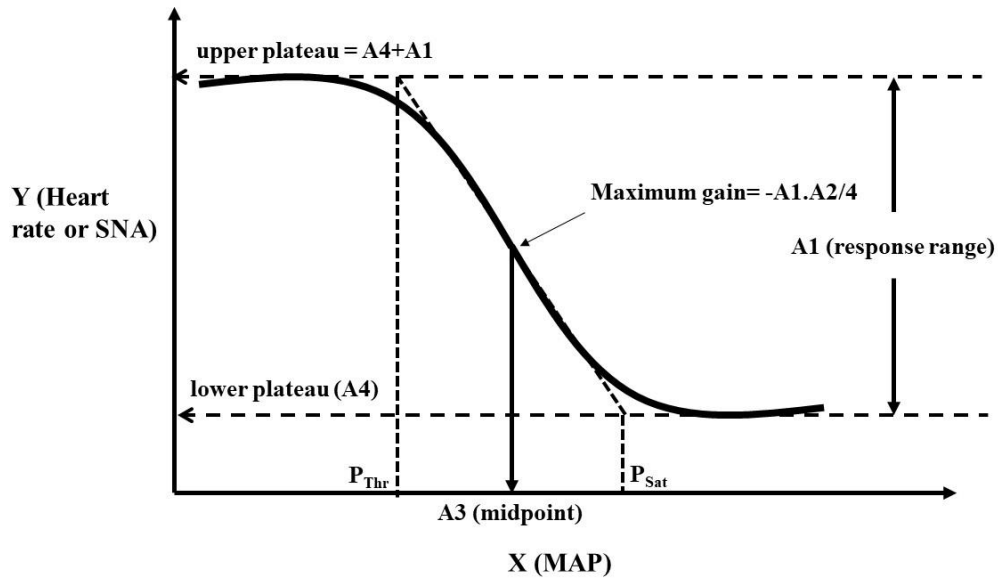


Figure 2.5. Logistic sigmoidal baroreflex function curve. P_{Thr} is threshold pressure at which the response begins and P_{Sat} is saturation pressure at which response start to reach its maximum. Maximum gain is the maximum sensitivity calculated at the midpoint pressure at which baroreceptors operate ($A3$). The slope (gain/curvature coefficient) is presented as $A2$. Upper ($A4+A1$) and lower ($A4$) plateaus reflect minimum and maximum responses. $A1$ is the RSNA/HR response range.

2.2.2. Second cohort experimental protocol

The experimental protocol of the second cohort study is shown in Figure 2.6 which is similar to the first cohort protocol with some exceptions. First, VE challenges and renal function measurements were not carried out. Therefore, saline was infused intravenously during the surgical protocol (3 ml/hr) instead of inulin. Second, intra-renal infusion of saline and CPZ was conducted into the right kidney and RSNA recording was from the left kidney. Third, animals were spontaneously breathing 27-32% O_2 through their tracheal cannula instead of room air.

The protocol involved exclusive assessment of the high-pressure baroreflex response in sham ($n=13$) and CIH-exposed ($n=10$) rats using PE and SNP during two successive phases. The first phase was after 30 minutes of intra-renal infusion of saline (17 μ l/min) and the second phase was after 30 minutes of intra-renal infusion of CPZ (5 μ g/ml at 17 μ l/min), similar to the first cohort protocol.

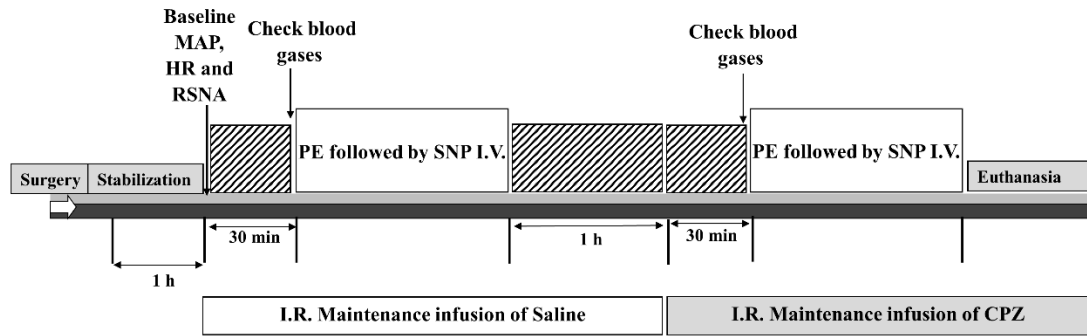


Figure 2.6. A schematic representation of the surgical protocol of the second cohort. Following a one-hour stabilization period, baseline cardiovascular parameters and RSNA were determined. After intra-renal infusion of saline to the right kidney for 30 minutes, phenylephrine and sodium nitroprusside were infused intravenously to elicit high-pressure baroreflex responses. Following the first assessment of the baroreflex (saline phase), one hour was allowed for parameters to recover during which intra-renal infusion of saline into the right kidney was maintained. For the second phase, intra-renal infusion of CPZ was initiated for 30 minutes into the right kidney followed by a second intravenous infusion of phenylephrine and sodium nitroprusside to assess high-pressure baroreflex (CPZ phase). Arterial blood was sampled before the beginning of each assessment to check blood gases using I-STAT. MAP, mean arterial blood pressure; HR, heart rate; RSNA, renal sympathetic nerve activity; I.V., intravenous; I.R., intra-renal; CPZ, capsaizepine; PE, phenylephrine; SNP, sodium nitroprusside.

2.2.2.1. Statistical analysis

Data in tables and within text are presented as mean \pm SD. Line figures are shown as mean \pm SE. Baseline analysis was carried out similar to cohort 1 described in section 2.2.1.5.

High pressure baroreflex function curves were fitted according to a four-parameter logistic sigmoidal function equation that shows the relationship between MAP and RSNA or HR $[y=A1/(1+\exp(A2(x-A3)))+A4]$ where y is the RSNA or HR; $A1$, response range over which baroreceptors operate; $A2$, gain coefficient; $A3$, mid-point blood pressure; $A4$, minimum response of RSNA or HR (166). Baroreflex function curve parameters (Figure 2.5) were compared between sham and CIH groups using independent sample t -tests. Baroreflex gain curve parameters during the first (saline) and second (CPZ) phase were compared using paired t -tests. Significance was taken at $P<0.0125$, accounting for multiple comparisons.

2.2.3. Third cohort experimental protocol

2.2.3.1. Intra-renal pelvic infusions

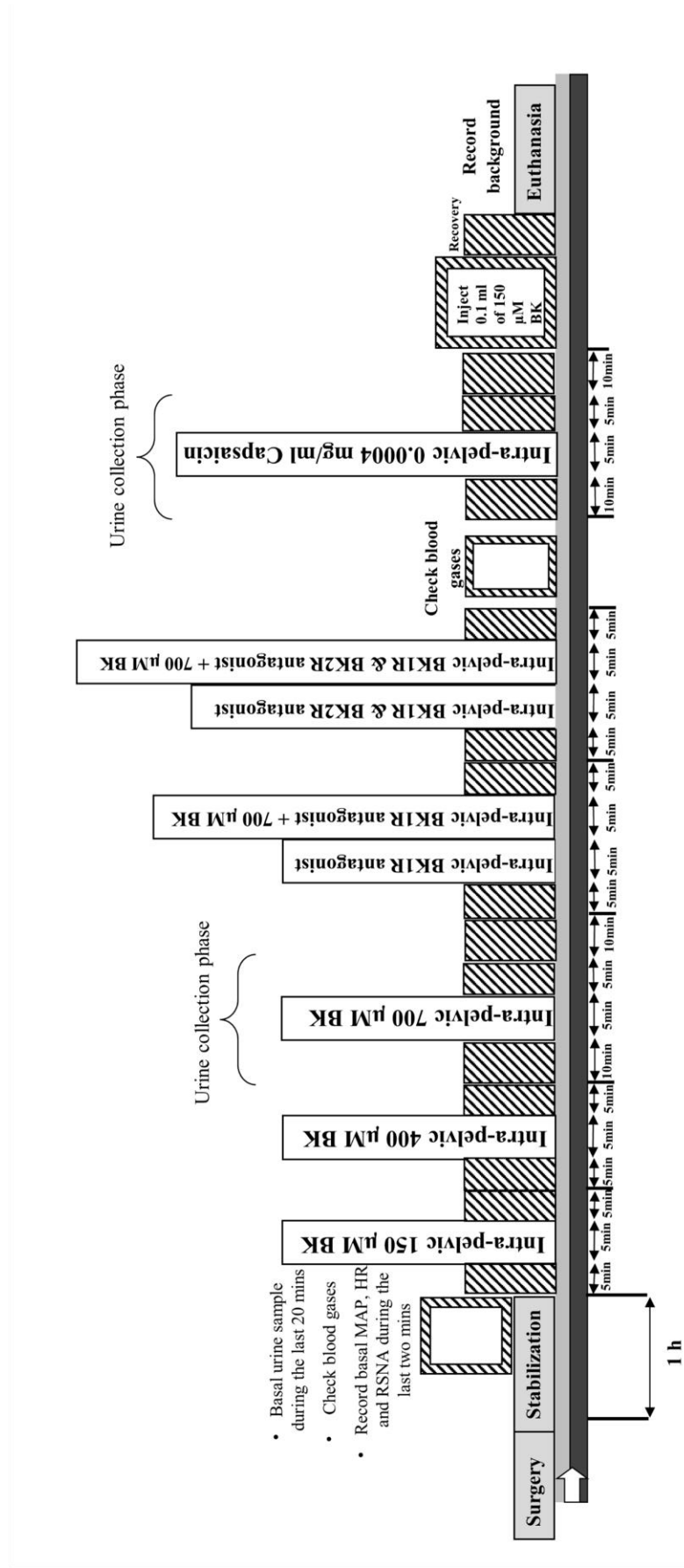
The experimental protocol of the third cohort study is described in Figure 2.7. Rats were spontaneously breathing 27-32% O₂ through their tracheal cannula instead of room air to maintain partial pressure of oxygen in arterial blood \geq 85 mmHg. After surgical instrumentation, a stabilization period of one hour was allowed and baseline MAP, HR and RSNA was recorded for two minutes. A blood sample was analysed using an I-STAT system (Abbott Laboratories, Abbott Park, IL, USA) at the end of the stabilization period to check blood gases and adjust percentage of oxygen supply. Intravenous inulin (FITC-inulin in saline, 10 mg/kg/hr) infusion started at the beginning of the stabilization period and continued throughout the whole surgical protocol. During the last 20 minutes of stabilization, a urine sample was collected from the contralateral left kidney to measure basal kidney function.

Thereafter, protocols of intra-renal pelvic infusion of different drugs were commenced. Each intra-renal pelvic infusion protocol involved: a 5-minute baseline period, during which saline was infused into the renal pelvis of the right kidney; an experimental phase for 5 minutes during which an agonist and/or an antagonist was infused; followed by 5 minutes infusion of saline to washout the renal pelvis (Recovery). Meanwhile, for 0.4 μ g/ml capsaicin and 700 μ M bradykinin, the baseline period was sustained for 10 minutes and an additional recovery phase of 10 minutes was added at the end of the protocol. All intra-renal pelvic infusions of the right kidney were carried out at 20 μ l/min. Using a random number generator, the order of infusion of bradykinin concentrations (150, 400 and 700 μ M) through the renal pelvic cannula was determined. Following the end of bradykinin infusions, a bradykinin receptor type 1 (BK1R) blocker, Lys-(des-Arg9, Leu8)-Bradykinin (42 μ M, Sigma-Aldrich), was infused into the renal pelvis for 5 minutes, followed by an immediate infusion of a mixture of Lys-(des-Arg9, Leu8)-Bradykinin with 700 μ M bradykinin for another 5 minutes, followed by a 5-minute recovery phase. The next protocol involved intra-renal pelvic infusion of Lys-(des-Arg9, Leu8)-Bradykinin (42 μ g/ml) and BK2R antagonist, Bradyzide (46 μ M, Sigma-Aldrich), for 5 minutes, followed by an immediate infusion of a mixture of Lys-(des-Arg9, Leu8)-Bradykinin, bradyzide and 700 μ M bradykinin for another 5 minutes. The protocol was completed with a 5-

minute recovery phase. Before proceeding to capsaicin infusion, a blood sample was taken from the arterial line for I-STAT system analysis to check blood gases. This was followed by an intra-renal pelvic infusion of capsaicin (0.4 µg/ml). During the basal, experimental and recovery phases of all aforementioned infusions, MAP, HR and RSNA were recorded.

At the end of the protocol, bradykinin was infused (150 µM, 0.1 ml, at 0.3 ml/min) through the intravenous line during which MAP, HR and RSNA responses were recorded. This step was performed to confirm that the intra-renal pelvic-induced responses were not baroreflex-mediated by blood pressure fluctuations due to spill-over of intra-pelvic infusion into the systemic circulation.

Similar to cohorts 1 and 2, animals were euthanized by an intravenous overdose of anaesthesia (mixture of 80 g/kg urethane and 55 mg/kg α-chloralose), during which RSNA reaches a maximum level due to the sudden drop of blood pressure. This was followed by a complete disappearance of RSNA peaks and this part of the recording was used to measure background noise, which was subtracted from all recordings.



Blood gases were analysed and followed by the adjustment of oxygen supply to have PO_2 level of >85 mmHg. For any metabolic acidosis, 0.2-0.3 ml of 1M sodium bicarbonate was injected.

Figure 2. 7. A schematic representation of the surgical protocol of the third cohort. At the end of one-hour stabilization period, baseline cardiovascular parameters and RSNA were determined. A urine sample was collected at the end of the stabilization period for the measurement of basal kidney function parameters. All subsequent infusions of drugs were carried out through the renal pelvis of the right kidney. The protocol of each infusion involved a baseline period of 5 minutes during which saline was infused, followed by the infusion of the agonist and/or antagonist for 5 minutes (experimental phase) and a washout period of 5 minutes, during which saline was infused (recovery phase). Meanwhile, the protocol of the highest concentration of bradykinin and capsaicin involved longer baseline durations of 10 minutes and longer washout periods of 15 minutes. The order of infusion of different bradykinin concentrations was selected randomly, and the order shown in the scheme is an example. The “Urine collection” phase represents the collection of a urine sample 10 minutes during the intra-renal pelvic infusion of saline (baseline), followed by subsequent collection of a urine sample for 5 minutes during drug infusion, and another urine sample for 5 minutes immediately after the end of infusion of drugs. BK, bradykinin; BK1R, bradykinin receptor type 1; BK2R, bradykinin receptor type 2; MAP, mean arterial pressure; HR, heart rate; RSNA, renal sympathetic nerve activity; PO_2 , partial pressure of oxygen in arterial blood.

2.2.3.2. Measurement of Excretory Parameters

Urine samples were collected from 6 sham rats and 6 CIH-exposed rats for the analysis of kidney function. At the end of stabilization period, a urine sample during a period of 20 minutes was collected to measure basal urine flow (UF) and basal absolute Na⁺ excretion. Urine samples were collected over 10-minute periods of baseline (U_{basal}) before the intra-renal pelvic infusion of 0.4 µg/ml capsaicin or 700 µM bradykinin. Moreover, two urine samples were collected during the 5-minute infusion of capsaicin (U_{Exp}) or 700 µM bradykinin, and during a 5-minute period post-infusion of capsaicin or 700 µM bradykinin (U_{Rec}).

Urine volume was measured gravimetrically and UF was calculated as: $UF = Uv/t$; Uv is urine volume, t is time of urine collection. Urinary Na⁺ concentration was measured using flame photometry (M410, Sherwood Scientific, Cambridge, UK). Absolute Na⁺ excretion was calculated using the formula: $[UNa^+].UF$; $[UNa^+]$ is urinary Na⁺ concentration.

2.2.3.3. Validation of concentrations of bradykinin and capsaicin

The concentrations of bradykinin used were based on previous reno-renal reflex studies (101, 187). Moreover, we conducted a pilot study on 6 control male Wistar rats of similar age to rats used in the main study. We infused 150, 400 and 700 µM bradykinin through the renal pelvic route of 4 rats, while 700, 1000 and 1500 µM bradykinin were infused into the renal pelvis of two other rats. The RSNA (% of baseline) responses during the last minute of the infusion were plotted against corresponding concentrations of bradykinin to draw a dose-response curve. As a result, concentrations of bradykinin of 150, 400 and 700 µM were selected for subsequent use in the main experiment. Additionally, we tested three concentrations of capsaicin that were used in a previous reno-renal reflex study (192): 0.4, 10 and 100 µg/ml. The first concentration i.e. 0.4 µg/ml was infused into the renal pelvic wall of 8 rats and the other two concentrations were tested in 3-4 rats. The maximum change in RSNA during infusion was compared and 0.4 µg/ml of capsaicin was chosen for the main study.

2.2.3.4. Possible desensitization of bradykinin receptors

In six control male Wistar rats of similar age to rats used in the main study, bradykinin of 700 μM was infused repeatedly three times through the intra-renal pelvic route. The protocol used was similar to the one used in the main study: a 5-minute baseline period, during which saline was infused into the renal pelvis of the right kidney; an experimental phase for 5 minutes during which 700 μM bradykinin was infused; followed by 5 minutes and further 10 minutes infusion of saline to washout the renal pelvis (Recovery). This protocol was repeated for another two successive times. During infusions, MAP, HR and RSNA were recorded.

2.2.3.5. Statistical analysis

Data in tables and within text are shown as mean \pm SD and line figures are displayed as mean \pm SE. Baseline MAP and HR were averaged for 2 minutes before arterial cannulation i.e. before retroperitoneal incisions to expose the kidneys. Additional baseline values of MAP and HR, in addition to RSNA, were recorded for two minutes at the end of the stabilization period. All baseline parameters were compared between sham and CIH-exposed rats using independent sample *t*-test. Baseline RSNA values were expressed as absolute values ($\mu\text{V.s}$) or as a percentage of maximum value (% of max). The latter is calculated by the normalization of RSNA values to the maximum RSNA obtained during euthanasia by an overdose of anaesthesia.

During the intra-renal pelvic infusion of bradykinin, capsaicin and bradykinin receptor antagonists, MAP, HR and RSNA were recorded and averaged for 5 minutes prior to the start of the infusion, which represents a baseline reading. Thereafter, during the infusion of each drug, MAP, HR and RSNA were recorded and averaged for every 30 seconds until the end of the 5-minute infusion period. This was followed by averaging parameters for every minute during the 5-minute period of recovery phase (during the intra-renal pelvic infusion of saline). Averaged values of MAP, HR and RSNA were plotted against time, taking into consideration the baseline averaged value at zero time. HR was expressed either as an absolute value or in terms of change in HR from baseline value (ΔHR). Similarly, RSNA responses during infusions were expressed in

two fashions; in terms of percentage change from baseline recording (% of baseline, baseline = 100%) and as absolute values normalized to maximum RSNA obtained during euthanasia (% of max).

Responses of MAP, HR, Δ HR, RSNA (% of baseline) and RSNA (% of max) to the intra-renal pelvic infusion of drugs were analysed using repeated measures two-way ANOVA followed by a Bonferroni *post hoc* analysis to test responses over time (Exposure x Time). The same analysis was carried out to test cardiovascular and RSNA responses during the intra-renal pelvic infusion of bradykinin receptor antagonists before the infusion of bradykinin, with $p < 0.05$ taken as significant.

The AUC of RSNA and HR responses vs. time was calculated using the trapezoidal rule, without considering the recovery phase. The AUC values were analysed using repeated measures two-way ANOVA followed by a Bonferroni *post hoc* test (Exposure x Bradykinin concentration). Similarly, the AUC of responses to the intra-renal pelvic infusion of 700 μ M bradykinin, 700 μ M bradykinin with an antagonist of BK1R, and 700 μ M bradykinin with BK1R and BK2R antagonists, were analysed using repeated measures two-way ANOVA followed by a Bonferroni *post hoc* test (Exposure x Drug). Significance was taken at $p < 0.05$.

To compare intra-renal pelvic with intravenous infusion of 150 μ M bradykinin, the minimum of MAP, an average of 30 seconds, that was attained during infusions were subtracted from basal MAP (Δ MAP) to compare between the two routes of infusion and exposure groups by repeated measures two-way ANOVA. Similarly, HR and RSNA were averaged every 30 seconds. The maximum change in HR (Δ HR) and RSNA (% of baseline) were analysed using repeated measures two-way ANOVA followed by Bonferroni *post hoc* analysis. Significance was taken at $p < 0.05$.

Basal UF and absolute Na^+ excretion were calculated from a urine sample that was collected over a period of 20 minutes, and were compared between groups using independent sample *t*-test. During the infusion protocol of capsaicin and the 700 μ M bradykinin, baseline urine sample was collected for 5 minutes prior to infusion, for 5 minutes during the infusion and 5 minutes post infusion. The three urine samples were used to compare between CIH-exposed and sham rats in terms of responses of UF and absolute Na^+ excretion using repeated measures two-way ANOVA (Exposure x time). Significance was taken as $p < 0.05$.

2.3. Tissue preparation

In separate studies, male Wistar rats were either exposed to 14 days of CIH or to normoxia as described previously (section 2.1). On day 15, rats were euthanized by an overdose of intra-peritoneal sodium pentobarbital (Dolethal (200 mg/ml), Vetoquinol, France, 60 mg/kg). The left kidney was collected and halved along its sagittal plane. Each half was cut transversely into three sections: top, middle (containing the pelvic wall) and bottom. Sections were preserved at -80°C for later use. Immediately after harvesting the left kidney, the left renal artery and vein were closed by a bulldog clamp. Intra-cardiac puncture via the left ventricle was performed and warmed heparinized saline (~ 63 U/ml) was infused. The rate of infusion was 35 ml/min, which was raised gradually to 60 ml/min until 250-300 ml of heparinized saline was infused into each animal. This was followed by infusion of 4% paraformaldehyde at an infusion rate of 60 ml/min (Formalin solution, neutral buffered, 10%, Sigma-Aldrich, St. Louis, MO, USA) to fix organs including the right kidney for staining purposes. The upper and lower poles of the right kidney were removed, and the remnant kidney was either post-fixed for 24 hours for immunofluorescence, or wax-embedded in paraffin. Some kidneys that were harvested from sham and CIH-exposed rats that underwent surgical procedures were also perfusion-fixed and wax-embedded in paraffin. Paraffin blocks were stored at 4°C until sectioning for histological assessment. In separate sham (n=6) and CIH-exposed rats (n=6) that were not perfusion-fixed, the right kidneys were removed and after removal of the upper and lower poles, were directly post-fixed in formalin solution for 24 hours. Then, fixed tissues were incubated in 20% sucrose until the tissue sank in solution. Next, kidneys were frozen in optimal cutting temperature compound and stored at -80°C for subsequent use in immunofluorescence studies.

The middle part of the left kidney was homogenized (Omni tissue homogeniser, Kennesaw, Georgia, USA) in a buffer made of: 10X RIPA lysis buffer, deionized H₂O, sodium fluoride (200mM), phenylmethylsulfonyl fluoride (100 mM) and protease cocktail inhibitor [(5 mM EDTA, 1 mM EGTA, 5 µg/ml leupeptin, 5 µg/ml aprotinin, 2 µg/ml pepstatin, 120 µg/ml Pefabloc, 2 mM 1,10-phenanthroline and sodium orthovanadate (200 mM) (Sigma-Aldrich)]. Samples were homogenized on ice using 10 X 10 sec bursts separated by 10 sec periods. Homogenates were kept on ice for 20

minutes with intermittent vortex. Samples were then centrifuged at 15,339 *g* at 4°C for 15 minutes. The supernatant was aliquot into ice-cold Eppendorf tubes and stored at -80°C for use in an Advanced Oxidation Protein Products (AOPP) assay (Cell Biolabs, San Diego, CA), superoxide dismutase (SOD) and catalase activity assays (sham, n=12; CIH, n=8) (Cayman Chemical, Ann Arbor, MI, USA). Supernatant was also used for TRPV1, bradykinin 1 and bradykinin 2 receptors (Mybiosource, Tokyo, Japan) ELISA assays to determine protein abundance. The same homogenization protocol was used to prepare samples for the assessment of NADPH oxidase (NOX) activity and to determine the concentrations of inflammatory cytokines in renal tissue (sham, n=11; CIH, n=10) except for the use of a lysis buffer made of Tris-HCL (20 mM, pH 7.5, Sigma-Aldrich), sodium chloride (150 mM) and 1% Triton-X-100 (Molekula, Dorset, UK) instead of RIPA during homogenization. In a separate cohort, pelvic walls of left kidneys were isolated and harvested from 4 CIH and 4 sham rats and were preserved at -80°. In addition, pelvic walls of left kidneys were isolated from 2 CIH and 2 sham rats post-surgery and were also preserved at -80°. The same homogenization protocol described above was carried out to homogenize pelvic wall samples for subsequent use in CGRP, bradykinin receptors 1 and 2 ELISA assays. A bicinchoninic protein assay (Pierce Biotechnology, Fisher scientific, Ireland) using bovine serum albumin standards was conducted prior to the performance of each biochemical assay to determine protein concentrations of kidney and pelvic wall tissue homogenates.

2.4. Biochemical assays

All assays were conducted in duplicate and readings were carried out using a microplate spectrophotometer (SpectraMax® M3, molecular devices, California, USA) and SoftMax Pro 6.2.2 software.

2.4.1. TRPV1 ELISA

TRPV1 cation channel expression in kidney tissues of sham (n=12) and CIH (n=8) rats was quantified using a competitive enzyme immunoassay ELISA kit as per the manufacturer's instruction. The plate was pre-coated with an anti-TRPV1 antibody. Samples and TRPV1-HRP conjugate were incubated in the plate together for one hour at 37° to compete for the antibody binding site. Then, a substrate for HRP enzyme is added to each well. The substrate and TRPV1-HRB conjugate forms a blue coloured complex and a stop solution will convert the blue coloured solution into yellow. The absorbance was measured at 450 nm using a microplate reader. The binding sites of TRPV1 antibody are limited and if TRPV1 from sample binds to the antibody, there will be less available binding sites to TRPV1-HRB conjugate. Therefore, colour intensity produced was inversely proportional to the amount of TRPV1 in samples. In blank wells, TRPV1-HRB conjugate was omitted and sample was replaced with an equivalent volume of phosphate-buffered saline. Absorbance obtained from kit standards were plotted against their concentration using a four-parametric logistic fit. Concentration of TRPV1 in each sample was calculated based on corresponding mean absorbance value from the standard curve and was multiplied by the appropriate dilution factor.

2.4.2. Bradykinin receptor 1 ELISA assay

Bradykinin receptor 1 expression in kidney tissues of sham (n=11) and CIH-exposed (n=8) rats and in pelvic wall of 6 sham and 6 CIH-exposed rats was quantified using a competitive enzyme immunoassay similar in principle to the TRPV1 ELISA. The kit involved a microplate pre-coated with a polyclonal bradykinin 1 receptor antibody. Wells were filled with samples or standards and incubated with bradykinin receptor

1-HRP conjugate for one hour at 37°. Then, a substrate for HRP enzyme is added to each well that resulted in a blue coloured complex formation. Stop solution turned solution colour into yellow and absorbance was measured at 450 nm using a spectrophotometer. Colour intensity was inversely proportional to the abundance of bradykinin receptor 1 in samples. Bradykinin receptor 1- HRP conjugate was omitted from blank wells and samples/standards were replaced with an equivalent volume of phosphate-buffered saline. Analysis of results was similar to that described for the TRPV1 ELISA.

2.4.3. Bradykinin receptor 2 ELISA assay

Bradykinin receptor 2 expression in kidney tissues of sham (n=12) and CIH-exposed (n=8) rats and in pelvic wall of 4 sham and 4 CIH-exposed rats was quantified using sandwich enzyme immunoassay kit as per manufacturer's instructions. The assay principle is similar to the CGRP assay and is based on the use of a microplate that is pre-coated with bradykinin receptor 2 specific antibody. Samples and standards were incubated for one hour at 37° which was followed by an hour incubation with biotin-conjugated antibody. Then, avidin attached to HRP was added to each well for 30 minutes at 37°. Then, tetramethylbenzidine substrate was added to each well to develop a blue colour. Blank wells were included containing an equivalent volume of phosphate-buffered saline instead of sample. The optical density was measured at 450 nm using a spectrophotometer and optical density values (Log x-axis) were plotted against standards concentrations (Log y-axis) and a fit-line was drawn. Protein concentration of bradykinin receptor type 2 in each sample was calculated based on corresponding mean optical density logarithmic values of the curve with subsequent multiplication of the appropriate dilution factor.

2.4.4. AOPP assay

AOPP OxiSelect assay kit is used as a measurement of total oxidative stress. These products are oxidative toxins such as chloramines and hypochlorous acid that are produced from the reaction of proteins with chlorinated oxidants. Kidney tissue homogenates from sham (n=12) and CIH-exposed (n=8) rats were de-frosted on ice

and the protocol was followed as per the manufacturer's instruction. In each well, a chloramine reaction initiator and sample were incubated together for 5 minutes at room temperature. AOPP in the biological sample will cause the formation of chloramines. Absorbance was measured at 340 nm which correspond to chloramine concentration as chloramine equivalents (μM). Sample diluent was added to blank wells instead of sample/standard. Absorbance obtained from kit standards were plotted against chloramine concentration (μM) and a linear best-fit line was drawn. Concentration of chloramine in sample was calculated corresponding to the mean optical density value of the standard curve and was multiplied by the appropriate dilution factor.

2.4.5. NOX activity assay

NOX activity in sham (n=11) and CIH-exposed (n=10) groups was assessed using a protocol that depends on formazan blue formation from the reaction of nitroblue tetrazolium (NTB) with superoxide radicals generated by NOX enzymes present in biological samples as previously detailed (301) (Figure 2.8). A cocktail was prepared that contained: NTB, sodium cyanide and diethylene-triamine-penta-acetic acid, all in Tris-HCl pH 8 buffer. A fresh solution of NADPH (1mM) was also prepared and kidney tissue homogenates were diluted using Tris-HCl pH 8. Each well was filled with 20 μl of sample, 250 μl of cocktail and 30 μl of NADPH solution. In blank wells, samples were replaced with an equivalent volume of diethylene-triamine-penta-acetic acid in pH 8 buffer. Absorbance was then measured at 560 nm at room temperature every 20 sec for 40 minutes. NOX activity was expressed as the slope of formazan blue formation, taking into consideration the linear part of the reaction curve (between 3 and 30 minutes).

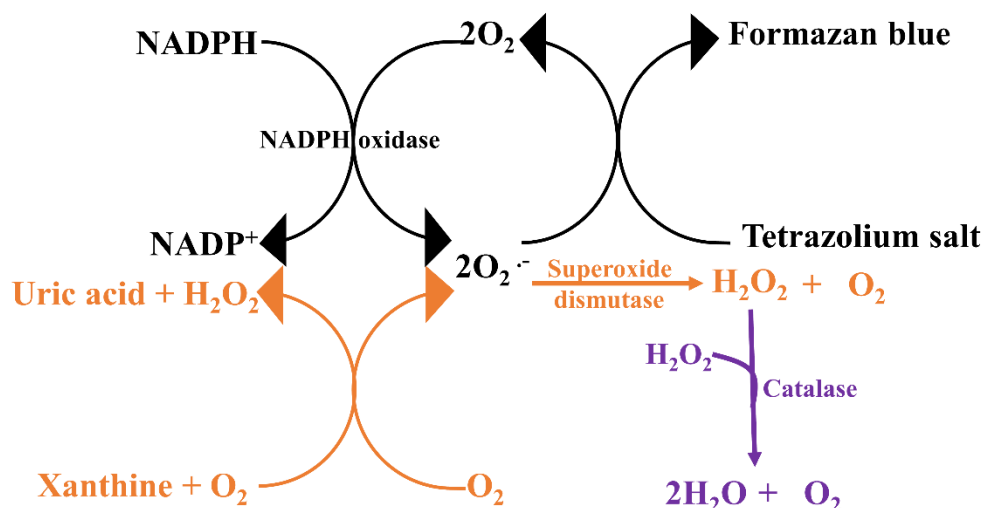


Figure 2.8. Formation and dismutation of superoxide radicals. The black scheme shows NADPH oxidation conjugated with the generation of superoxide radicals. NADPH oxidase assay is based on the conversion rate of tetrazolium salt to formazan blue through redox reaction mediated by superoxide radicals. The orange scheme shows the principle of the superoxide dismutase assay which depends on the dismutation of superoxide radicals to hydrogen peroxide (H₂O₂). Each two molecules of H₂O₂ are subsequently detoxified to water and oxygen molecules through the reductive activity of catalase enzyme (purple scheme).

2.4.6. SOD activity assay

SOD catalyses the conversion of oxygen radicals to oxygen and H₂O₂ (an antioxidant mechanism, Figure 2.8). SOD activity in sham (n=12) and CIH-exposed (n=8) groups was assessed as per the manufacturer's instructions. The assay protocol reflects SOD total activity and does not differentiate the activity of Cu/Zn, Mn and FeSOD. The assay utilizes tetrazolium salt which is converted to formazan blue by superoxide radicals. Superoxide radicals were generated in each well by the addition of xanthine oxidase enzyme and hypoxanthine. Higher activity of SOD in wells is associated with greater dismutation of superoxide radicals; thus less formation of formazan blue and less colour intensity. SOD standard/tissue sample were incubated with assay reagents for 30 minutes at room temperature. A blank was carried out for each sample while wells of zero standard concentration were considered as a blank for all standards wells. All reagents were added to blank wells except that xanthine oxidase was replaced by sample buffer. Absorbance was measured at 450 nm and SOD activity was expressed

as unit/ml using a linear standard curve. The background absorbance of each blank well was subtracted from corresponding average sample absorbance. One unit of SOD reveals the amount of enzyme needed to exhibit 50% dismutation of superoxide radicals.

2.4.7. Catalase activity assay

This protocol was performed for kidneys harvested from sham (n=12) and CIH-exposed (n=8) groups. Catalase is an oxidoreductase enzyme that retains reduction and peroxidation activities. The reductive activity of catalase enzyme involves the conversion of H₂O₂ to two molecules of water and one molecule of oxygen (Figure 2.8, purple scheme). The peroxidative activity principle is used in the assay protocol to convert H₂O₂ in presence of methanol to formaldehyde and two molecules of water (Figure 2.9). The reaction was carried out for 20 minutes at room temperature. As a final step, purpald (4-Amino-3-hydrazino-5-mercapto-1,2,4-triazole) was added to each well which was oxidized by the formaldehyde generated to a purple product. Blank wells were composed of all reagents except for the sample/standard. Absorbance was measured at 540 nm and absorbance values were plotted against formaldehyde standards concentrations. One unit is equivalent to the amount of enzyme required to generate 1 nmol of formaldehyde per minute.



Peroxidase activity

Figure 2.9. The peroxidase activity of catalase enzyme.

2.4.8. Renal inflammatory cytokines

Pro-inflammatory and anti-inflammatory cytokines (IFN- γ , IL-1 β , IL-4, IL-5, IL-6, keratinocyte chemoattractant/growth related oncogene, IL-10, IL-13, and TNF- α) were analysed by sandwich immunoassay method using V-plex proinflammatory panel 2 rat kit (Meso Scale Discovery, Rockville, MD, USA), as per the manufacturer's instructions. One-hundred micrograms of protein from tissue

homogenate was added to sample wells of a multi-spot plate. The bottom of each well was made of a high binding carbon electrode attached to 9 different capture antibodies at 9 different specific locations of each well to detect different cytokines. Standards/samples were incubated in wells for two hours at room temperature. After multiple washings, a detection antibody conjugated with sulfo-tag labels was added to each well for one hour at room temperature. Plate was analysed using QuickPlex SQ 120 plate reader (Meso Scale Discovery) that applies electricity to plate electrodes which generates electrochemiluminescence from attached sulfo-tag labels. The intensity of each emitted light is directly proportional to the amount of each different cytokine in samples. A linear standard curve was constructed and the amount of cytokines in samples was calculated, taking into consideration dilution factor thereafter. IL-1 β , TNF- α and keratinocyte chemoattractant/growth related oncogene were successfully measured. All other cytokines were below the detection limits of this kit.

2.5. Immunofluorescence

Frozen, formalin-fixed kidneys were sectioned to 20 µm sagittal sections using a cryostat (Leica Biosystems, Wetzlar, Germany). Every two subsequent sections were mounted onto polysine-coated glass slides (VWR, Belgium) and stored at -80°C. Three sections that contained the renal pelvic wall were randomly selected from each kidney by systematic random sampling. Generally, slides were washed in phosphate-buffered saline three times each of 15 minutes duration. Following each incubation in blocking solution, with primary and secondary antibodies, slides were washed in phosphate-buffered saline three times each of 15 minutes duration. At the end of each protocol, sections were covered with anti-fade mounting medium (Vectashield, Vector laboratories, Burlingame, CA, USA) and coverslip (Thickness No 1.5, VWR, Belgium).

2.5.1. TRPV1 receptors

Immunofluorescence for TRPV1 protein expression in the renal pelvic wall was carried out on 3 CIH-exposed and 3 sham kidneys that were perfusion-fixed and post-fixed, in addition to 6 CIH-exposed and 5 sham kidneys that were only post-fixed. Non-specific binding was blocked by incubating sections in 5% goat serum and 1% bovine serum albumin (with 0.5% triton-X) for one hour. Then, sections were incubated with rabbit polyclonal anti-TRPV1 antibody (1:200, ACC-030, Alomone labs) diluted with 5% goat serum, 1% bovine serum albumin and 0.5% triton-X for two hours at 37°C. Sections were incubated with goat anti-rabbit FITC secondary antibody (1:100, Sigma-Aldrich, St. Louis, MO, USA) diluted in phosphate-buffered saline (mixed with 2µg/ml DAPI, Sigma-Aldrich, Saint Louis, MO, USA) for two hours at room temperature.

2.5.2. CGRP and NK1 receptor

Indirect immunofluorescence was carried out to examine the protein expression and the co-localization of CGRP and NK1 receptor in renal pelvic wall. Kidneys were harvested from 3 CIH-exposed and 2 sham rats that were perfusion-fixed and post-

fixed, in addition to, kidneys harvested from 6 CIH-exposed and 7 sham rats that were post-fixed only. Sections were blocked for one hour in 5% goat serum and 1% bovine serum albumin (mixed with 0.3% Triton-X). Sections were incubated with rabbit polyclonal anti-CGRP IgG antibody (1:500, Sigma-Aldrich, Saint Louis, MO, USA) or mouse monoclonal anti-NK1 IgG1 antibody (1:200, Invitrogen, Illinois, USA) diluted with 5% goat serum and 1% bovine serum albumin (mixed with 0.3% Triton-X) for two hours at 37°. For co-localization purpose, both primary antibodies were mixed in one solution of the same diluent and composition.

For CGRP detection, sections were then incubated with goat anti-rabbit FITC IgG secondary antibody (1:100, Sigma-Aldrich, St. Louis, MO, USA) diluted with 1% bovine serum albumin for two hours at room temperature. For NK1 receptor analysis, sections were incubated with goat anti-mouse IgG Fc γ subclass 1 Alexafluor 594 antibody (Jackson ImmunoResearch, West grove, Pennsylvania, USA) diluted with 5% goat serum, 1% bovine serum albumin and 0.3% Triton-X in phosphate-buffered saline. All secondary antibody solutions contained 4 μ g/ml DAPI. For co-localization, both secondary antibodies were prepared in one solution and using same concentrations in 5% goat serum, 1% bovine serum albumin and 0.3% Triton-X.

2.5.3. Image analysis

Images were captured using a laser scanning confocal microscope (Olympus FV1000-IX71, Tokyo, Japan) provided with excitation lasers of 488 nm (for CGRP and TRPV1 detection), 543 nm (for NK1 receptor detection) and 408 nm (DAPI). Before imaging, slides labels were covered with a sticker and marked with a random number to blind from the treatment group during imaging.

For TRPV1 analysis, sections were initially visualized using 20X magnification under the DAPI filter and three regions of the pelvic wall were randomly selected from each section. After selection, the 488 nm laser was switched on to capture images. Positive staining was detected in the uroepithelial layer and submucosa/ muscularis propria layers of the pelvic wall. A similar imaging procedure was used for CGRP and NK1 detection except that one region of the pelvic wall was randomly selected from each section and the 543 nm laser was switched on to capture NK1 images of selected

regions. Positive staining of CGRP and NK1 was mainly detected within the muscularis propria of renal pelvic wall.

Images were transferred to greyscale and the threshold was adjusted to highlight the area occupied by positive fluorescent labelling using Image J software. Threshold area was calculated and normalized to the total area of the uroepithelium within the image to quantify the expression of TRPV1 in that region. Similarly, threshold TRPV1 area in the submucosa and muscularis propria layers were calculated and normalized to the total layer area identified in the image. For CGRP and NK1, threshold area was normalized to the total area of the pelvic wall in each image. Data are expressed as a percentage of area occupied by positive labelling.

For CGRP analysis, results were collected from 9 CIH-exposed and 9 sham kidneys. For NK1 receptor analysis, a kidney from each group was excluded due to poor signal to noise ratio; thus, thresholding difficulty. Therefore, for the latter, data were obtained from 8 CIH-exposed and 8 sham kidneys. Meanwhile, data from 9 CIH-exposed and 8 sham kidneys were analysed for TRPV1 detection.

2.6. Renal histopathological staining

Paraffin blocks were cross-sectioned to 10 μ m tissue sections using a rotary microtome (Leica RM2135, Germany). Kidneys were taken from sham (n=3) and CIH-exposed (n=5) rats that underwent surgical procedures as well as from rats euthanized following exposure to gasses without undergoing surgery (sham, n=5; CIH, n=3). Four of 10 kidney sections were held on polysine-coated glass (VWR, Belgium). Two sections were randomly selected by random number generator each from the upper, middle and bottom parts of the paraffin block (a total of 6 sections from each kidney block).

2.6.1. Haematoxylin and eosin stain

The protocol for staining was carried out as follows:

- Sections were de-waxed using Neo-Clear® xylene substitute (Merck, Darmstadt, Germany) three times each of 3 minutes.
- Sections were washed with down-graded levels of ethanol (100% for two minutes, 95% for one minute and 70% for one minute). This was followed by immersing sections in distilled water for one minute.
- Tissue sections were then stained in haematoxylin (Haematoxylin Solution, Harris Modified, Sigma-Aldrich, St. Louis, MO, USA) for 6 minutes followed by washing in distilled water for one minute.
- Haematoxylin stain was differentiated by immersing sections in 0.3% hydrochloric acid prepared in 70% ethanol.
- Sections were washed in distilled water for one minute followed by another washing in Scott tap water (Sigma-Aldrich, St. Louis, MO, USA) for another minute.
- Sections were then stained with eosin (Surgipath Europe LTD, Cambridgeshire, UK) for two minutes.
- Sections were dehydrated in 95% ethanol (one minute) and 100% ethanol (three times, each of one minute duration).
- As a final step, sections were cleared in Neo-Clear® xylene substitute (three times, each of one minute duration)

- Sections were mounted with DPX mounting medium (Sigma-Aldrich, St. Louis, MO, USA) and cover-slipped (Thickness No 1, VWR, Belgium).

2.6.2. Sirius red stain

The protocol for staining was carried out as follows:

- Sections were cleared using Neo-Clear® xylene substitute and washed in graded levels of ethanol in a similar fashion as for the haematoxylin and eosin staining protocol.
- Slides were dipped in 0.1% Direct red 80 (Sigma-Aldrich, India) for an hour.
- Sections were then washed in 0.5% acetic acid prepared in distilled water twice each of two minutes' duration.
- Similar to haematoxylin and eosin, sections were dehydrated with ethanol and cleared in Neo-Clear® xylene substitute, mounted with DPX mounting medium and cover-slipped.

2.6.3. Histological analysis

Haematoxylin and Eosin staining was used for the assessment of total glomerular tuft area. A virtual grid comprised of 91 squares was created to enable random sampling of cortical areas of each kidney section. The grid was drawn over the kidney under 4X magnification. Selected squares were magnified using 40X magnification lens to image selected glomeruli (only when the juxtaglomerular apparatus was evident). As some squares did not include any glomeruli and/or the juxtaglomerular apparatus was not visible in some glomeruli, other squares were randomly chosen so that overall total of 3 glomeruli per kidney section were analysed. As 6 sections were randomly selected from each animal, a total of 18 glomeruli per animal were chosen to measure glomerular tuft area. Images were taken using 40X magnification (Olympus inverted BX53F microscope, Tokyo, Japan) and tuft area was measured using ImageJ software.

Sirius red stain was used to semi-quantify collagen areas in the cortex and outer medulla. We used another virtual grid with 25 squares to enable random selection of cortical and medullary areas. The grid was drawn over the kidney using 4X

magnification lens and selected squares were magnified using 20X magnification to capture images. Three cortical areas and two outer medullary areas per kidney section were randomly chosen. As 6 sections were stained from each animal, a total of 18 cortical areas and 12 areas from the outer medulla were selected for analysis. Glomeruli and perivascular fibres were blanked from images to analyse tubulointerstitial fibrosis. Images were transformed to grey scale and the black area was marked with red colour which presented the collagen area (Figure 2.10). The fibrotic area of each image was normalized to the total area of the captured image to generate the % fibrotic area.

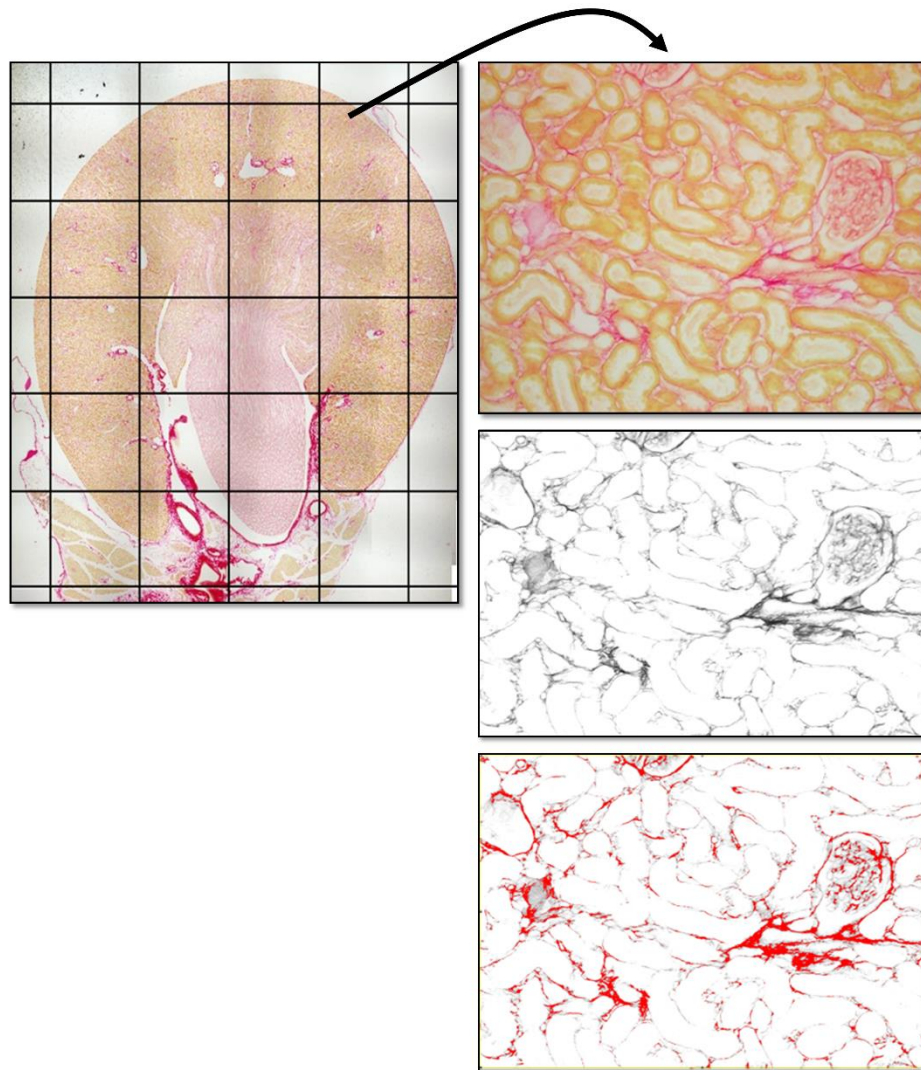
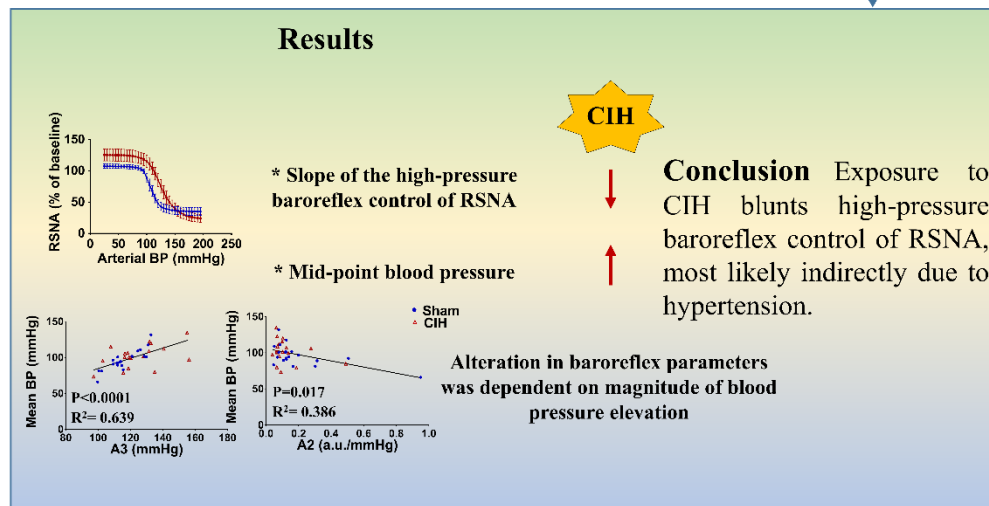
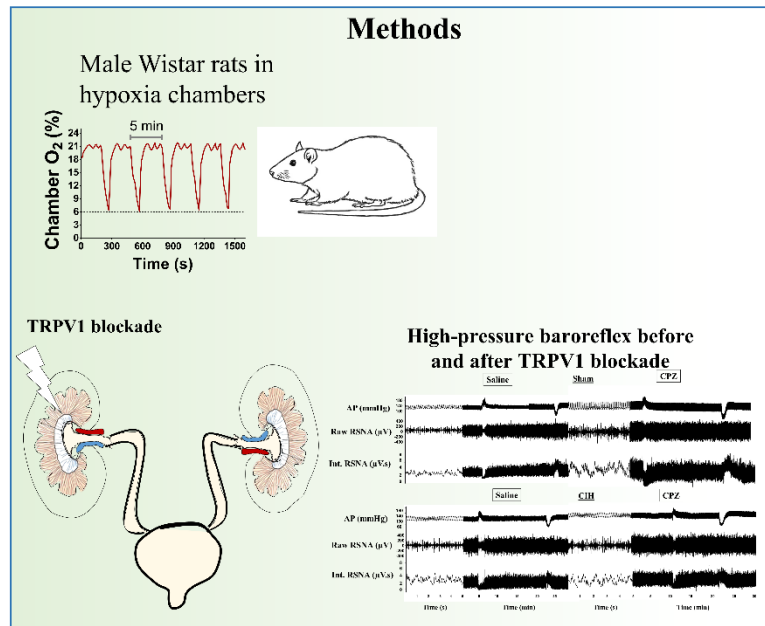


Figure 2.10. Assessment of renal fibrosis. A virtual grid was used for the random selection of kidney regions. Sirius red stained images were converted to grey scale and a colour threshold function was used to highlight collagen in red.

2.6.4. Statistical analysis

Comparisons of TRPV1 and bradykinin receptor 1 and 2 protein abundance, cytokine concentrations, enzymatic activities, histology and immunofluorescence between sham and CIH-exposed rats were performed using independent sample *t*-tests or Mann-Whitney tests, and significance was taken at $P < 0.05$. All statistical analyses were performed using SPSS software (SPSS Statistics for Windows, v25.0. IBM corp., NY, USA). All graphs were plotted using GraphPad® Prism (v6, GraphPad software, San Diego, CA, USA).

Chapter 3: Effect of chronic intermittent hypoxia on the high-pressure baroreflex control of heart rate and renal sympathetic nerve activity



List of Abbreviations

AMPA	α -amino-3-hydroxy-5-methyl-4-isoxazolepropionic acid
ARNA	Afferent renal nerve activity
AT-1	Angiotensin II type 1
BP	Blood pressure
CIH	Chronic intermittent hypoxia
CNS	Central nervous system
CPZ	Capsaizepine
DBP	Diastolic blood pressure
HIF-1 α	Hypoxia-inducible factor-1alpha
HR	Heart rate
IH	Intermittent hypoxia
IL-10	Interleukin-10
MAP	Mean arterial pressure
MSNA	Muscle sympathetic nerve activity
NF- κ B	Nuclear factor kappa B
NMDA	N-methyl-D-aspartate
NTS	Nucleus tractus solitarius
OSA	Obstructive sleep apnoea
PO ₂	Partial pressure of oxygen
PVN	Paraventricular nucleus
ROS	Reactive oxygen species
RSNA	Renal sympathetic nerve activity
RVLM	Rostral ventrolateral medulla
SBP	Systolic blood pressure
SFO	Subfornical organ
sLTF	Sensory long-term facilitation
SNP	Sodium nitroprusside
SOD	Superoxide dismutase
TNF- α	Tumour necrosis factor-alpha
TRPV1	Transient receptor potential vanilloid 1

3.1. Introduction

A rapid surge of sympathetic nerve activity (SNA) and blood pressure occurs in the last phase of each apnoea cycle during sleep in people with obstructive sleep apnoea (OSA) (250). This is necessary to maintain adequate oxygen supply to peripheral tissues. Lowering of arterial PO_2 (partial pressure of oxygen) during recurrent apnoeas stimulates the carotid bodies, which in turn triggers sympathetic outflow and nocturnal hypertension (251, 281). However, clinical studies have shown that people with OSA, during normal breathing while awake, exhibit normal resting blood pressure with heightened sensitivity of carotid bodies (250) or diurnal hypertension and sympathetic over-activity (35, 64). Enhanced neural firing of the carotid bodies modulates second-level neurons of the central nervous system (CNS) that receive inputs from baroreceptors. Subsequently, heightened chemoreflex drive disrupts the balance between sympathetic and parasympathetic outflow (250). Baroreflex control of heart rate (HR) is impaired in normotensive and hypertensive people with OSA (35, 64), while it was unaltered in another study of normotensive OSA (250). These differences are likely related to variable severity of hypoxaemia and apnoea duration between individuals. Therefore, whether impaired cardiac baroreflex contributes to the onset of hypertension or exacerbates blood pressure elevation at later stages of the disease, remains unclear.

Exposure to chronic intermittent hypoxia (CIH) in animals mimics the episodic arterial hypoxaemia of OSA, which is the primary stimulus for autonomic dysfunction and sympatho-excitation (318, 324, 417). Of note, repetitive apnoeas during room air breathing was not associated with an increase in muscle sympathetic nerve activity (MSNA) or blood pressure elevation in humans (207). Meanwhile, voluntary intermittent hypoxic apnoea for 20 minutes resulted in an increase in MSNA shortly after 5 minutes of the beginning of the protocol which lasted for three hours following the last apnoea cycle during normoxia (69). Furthermore, the increase in blood pressure and MSNA was comparable during intermittent isocapnic and hypercapnic hypoxic apnoeas (69). This illustrates that the neurogenic manifestation of hypertension in OSA is predominantly related, yet not confined to arterial hypoxaemia. Thus, other pathological features of OSA, not modelled in CIH, such as hypercapnia and inputs from lung stretch receptors in response to intra-thoracic

pressure swings, are not crucial for autonomic dysfunction and excessive sympathetic outflow observed in OSA.

The impact of CIH on baroreflex control of HR has been widely explored. Exposure to a relatively moderate protocol of CIH showed either no change (202, 392) or increased sensitivity of HR baroreflex (416). Conversely, baroreflex control of HR was blunted in response to CIH of long duration and/or of high frequency of episodes (74, 217). However, it is not established if impaired baroreflex is a direct consequence of CIH exposure or secondary to hypertension, or both together. Moreover, there is insufficient knowledge about high-pressure baroreflex control of renal sympathetic nerve activity (RSNA). This is of significance as previous studies have shown that the response of RSNA to the activation of high-pressure baroreceptors might be modified differently from the HR response in the same physiological model (243) and in pathophysiological models (133, 363). Accordingly, we hypothesized that exposure to CIH, sufficient to cause hypertension, disrupts the high-pressure baroreflex control of RSNA.

Afferent renal nerves are densely located in the renal pelvic wall, ureter and to a lesser extent in the renal cortex (237). Selective renal deafferentation was associated with attenuation of hypertension, similar to the extent of blood pressure decrease obtained following total renal denervation (46, 101). Moreover, renal denervation resulted in restoration of blunted high-pressure baroreflex in hypertensive models that involve kidney injury (168). As discussed in chapter 1, transient receptor potential vanilloid 1 (TRPV1) channels in the renal pelvic wall are co-localised with SP and CGRP neurotransmitters that mediate the activity of afferent renal nerves (15, 385). TRPV1 channels modulate afferent renal nerve activity (ARNA) by increasing intracellular Ca^{2+} and by stimulating the release of SP and CGRP (15, 414). Using whole-cell patch clamp, the membrane conductance of HEK293T cells, transfected with rat TRPV1 channels, was increased during exposure to 3% O_2 . This was revealed by an increase in the amplitude of rectified TRPV1 currents which was associated with an increase in the concentration of intracellular calcium. The addition of tiron, an intracellular oxygen radical scavenger, attenuated the basal conductance of TRPV1 channels during hypoxia, suggesting that the activity of TRPV1 was enhanced by reactive oxygen species (ROS) (172). Furthermore, intra-renal pelvic infusion of an agonist

dose of capsaicin increases RSNA and blood pressure, indicating an excitatory afferent renal reflex mediated by TRPV1 channels. This is associated with increased c-fos labelling and superoxide radicals in the paraventricular nucleus (PVN) (287, 397). Afferent renal inputs are transmitted to nucleus tractus solitarius (NTS), rostral ventrolateral medulla (RVLM) and PVN, which are the integration centers of the baroreflex loop (151). Therefore, we propose that the activity of TRPV1 channels located in the renal pelvic wall is enhanced following exposure to CIH due to altered oxidative signalling in the kidney, which elicits an excitatory afferent renal reflex. We hypothesized that TRPV1 blockade restores the anticipated CIH-induced blunting of the high-pressure baroreflex control of RSNA.

We tested our hypothesis using vasoconstrictor and vasodilator agents to induce blood pressure changes and assess high-pressure baroreflex activity. RSNA (% change from baseline) and HR were recorded during blood pressure fluctuations. This protocol was conducted in two phases: a first phase when saline was infused into the kidney in cohort 1 and 2, and a second phase when intra-renal capsaizepine (CPZ, TRPV1 blocker) was infused in cohort 2.

3.2. Results

3.2.1. General

Body weight gain in rats exposed to CIH was lower than the corresponding shams during 14 days of exposure in all cohorts (Appendix I, Figure 8.2 and Table 8.3). Body weights on the day of the surgical experiments (one day after day 14) were not significantly different between CIH-exposed and sham rats of both cohorts. In cohort 1, rats were not provided with supplementary oxygen during surgery and there was no significant difference in arterial PO_2 or partial pressure of carbon dioxide (PCO_2) between CIH-exposed and sham rats (Table 8.4). Blood gases remained relatively stable before the first VE vs. the second VE, as shown in Table 8.4. However, under anaesthesia, CIH-exposed and sham rats had low arterial PO_2 , which can activate peripheral chemoreceptors and causes an increase in the sympathetic outflow. Therefore, rats of the second cohort were provided with supplementary oxygen during the surgical protocol. PO_2 and PCO_2 were not significantly different between CIH-exposed and sham rats of the second cohort. However, CIH-exposed rats required less

percentage of supplementary oxygen compared with shams to maintain PO₂ levels above 80 mmHg during surgery (Table 8.4). Moreover, rats of cohort 2 were acidotic, which was comparable between CIH-exposed and sham rats. Haematocrit levels were comparable between CIH-exposed and sham rats of both cohorts (Table 8.4).

3.2.2. Effect of CIH on baseline values of MAP, HR and RSNA

A representative recording of baseline parameters is shown in Figure 3.1. In the first cohort study, CIH-exposed rats had higher mean arterial pressure (MAP) values before and immediately after the stabilization period (97 ± 11 vs. 84 ± 9 mmHg, $\uparrow 15.5\%$, $p=0.028$, Table 3.1) compared with sham rats. Baseline RSNA was greater in CIH-exposed rats compared with sham rats (RSNA (% of max), $36 \pm 15\%$ vs. $17 \pm 7\%$, $p=0.006$), when normalized to maximum RSNA values obtained during euthanasia. Before retroperitoneal incisions and before the stabilisation period, MAP was greater in CIH-exposed rats (by $\sim 10.4\%$) of the second cohort compared with sham rats, but to a lesser extent compared with rats of the first cohort study (by $\sim 15.3\%$).

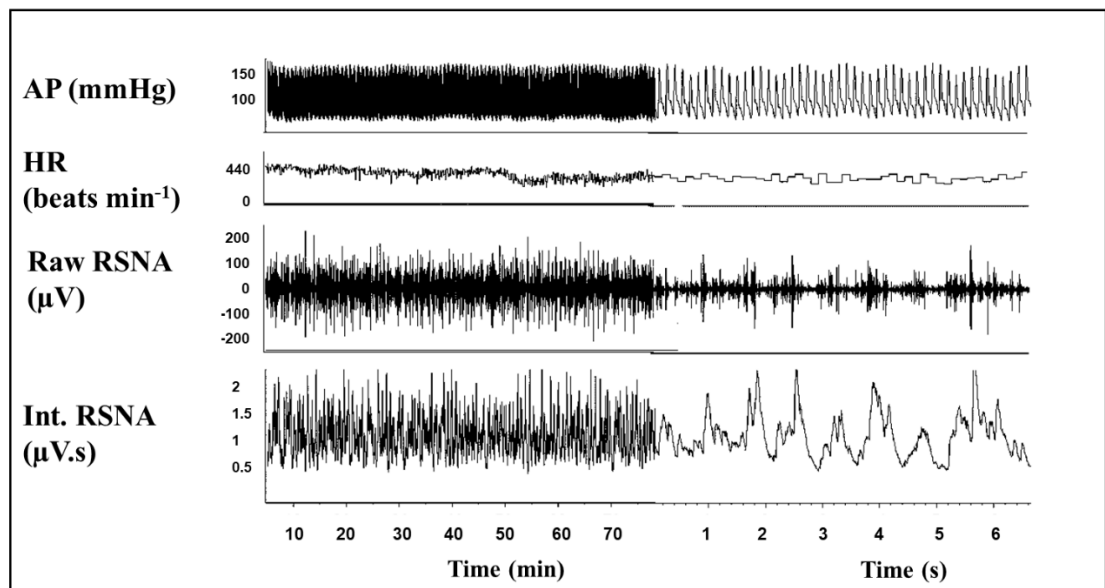


Figure 3. 1. Original recordings of cardiovascular parameters and RSNA in an anaesthetised rat. Representative original recordings of baseline arterial pressure (AP), heart rate (HR) which was derived from the AP recording, and raw and integrated RSNA (Int. RSNA) recordings from a sham rat.

Table 8.6 (Appendix I) illustrates baseline parameters in CIH-exposed and sham rats between cohorts 1 and 2. Rats of cohort 2 showed modest MAP and HR compared with rats of cohort 1. This was revealed by lower MAP (Cohort, $p < 0.001$) and HR (Cohort, $p = 0.010$) values, measured before retroperitoneal incisions, in sham and CIH-exposed rats of the second cohort compared with sham and CIH-exposed rats of the first cohort. MAP was significantly higher in CIH-exposed rats compared with sham rats of both cohorts (Exposure, $p < 0.001$). Meanwhile, following retroperitoneal incisions and after the stabilization period, rats of cohort 2 had higher MAP compared with rats of cohort 1 (Cohort, $p = 0.002$). Moreover, basal MAP, measured after the stabilization period, was comparable between CIH-exposed rats and sham rats of both cohorts. We suggest that the use of anesthesia caused the variability observed in baseline parameters after the stabilization period compared with baseline parameters before retroperitoneal incisions. Stabilization period was attained following 3-4 hours of surgical instrumentation under adequate anaesthesia. Nonetheless, RSNA and HR were significantly elevated in CIH-exposed rats compared with sham rats in both cohorts (Exposure, $p = 0.003$).

Table 3. 1. Baseline cardiovascular and RSNA parameters in sham and CIH-exposed rats.

Parameter	Sham	CIH	p-value	Sham	CIH	p-value
After arterial cannulation (before renal surgical instrumentation)						
	<u>First cohort</u>			<u>Second cohort</u>		
<i>MAP (mmHg)</i>	124±13	143±7*	0.001	115±11	127±9*	0.014
<i>SBP (mmHg)</i>	143±17	163±11*	0.008	137±13	144±12	0.154
<i>DBP (mmHg)</i>	114±12	133±5*	<0.0001	104±11	118±10*	0.005
<i>HR (beats min⁻¹)</i>	432±28	461±39	0.083	411±29	425±41	0.355
After stabilization (after renal surgical instrumentation)						
<i>MAP (mmHg)</i>	84±9	97±11*	0.028	103±12	107±18	0.565
<i>SBP (mmHg)</i>	116±14	125±15	0.262	134±15	132±22	0.871
<i>DBP (mmHg)</i>	69±8	82±11*	0.043	88±13	94±19	0.365
<i>HR (beats min⁻¹)</i>	400±52	445±47	0.084	436±19	450±34	0.204
<i>RSNA (% of max)</i>	17±7	36±15*	0.006	24±10	32±18	0.387
<i>RSNA (μV.s)</i>	0.66±0.30	1.34±0.73	0.231	1.39±0.84	1.67±0.65	0.878
<i>Maximum RSNA (μV.s)</i>	4.70±2.03	4.03±2.18	0.349	7.04±5.29	6.60±3.54	1.000

Data are presented as mean±SD and were collected from the first (sham, n=10; CIH-exposed, n=9) and second cohorts of animals (sham, n=13; CIH-exposed, n=10). Baseline cardiovascular parameters were recorded for 2 minutes after ~4-5 minutes of arterial cannulation i.e. before retroperitoneal incisions were performed to expose the kidneys. Cardiovascular parameters and RSNA were also recorded for 2 minutes after the stabilization period, 1 hour following renal surgical instrumentation. Parameters were analysed using independent samples *t*-test or Mann-Whitney test. * *p*<0.05 between exposure groups. CIH, chronic intermittent hypoxia; MAP, mean arterial blood pressure; SBP, systolic blood pressure; DBP, diastolic blood pressure; HR, heart rate; RSNA (% of max), renal sympathetic nerve activity normalized to maximum activity recorded during baroreflex activation during euthanasia.

3.2.3. Effect of CIH on the high-pressure baroreflex

Representative recordings from high-pressure baroreflex trials are shown in Figure 3.2. The slope of the RSNA baroreflex function curve of CIH-exposed rats was less than that of sham rats (A2 parameter: 0.09±0.05 vs. 0.29±0.27 mmHg⁻¹, *p*=0.016, Figure 3.3a). This was related to a significant elevation in the response range (A1 parameter: 73±26 vs. 104±32%, *p*=0.043) and operating range in CIH-exposed rats

compared with sham rats (Table 3.2). A rightward shift in the pressure at which the baroreceptors operate (A3 parameter), by ~20 mmHg ($p=0.005$), in CIH-exposed rats was observed (Figure 3.3a). This is consistent with the elevated MAP in CIH-exposed rats (by 13 mmHg) compared with sham rats, measured after the stabilisation period (Table 3.1) and immediately before the assessment of the high-pressure baroreflex. Conversely, data from the second cohort study (with a more modest increase in MAP in CIH-exposed rats) revealed no difference in any of the parameters between CIH-exposed and sham rats (Figure 3.3b, Table 3.2). Parameters of the baroreflex control of HR were not significantly different between CIH-exposed and sham rats in either of the two cohort studies (Table 3.2). Baroreflex curves of raw data obtained from a sham rat and a CIH-exposed rat in each cohort are shown in Figure 8.3 in Appendix I.

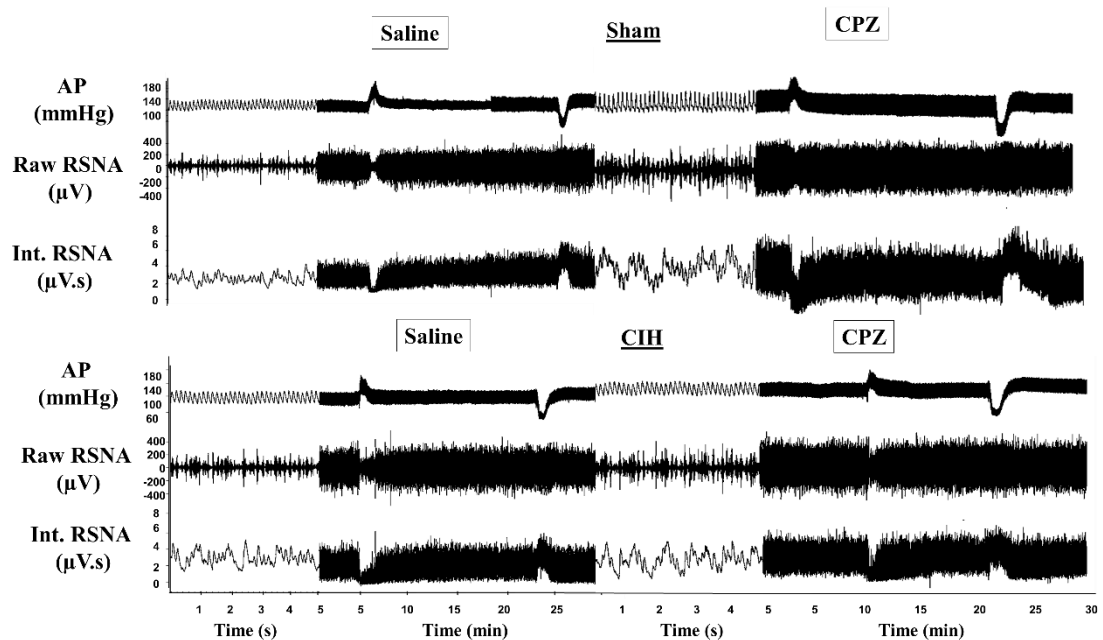


Figure 3. 2. Original recordings illustrating high-pressure baroreflex control of RSNA in anaesthetised rats. Representative original recordings of arterial blood pressure, raw and integrated RSNA responsiveness to blood pressure manipulations evoking the high-pressure baroreflex. Recordings are shown for representative sham and CIH-exposed rats showing responses during intra-renal infusion of saline and intra-renal infusion of CPZ, (TRPV1 blocker). AP, arterial blood pressure; RSNA, renal sympathetic nerve activity; Int. RSNA, integrated RSNA; CPZ, capsaizepine.

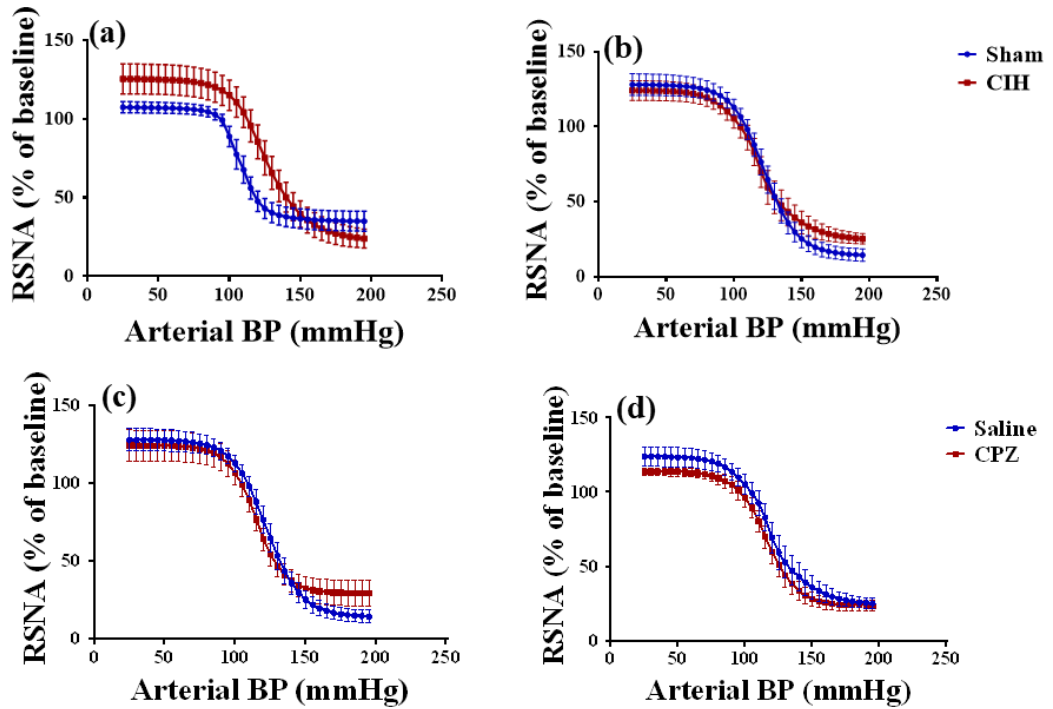


Figure 3.3. High-pressure baroreflex control of RSNA. Data (mean±SE) are shown for RSNA (% of baseline) as a function of arterial blood pressure in sham and CIH-exposed rats of the first (a; sham, n=10; CIH, n=8) and second cohort (b; sham, n=10; CIH, n=10). In each animal, the mean arterial blood pressure (MAP) was binned by 5 mmHg and corresponding values of RSNA (% of baseline) within each bin were averaged. A sigmoidal curve of RSNA-MAP relationship was drawn for each rat using the four-parameter equation. Then, the baroreflex curve for each exposure group was constructed by using the four parameters obtained from each rat in each exposure group to calculate the RSNA (% of baseline) at fixed points of MAP using the four-parameter equation. In graphs (c) and (d), data (mean±SE) are shown for RSNA (% of baseline) as a function of arterial blood pressure during intra-renal infusion of saline and CPZ (TRPV1 blocker) of sham (c) and CIH-exposed rats (d) of the second cohort. Data for baroreflex parameters are shown in table 3.2 and table 3.3. RSNA, renal sympathetic nerve activity; BP, blood pressure.

These apparently conflicting results obtained from the two cohorts are likely explained by the moderate correlation (Figure 3.4) that we found between baseline blood pressure recorded after the stabilization period and the slope (A2, $R^2=0.386$, $p=0.017$) and mid-point pressure (A3, $R^2=0.639$, $p<0.0001$) of baroreflex gain curves of all rats in both cohorts.

Table 3. 2. High-pressure baroreflex parameters during intra-renal infusion of saline in sham and CIH-exposed rats (cohort 1 and cohort 2).

Parameter	Sham	CIH	p-value	Sham	CIH	p-value
RSNA baroreflex						
	First cohort			Second cohort		
A1 (%)	73±26	104±32*	0.043	114±30	100±22	0.280
A2 (mmHg ⁻¹)	0.29±0.27	0.09±0.05*	0.016	0.10±0.03	0.15±0.14	0.912
A3 (mmHg)	109±6	129±14*	0.005	123±8	121±17	0.757
A4 (%)	35±20	22±13	0.131	14±13	24±10	0.062
Max. gain (%.mmHg ⁻¹)	5.0±4.9	2.4±1.3	0.237	2.8±0.9	3.4±2.5	0.739
HR baroreflex						
	First cohort			Second cohort		
A1 (beats min ⁻¹)	59±25	65±44	0.732	88±31	92±40	0.843
A2 (mmHg ⁻¹)	0.16±0.18	0.19±0.19	0.673	0.12±0.08	0.11±0.04	0.674
A3 (mmHg)	116±9	122±15	0.341	125±17	125±15	0.999
A4 (beats min ⁻¹)	370±46	410±59	0.139	387±38	397±76	0.707
Max. gain (beats min ⁻¹ . mmHg ⁻¹)	1.8±1.5	2.1±1.5	0.423	2.2±0.8	2.2±0.9	0.821

Data are expressed as mean±SD and represent baroreflex parameters of cohort 1 (sham, n=10; CIH, n=9) and cohort 2 (sham, n=10; CIH, n=10). Data were analysed using independent sample *t*-tests. * p<0.05 vs. sham group. CIH, chronic intermittent hypoxia; RSNA, renal sympathetic nerve activity; HR, heart rate; A1, response range of RSNA/HR; A2, the gain coefficient; A3, midpoint pressure of input; A4, the minimum response.

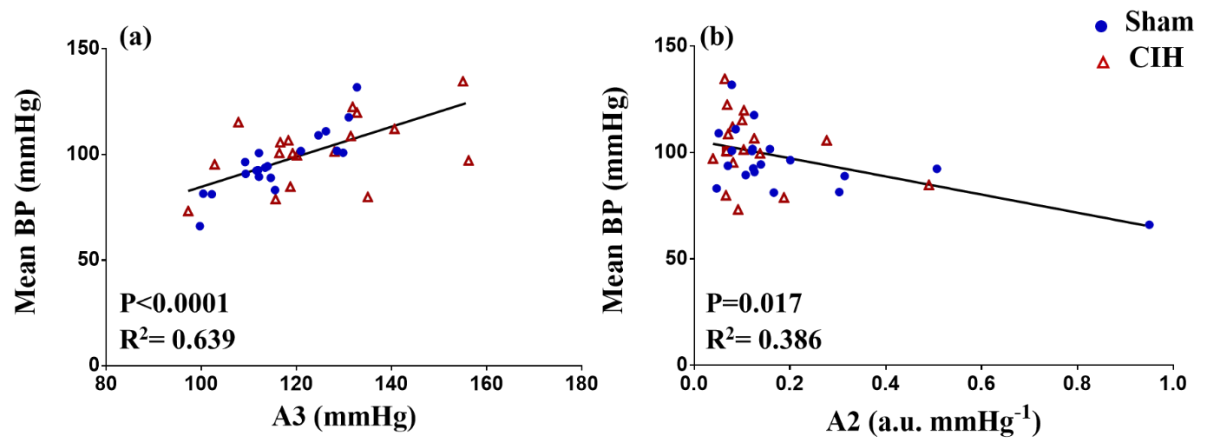


Figure 3. 4. Correlations between baseline MAP and baroreflex parameters. The relationship between mean arterial blood pressure and the baroreflex parameters, A3 and A2, are shown for all sham (n=20) and CIH-exposed rats (n=18). Linear regression analysis was performed. Significance was taken at $P < 0.05$. MAP, mean arterial blood pressure; A3, midpoint pressure of the response; A2, gain coefficient.

3.2.4. Effects of intra-renal TRPV1 blockade

Baseline MAP was decreased during intra-renal infusion of CPZ in CIH-exposed and sham rats compared with before infusion of CPZ. However, HR and RSNA were not changed during intra-renal infusion of CPZ (Table 3.3). Intra-renal CPZ did not significantly affect high-pressure baroreflex of RSNA or HR in CIH-exposed and sham rats of cohort 2 (Figure 3.3c and 3.3d, and Table 3.4).

Table 3. 3. Baseline MAP, HR and RSNA in sham and CIH-exposed rats (cohort 2).

Parameter	Saline phase					CPZ phase				
	MAP	HR	RSNA	RSNA	MAP	HR	RSNA	RSNA		
	(mmHg)	(beats min ⁻¹)	(% of max)	(μV.s)	(mmHg)	(beats min ⁻¹)	(% of max)	(μV.s)		
	Before intra-renal saline					Before intra-renal CPZ				
<i>Sham</i>	107±10	438±23	27±20	1.25±0.72	103±12	439±42	26±7	1.56±1.10		
<i>CIH</i>	111±14	437±39	26±12	1.59±0.62	112±13	448±30	29±6	1.96±0.93		
	After intra-renal saline					After intra-renal CPZ				
	(before high-pressure baroreflex)					(before high-pressure baroreflex)				
<i>Sham</i>	103±13	434±20	35±41	1.39±0.84	100±9*	443±35	27±7	1.75±1.32		
<i>CIH</i>	110±15	446±33	27±12	1.67±0.65	105±13*	446±33	30±6	2.12±1.19		
2x2 ANOVA										
<i>Exposure</i>	P=0.275	P=0.742	P=0.682	P=0.241	P=0.602	P=0.520	P=0.494	P=0.861		
<i>Time</i>	P=0.132	P=0.209	P=0.179	P=0.327	P=0.005	P=0.999	P=0.374	P=0.109		
<i>Exposure x time</i>	P=0.181	P=0.037	P=0.261	P=0.688	P=0.676	P=0.664	P=0.662	P=0.659		

Data were collected from sham (n=13) and CIH-exposed rats (n=10) and are expressed as mean±SD. Baseline values over a 2-minute period were averaged before and after the infusion of saline or CPZ and were analysed using repeated-measures two-way ANOVA. * p<0.05 vs. corresponding value before intra-renal infusion of drug. MAP, mean arterial blood pressure; HR, heart rate; VE, volume expansion; CPZ, capsaizepine; normalized RSNA, renal sympathetic nerve activity normalized to maximum activity recorded during baroreflex activation during euthanasia.

Table 3. 4. High-pressure baroreflex parameters during intra-renal infusion of capsaizepine in sham and CIH-exposed rats (cohort 2).

Parameter	Sham	CIH	p-value	Sham	CIH	p-value
	RSNA baroreflex			HR baroreflex		
<i>A1 (% or beats min⁻¹)</i>	95±46	90±17	0.780	67±36	82±40	0.370
<i>A2 (mmHg⁻¹)</i>	0.15±0.08	0.13±0.04	1.000	0.23±0.21	0.11±0.04	0.180
<i>A3 (mmHg)</i>	113±8	116±15	0.588	112±11	116±15	0.586
<i>A4 (% or beats min⁻¹)</i>	29±26	24±12	0.533	390±43	386±51	0.650
<i>Max. gain (%mmHg⁻¹ or beats min⁻¹. mmHg⁻¹)</i>	3.1±1.4	2.9±1.1	0.692	3.5±4.7	2.1±1.0	0.880

Data are expressed as mean±SD from sham (n=10) and CIH-exposed (n=10) groups and were analysed using independent sample *t*-tests. CIH, chronic intermittent hypoxia; RSNA, renal sympathetic nerve activity; HR, heart rate; A1, response range of RSNA/HR; A2, the gain coefficient; A3, midpoint pressure of input; A4, the minimum response.

3.2.5. Validation of intra-renal (cortico-medullary) cannulation

Lissamine green stain was infused into the kidney of three control rats for 30 minutes through the cortico-medullary cannula used to infuse CPZ. Tissue sections (30 µm) were imaged using a 4X magnification lens. All image shots were stitched together to generate a full image of each kidney section. In two out of three kidneys, the renal pelvic wall area was clearly stained by the green dye (Figure 3.5a and 3.5b). In the third kidney, the intra-renal cannula was correctly positioned to reach the renal pelvic area (Figure 3.5c), so we conclude that the lack of staining relates to a technical fault during sectioning using the cryostat. Accordingly, we conclude that intra-renal infusion for 30 minutes was sufficient to deliver CPZ to TRPV1 channels located in the renal pelvic wall.

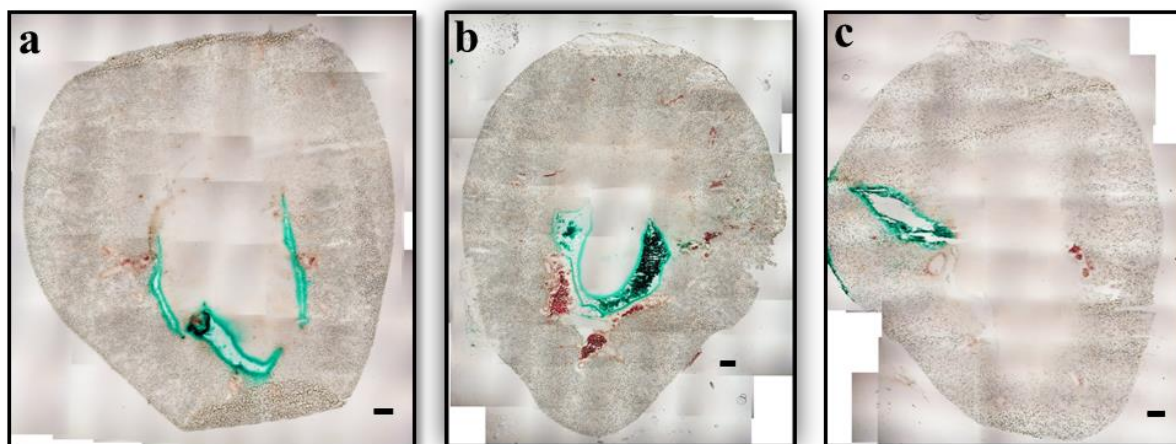


Figure 3. 5. Validation of intra-renal (cortico-medullary) infusion of TRPV1 blocker, capsaizepine. Lissamine dye was infused for 30 minutes into the right kidney of three control rats using a cortico-medullary cannula similar to the one used to infuse capsaizepine into the kidney of experimental rats. Each image in the figure represents multiple shots captured and stitched together from a single kidney section of each control rat. Cortico-medullary infusion of lissamine green shows successful staining of the renal pelvic wall after 30 minutes of infusion in two (a and b) out of three rats. The cannula reached the renal pelvis area in the kidney of the third rat (c). Scale bar 500 μ m.

3.3. Discussion

Exposure to CIH resulted in ~16 mmHg increase in MAP recorded under anaesthesia and was associated with greater RSNA compared with sham rats (Table 3.1, Table 8.6 in Appendix I). The high-pressure baroreflex was modestly affected in CIH-exposed rats, an outcome that was related to the magnitude of blood pressure increase after exposure to CIH, as high-pressure baroreflex control of RSNA was intact in CIH-exposed rats with modest hypertension (+12 mmHg basal MAP, second cohort) but was altered in rats with more severe hypertension (+19 mmHg basal MAP, first cohort).

3.3.1. Chronic intermittent hypoxia causes hypertension

The CIH paradigm used in the present study was relatively modest, yet sufficient to induce hypertension, which was associated with increased RSNA. The current CIH model caused ~15.3% increase of MAP in CIH-exposed rats vs. control of first cohort

and ~10.4% increase of MAP in CIH-exposed rats of second cohort. Similar increases in MAP were reported after 4, 7 and 14 days of CIH exposure (74, 97, 392). Using the same CIH protocol to that of our study, increases in basal MAP (+9.2% and +18.5%) were reported in separate studies from our laboratory (226, 257). However, Del Rio et al. (75), using similar CIH paradigm, showed an increase in blood pressure after 21 days, but not after 7 or 14 days of exposure. The same model elicited augmented chemosensory drive and enhanced ventilatory response to acute hypoxia after 7 and 14 days of CIH exposure, despite no change in MAP before day 21 (75). The variability in blood pressure elevation reported by different studies using similar CIH protocols is likely to be related to the anaesthetic agent used and depth of anaesthesia that was attained during blood pressure recording. Del Rio et al. (75) used sodium pentobarbital of 40 mg/kg to induce and maintain an adequate level of anaesthesia, a dose that can cause a 20% decrease in MAP during two hours of recording (377). In our study, sodium pentobarbital was used at a lower dose (33 mg/kg) to induce anaesthesia and was omitted from maintenance doses where urethane and α -chloralose were used. In other aforementioned studies conducted in our lab, urethane alone was used to maintain anaesthesia. Subsequently, studies are needed to compare the effect of different anaesthetic agents on cardiovascular modulation mediated by CIH.

Nevertheless, the method used to record blood pressure has a profound effect on the magnitude of MAP increase reported in different CIH studies. In addition to arterial catheterization used in our experiment, other studies have used radiotelemetry and cuff-tail methods to monitor blood pressure changes during CIH exposure (81). For example, Fletcher et al. (99) implemented a CIH paradigm of 35 days (120 cycles/hr, 6-8 hr/day, 3-5% O₂) and reported an increase in MAP by 13.5 mmHg in CIH-exposed rats recorded by catheterization of the abdominal aorta, compared with 21 mmHg increase when blood pressure was measured by tail-cuff method. Interestingly, telemetry recording in conscious rats revealed that exposure to CIH for 3 to 5 days is associated with a prompt increase in MAP without progressive elevation of blood pressure after longer durations of CIH exposure (75, 138, 201, 236). Exposure to CIH for 30 days (48 cycles/hr, 6 hr/day, 2-6% O₂) resulted in a maximum increase in MAP by ~12.2%, reached after 7 days and was maintained during 30 days of continuous CIH exposure (201), which is similar to the magnitude of increase in MAP shown in our study. Moreover, MAP was elevated by ~10 mmHg after 3 days of CIH exposure

(15 cycles/hr, 12 hr/day, 10% O₂), with no further elevation of blood pressure during the exposure period of 28 days (236).

Our findings illustrated that basal HR in CIH-exposed rats was similar to shams. CIH exposure (12 cycles/hr, 8 hr/day, 10% O₂) in rats was associated with a significant increase in HR during the light (sleep) cycle, which was restored to levels that are equivalent to shams the following day, after the end of CIH protocol, during normoxic breathing (138). Indeed, no change or an increase in resting HR has been described in rats exposed to CIH (56, 226).

The magnitude of blood pressure increase depends on the parameters of the CIH model used, including duration of CIH exposure, frequency of hypoxia cycles and intensity of hypoxia (minimum FiO₂ attained in the hypoxia cycle) (15). Peng et al. (272) have shown that 10 days of CIH exposure of multiple hypoxic episodes per day (9 cycles/hr, 8 hr/day, 5% O₂) was associated with 32% increase in MAP, while there was no blood pressure elevation in rats exposed to a CIH paradigm of less frequent cycles (4 hours of 5% O₂, once per day for 10 days) (272). Basal discharge of carotid bodies and sensory long term facilitation (sLTF, persistent elevation of basal chemoafferent activity in normoxia), was heightened in rats exposed to the former CIH paradigm of frequent episodes, but were not altered following exposure to the latter CIH protocol (272). Moreover, adrenaline and noradrenaline efflux of the adrenal medulla was greatly induced in response to acute hypoxia in rats pre-treated with CIH paradigm of frequent episodes compared with rats pre-treated with less frequent episodes of CIH (199). In support of this, it was previously shown that the severity of systemic inflammation is heightened in response to a CIH protocol composed of more frequent hypoxia cycles (406). Serum levels of tumour necrosis factor alpha (TNF- α), nuclear factor kappa B (NF- κ B) and hypoxia-inducible factor-1 alpha (HIF-1 α) were elevated after exposure to 6 weeks of 10, 20, 30 and 40 cycles/hr of intermittent hypoxia (IH), with more significant elevation of inflammatory cytokines in rats exposed to more frequent IH cycles. In addition, the decrease of interleukin-10 (IL-10, an anti-inflammatory cytokine) level was greater when rats were exposed to more frequent cycles of IH (406). Administration of a superoxide dismutase (SOD) mimetic eliminated the increase in blood pressure and prevented the enhanced chemoreflex drive induced by acute hypoxia in CIH-exposed rats (272). Furthermore, tempol, an

SOD mimetic, attenuated the CIH-induced modulation of pro-inflammatory / anti-inflammatory cytokine profile (406). Therefore, it is strongly suggested that the cyclical pattern of hypoxia and re-oxygenation plays a major role in the autonomic and cardiorespiratory alterations induced by CIH, due to the generation of superoxide radicals during the re-oxygenation phase of each cycle. Hence, available evidence focuses on the role of frequency of hypoxia cycles in CIH-induced cardiorespiratory modulation. However, the parameter of CIH model that induces the predominant effect at the level of tissue injury, autonomic disruption and cardiorespiratory changes is not fully understood.

Consistent with other models of hypertension (198, 227), a neurogenic mechanism leading to increased renal sympathetic tone is activated early in CIH models (123, 224). We analyzed the integrated RSNA and presented our results in terms of absolute RSNA ($\mu\text{V.s}$) and values normalized to the maximum RSNA obtained during euthanasia. Our comparisons showed that absolute basal RSNA in CIH-exposed rats was not significantly different from sham group (Table 3.1). Normalisation of RSNA reduces the variability obtained from different recording conditions on different days from multiple groups. To minimize the variability in RSNA recordings, a dramatic increase in RSNA is induced and data are expressed in terms of percentage of maximum activity. Previous studies have shown that nasopharyngeal reflex in response to cigarette smoking induces a substantial increase in RSNA and complete attenuation of renal blood flow. This protocol was commonly used to normalize RSNA recordings to a maximum value in conscious rabbits and was reported in some pre-clinical studies of conscious rats (32, 42, 213, 241, 242). Another method of normalization involves the recording of maximum RSNA obtained during injection of sodium nitroprusside (SNP) (208). However, in our study, we observed that maximum RSNA obtained in response to blood pressure decrease during SNP injection (Cohort 1: Sham, $1.05 \pm 0.92 \mu\text{V.s}$; CIH, $1.46 \pm 0.97 \mu\text{V.s}$; Cohort 2: Sham, $1.96 \pm 1.28 \mu\text{V.s}$; CIH, $2.35 \pm 1.45 \mu\text{V.s}$) was less than the maximum RSNA observed during euthanasia in response to the profound drop in blood pressure caused by an overdose of anaesthesia (Cohort 1: Sham, $4.70 \pm 2.03 \mu\text{V.s}$; CIH, $4.03 \pm 2.18 \mu\text{V.s}$; Cohort 2: Sham, $7.04 \pm 5.29 \mu\text{V.s}$; CIH, $6.60 \pm 3.54 \mu\text{V.s}$). Therefore, our basal values were expressed in terms of percentage of maximum obtained (average of 5 s) during euthanasia. Our

results showed a significant increase in basal RSNA (% of max) in CIH-exposed rats compared with sham rats of cohort 1.

Previous studies have reported an increase in splanchnic, muscle, lumbar, thoracic and renal nerve activity in different models of CIH (224, 235, 280, 324, 417). Prior evidence has shown that exposure to 5 or 10 cycles of acute IH caused a ramp increase in RSNA and splanchnic sympathetic nerve activity, which was gradually progressing one hour after the end of the last hypoxia cycle (323). Acute optogenetic intermittent stimulation of neurons in the caudal NTS generated a similar ramp increase of RSNA and phrenic nerve activity, but of a lesser magnitude (393). This suggests that disrupted RSNA in IH might be induced by central plasticity of NTS neurons, independent of afferent signals coming from peripheral chemoreceptors (393). Overall, heightened RSNA might be related to down regulation of potassium/ATP channels in NTS neurons, activation of angiotensin II type 1 (AT1) receptors in the subfornical organ (SFO) and activation of neurons within the NTS in response to afferent inputs from the carotid bodies (323, 393) and possibly other sites such as the kidney (15).

3.3.2. High-pressure baroreflex control of HR

Disrupted autonomic control of blood pressure is associated with the pathogenesis of CIH-induced hypertension (320, 416). In relation to that, impaired cardiac baroreflex function was previously reported in people with OSA (64, 300) and conflicting results were reported regarding baroreflex control of HR in rats exposed to CIH (202, 392, 416). Our data showing no change in the baroreflex control of HR in CIH-exposed rats, is in agreement with previous studies utilizing 5, 7 and 10 days of CIH exposure (202, 392). Indeed, long-term exposure to CIH was associated with decreased cardiac baroreflex gain (74, 122, 217). In contrast, Zoccal et al. (416) showed enhanced cardiac baroreflex sensitivity after exposing juvenile rats to CIH for 10 days. Indeed, their finding were supported by subsequent studies by Moraes et al. (246) who revealed enhanced inhibitory baroreflex inputs in juvenile rats exposed to CIH. Enhanced inhibitory inputs was associated with an increase in the inhibition of RVLM pre-sympathetic neurons during the expiratory phase (246). Lai et al. (202) analysed day-to-day arterial blood pressure and baroreflex sensitivity of the heart in conscious

rats. They found that MAP was higher by 15 mmHg after 5 days of exposure to CIH, but with no measurable alteration in baroreflex function. This was followed by a decline in baroreflex sensitivity starting 10 days after the onset of exposure to CIH (202). Of note, parameters other than duration of exposure must be taken into account in the comparison of severity of exposure between different studies and in the determination of the stage of the disease. Altogether, previous studies proposed that cardiac baroreflex sensitivity increases during the early phase of CIH exposure decreasing the sympatho-excitatory response to carotid body hypersensitivity and acts to bring blood pressure back to normal (246). However, with the disease progression, the augmented chemoreflex drive overwhelms the activity of the baroreceptors to control blood pressure (246). Other studies indicated that resetting of the cardiac baroreflex after 28 days of CIH exposure was restored to sham levels after bilateral carotid body ablation (62, 74).

Impaired baroreflex control of HR following CIH exposure could be related to a dysfunction of multiple components of the baroreflex circuit, which results in an imbalance between sympathetic and parasympathetic activities. A previous study has shown that the electrical stimulation of cardiac vagal efferent neurons produced bradycardia, which was enhanced in CIH-exposed rats (217). Moreover, using anterograde tracing, the density of synapse-like endings of efferent vagal neurons was increased in CIH-exposed rats, suggesting that efferent postganglionic vagal neurons do not contribute to blunted baroreflex control of HR in CIH (217). On the other hand, immunofluorescence labelling revealed downregulation in glutamate, N-methyl-D-aspartate (NMDA) and α -amino-3-hydroxy-5-methyl-4-isoxazolepropionic acid (AMPA) receptors in the nucleus ambiguus region in the brain. Therefore, injection of glutamate, NMDA or AMPA into nucleus ambiguus produced a decrease in HR that was attenuated in CIH-exposed rats (217, 394). In support of this notion, exposure to CIH mixed with hypercapnia blunted the spontaneous excitatory glutamatergic transmission into the preganglionic vagal neurons of nucleus ambiguus in rats (89). Therefore, current evidence shows that blunted cardiac baroreflex is mediated by dysfunction in the central baroreflex component controlling the parasympathetic outflow. In addition, a heart rate variability study showed an increase in the low frequency to high frequency ratio after 14 days of CIH exposure indicating a shift towards sympathetic over parasympathetic control of HR (75). In normotensive

individuals with OSA, Cortelli et al. (65) showed enhanced bradycardia response to cold pressor test despite attenuated baroreflex sensitivity. This agrees with enhanced vagal efferent neurotransmission reported in CIH-exposed rats (217).

In the first cohort, RSNA- and HR-MAP relationship curves had no evidence of asymmetry around the mid-pressure point, as shown in Figure 8.1 in appendix I. A previous study showed a comparison between the four- and the five-parameter models in the analysis of the high-pressure baroreflex control of RSNA and HR (302). It was shown in that study that the five-parameter equation composed of two curvature (gain) coefficients can be reduced to four parameters accounting one curvature (gain, A2) coefficient, if there is no asymmetry. Therefore, the four-parameter model was used to analyse the high-pressure baroreflex control of RSNA and HR.

3.3.3. High-pressure baroreflex control of RSNA

CIH-exposed rats of the first cohort showed a significant shift in mid-point blood pressure by almost 20 mmHg, which was associated with an increase in the operating range of the RSNA baroreflex. Moreover, a marked increase in response range (A1 parameter) of the RSNA baroreflex was evident in CIH-exposed rats. Elevation in the operating and response range of RSNA resulted in decreased slope of the baroreflex gain curve (A2 parameter). These changes were concomitant with a substantial hypertensive phenotype (Table 3.1). Conversely, CIH-exposed rats of the second cohort which showed modest hypertension displayed baroreflex responsiveness that was equivalent to the respective sham group. Interestingly, a significant correlation between basal MAP and the slope of the baroreflex curve (A2) and between MAP and mid-point pressure (A3) was evident (Figure 3.4). This indicates that resetting of the RSNA baroreflex and the decreased slope of the curve are associated with elevated blood pressure. It is likely that baroreflex adjustments following exposure to CIH in this study and marked attenuation of baroreflex function of HR observed in severe CIH protocols, are secondary to the development of hypertension following exposure to CIH. This is supported by the notion that the second cohort of rats were hypertensive (modest compared with cohort 1), but displayed no changes in baroreflex parameters indicating that the latter was not obligatory for the manifestation of CIH-induced hypertension. Hypertension overrides the baroreceptors' capacity to control blood

pressure, causing resetting of the baroreflex and decreasing the baroreflex sensitivity. Additionally, hypertension is associated with vasoconstriction, which in turn exacerbates the tonic activity of chemoreceptors and aggravates sLTF. Subsequently, excessive chemoreflex drive mediates central plasticity in brain regions involved in baroreflex regulation (75). In support of this argument, exposure to CIH in neonatal rats (20 cycles/hr, 12 hr/day, 8% O₂) for 30 days did not blunt baroreflex control of RSNA. However, following exposure to acute IH (6 cycles of 10% O₂ for 90s), neonatal rats pre-exposed to CIH had augmented sLTF of carotid bodies and showed decreased baroreflex control of RSNA (332). Nonetheless, in humans with OSA, a normal baroreflex control of HR was reported with no changes in MSNA response to phenylephrine, but with selective attenuation of MSNA increase in response to SNP injection (250).

The high-pressure baroreflex loop of RSNA is composed of afferent inputs from baroreceptors, central integration, efferent sympathetic preganglionic neurons and post ganglionic neurons with their synapse-like terminals (395). Different models of CIH showed elevated pro-inflammatory cytokines and c-fos labelling in NTS and RVLM, brainstem regions of preganglionic sympathetic neurons (263, 332). Exposure to CIH depletes ATP levels required for potassium efflux to cause hyperpolarization in neuronal cells, which results in enhanced neuronal excitability in NTS and augmented sympathetic outflow (407). Furthermore, blunted cardiac baroreflex in chronic kidney disease-induced hypertension was found to be associated with increased glutamate and decreased GABA levels, and downregulation of GABA receptors in the NTS (54). In the latter study, elevated blood pressure and the blunted baroreflex were normalized following renal denervation. Therefore, based on the available evidence, it is suggested that modulation of the sympathetic baroreflex is mediated by dysfunction in the central nervous system component, and whether other components of the baroreflex loop are impaired warrants investigation.

In our study, baroreflex control of RSNA was altered in CIH-exposed rats of cohort 1 that had more severe hypertension, while baroreflex control of HR was maintained in all CIH-exposed rats of both cohorts. The difference between baroreflex control of RSNA and HR in the present study may be explained by the fact that the heart is regulated by the sympathetic and parasympathetic systems such that both systems

work together to sustain normal baroreflex control of HR (243). Moreover, we can speculate that distinctive sites within the NTS and RVLM control sympathetic outflow to the kidney and the heart. These sites might be modulated differently in response to CIH and hypertension, in addition to the presence of different ganglionic connections which requires investigation. Divergence has also been previously observed in other hypertensive disease models where baroreflex control of HR was decreased, while the baroreflex control of RSNA was unaltered (133, 363).

3.3.4. Blockade of TRPV1 channels

In our study, we aimed to test if blockade of renal TRPV1 channels restores the blunted baroreflex control of RSNA. The basis of this hypothesis was that PVN and RVLM are the main integration centres of baroreceptors inputs. The stimulation of renal afferent nerves induces an excitatory afferent reflex, activating neurons located in the supraoptic nucleus and PVN, which regulate the activity of preganglionic sympathetic neurons of RVLM (50, 325). This reflex increases blood pressure, which is clearly observed in cats, rats and mice (50, 261, 325). Of note, electrical stimulation of carotid sinus nerves activated 70-80% of hypothalamic regions that are activated during the electrical stimulation of renal afferent nerves (43). Inputs from carotid sinus nerve inhibit ~60% of hypothalamic units that are inhibited by renal afferent nerves, including PVN, lateral hypothalamus and preoptic region (43). Electrical stimulation of sensory renal nerves in mice results in an increase in splanchnic, lumbar and renal SNA (261). A subset of sensory renal nerves express TRPV1 channels that induce the entry of Ca^{+2} ions when activated, which stimulates SP and CGRP release, resulting in the activation of afferent renal nerves (160, 414). In our study, we used CPZ at a similar dose to that used in previous studies to block TRPV1 with marked changes in RSNA (209). Our intention was to deliver CPZ into the renal pelvic wall, to target TRPV1 channels which are part of renal afferent nerves (Figure 3.5). However, we cannot exclude the possibility of spill-over of CPZ to the surrounding renal cortical areas, where TRPV1 mediates vasodilation of renal arterioles (210). Furthermore, a previous study has shown that activation of TRPV1 located in the renal interstitium increases ARNA (82). Therefore, based on lissamine green images (Figure 3.5), we expect that we did not inhibit all renal afferent nerves that contain TRPV1. In addition, during the first cohort, we cannulated the left kidney and measured the ipsilateral

RSNA. However, a previous study has shown that the contralateral reno-renal reflex is more apparent than the ipsilateral arm of the reflex. Therefore, in the second cohort, we aimed to infuse saline/CPZ to the contralateral right kidney. Nevertheless, we don't expect this difference between cohort 1 and 2 to affect our results because we did not study the effect of TRPV1 blockade in the first cohort rather than CPZ was infused during the second cohort only.

Following 30 minutes of intra-renal infusion of CPZ, MAP was decreased in CIH-exposed and sham rats with no change in RSNA and HR. This finding disagrees with prior studies that showed no change in basal MAP in sham rats following CPZ infusion into the kidney (209). In animal models of CIH, increases in systemic and renal inflammatory biomarkers and ROS have been reported together with impaired baroreflex control of HR (74, 202, 392). Pharmacological inhibition of inflammation and renal denervation restored the blunted high-pressure baroreflex control of RSNA in obese rats (170). Moreover, ROS modulate the downstream signalling pathway of TRPV1 channels (172) and cortico-medullary TRPV1 blockade normalised the blunted high-pressure baroreflex control of RSNA in a cisplatin model of renal failure (1). For logistical reasons, the high-pressure baroreflex function was not assessed after intra-renal CPZ in rats of cohort 1, where baroreflex changes were subsequently revealed. The effect of intra-renal CPZ was assessed in rats of cohort 2, but high-pressure baroreflex control of RSNA was not altered in these rats with modest hypertension. Therefore, a possible role for TRPV1 signalling in modulating high-pressure baroreflex control of RSNA in CIH-exposed rats cannot be excluded and this warrants further attention.

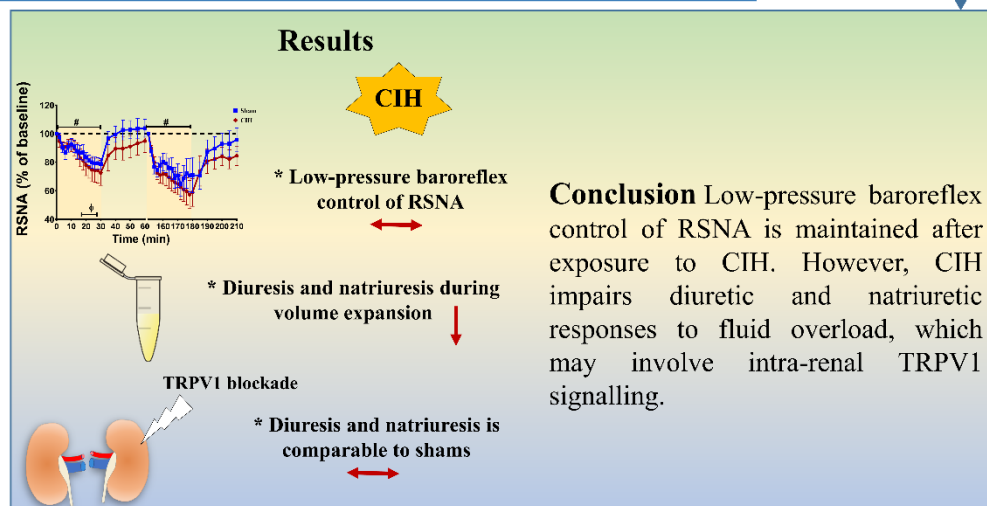
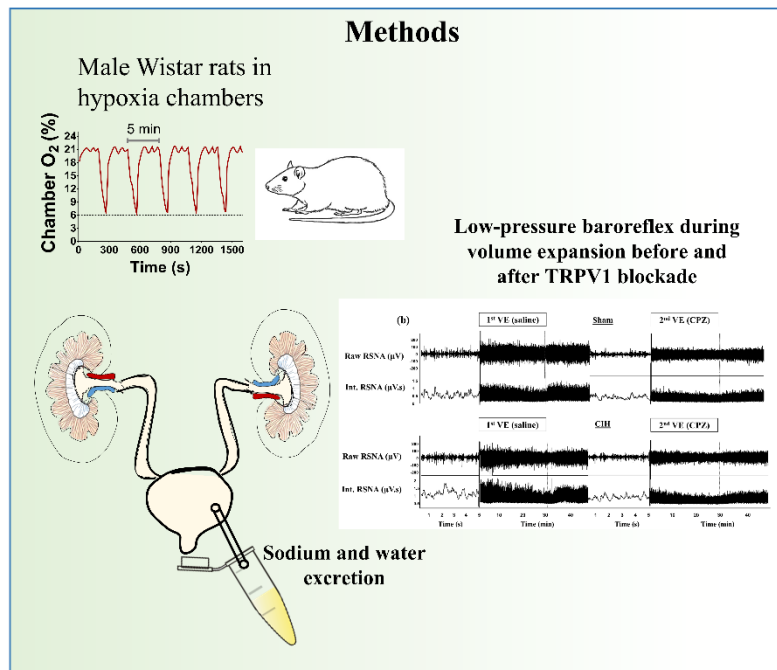
In cohort 2, CIH-exposed and sham rats had respiratory acidosis, which is related to the use of anaesthesia (404). It was previously shown that hypercapnic acidosis increases baroreflex sensitivity (371). However, in our cohort and before the intra-renal infusion of saline, the magnitude of respiratory acidosis was comparable between CIH-exposed and sham rats. In addition, baroreflex parameters were not different between CIH-exposed and sham rats during the saline phase of cohort 2 (Table 8.4, Appendix I). Meanwhile, after the end of the intra-renal saline phase and before the intra-renal infusion of CPZ, blood gases of CIH-exposed rats were different from sham rats of the second cohort. CIH-exposed rats displayed metabolic acidosis and normalised levels of PCO₂ compared with sham rats (Table 8.4, Appendix I). This

might be due to increased hyperventilation in CIH-exposed rats compared with sham rats in response to phenylephrine and sodium nitroprusside during the preceding intra-renal saline phase. Nevertheless, baroreflex parameters were not changed during the intra-renal infusion of CPZ compared with intra-renal infusion of saline in any of the exposure groups.

3.4. Conclusion

In conclusion, our findings show that rats exposed to CIH with established hypertension have moderate alterations in the high-pressure baroreflex control of RSNA with no changes in the baroreflex control of HR. We suggest that modulation of high-pressure baroreflex control of RSNA in this model is a consequence of hypertension and is less likely related to hypoxia per se, but might proceed to a pathological level and contribute to the maintenance of hypertension. Similarly, high-pressure baroreflex control of HR can possibly be impaired at later stages of the disease.

Chapter 4: Effect of chronic intermittent hypoxia on renal sympatho-inhibition and renal functional responses to volume expansion before and after TRPV1 blockade



List of abbreviations

ADH	Antidiuretic hormone
AHI	Apnoea hypopnoea index
Ang II	Angiotensin II
ANP	Atrial natriuretic peptide
AT-1	Angiotensin II type 1
AUC	Area under the curve
CGRP	Calcitonin gene-related peptide
CIH	Chronic intermittent hypoxia
CKD	Chronic kidney disease
CPAP	Continuous positive airway pressure
CPZ	Capsaizepine
CSNA	Cardiac sympathetic nerve activity
eGFR	Estimated glomerular filtration rate
eNOS	Endothelial nitric oxide
ESRD	End-stage renal disease
GFR	Glomerular filtration rate
H ₂ O ₂	Hydrogen peroxide
HR	Heart rate
MAP	Mean arterial blood pressure
NOX4	NADPH oxidase 4
OSA	Obstructive sleep apnoea
PO ₂	Partial pressure of oxygen
PVN	Paraventricular nucleus
RAAS	Renin-angiotensin-aldosterone system
ROS	Reactive oxygen species
RSNA	Renal sympathetic nerve activity
RVLM	Rostral ventrolateral medulla
SHR	Spontaneously hypertensive rat
SNA	Sympathetic nerve activity
SON	Supraoptic nucleus
SP	Substance P

TRPV1	Transient receptor potential vanilloid 1
UF	Urine flow
VE	Volume expansion

4.1. Introduction

Obstructive sleep apnoea (OSA) is prevalent in 50% of individuals with chronic kidney disease (CKD) (228). A clinical trial of 200 participants has shown that the diagnosis of OSA becomes more frequent as kidney function deteriorates: 25% of participants with estimated glomerular filtration rate (eGFR) >60 ml/min/1.73 m² and 35% of participants with eGFR >30 ml/min/1.73 m² had OSA compared with 45% of participants with eGFR <30 ml/min/1.73 m² diagnosed with OSA (13). Hypertension, OSA and CKD were described as a “triad” wherein each contributes to the onset and progression of the other complication (21). OSA worsens renal function through a direct effect of hypoxia and indirectly through sympathetic over-activity, endothelial dysfunction, activation of renin-angiotensin-aldosterone system (RAAS), and hypertension (21). All of these pathophysiological features are similarly presented in different models of chronic intermittent hypoxia (CIH) (15, 196).

OSA severity, as determined by apnoea hypopnoea index (AHI), and deterioration of kidney function are linked through the volume status and body water content, as OSA is characterised by fluid accumulation and rostral fluid shift from legs into the neck and upper airway region during sleep. Individuals with CKD have 12% decreased pharyngeal area and increased neck circumference (21). Moreover, individuals with end-stage renal disease (ESRD) and OSA have markedly increased extracellular volume in the legs, neck and thoracic area. They have also greater reduction in nocturnal fluid volume in their legs compared with individuals with ESRD without OSA. In addition, AHI correlates with serum urea and creatinine clearance in individuals with CKD (11). Thus, dialysis using nocturnal ultrafiltration decreased AHI and fluid volume in ESRD (228). There was also a significant correlation between improvements in AHI and neck circumference (21). Subsequently, administration of diuretics caused improvements in AHI. In addition, treatment with continuous positive airway pressure (CPAP) resulted in decreased proteinuria and glomerular filtration fraction, and increased renal blood flow (11, 21). On the other hand, OSA worsens kidney function due to enhanced sympathetic outflow which causes RAAS activation, hyperaldosteronism, increased endothelin release, and subsequently endothelial dysfunction and blood pressure elevation. Indeed, treatment with CPAP was

associated with an increase in nitric oxide and a decrease in blood pressure in hypertensive individuals (21, 410).

Volume status of the body is mainly maintained by the diuretic and natriuretic functions of the kidney. Under physiological conditions, blood pressure increase causes pressure diuresis and natriuresis to protect against blood pressure elevation (130). Fluid overload, defined as an increase in blood volume, activates low-pressure baroreceptors located in the cardiopulmonary region of the heart (260). These volume receptors are located in the atria, ventricles and lungs (245). Afferent inputs from low-pressure baroreceptors induce reflex sympatho-inhibition, which causes a fall in renal sympathetic nerve activity (RSNA) followed by diuresis and natriuresis (291). A previous study has shown that cardiac receptors are the primary source for vagal afferent inputs in response to fluid overload, while receptors located in the lungs have a minor impact on the reflex (245).

Low-pressure baroreflex is not widely examined in hypertension disease models. Clinical trials of essential hypertension have revealed that high-pressure baroreflex sensitivity is blunted in individuals with borderline hypertension and with moderate and severe hypertension (233). Meanwhile, low-pressure baroreflex control of splanchnic nerve activity is heightened in response to lower body negative pressure in individuals with borderline hypertension (233). The increased sensitivity of cardiopulmonary receptors in borderline hypertension is compensatory to decreased high-pressure baroreflex control of sympathetic nerve activity (SNA) and vascular tone. Meanwhile, the function of low-pressure baroreflex deteriorates with the progressive elevation of blood pressure in individuals with moderate-to-severe hypertension (233). In addition, the low-pressure baroreflex is blunted at advanced stages of hypertension when changes in cardiac structure begin. Cardiopulmonary reflex sensitivity was higher in normotensive individuals that have relatives with essential hypertension than in normotensive individuals with no evidence of familial hypertension (356). In contrast, Grassi et al. (121) reported a decrease in the sensitivity of the low-pressure baroreflex control of renin release and vascular tone in individuals with mild hypertension. The sensitivity was progressively deteriorated in individuals that have severe hypertension and left ventricular hypertrophy (121). In relation to that, a significant correlation was shown between decreased sensitivity of the

cardiopulmonary baroreflex with heart thickness and with renal vascular tone in humans (356). Interestingly, normotensive individuals with OSA have increased left ventricular mass similar to hypertensive individuals with no OSA (21). It was suggested that repetitive hypoxaemia during apnoeic episodes causes continuous activation of intra-thoracic pressure, and subsequently results in blood pressure increase and left ventricular hypertrophy (21). AHI was correlated with left ventricular mass (72), indicating that low-pressure baroreflex control could be altered in the early stages of OSA and CIH models.

Previous studies have revealed blunted low-pressure baroreflex control of RSNA in response to fluid overload in disease models that involve kidney injury (3, 168, 169). In this regard, similar renal pathophysiological changes to that observed due to exposure to CIH were reported in renal injury disease models (80, 224, 380, 381, 409). However, the influence of exposure to CIH on the low-pressure baroreflex control of RSNA and kidney function has not yet been examined.

Kidneys are innervated by afferent and efferent sympathetic nerves that interact to maintain normal water and electrolyte balance, through reno-renal reflex mechanisms (6). Studies have shown that activation of afferent renal nerves induces sympatho-excitation and a decrease in renal blood flow (24, 135, 180, 256, 267, 383). Electrical stimulation of afferent renal nerves in cats and rats enhanced the activity of neurons in the paraventricular nucleus (PVN) and supraoptic nucleus (SON) and subsequently, this increased plasma levels of antidiuretic hormone (ADH) in the absence of any change in plasma osmolality (50, 325). Studies utilizing selective renal deafferentation techniques reported attenuation of hypertension (46, 101). Ditting et al. (83) have shown that dendritic cells and macrophages are in close proximity to renal afferent nerve endings. Accordingly, pharmacological inhibition of renal inflammation and/or oxidative stress was associated with normalization of low-pressure baroreflex control of RSNA in many hypertensive disease models (3, 170). TRPV1 channels are involved in the activation pathway of renal afferent nerves (172), and their activity is enhanced following exposure to hypoxia (15). Moreover, the PVN is the main control site for efferent RSNA, and it receives inputs from low-pressure baroreceptors and from renal afferent nerves. Indeed, renal afferent nerves were found to be activated by TRPV1 agonists (151, 287, 397).

We aimed to explore the impact of CIH exposure on low-pressure baroreflex control of RSNA with possible changes in renal excretory responses to fluid overload. We hypothesised that renal TRPV1 blockade improves the baroreflex regulation of RSNA and alters kidney diuretic and natriuretic responses. Therefore, we induced volume expansion (VE) using IV saline infusion for 30 minutes and we recorded RSNA and sodium and water excretion before, during and after VE. This was performed in two phases in study cohort 1. The first phase was performed in the presence of a background of intra-renal infusion of saline (vehicle) while the second phase was done in the presence of a background intra-renal infusion of capsaizepine (CPZ, TRPV1 blocker). We also examined TRPV1 expression in the renal pelvic wall and kidney tissue. The plasma levels of atrial natriuretic peptide (ANP) in response to VE was also analysed in CIH-exposed and sham rats.

4.2. Results

4.2.1. Basal haemodynamic and renal excretory parameters before VE

Exposure to CIH had no significant effect on any of the basal renal excretory parameters (Table 4.1). During intra-renal infusion of CPZ, there was a significant increase in urine flow (UF) and sodium excretion, both in CIH-exposed and sham rats compared with respective values measured during saline infusion (Table 4.1).

Prior to VE challenge, intra-renal infusion of saline had no significant effect on blood pressure, heart rate (HR) and RSNA. In contrast, mean arterial pressure (MAP) was lower during intra-renal infusion of CPZ, both in CIH-exposed and sham rats, compared with respective baseline values measured prior to CPZ infusion, whereas RSNA and HR were unchanged (Table 4.2).

Table 4. 1. Baseline renal excretory parameters in sham and CIH-exposed rats.

	GFR (ml min ⁻¹ kg ⁻¹)	UF (μl min ⁻¹ kg ⁻¹)	Absolute Na ⁺ excretion (μmol min ⁻¹ kg ⁻¹)	Fractional Na ⁺ excretion (%)
After intra-renal infusion of saline/before VE				
<i>Sham</i>	11.19±8.43	32.87±15.53	4.08±3.07	0.25±0.20
<i>CIH</i>	8.94±3.42	46.18±23.60	7.05±4.73	0.57±0.45
After intra-renal infusion of CPZ/before VE				
<i>Sham</i>	11.78±4.48	81.71±35.59*	17.02±6.95*	1.22±0.87*
<i>CIH</i>	10.53±3.02	101.26±43.85*	23.64±11.19*	1.53±0.64*
2x2 ANOVA				
<i>Exposure</i>	P=0.169	P=0.155	P=0.090	P=0.166
<i>Drug</i>	P=0.242	P<0.001	P<0.001	P<0.001
<i>Exposure x drug</i>	P=0.585	P=0.760	P=0.394	P=0.976

Data are expressed as mean±SD in sham (n=9) and CIH-exposed rats (n=9). Two basal urine samples were averaged and data were compared between CIH-exposed and sham rats during saline and CPZ phases by repeated-measures two-way ANOVA. * p<0.05 vs. corresponding value during intra-renal infusion of saline. GFR, glomerular filtration rate; UF, urine flow; CPZ, capsaizepine.

Table 4. 2. MAP, HR and RSNA before and during VE challenges in sham and CIH-exposed rats.

Parameter	First VE (saline phase)				Second VE (CPZ phase)			
	MAP (mmHg)	HR (beats min ⁻¹)	RSNA (% of max)	RSNA (μV.s)	MAP (mmHg)	HR (beats min ⁻¹)	RSNA (% of max)	RSNA (μV.s)
	Before intra-renal infusion of saline				Before intra-renal infusion of CPZ			
<i>Sham</i>	90±9	409±35	15±5	0.71±0.34	94±11	430±41	18±6	0.87±0.43
<i>CIH</i>	99±10	444±49	32±18 [†]	1.19±0.82	98±11	448±42	23±6	0.95±0.72
	After intra-renal saline (before VE)				After intra-renal CPZ (before VE)			
<i>Sham</i>	90±8	408±49	18±8	0.86±0.50	83±5 [#]	412±45	18±6	0.86±0.41
<i>CIH</i>	90±4	428±46	30±14 [†]	1.14±0.78	90±5 [#]	431±46	22±8	0.94±0.74
	Last two minutes of VE				Last two minutes of VE			
<i>Sham</i>	92±15	451±35*	15±6*	0.69±0.36*	76±10	443±33*	12±6*	0.53±0.71*
<i>CIH</i>	91±9	458±31*	18±5*	0.78±0.68*	90±9	450±25*	11±8*	0.58±0.38*
	2X2 ANOVA (before vs. after intra-renal saline/CPZ)							
<i>Exposure</i>	P=0.075	P=0.131	P=0.035	P=0.180	P=0.225	P=0.165	P=0.158	P=0.567
<i>Time</i>	P=0.102	P=0.084	P=0.894	P=0.330	P=0.024	P=0.100	P=0.722	P=0.396
<i>Exposure X time</i>	P=0.065	P=0.007	P=0.044	P=0.137	P=0.502	P=0.748	P=0.975	P=0.838
	2X2 ANOVA (after intra-renal saline/CPZ vs. last two minutes of VE)							
<i>Exposure</i>	P=0.516	P=0.404	P=0.077	P=0.527	P=0.045	P=0.205	P=0.581	P=0.942
<i>Time</i>	P=0.072	P<0.001	P=0.01	P=0.026	P=0.168	P=0.002	P=0.001	P=0.010
<i>Exposure X time</i>	P=0.786	P=0.182	P=0.115	P=0.388	P=0.073	P=0.218	P=0.252	P=0.591

Data were collected from sham (n=8) and CIH-exposed rats (n=9) of the first cohort. Data are expressed as mean±SD. Baseline values over a 2-minute period were averaged before and after the infusion of saline or CPZ and were analysed using repeated-measures two-way ANOVA. The last two minutes of each VE trial were averaged and compared with baseline values collected immediately before VE using repeated-measures two-way ANOVA. * p<0.05 vs. corresponding value after intra-renal infusion of saline/drug. [#] p<0.05 vs. corresponding value before intra-renal infusion of drug. [†] p<0.05 vs. sham. MAP, mean arterial blood pressure; HR, heart rate; VE, volume expansion; CPZ, capsaizepine; RSNA (% of max), renal sympathetic nerve activity normalized to maximum activity recorded during baroreflex activation during euthanasia.

4.2.2. Effect of CIH on the low-pressure baroreflex control of RSNA

RSNA recordings during VE challenge are shown in Figure 4.1. The low-pressure baroreflex was examined in terms of RSNA response to VE challenge. VE caused a progressive significant decrease in RSNA, which reached its maximum after 28-30 minutes. The drop in RSNA during VE in the presence of intra-renal infusion of saline was not significantly different between CIH-exposed and sham rats (Figure 4.2).

4.2.3. RSNA response to VE during intra-renal TRPV1 blockade

During intra-renal infusion of CPZ, the decrease in RSNA (% of max) in response to VE was equivalent in CIH-exposed and sham rats (Figure 4.2). However, an apparent potentiation of the RSNA sympatho-inhibitory response to VE was observed in both groups when RSNA (% of baseline) was considered.

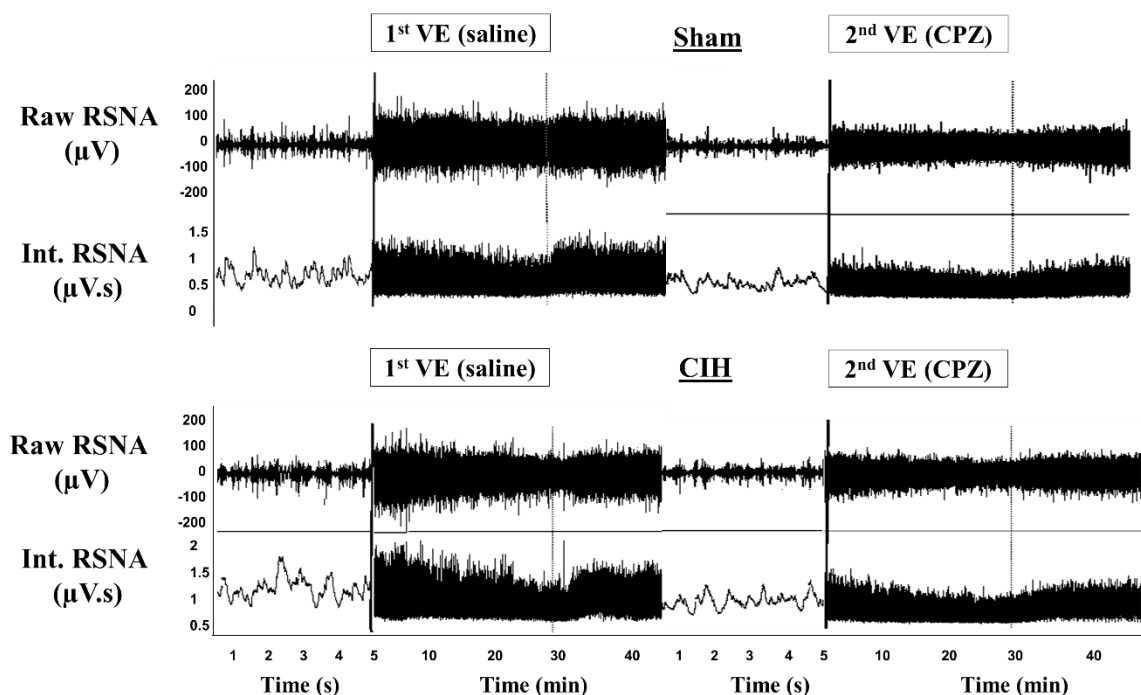


Figure 4. 1. Representative recordings of RSNA response to VE in anaesthetised rats. Raw and integrated RSNA responsiveness to VE evoking the low-pressure baroreflex. Recordings are shown for representative sham and CIH-exposed rats showing responses during intra-renal infusion of saline and intra-renal infusion of CPZ, (TRPV1 blocker). RSNA, renal sympathetic nerve activity; Int. RSNA, integrated RSNA; VE, volume expansion; CPZ, capsaizepine.

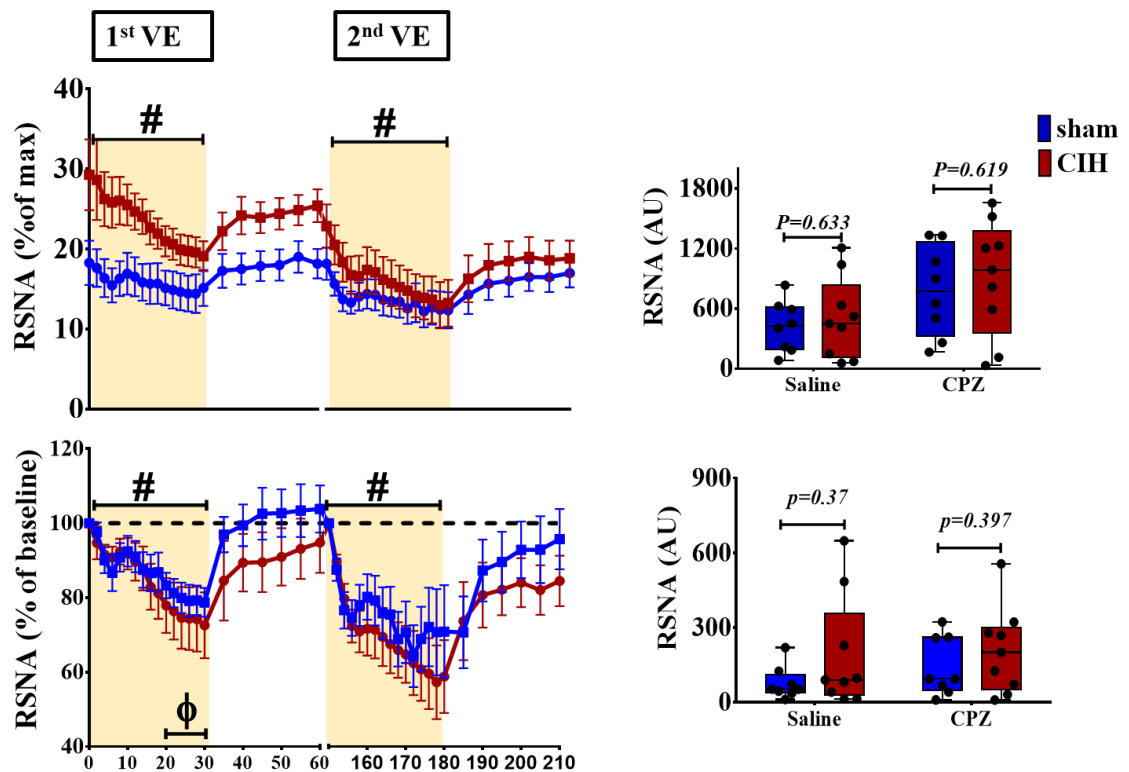


Figure 4. 2. RSNA responses to VE. In sham (n=8) and CIH-exposed rats (n=9), RSNA responses to VE challenges were determined. In the left-hand panels, the time course of responses to and recovery from VE during intra-renal infusion of saline or CPZ (TRPV1 blocker) are shown. Integrated RSNA values were averaged every two minutes during both VE challenges and every 5 minutes during the recovery after VE (mean±SE). Each averaged RSNA value was either normalized to baseline RSNA, which was taken as 100% (upper left panel), or normalized to the maximum RSNA (lower left panel). Maximum RSNA was obtained during euthanasia and was calculated as an average of 5s. Two-way ANOVA (time x exposure) was used to statistically compare the data. # $p<0.05$ for time; Φ $p<0.05$ for time points significantly different from respective baseline (post-hoc analysis). In the right-hand panels, area under the curve (AUC) analysis for the respective responses were calculated using the trapezoidal rule by the summation of the VE period. AUC data are expressed in arbitrary units (AU) and represent the sum of small areas (trapezoids) that are calculated for every two minutes of the VE challenge. Data are shown as individual data points for each rat, with box and whiskers plots representing the interquartile range and maximum and minimum values. AUC data were compared using independent *t*-tests. Significance was taken at $p<0.0125$, accounting for multiple comparisons. RSNA, renal sympathetic nerve activity; CPZ, capsaizepine; VE, volume expansion.

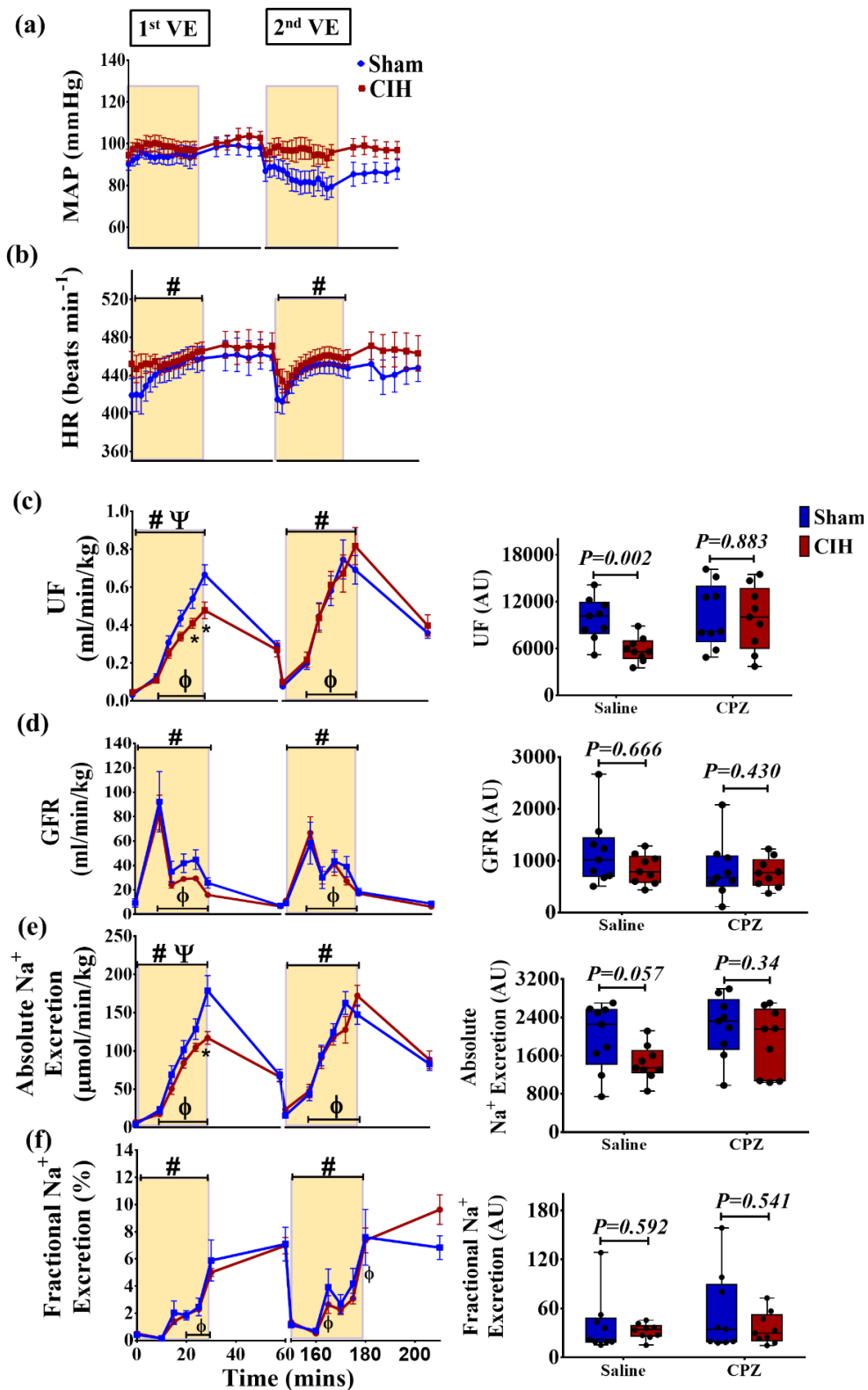


Figure 4. 3. Cardiovascular and renal excretory responses to VE. In sham (n=8) and CIH-exposed rats (n=9), MAP, HR, UF, GFR, absolute and fractional Na⁺ excretion responses to VE challenges were determined. In the left-hand panels, the time course of responses to and recovery from VE during intra-renal infusion of saline or CPZ (TRPV1 blocker) are shown. Data (mean±SE) were averaged over each 2-minute period during VE trials. Two-way ANOVA (time x exposure) was used to

statistically compare the data. # $p < 0.05$ for time; Φ $p < 0.05$ for time points significantly different from respective baseline (post-hoc analysis); Ψ $p < 0.05$ for exposure; * $p < 0.05$ compared with corresponding time point in sham rats. In the right-hand panels, area under the curve (AUC) analysis for the respective responses is shown (expressed in arbitrary units, AU), calculated using the trapezoidal rule, by the summation of the VE period. Data are shown as individual data points for each rat, with box and whiskers plots representing the interquartile range and maximum and minimum values. Data were compared with independent t -tests. Significance was taken at $p < 0.0125$, accounting for multiple comparisons. MAP, mean arterial pressure; UF, Urine flow; GFR, glomerular filtration rate; MAP, mean arterial blood pressure; HR, heart rate; CPZ, capsaizepine.

4.2.4. Effect of CIH on renal excretory responses to VE

VE in CIH-exposed and sham rats resulted in significant increases in GFR, UF and Na^+ excretion (Figure 4.3c-f). The response pattern and magnitude of GFR and fractional Na^+ excretion during VE were similar in sham and CIH-exposed rats. Diuresis in response to VE was of significantly lesser magnitude in CIH-exposed rats compared with sham rats after 25 and 30 minutes (Figure 4.3c). Similarly, absolute Na^+ excretion was significantly less in CIH-exposed rats after 30 minutes of VE (Figure 4.3e). Analysis of area under the curve (AUC), reflecting the temporal cumulative response to VE, revealed that UF was significantly less in CIH-exposed rats compared with sham rats (Figure 4.3c).

4.2.5. Renal excretory responses to VE during intra-renal TRPV1 blockade

During intra-renal infusion of CPZ, significant increases in UF and absolute Na^+ excretion in response to VE were observed in CIH-exposed and sham rats, with no significant difference between the experimental groups (Figure 4.3).

4.2.6. Cardiovascular responses to VE

Baseline ANP concentration in plasma prior to VE challenge was not significantly different between CIH-exposed and sham rats (CIH vs. sham; 157 ± 17 vs. 167 ± 36 pg/ml). In response to VE, the estimated ANP amount in plasma was increased in both groups. However, there was a lesser increase of ANP in CIH-exposed compared with sham group (Δ ANP: CIH vs. sham; 1.54 ± 0.28 vs. 4.36 ± 1.55 ng, $p = 0.026$). MAP and

HR data during each VE trial are shown in Figure 4.3a and 4.3b. During the last 2 minutes of each VE trial, MAP was not significantly different from respective baseline values recorded prior to VE (Table 4.2). HR was significantly elevated during the last 2 minutes of each of the VE trials, both in CIH-exposed and sham rats (Table 4.2).

4.2.7. Content of TRPV1 in renal tissue

TRPV1 channels are mainly expressed in the nerve fibres located between the muscular layer and the uroepithelium of the renal pelvic wall (Figure 4.4). Positive staining was also expressed in the uroepithelium (Figure 4.4). TRPV1 fluorescence occupied $5.1 \pm 1.0\%$ of the area of the muscularis propria of the pelvic wall of CIH-exposed rats, which was equivalent to sham rats ($6.4 \pm 1.9\%$, Figure 4.4f). Similarly, TRPV1 expression in the uroepithelium was equivalent between CIH-exposed and sham rats ($3.7 \pm 0.9\%$ vs. $3.9 \pm 1.1\%$). TRPV1 protein concentration in whole kidney tissue measured by ELISA (Figure 4.4f, bottom) was not significantly different between CIH-exposed and sham rats.

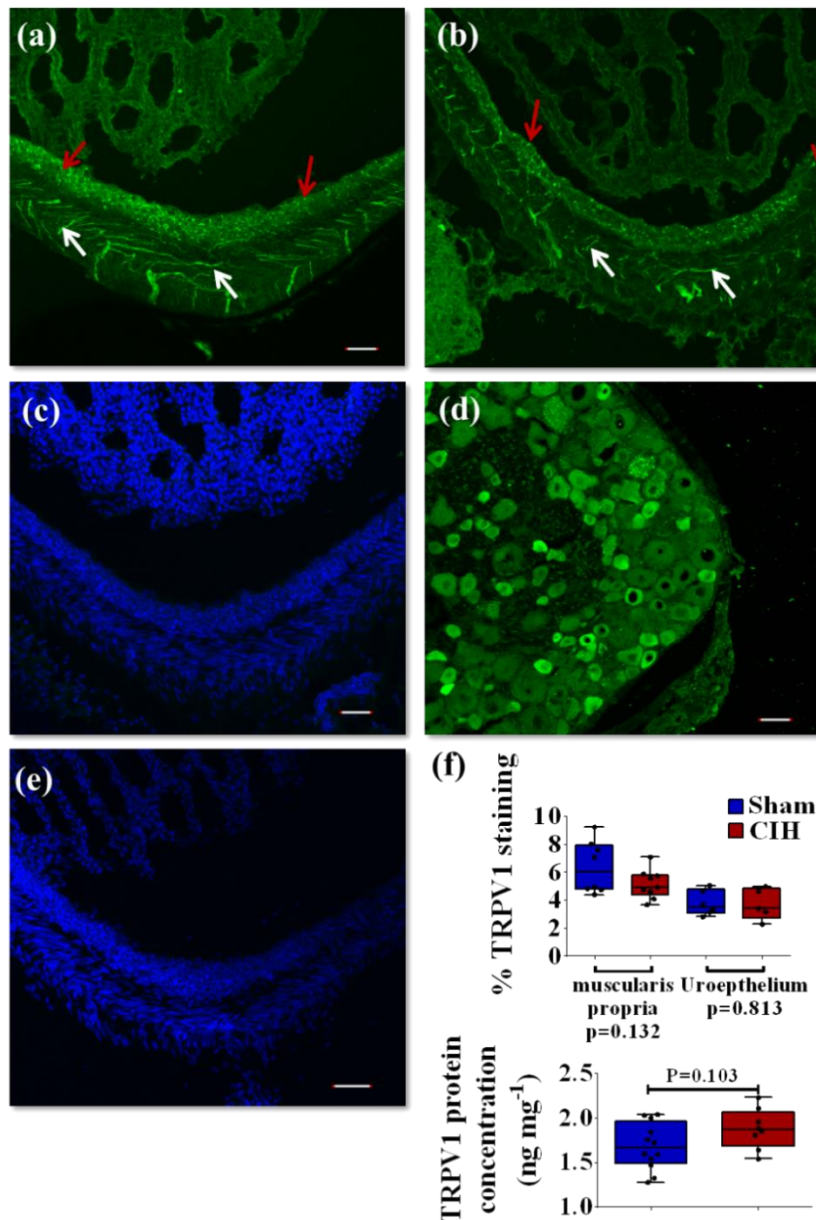


Figure 4. 4. TRPV1 immunofluorescence in the renal pelvic wall. Immunofluorescence labelling of renal pelvic wall showing TRPV1-positive labelling within the muscularis propria (white arrows) and uroepithelium layer (red arrows). (a) is a representative image from a sham kidney and (b) is a representative image from a CIH-exposed kidney. Negative controls demonstrate specificity of the antibodies used in the study (c, primary antibody omitted; e, secondary antibody omitted); Blue labelling of nuclei by DAPI. (d) Immunofluorescence labelling of TRPV1 channels in neuronal cell bodies of lumbar dorsal root ganglia as a positive control. Scale bar 50 μ m. Data for TRPV1-positive staining (% of total area) in sham (n=8) and CIH-exposed rats (n=9) are shown as individual data points for each rat, and box and whiskers plots representing the interquartile range and maximum and minimum values (f, top). Data for TRPV1 protein concentration of kidney tissue homogenate in sham (n=12) and CIH-exposed rats (n=8) are shown as individual data points for each rat, with box and whiskers plots representing the interquartile range and maximum and minimum values (f, bottom). Data were compared with independent *t*-tests. Significance was taken at $p < 0.05$.

4.3. Discussion

The key new findings of the present chapter are as follows: 1) In CIH-exposed rats, diuretic and natriuretic responses to VE were impaired, notwithstanding that the sympatho-inhibitory response of RSNA to fluid overload was preserved. 2) Preliminary observations suggest that intra-renal TRPV1 blockade with CPZ restored the renal excretory responses to VE in CIH-exposed rats, but this requires further testing.

4.3.1. Low-pressure baroreflex control of RSNA

VE has been previously used to study the integrity of the low-pressure baroreflex and associated RSNA and kidney functional changes (168, 169). During VE, a marked decline (~30%) in RSNA was observed in sham rats of the current study, which is similar to previous studies (41, 168). HR was significantly elevated during VE which might be related to the Bainbridge reflex and increased cardiac sympathetic nerve activity (CSNA) in response to fluid overload (129). An increase in blood volume induces distinct SNA responses such as an increase in CSNA, a decrease in splanchnic and renal SNA, but was not shown to change lumbar SNA (19, 129, 260, 292). There was no significant change in MAP during VE in this study, which was also observed in previous studies (3, 41).

Exposure to CIH did not affect the sympatho-inhibitory response of RSNA to VE. This suggests that altered low-pressure baroreflex control of RSNA does not contribute to CIH-induced hypertension. However, impaired low-pressure baroreflex was indeed evident in cisplatin-induced renal failure and other models of severe hypertension such as spontaneously hypertensive rats (SHR) (120, 168, 374). Moreover, central activation of angiotensin II type 1 (AT-1) receptor, which are upregulated in the SON of CIH-exposed rats (319), blunts the sympatho-inhibitory response of RSNA to VE (7). Therefore, we predict that altered low-pressure baroreflex control of RSNA in our model might manifest later, suggesting it is a consequence of hypertension during disease progression. Further studies to explore the low-pressure baroreflex in severe models of CIH are therefore warranted.

Low-pressure baroreflex is composed of afferent inputs from volume receptors in the cardiopulmonary region, inter-neurons in the brainstem and hypothalamus, and efferent pre- and post-ganglionic sympathetic and parasympathetic neurons. In hypertensive disease models such as SHR (107, 357), cardiac remodelling was associated with impaired RSNA sympatho-inhibitory response to VE and reduced fall in forearm vascular resistance (232, 357). Treatment of individuals with anti-hypertensive agents resulted in greater decrease in forearm vascular resistance and reduced left ventricular weight (232). Moreover, in essential hypertension in humans, the decrease in forearm vascular tone and renin release in response to an increase in central venous pressure by leg elevation was markedly blunted. The responses were further attenuated in hypertensive participants with cardiac hypertrophy (121). A coherent correlation between the degree of cardiac remodelling and impaired RSNA response to VE was evident, indicating a change in the sensitivity of cardiopulmonary receptors at peripheral level. In relation to this, severe models of CIH revealed cardiac hypertrophy (396, 398). At the same time, aggravated chemoreflex drive occurs at an early stage of CIH exposure which induces central modulation and dysregulation of sympathetic outflow (75), suggesting that altered low-pressure baroreflex might occur at later stages of the disease. This alteration in the baroreflex is suggested to be a consequence of the dysfunction in the central circuit or in the peripheral vagal receptors in association with cardiac structural changes during persistent hypertension.

In our study, we examined the overall change in RSNA in response to VE. Our analysis did not measure the frequency of neural bursts distinctively from the amplitude of RSNA signal. Indeed, an increase in the amplitude indicates recruitment of nerve fibres. In sheep, VE induced a decrease in the frequency of bursts and amplitude of RSNA (293). In contrast, a decrease in the amplitude with no change in the frequency of bursts in response to VE was revealed in rabbits (204).

Of note, VE challenges were performed following the assessment of the high-pressure baroreflex, discussed in chapter 3. The effects of phenylephrine and sodium nitroprusside on the RSNA and cardiovascular parameters are short-lived, as shown in Figure 3.2. Sufficient time (~30 minutes) was allowed before the beginning of the first VE phase to ensure the return of parameters to baseline levels. Therefore, it is less likely that the assessment of the high-pressure baroreflex using vasoactive agents had

an effect on the low-pressure baroreflex. Moreover, previous studies in our laboratory utilized this approach (2, 141).

4.3.2. Renal excretory responses to VE

Basal renal function was not significantly different between sham and CIH-exposed rats despite increased basal RSNA in the CIH group (Table 3.1). Nevertheless, the renal excretory response to VE in CIH-exposed rats was blunted with a resultant sodium and water retention (Figure 4.3c and 4.3e). These findings suggest that compensatory mechanisms in the kidney ensure maintenance of normal basal kidney function in the face of CIH-related stress and sympathetic over-activity. Dysfunction was revealed however, during VE challenge, with evidence of blunted diuretic and natriuretic responses, which appear independent of neural control of the kidney. Similarly, in streptozotocin-induced diabetic rats, basal diuresis and natriuresis was equivalent to non-diabetic rats, but excretory responses were impaired during VE (379). The underlying mechanisms that contribute to impaired excretory responses during VE are multifactorial and do not depend solely on changes in RSNA. Such mechanisms include alterations in RAAS activity, renal perfusion pressure, and glomerular filtration rate (GFR). Thus, our findings of blunted sodium and fluid excretion during VE in CIH-exposed rats, despite preserved reflex reduction in RSNA, highlighted that other mechanisms might contribute to diuretic and natriuretic responses to VE and revealed that one or more of these mechanisms are perturbed by exposure to CIH.

In conscious and anaesthetized rats, diuresis and natriuresis responses were eliminated following bilateral removal of atrial appendages which were comparable to responses obtained after selective right atrial appendectomy, indicating that vagal receptors, located in the right atrium, are linked to the VE-mediated renal excretory responses (308). However, vagotomy in another study in rats decreased the diuretic but it did not have any effect on the natriuretic response to VE (361). Vagotomy was also associated with 75% attenuation in RSNA sympatho-inhibitory response in dogs (19). It is worth mentioning that balloon inflation in the left atrium and negative pressure breathing were associated with diuresis, but not natriuresis (19). Moreover, an increase in extracellular volume with no alteration in plasma volume was associated with

natriuresis (315). This provides evidence for differential mechanisms involved in the regulation of diuretic and natriuretic responses to VE. In response to VE in dogs, the increase in sodium excretion preceded the increase in diuresis (19). Based on these observations, it was hypothesized that there are extrathoracic receptors that detect increased blood volume, in addition to other receptors in the interstitial compartment of the body (19). In support of this notion, infusion of hyperoncotic saline, a colloidal fluid of 5% albumin, during haemorrhage restored the blunted water excretion to baseline, while sodium retention persisted along with excessive aldosterone levels (19), suggesting a distinct mechanism controlling sodium excretion in response to changes in blood volume.

Diuresis occurred without any consistent and uniform change in GFR between groups. Sodium and fluid excretion reached its maximum at the end of VE (after 25 to 30 minutes), while GFR showed a transient increase at the beginning of the challenge, followed by a decline until the end of the 30-minute period. Previous VE studies reported either no change, or small inconsistent changes in GFR, concomitant with increased sodium and fluid excretion (19, 134). Hegde et al. (134) using 60 minutes of VE in normal rats, showed a transient increase in GFR after 30 minutes of VE initiation followed by a decline until the end of the 60 minute period. Furthermore, in humans, a decrease in venous return was associated with a decline in GFR and sodium excretion. When venous return was restored to normal, GFR was normalized but with sustained decrease in sodium excretion, which was later restored to normal (315). Therefore, variable GFR responses in our study were in line with previous studies using similar VE challenges. Possible alterations in GFR during VE result from changes in renal haemodynamics (an increase in renal blood flow and a decrease in renal vascular resistance). Franchini et al. (102) showed that changes in renal haemodynamics are not strictly dependent on neural control of the kidney. VE using isotonic saline results in haemodilution and decreased blood viscosity, which was associated with a decrease in renal vascular resistance and an increase in renal blood flow. However, VE using whole blood infusion was associated with no changes in renal haemodynamics, suggesting that rheological changes of blood induce renal haemodynamic changes during VE. In the current study, the change of haematocrit during VE in saline and CPZ phases was not significantly different between exposure

groups (Appendix I, Figure 8.4), indicating that haemodilution is less likely to contribute to the differences in excretion between CIH-exposed and sham rats.

A decrease in oncotic pressure in response to VE inhibits water and sodium reabsorption from proximal tubules (39). It was shown that the addition of albumin to the volume-expanded fluid restored water and sodium reabsorption in proximal tubules. We performed volume expansion using saline which resulted in a decrease in blood oncotic pressure, reducing the oncotic gradient between peritubular capillaries and the lumen of proximal tubules. Accordingly, oncotic pressure changes during VE contribute to diuresis and natriuresis by decreasing sodium and water fractional reabsorption through the proximal tubule (331). Proteinuria was evident after exposure to a CIH paradigm similar to the one used in this study (258), suggesting higher luminal oncotic pressure in CIH-exposed rats compared with shams. Therefore, it is less likely that differences in the oncotic pressure gradient between CIH and sham groups contribute to differences in diuresis and natriuresis observed in this study. Although we did not observe differences in the GFR response to VE between CIH-exposed and sham rats, indicating less likelihood of differences in glomerular hydrostatic pressure, the possibility of changes in peritubular capillary hydrostatic pressure exerting an effect on tubular water and sodium reabsorption cannot be ruled out (145).

On the other hand, it has been shown that acute VE is associated with suppressed levels of renal and plasma angiotensin II (Ang II) with no change in the intraluminal content of Ang II in the proximal tubule (34). A dissociation between extraluminal and intraluminal renal tubular levels of Ang II was reported during VE. It was suggested that Ang II production and degradation are differentially altered inside proximal tubules compared with renal interstitium (34). Remarkably, chronic hypoxia was associated with reduced protein and gene expression of neutral endopeptidase 24.11, responsible for Ang II degradation in the proximal tubule (362). Moreover, decreased cortical PO₂ (partial pressure of oxygen) with unaltered oxygen tension in the medulla was shown in a model of CIH, similar to the one used in this study (258). The latter suggests altered sodium transport at superficial segments of the nephron. Further studies are required to examine whether the regulation of Ang II in proximal tubules is altered and if it contributes to the blunted diuresis during VE. Together, these

observations suggest the presence of a tubular-related mechanism controlling diuresis and natriuresis (30, 52, 306), which is adversely affected in CIH.

Of note, our results showed a concomitant increase in natriuresis and diuresis during 30-minute VE. We measured total urine volume which does not indicate free water excretion. VE studies provided evidence that the natriuretic response to VE is independent of increased diuresis. A previous study showed that fractional sodium excretion is increased while free water excretion is decreased during isotonic saline VE (238). Nonetheless, blunted natriuresis in CIH-exposed rats of this study was linked to decreased absolute sodium excretion, while fractional sodium excretion was comparable between CIH-exposed and sham rats. This might indicate that sodium load into the kidney was less in CIH-exposed rats. In support of this notion, there was a linear correlation between increased fractional sodium excretion and decreased filtration fraction (i.e. decreased sodium load on tubules) in a previous study (288). Sodium load is affected by renal haemodynamics (renal blood flow and vascular resistance) and by Starling forces (hydrostatic and oncotic pressures). However, these measurements were beyond the scope of this study and this requires further investigation.

Martinez-maldonado et al. (238) have shown that medullary and papillary solute concentration is increased in response to isotonic saline VE although fractional sodium excretion is increased. This strongly indicates that sodium reabsorption increases during VE across the early segment of the nephron. Subsequently, impaired sodium reabsorption occurs beyond the ascending limb of the loop of Henle (238), through a mechanism that is not fully understood. Similarly, Sonnenberg et al. (331) showed that absolute proximal transport did not change during VE and suggested that excretory responses are due to changes at the distal parts of the nephron.

Natriuretic peptides are stored in cardiomyocytes and are released in response to stretch of the cardiac wall. ANP is the most abundant natriuretic peptide, which binds to natriuretic peptide receptor A located in the kidney to boost diuresis and natriuresis (378). During VE, it was suggested that ANP mediates natriuresis by acting on the distal segment of the nephron (23). In the current study, the magnitude of ANP increase during VE was less in CIH-exposed rats compared with sham rats. In a previous study, VE in anaesthetized rats resulted in diuresis and natriuresis in the

presence of increased plasma ANP (308), similar to our observation. In another group of rats, synthetic ANP bound to bovine thyroglobulin was injected to produce antibodies and autoimmunity to ANP. These rats had no increases in water and sodium excretion during VE (308). Interestingly, bilateral removal of atrial appendages resulted in no change in plasma ANP and eliminated the diuretic and natriuretic responses (308), indicating that renal excretory responses to VE in anaesthetized rats is dependent upon ANP. A previous study from our laboratory has shown that exposure to the same CIH protocol was associated with hypertrophy of the right and left interventricular septum, and increased cardiac output (226). Thickening of the right side of the heart is usually caused by pulmonary hypertension, which was observed following exposure to a different protocol of CIH (255). VE studies indicated that volume receptors are located in the left and the right atria of the heart. Therefore, the presence of hypertrophy and apoptosis of cardiomyocytes, which was observed previously in a CIH model (388), suggests that the attenuated release of ANP in CIH-exposed rats during VE might be related to decreased elasticity of the heart. Meanwhile, the main stimulus for the myocardial stretch and the release of ANP is the increase in atrial pressure during fluid overload, which could be different between CIH-exposed and sham rats. The measurement of atrial pressure during VE challenges was beyond the scope of this study, which requires investigation.

Of note, however, VE in conscious rats caused diuresis and natriuresis with no change in plasma ANP. On another hand, in conscious ANP autoimmune rats, there was a similar diuresis and natriuresis response during VE compared with control rats (308). Moreover, it has been shown that ANP rises within 5 minutes of VE initiation, whereas natriuresis peaked between 15-20 minutes after challenge (25). The latter study suggested that ANP is responsible for the initial natriuretic response, whereas the subsequent sodium excretion is due to prolonged suppression of RAAS by an ANP-independent mechanism (378). Based on these studies, blunted diuresis and natriuresis responses to VE in CIH-exposed rats are also related to additional factors beyond the demonstrated suppressed release of ANP. Changes in other humoral factors such as inhibition of ADH secretion and decreased aldosterone levels may also explain the diuretic and natriuretic responses (19). Indeed, a more modest CIH paradigm than that used in the current study, resulted in up-regulation of ADH receptors in the rostral ventrolateral medulla (RVLM) and rostral ventral respiratory column (278). In

addition, exposure to CIH for 7 days was sufficient to increase the activity of the adrenal gland with marked elevation in aldosterone (289). In relation to that, elevated levels of aldosterone was also reported in OSA patients (284). Both ADH and aldosterone exert a direct tubular effect on the reabsorption of sodium and water (19).

In contrast, Brattleboro rats (a strain of rats which lacks the ability to produce ADH) showed similar diuretic and natriuretic responses to VE compared with ADH-supplied rats under both anaesthetic and conscious conditions (308). In another study, blunted natriuresis during VE was attributed to reduced dopamine in healthy rats and elevated nitric oxide in diabetic rats (134, 379). However, this is a weak argument regarding the CIH model, as elevated dopamine levels and reduced nitric oxide bioavailability were reported after CIH exposure (22, 171). Nonetheless, further studies are required to explore further mediators that account for impaired diuresis and natriuresis in the CIH model.

In summary, we exposed rats to 14 days of CIH which was not associated with significant changes in basal kidney function but resulted in blunted diuresis and natriuresis in response to fluid overload. Exposure to CIH for longer durations was associated with marked deterioration of kidney function at basal levels including increased serum creatinine level, proteinuria and decreased GFR (9, 303). It is likely that impairment in kidney function in CIH models develops gradually and originates from a combination of factors that are directly related to hypoxia and as a major player, a vicious cycle of sympatho-excitation and hypertension.

4.3.3. Blockade of TRPV1 channels

A subgroup of afferent renal nerves are positively labeled with TRPV1 channels, which are co-localized with substance P (SP) sensory neurotransmitter in the renal pelvic wall (160, 385). In rats, cortico-medullary infusion of the TRPV1 agonist, capsaicin, induces an increase in contralateral RSNA (287, 397). Capsaicin also increases c-fos labelling in the PVN, where magnocellular neurons responsible for ADH release are located (325). Reactive oxygen species (ROS) increase the activity of TRPV1 receptors. Acute hypoxia increases the tonic activity of TRPV1, which was suppressed using CPZ and Tiron, a membrane permeable ROS scavenger (172). On another hand, overnight exposure to chronic hypoxia was associated with reduced de-

sensitization of TRPV1 channels normally observed during their continuous stimulation (304). It was shown that TRPV1 activation decreases cell viability and induces apoptosis (343). P38 MAPK-mediated apoptosis is one of the pathways activated by TRPV1 receptors, which was also found to be activated in kidney tissue of CIH-exposed rats (382). Moreover, endogenous hydrogen peroxide (H_2O_2) released by the activation of renal pelvic NADPH oxidase 4 (NOX4) stimulates TRPV1 containing afferent renal nerves (216). Therefore, in the CIH model, we investigated the role of renal TRPV1 receptors in baroreflex regulation of RSNA during VE, in addition to their putative effect on diuretic and natriuretic responses to VE. We aimed to target TRPV1 receptors that are involved in the activation of afferent renal nerves.

Intra-renal infusion of CPZ caused a significant reduction in MAP, but without an attendant decrease in RSNA (Table 4.2). CPZ was also associated with increased diuretic and natriuretic responses to VE in CIH-exposed and sham rats. However, the renal sympatho-inhibitory response (RSNA % of max) to VE after CPZ administration was unaffected, both in CIH-exposed and sham rats. The effect of CPZ on the renal excretory function in CIH group suggests a potential role of renal TRPV1 receptors in CIH-induced impairment of renal excretory function. In the two-kidney, one-clip model, unilateral selective denervation of afferent renal nerves containing TRPV1 channels by high dose of periaxonal application of capsaicin decreased blood pressure and attenuated renal cytokines in the clipped kidney (261). In addition, *in vitro* studies showed that TRPV1 activation increases ROS and intra-cellular calcium influx, which was associated with enhanced apoptosis. Treatment of H9C2 cardiomyocytes with CPZ improved cell viability after hypoxia-reperfusion injury (343). The increased basal activity of TRPV1 in response to hypoxia was associated with increased amplitudes of TRPV1 currents. This was associated with no alteration in protein expression (172), similar to our observation in this study.

Conversely, other studies have revealed cardiac and renal protective effects of TRPV1 in an ischaemia-reperfusion injury model because TRPV1 channels are distributed in tubules and expressed in the endothelial cells of renal arterioles (57, 160, 210, 401). TRPV1 activation by subcutaneous injection of capsaicin after ischaemia-reperfusion injury reduced tubular damage and elevated urine to water intake ratio compared with healthy rats after high-salt diet (401). This was mediated by arteriolar vasodilatation and increased GFR and was completely inhibited when SP and calcitonin gene-related

peptide (CGRP) were blocked (210). These conflicting reports suggest that TRPV1 activation elicits protective effects due to SP and CGRP release, while calcium influx provokes pathological consequences (343).

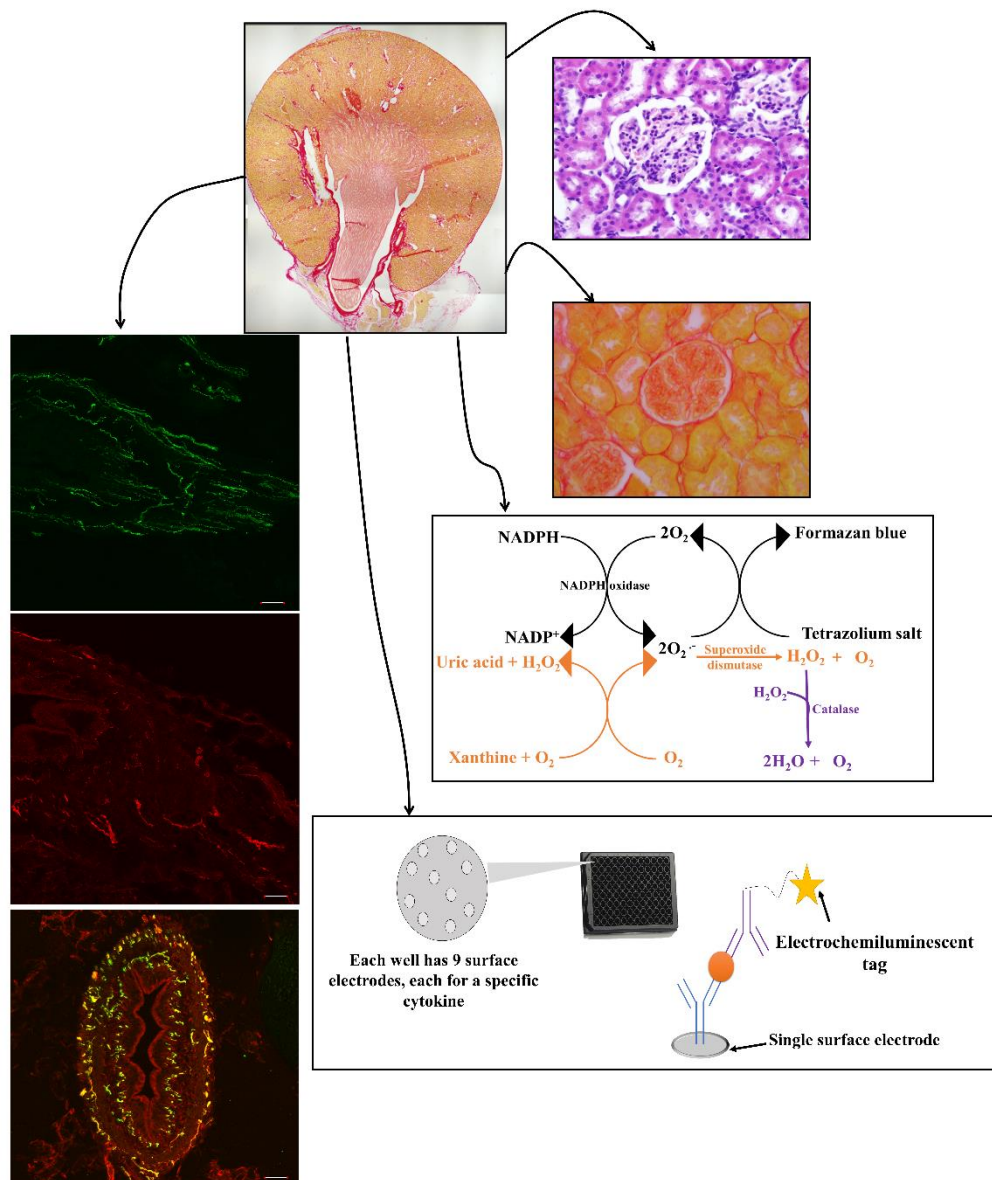
On the other hand, TRPV1 channels are involved in the sensory mechanism of different peripheral organs. They are located in the carotid sinus and the walls of aortic arch as part of the mechanosensing mechanism of baroreceptors (341). Vascular TRPV1 channels mediate vasorelaxation when activated (418). Accordingly, systemic inhibition of TRPV1 and/or gene knockout eliminates the protective activity of TRPV1 channels at some peripheral sites. Meanwhile, activation of TRPV1 located at other regions, such as kidney and adipose tissue, mediates an excitatory reflex, resulting in an increase in SNA (71, 135, 397). Therefore, we surmise that TRPV1 receptors have dual neural and peripheral (vascular) effects, and the pathological deterioration that was observed in TRPV1 knockout mice in cardiovascular disease models (57, 368) might be related to the blockade of TRPV1 at sites other than renal or adipose tissues. It was found that selective blockade of TRPV1 at the latter induces a decrease in SNA with protective consequences. In support of this notion, incorporating capsaicin as an agonist into the diet of two-kidney, one-clip rats resulted in attenuation of high blood pressure and was associated with enhanced phosphorylation of endothelial nitric oxide synthase (eNOS). The co-administration of a NOS inhibitor with capsaicin eliminated the protective effects of capsaicin with blood pressure values that remained similar to untreated kidney clipped rats (313).

In the current study, RSNA and renal excretory responses to VE were measured during two subsequent challenges. A previous study that was performed in our laboratory has shown that the RSNA sympatho-inhibitory response to two successive VE challenges were comparable (7). However, the enhanced renal excretory response during the second VE might be affected by the preceded first VE. Moreover, we cannot exclude the possibility that intra-renal CPZ induced diuresis and natriuresis per se, which was independent of RSNA. This effect of CPZ may have contributed to the recovery of renal excretory responses to VE in CIH-exposed rats and masked the original mechanism contributing to impaired renal excretory function. Therefore, our results should be viewed as preliminary and the molecular mechanisms contributing to CIH-induced impairment in renal excretory function requires further exploration.

4.4. Conclusion

Our study confirmed that the low-pressure baroreflex control of RSNA during VE was unaltered in CIH-exposed rats with established hypertension. Notwithstanding, sodium and water excretion was blunted following exposure to CIH. Our results suggest that exposure to CIH is associated with impaired excretory function, which may be relevant to OSA. Blockade of TRPV1 channels increased sodium and water excretion during VE in CIH-exposed rats to levels equivalent to shams. Impaired renal excretory response to VE in CIH was associated with blunted increase in ANP. Further studies are required to examine other humoral factors potentially involved in impaired kidney function and to determine conclusively if TRPV1 channels contribute to the altered renal function responses observed in CIH.

Chapter 5: Molecular changes in kidney tissue exposed to chronic intermittent hypoxia



List of abbreviations

Ang II	Angiotensin II
ANP	Atrial natriuretic peptide
CGRP	Calcitonin gene-related peptide
CIH	Chronic intermittent hypoxia
CKD	Chronic kidney disease
CTGF	Connective tissue growth factor
ECM	Extracellular matrix
H ₂ O ₂	Hydrogen peroxide
HIF-1 α	Hypoxia inducible factor-1 alpha
HO-1	Heme oxygenase-1
HR	Heart rate
ICAM	Intercellular adhesion molecule 1
IL-6	Interleukin-6
MAPK	Mitogen-activated protein kinase
NF- κ B	Nuclear factor kappa B
NK1	Neurokinin-1
NO	Nitric oxide
NOX	NADPH oxidase
NQO1	NADPH quinone dehydrogenase 1
Nrf2	Nuclear factor erythroid 2-related factor 2
NTS	Nucleus tractus solitarius
OSA	Obstructive sleep apnoea
PAI-1	Plasminogen activator inhibitor-1
RAAS	Renin-angiotensin-aldosterone system
ROS	Reactive oxygen species
RSNA	Renal sympathetic nerve activity
RVLM	Rostral ventrolateral medulla
SHR	Spontaneously hypertensive rat
sLTF	Sensory long-term facilitation
SNA	Sympathetic nerve activity
SOD	Superoxide dismutase

SP	Substance P
TGF- β	Transforming growth factor-beta
TNF- α	Tumour necrosis factor-alpha
TRPV1	Transient receptor potential vanilloid 1
VCAM	Vascular cell adhesion molecule 1

5.1. Introduction

Clinical studies have shown that obstructive sleep apnoea (OSA) induces a decline in kidney function and accumulating evidence has indicated that OSA alleviation improves kidney performance in individuals with chronic kidney disease (CKD) (11, 21, 410). Repetitive re-oxygenation during hypoxia (i.e. intermittent phenomenon) provokes reactive oxygen species (ROS) production and inflammatory cytokine release, causing multisystem injury and pathological consequences in different organs (146, 273, 342). Previous studies of chronic intermittent hypoxia (CIH) have shown oxidative stress and increased inflammatory cytokines in renal tissues (9, 224, 342). NADPH oxidase 2 (NOX2) in carotid bodies and NOX4 in kidney tissue are upregulated in CIH, promoting the production of ROS (200, 223). NOX activation induces hypoxia-inducible factor-1 alpha (HIF-1 α) upregulation in kidney, rostral ventrolateral medulla (RVLM), nucleus tractus solitarius (NTS) and carotid bodies, which regulates the transcription of genes responsible for the release of tumour necrosis factor-alpha (TNF- α), interleukin-6 (IL-6) and IL-1 β (200, 224, 273, 330, 382, 409). However, it is unclear if renal inflammation results from episodic hypoxia per se or if it is secondary to sympatho-excitation and hypertension. Decreased oxygen concentration in the kidney enhances ROS production and causes fibrinogenesis, which leads to a vicious cycle of hypoxia, causing glomerular sclerosis and proteinuria, the primary clinical manifestations of CKD (11). The inhibition of mitochondrial release of ROS attenuated kidney damage in diabetic rats (264). Meanwhile, sympathetic over-activity increases vascular tone, depletes nitric oxide (NO) and causes endothelial dysfunction (345), thus, decreasing kidney oxygen supply. This causes renin-angiotensin-aldosterone system (RAAS) activation and increased sodium reabsorption. The renal medulla is vulnerable to hypoxia due to high demand of O₂ required for sodium reabsorption in the thick ascending limb of the loop of Henle (264). Of note, reduced oxygen tension in renal cortex was observed in a CIH model similar to the model used in our study (258).

Renal denervation in a CIH animal model was associated with attenuation of hypertension, and inflammation and oxidative stress in kidney and brainstem regions (RVLM, NTS) that are responsible for sympathetic outflow (164). In obese rats, impaired baroreflex control of renal sympathetic nerve activity (RSNA) was

associated with renal inflammation (170). Treatment with tacrolimus, an anti-inflammatory agent, eliminated kidney inflammation and restored high- and low-pressure baroreflex function (170), suggesting that inflammation contributes to baroreflex dysfunction and disruption in the autonomic control of blood pressure, through a renal nerve-dependent mechanism.

Immunofluorescence studies have shown co-localisation between TRPV1, NOX4 and hydrogen peroxide (H_2O_2) in the renal pelvic wall (216). H_2O_2 sensitises TRPV1 channels and is produced in response to NOX activation and/or decreased expression and activity of catalase (216). Moreover, it was shown that the activation of neurokinin-1 (NK1) receptor *ex vivo* stimulates superoxide production with subsequent augmentation of capsaicin-induced activation of peripheral neurons (218). Of note, sensory long term facilitation (sLTF) of carotid bodies in CIH-exposed animals was associated with increased levels of superoxide and H_2O_2 , which was abolished by catalase (270).

Overall, the interaction between sympathetic over-activity and inflammation/oxidative stress is evident at peripheral and central sites in CIH models. However, each CIH protocol mimics a certain stage of the OSA disorder. Whereas many CIH studies have examined kidney pathology, they did not include concomitant measurement of sympathetic nerve activity (SNA) and/or blood pressure. The mechanism by which kidney injury occurs, i.e. either due to intermittent hypoxia itself or secondary to hypertension and sympatho-excitation, or combinations of these stressors, remains unclear.

5.2. Results

5.2.1. Renal histopathological assessment

Hematoxylin and eosin staining was used to examine glomerular tuft area of ~18 glomeruli per kidney. The average glomerular tuft area of the CIH-exposed group was not different from sham rats (CIH vs. sham; 7364 ± 902 vs. $7831 \pm 486 \mu m^2$, $p=0.219$, Figure 5.1). A slightly greater degree of fibrosis was observed in the cortex of CIH-exposed kidneys compared with sham kidneys (CIH vs. sham; 7.47 ± 0.60 vs. $6.73 \pm 0.70\%$, $p=0.04$, Figure 5.1b and d). In contrast, there was no significant

difference in collagen expression in the outer medulla between CIH-exposed and sham kidneys (Figure 5.1c and d).

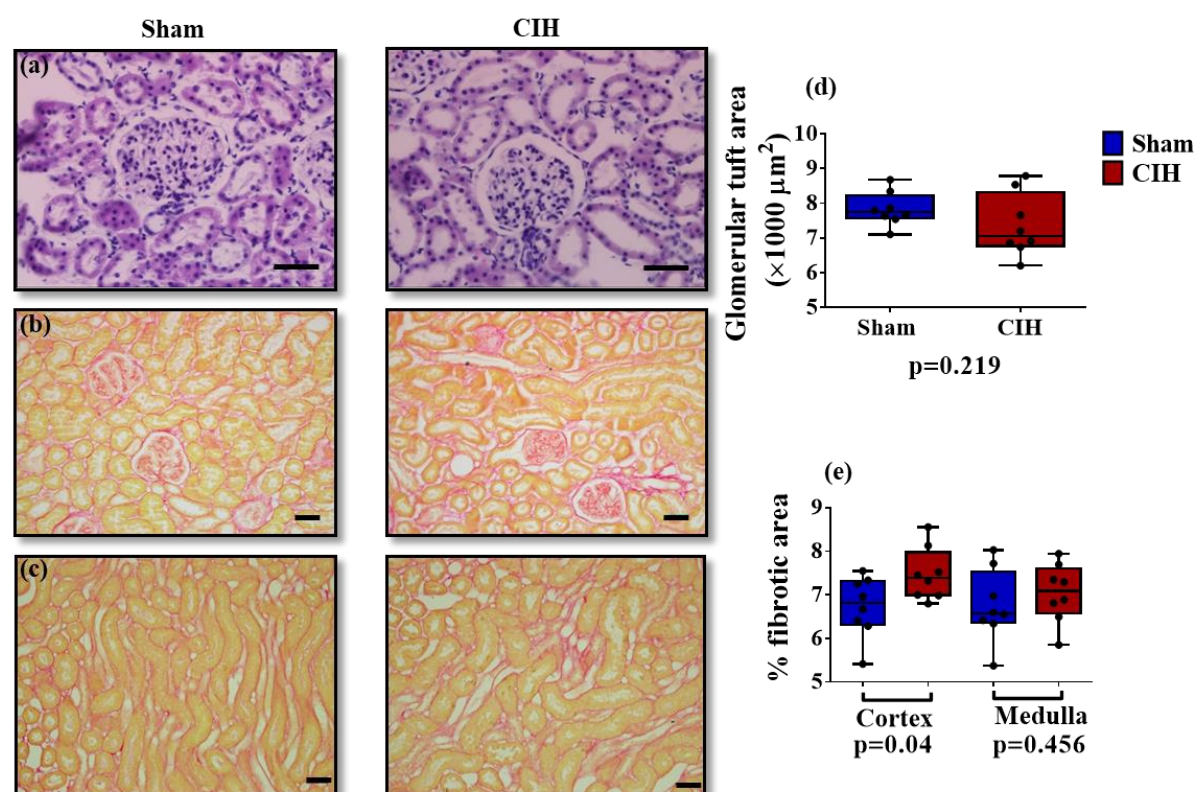


Figure 5. 1. Renal histology. Representative images from a sham and CIH-exposed rat are shown. (a) shows hematoxylin and eosin staining; (b) shows Sirius red staining of renal cortex; (c) shows Sirius red staining of renal outer medulla. Scale bar 50 μm. Data for glomerular tuft area and percentage fibrotic area are presented in (d) and (e) as individual data points for each rat, with box and whiskers plots representing the interquartile range and maximum and minimum values. Data from sham (n=8) and CIH-exposed rats (n=8) were compared using independent *t*-tests. Significance was taken at $p < 0.05$.

5.2.2. Renal oxidative stress, inflammation and protein oxidation

The activity of NOX, superoxide dismutase (SOD) and catalase enzymes was measured in whole kidney tissue and there was no significant change in the activity of these enzymes after exposure to CIH (Table 5.1). Furthermore, there was no evidence of greater protein oxidation in the kidneys of CIH-exposed rats (Table 5.1). Cytokine concentrations (IL-1 β , keratinocyte chemoattractant/growth related oncogene and TNF- α) were not significantly different between CIH-exposed and sham rats (Table 5.1).

Table 5. 1. Biomarker concentrations in kidney tissue homogenates of sham and CIH-exposed rats.

Parameter	Sham	CIH	p-value
AOPP (μM)	15.6 \pm 2.2 (n=12)	14.8 \pm 3.1 (n=8)	0.728
NADPH oxidase activity (mU min^{-1})	3.54 \pm 0.87 (n=8)	4.37 \pm 1.27 (n=9)	0.167
SOD activity (U ml^{-1})	803.5 \pm 125.0 (n=11)	792.3 \pm 120.8 (n=8)	0.846
Catalase activity (U ml^{-1})	15939 \pm 2888 (n=12)	17448 \pm 2539 (n=8)	0.105
TNF- α (pg mg^{-1})	0.22 \pm 0.22 (n=8)	0.16 \pm 0.14 (n=10)	0.790
IL-1 β (pg mg^{-1})	5.04 \pm 1.34 (n=11)	6.15 \pm 1.31 (n=10)	0.070
Keratinocyte chemoattractant/growth related oncogene (pg mg^{-1})	1.59 \pm 0.55 (n=11)	1.98 \pm 0.78 (n=9)	0.137

Data are expressed as mean \pm SD. AOPP, advanced oxidation protein products; SOD, superoxide dismutase. SOD activity, keratinocyte chemoattractant/growth related oncogene and IL-1 β concentrations were analysed using independent samples *t*-test. Other biomarkers were analysed using Mann-Whitney test.

5.2.3. Adjunct molecular analysis on renal tissue

Expression of CGRP and NK1 receptor

Immunofluorescence labelling showed positive staining of calcitonin gene-related peptide (CGRP) in uroepithelium, lamina propria and the muscular layer of renal pelvic wall. The percentage of renal pelvic area occupied by positive staining of CGRP was equivalent in CIH-exposed and sham kidneys (CIH, 6.8 \pm 1.8%; Sham, 5.5 \pm 2.5%, Figure 5.2a and Figure 5.4i). NK1 was abundant in the outer muscular layer and occupied 2.9 \pm 0.7% of the total renal pelvic wall area of CIH-exposed kidneys, which was equivalent to the percentage of renal pelvic wall area positively labelled with NK1 in sham kidneys (3.1 \pm 0.8%, Figure 5.3a and Figure 5.4j). No labelling was detected in negative control images of renal pelvic wall (Figure 5.2b and c; Figure 5.3b and c).

Most of the NK1 fluorescence was co-localised with sensory neurotransmitter CGRP in the muscular layer of renal pelvic wall (Figure 5.4c and g). Representative images of immunofluorescence of CGRP and NK1 co-labelling in the ureter are provided in Figure 8.5 of Appendix I.

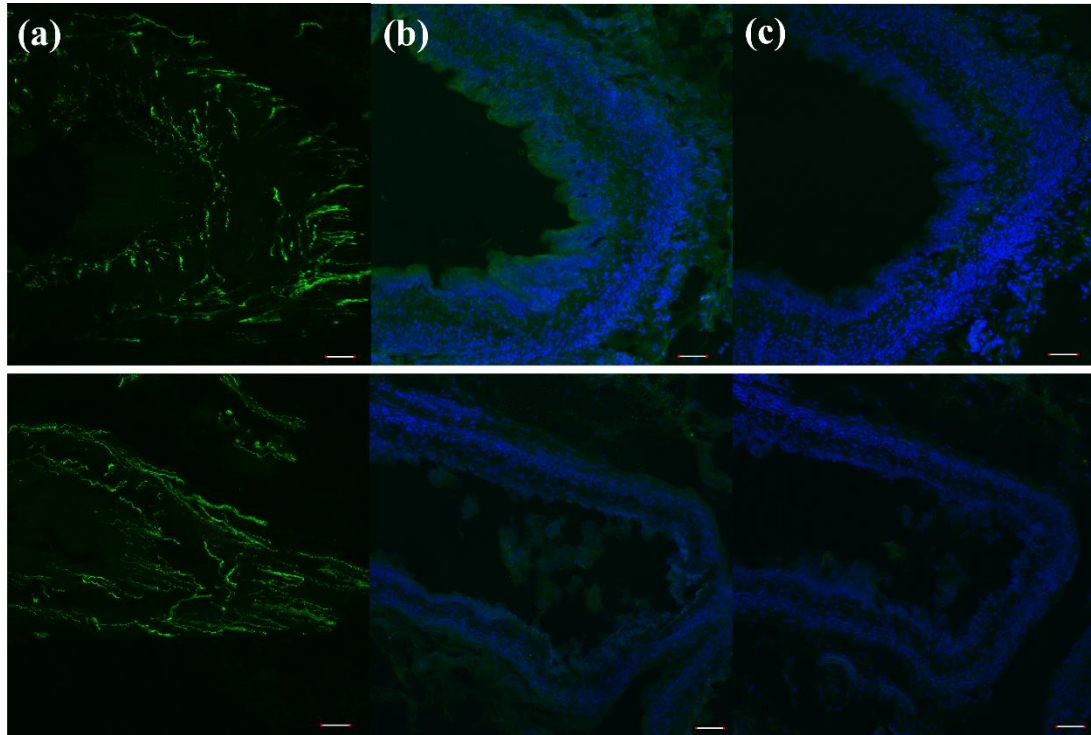


Figure 5. 2. Immunofluorescence labelling of CGRP in the renal pelvic wall. Immunofluorescence staining of the renal pelvic wall showing CGRP-positive labelling of renal afferent nerves. CGRP labelling is distributed from the outermost adventitia to the innermost layer of uroepithelium. (a, top) is a representative image from a sham kidney and (a, bottom) is a representative image from a CIH-exposed kidney. Negative controls demonstrate specificity of the antibodies used in the study (b, primary antibody omitted; c, secondary antibody omitted); Blue labelling of nuclei by DAPI (4, 6-diamidino-2-phenylindole). CGRP, calcitonin gene-related peptide.

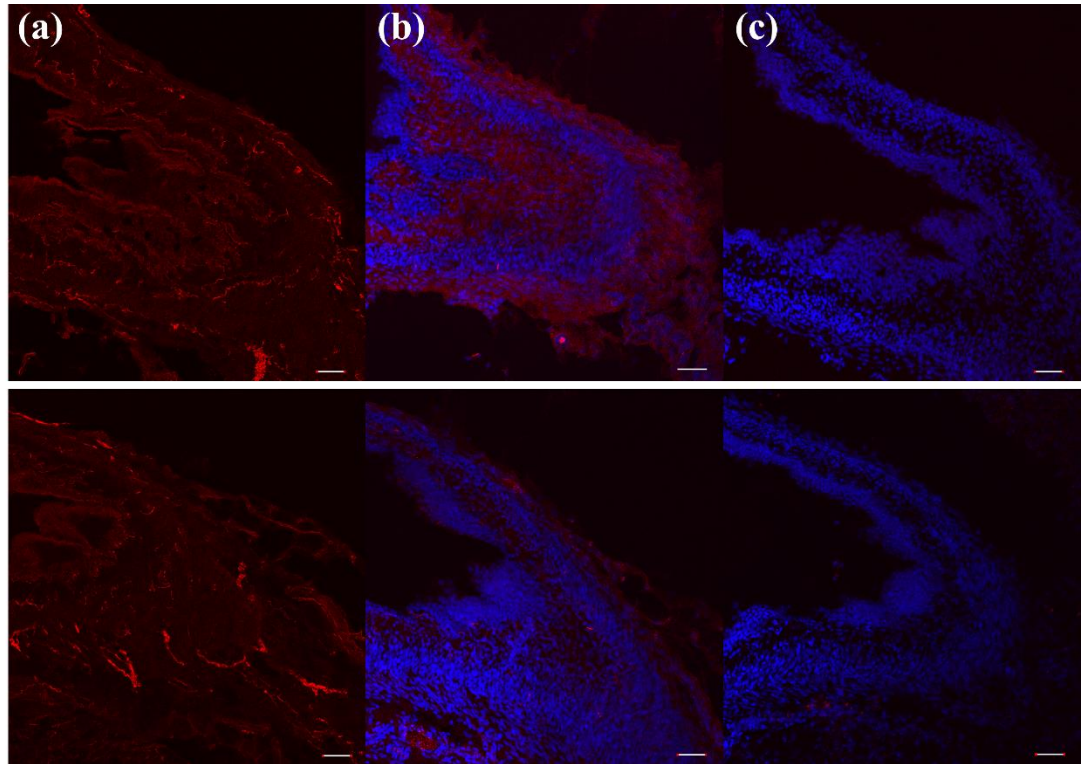


Figure 5. 3. Immunofluorescence of NK1 in the renal pelvic wall. Immunofluorescence staining of the renal pelvic wall showing NK1 receptor-positive labelling. NK1 labelling is mainly located in the outermost muscular layer of the renal pelvic wall. (a, top) is a representative image from a sham kidney and (a, bottom) is a representative image from a CIH-exposed kidney. Negative controls demonstrate specificity of the antibodies used in the study (b, primary antibody omitted; c, secondary antibody omitted); Blue labelling of nuclei by DAPI (4, 6-diamidino-2-phenylindole). NK1, neurokinin-1 receptor.

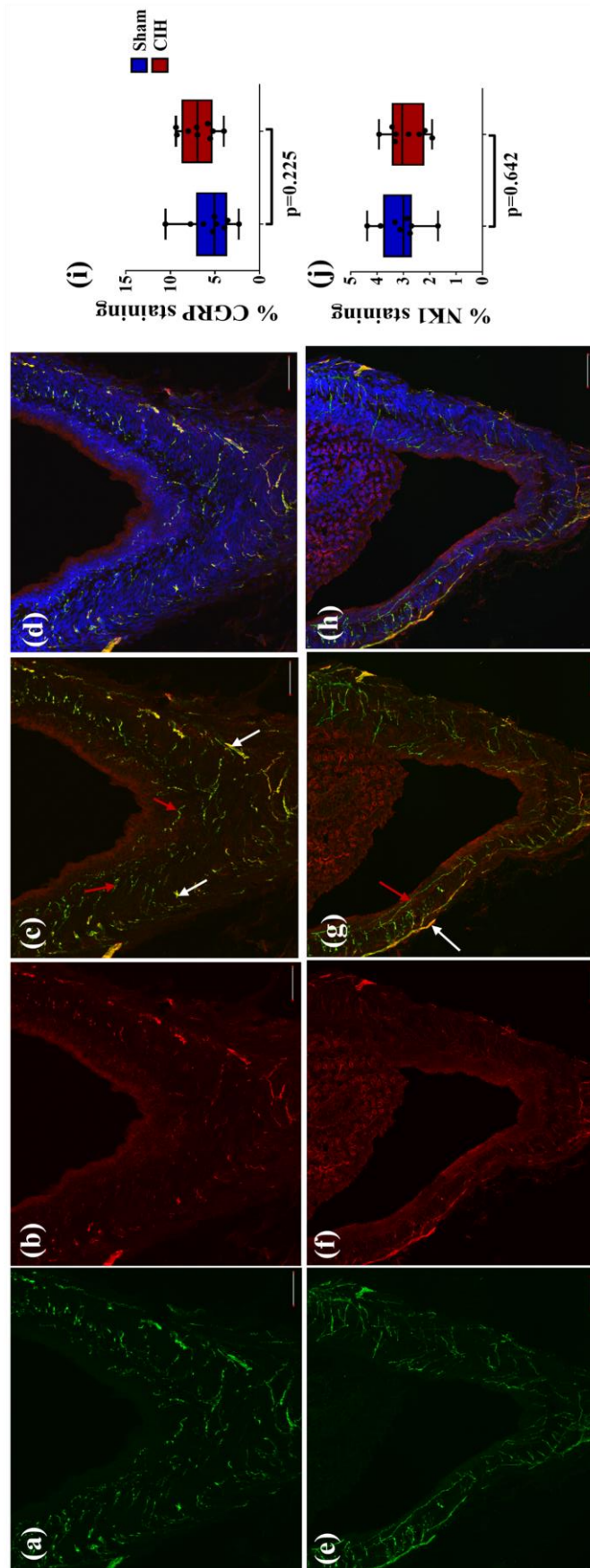


Figure 5. 4. CGRP and NK1 immunofluorescence in renal pelvic wall. CGRP is FITC-labeled (green channel (a and e)) and NK1 is Alexafour 594-labeled (red channel (b and f)). Images of the upper panel are representative images captured from a sham kidney and images in the lower panel are representative images of a CIH-exposed kidney. (c) and (g) shows immunofluorescence doubling labelling of CGRP and NK1 receptor from a sham kidney (c) and a CIH-exposed kidney (g). White arrows point towards the yellow staining which represents the co-localization of CGRP and NK1 receptor, mostly in the outer region of pelvic wall i.e. muscular and adventitia layers. Red arrows point towards CGRP green labelling which shows that CGRP is more abundant than NK1 and less co-localised with NK1 in the muscular and lamina propria layers. (d) and (h) are co-localization images in addition to nuclei blue labelling by DAPI (4, 6-diamidino-2-phenylindole). Scale bar 50 μ m. (i) and (j) are box and whiskers plots representing the interquartile range and maximum and minimum values resulting from image analysis. Each data point represents the average % of total renal pelvic area occupied by positive labelling of CGRP or NK1 from each rat of each group. Data were compared between sham (CGRP: n=9; NK1: n=8) and CIH-exposed (CGRP: n=9; NK1: n=8) kidneys using independent *t*-test. Significance was taken at $p<0.05$. CGRP, calcitonin gene-related peptide; NK1, neurokinin-1 receptor.

5.3. Discussion

5.3.1 No evidence of kidney injury

Previous studies of CIH have suggested that protective compensatory mechanisms are activated in response to acute oxidative stress in the early phase and/or after short duration of CIH exposure (342, 380). Meanwhile, after long-term exposure to CIH, anti-oxidative mechanisms become overwhelmed and incapable of maintaining efficient oxygen balance, leading to renal fibrosis, tissue peroxidation and inflammation (380, 409).

A relatively moderate paradigm of CIH was utilized in the present study, sufficient to elaborate sustained hypertension, yet with only subtle pathological consequences at the tissue level (226). Histological assessment in the CIH-exposed rats showed modest cortical tubulointerstitial fibrosis, which may relate to decreased cortical oxygen tension, reduced renal blood flow and decreased cortical NO previously reported by our group using a similar CIH protocol (258). Exposure to more severe protocols of CIH (more frequent cycles and/or longer duration) resulted in significant fibrosis along with an increase in the expression of transforming growth factor- β (TGF- β), collagen type 1 and type IV and connective tissue growth factor (CTGF) (9, 224, 380, 409). Hypoxia accelerates fibrosis and kidney function deterioration. Genes of extracellular matrix (ECM) proteins are activated by ROS, which in turn exacerbates hypoxia, causing a vicious cycle (224). Zhang et al. (409) showed that fibroblasts in the kidneys of CIH-exposed rats were co-localised with increased expression of CD68 macrophages. Of note, the susceptibility of tissues to changes induced by CIH varies among different animal species. For example, exposure to 30 cycles of CIH per hour (5% O₂) for 3 weeks was not associated with renal histopathological changes in mice (380); meanwhile, a similar protocol induced renal fibrosis and an increase in the expression of growth factors after 2 weeks in rats (224).

In chronic hypertension and when autoregulatory mechanisms are saturated, intraglomerular pressure increases (359). The activation of RAAS causes efferent arteriolar vasoconstriction through Ang II (359). This eventually causes mesangial expansion, which increases glomerular tuft area and develops to glomerulosclerosis (143, 399). The increase in glomerular pressure causes an increase in the capillary wall strain and promotes the release of ROS and endothelin-1 (100). These factors induces

mesangial proliferation and causes an imbalance between glomerular matrix generation and degradation (9). Intermittent hypoxia per se, through the generation of ROS, increases the levels of growth factors. Chronic hypertension accompanying intermittent hypoxia induces structural changes in the glomerulus, as was described in severe models of IH (9, 382). However, in our study, no glomerular hypertrophy was observed in rats exposed to CIH and had developed hypertension. Nevertheless, structural changes might occur at an advanced stage of CIH and hypertension. Previous studies have shown that exposure to CIH of more frequent episodes (40 cycles/hr) or of long duration (>4 weeks) was associated with glomerular hypertrophy, mesangial expansion, tubular atrophy and necrosis along with increased blood urea nitrogen and serum creatinine (9, 277, 382).

Although previous CIH studies reported attenuated protein expression of SOD and catalase enzymes (224, 277, 381), their enzymatic activities were not altered in the CIH model of this study. Moreover, there was no sign of protein oxidation in renal tissue of CIH-exposed rats. The differences between results from the current study and prior studies, which reported a decrease in anti-oxidant protein expression and an increase in pro-fibrotic factors (224, 277, 330, 380), is likely related to differences in the CIH paradigm used. In this regard, Wu et al. (380) showed that the protein expression of Nrf2, the main defence antioxidant controlling redox signalling, and metallothionein, and the mRNA expression of downstream antioxidant genes (HO-1, NQO1) were increased following 3-7 days of exposure to CIH (30 cycles/hr, 8% O₂, 12 hr/day) (342). Potentiation of anti-oxidative mechanisms persisted but of lesser magnitude after exposure to 1 week and up to 3 weeks of CIH. However, these anti-oxidative markers were depressed after 3 weeks of CIH exposure to levels lower than the sham group. Malonaldehyde, a marker for lipid peroxidation, was significantly elevated in renal tissue after 3 and 7 days (342, 380), indicating that kidneys sense decreased partial pressure of oxygen at an early stage of exposure to CIH. Furthermore, an increase in the levels of the inflammatory markers including ICAM, VCAM and PAI-1 was evident after 3 days of CIH (342, 380). However, the lack of cardiovascular measurements in these latter studies makes it difficult to propose the temporal sequence of renal hypoxia and inflammation, kidney function deterioration and hypertension.

Inflammatory cytokine concentrations were unchanged or below the level of detection in this study. A previous study has indicated that oxidative stress precedes inflammation in a model of CIH (146). Treatment with an anti-oxidant eliminated oxidative stress and the increase in inflammatory cytokines in carotid bodies. However, administration of an anti-inflammatory agent did not abolish the oxidative stress (146). In support of this notion, ROS release activates NLRP3 inflammasome, which was found in renal tissue of CIH-exposed rats (381). Elevated levels of inflammatory cytokines such as nuclear factor- κ B (NF κ B), TNF- α and IL-1 β were only reported in studies of prolonged CIH protocols (≥ 21 days) and/or relatively severe hypoxia cycles (≥ 30 cycles/hr) (224, 382, 409). Moreover, we did not observe changes in NOX activity in renal tissue of CIH-exposed rats. However, NOX4 upregulation in kidney was described following exposure to another protocol of CIH (223). The antioxidant, N-acetyl cysteine, increased renal SOD, decreased blood pressure and RSNA in CIH-exposed rats (223). Therefore, it appears that variable renal outcomes occur at the molecular level related to the pattern, duration and intensity of CIH as summarized in Appendix I, Table 8.1 (15). Nevertheless, we acknowledge that many other oxidative signalling pathways/mediators were not explored in this model and these could be altered in our model. This includes the measurement of the activity of xanthine oxidase enzyme, which is altered in different tissues following exposure to severe protocols of CIH (85, 147). Moreover, xanthine oxidase and aconitase enzymes activities are altered in other tissues when exposed to CIH protocol similar to the one used in this study (249, 271, 375). Anti-oxidative biomarkers, other than catalase and SOD, were shown to be altered in different tissues following exposure to CIH (152, 342, 375, 380). This includes glutathione peroxidase, glutathione reductase and the expression of nuclear factor erythroid 2 (Nrf2), the main transcription factor that regulates the expression of antioxidative enzymes. Importantly, however, our study revealed that kidney oxidative stress and inflammation are not obligatory for the development of CIH-induced hypertension.

5.3.2. Expression of other receptors in the renal pelvic wall

In the present study, we focused on the role of renal TRPV1 channels in the baroreflex control of RSNA. Meanwhile, other receptors located in the renal pelvic wall regulate

the release of substance P (SP) and CGRP from afferent renal nerve endings. Activation of TRPV1 and bradykinin receptors stimulates the release of SP, which is the primary neurotransmitter that binds to NK1 receptors to activate afferent renal nerves (15). Down-regulation of NK1 receptor in small dendrites of caudal NTS neurons was shown following 10 days of CIH (206). Moreover, in DOCA hypertension, NK1 antagonism attenuated proteinuria and tubulointerstitial damage (370). However, we revealed no change in NK1 receptor or CGRP expression in the renal pelvic wall of CIH-exposed rats.

5.4. Conclusion

Overall, a relatively modest CIH paradigm used in this study was sufficient to induce hypertension, without evidence of renal inflammation and/or oxidative stress. This suggests that pathophysiological changes at the tissue level, when they occur, are more likely to be secondary to hypertension rather than a direct effect of exposure to CIH, although they may present due to the direct effect of exposure to severe CIH. These changes may also arise due to synergistic effects of hypertension and hypoxia at an advanced stage of the disease.



AlMarabeh, S. Y. A. R. 2021. The role of renal afferent signalling in chronic intermittent hypoxia-induced sympathoexcitation and hypertension. PhD Thesis, University College Cork.

Please note that Chapter 6 (pp. 176-220) is unavailable due to a restriction requested by the author.

CORA Cork Open Research Archive <http://cora.ucc.ie>

Chapter 7: Summary and Conclusion

List of abbreviations

ANP	Atrial natriuretic peptide
ADH	Antidiuretic hormone
ARNA	Afferent renal nerve activity
BK1R	Bradykinin receptor type 1
BK2R	Bradykinin receptor type 2
CGRP	Calcitonin gene-related peptide
CIH	Chronic intermittent hypoxia
CKD	Chronic kidney disease
CPAP	Continuous positive airway pressure
ERK	Extracellular signal-regulated kinase
GFR	Glomerular filtration rate
IL-6	Interleukin-6
MAPK	Mitogen-activated protein kinase
NK1	Neurokinin 1
NO	Nitric oxide
NTS	Nucleus tractus solitarius
OSA	Obstructive sleep apnoea
PO ₂	Partial pressure of oxygen
PVN	Paraventricular nucleus
RSNA	Renal sympathetic nerve activity
RVLM	Rostral ventrolateral medulla
SNA	Sympathetic nerve activity
SON	Supraoptic nucleus
TNF- α	Tumour necrosis factor-alpha
TRPV1	Transient receptor potential vanilloid 1
VE	Volume expansion

7.1. Summary

In response to low partial pressure of oxygen (PO_2), protective mechanisms are activated to increase sympathetic nerve activity (SNA) and blood pressure to defend against tissue hypoxia. Persistent activation of these protective mechanisms results in pathophysiological changes and the development of pathological conditions such as hypertension, arrhythmias and stroke. It is suggested that the carotid bodies and the kidneys are involved in the adaptive mechanisms in response to low PO_2 levels (268). Hypoxia ($PO_2 \sim 60$ mmHg) induces increased activation of glomus cells of the carotid bodies which persists in chronic intermittent hypoxia (CIH)-exposed rats even during normoxic breathing (270). Type I glomus cells have high oxygen consumption (87), such that despite high blood supply to carotid bodies, they are highly sensitive to decreased blood oxygen levels. Therefore, enhanced tonic activity of carotid bodies and increased responsiveness to acute challenges following hypoxic exposure is a well-established mechanism in the development of hypertension in CIH models (74, 320). In addition, Ashton et al. (18) have shown that perfusion of the kidney with hypoxic blood ($PO_2 \sim 36$ mmHg) caused ~ 34 mmHg increase in the femoral perfusion pressure. This was eliminated following denervation of the perfused kidney. Indeed, in models that involve chronic hypoxia, such as renovascular hypertension, dorsal rhizotomy resulted in the attenuation of hypertension (383). Therefore, Patinha et al. (268) have proposed that the carotid bodies and kidneys cooperate to induce reflex sympatho-excitation and elevated blood pressure in response to hypoxia. In CIH models, the decrease in PO_2 in kidney tissue is mostly related to endothelial dysfunction with subsequent decrease in renal blood flow and oxygen supply, resulting in acute hypoxia (125, 215, 345). This was reported in a previous study from our laboratory using a CIH model similar to the one used in this study (258), where a decrease in cortical PO_2 and nitric oxide (NO) bioavailability were observed. However, the threshold of PO_2 needed for the activation of renal afferent nerves remains unknown. Interestingly, it was found that the threshold for the increase of femoral perfusion pressure in response to kidney perfusion with hypoxic blood was at PO_2 of ~ 73 mmHg in rabbits (18), showing an activation threshold higher than that needed to activate the carotid bodies. Despite the decrease in renal blood flow and GFR reported earlier in CIH, our findings have shown that basal sodium and water excretion tend to be higher in CIH-exposed rats, where diuresis was significantly

elevated in CIH-exposed rats of cohort 3. These changes in the excretory function were against a backdrop of heightened basal RSNA in CIH-exposed rats of all cohorts. This suggests the presence of humoral mechanisms that supersede sympathetic over-activity at rest and encourages kidney excretory function in CIH-exposed rats, independent of neural control and renal haemodynamic changes. Our findings have shown that the decrease in PO_2 in CIH (258) might also be related to increased oxygen demand, as the kidney of CIH-exposed rats of this study displayed sodium and water retention in response to fluid overload. In support of this notion, it was shown that renal denervation in CIH-exposed rats (164) and in individuals with obstructive sleep apnoea (OSA) (376) attenuates hypertension for up to 6 months.

Chemosensory inputs from the kidney and carotid bodies are transmitted to brain regions involved in the integration of baroreflex inputs such as nucleus tractus solitarius (NTS), paraventricular nucleus (PVN) and rostral ventrolateral medulla (RVLM). Many studies have shown that exposure to CIH is associated with hypertension, enhanced sensory drive of the carotid bodies and blunted cardiac baroreflex gain (74, 75, 122). Whereas it was shown that enhanced carotid body activity precedes hypertension development in CIH (75), the temporal sequence of the disrupted baroreflex function and the onset of blood pressure elevation remains uncertain. Moreover, the contribution of baroreflex control of renal sympathetic nerve activity (RSNA) in CIH-induced hypertension remains unclear. Therefore, we hypothesised that high- and low-pressure baroreflex control of RSNA and heart rate contributes to hypertension development at an early stage of the disease. We used a CIH protocol of 12 cycles/hr mimicking mild-to-moderate OSA, causing hypertension in rats. We found that high-pressure baroreflex control of RSNA was maintained in rats exposed to CIH despite their hypertensive phenotype. Meanwhile, rats displaying a higher magnitude of blood pressure elevation (rats of cohort 1), had decreased baroreflex control of RSNA, and a clear correlation was found between decreased slope of the baroreflex curve and resting levels of blood pressure in CIH-exposed and sham rats. Baroreflex control of heart rate was less sensitive to CIH exposure and was not modulated in CIH-exposed rats of both cohorts displaying modest or severe hypertension. This indicates that cardiac baroreflex control is preserved for a longer time during CIH exposure, which could be due to a compensatory mechanism mediated by an increase in the parasympathetic activity that has been shown in

previous CIH studies (217). In a further study described in this thesis, RSNA response to the hypotensive effect of intravenous bradykinin was blunted in CIH-exposed rats of cohort 3 and the increase in heart rate was similar in both exposure groups. Our findings indicate that blunted baroreflex control of RSNA and heart rate do not contribute to the onset of CIH-induced hypertension. However, at severe stages of the disease, the protective autonomic baroreflexes become overloaded by the sustained hypertension and the persistent sympatho-excitation, leading to dysfunction. This is consistent with CIH studies that showed blunted baroreflex control of heart rate after long durations of exposure to CIH (122, 217). However, this is in contrast with a previous clinical study that showed blunted baroreflex sensitivity in normotensive individuals with OSA; however, participants in this study had severe OSA of 50 apnoeas/hr (65).

Low-pressure baroreflex control of RSNA, which is blunted in many hypertensive disease models (3, 169), was unchanged in our CIH model of mild-to-moderate OSA. This indicates that impaired low-pressure baroreflex does not contribute to the initiation of hypertension. The assessment of low-pressure baroreflex control of RSNA is worth investigating using prolonged CIH exposure or a CIH protocol of more frequent cycles of hypoxia. This is relevant to left ventricular hypertrophy observed in severe CIH (396, 398) and humans with OSA (21). Although previous studies have shown blunted low-pressure baroreflex control of RSNA was associated with increased weight of the heart (121), it is not necessary that blunted low-pressure baroreflex is related to the resetting in the peripheral cardiac receptors. In this regard, the impaired baroreflex is possibly caused by oxidative stress and inflammation in brain regions involved in the baroreflex loop (263, 332). However, during the assessment of low-pressure baroreflex which showed no change in the renal sympatho-inhibitory response to volume expansion (VE), kidney excretory responses to VE were impaired in CIH-exposed rats. Meanwhile, basal sodium and water excretion in CIH-exposed rats showed an increase compared with sham rats despite heightened basal RSNA in the CIH rats. Therefore, we conclude that the diuretic and natriuretic response to VE was independent of the neural control of the kidney. The impaired diuresis and natriuresis was associated with an impaired increase in the plasma level of the atrial natriuretic peptide (ANP) during VE, suggesting a possible contribution of decreased ANP to the sodium and water retention in CIH-exposed rats.

This notion agrees with a previous study that showed diuretic and natriuretic response to VE to be dependent on ANP (308). Nevertheless, impaired diuresis and natriuresis could be related to other humoral factors that normally regulate body fluid homeostasis including aldosterone and antidiuretic hormone (ADH). Altered humoral control of kidney function observed during VE may also be relevant to basal renal function in the light of increased diuresis and natriuresis in CIH-exposed rats, which reached statistical significance in cohort 3 for water excretion. Moreover, it was shown previously that exposure to high altitude decreased ADH and aldosterone levels (112, 128). This indicates that changes in humoral factors such as decreased ADH and aldosterone could be responsible for the augmented excretory function at baseline, which counters the effect of heightened basal RSNA. During fluid overload, it is known that the physiological response includes an increase in ANP and a decrease in ADH and aldosterone (19, 308), and blunted increase in ANP was found in CIH-exposed rats. This suggests that the humoral system is activated in CIH perhaps near to saturation levels compared with shams, and a further decrease in ADH and aldosterone could not be attained during fluid overload resulting in impaired diuresis and natriuresis.

Interestingly, denervation of the carotid bodies in CIH-exposed rats resulted in the restoration of normal blood pressure and the resetting of the mid-pressure of the cardiac baroreflex curve to near normal levels (74). However, the blunted cardiac baroreflex gain in response to phenylephrine and sodium nitroprusside was maintained following the ablation of the carotid bodies. Moreover, in guinea pigs, which are known to be hypoxia insensitive, a blunted bradycardic response to phenylephrine was observed after exposure to a mild protocol of CIH (6 cycles/hr, 6.5% O₂, 12 days) (225). This suggests the presence of other peripheral sensory mechanisms and/or central disruption causing alteration in the baroreflex autonomic control.

Since the kidney is highly sensitive to decreased oxygen levels and a decrease in cortical PO₂ was shown in this CIH protocol (258), we hypothesized that heightened afferent renal nerve activity is responsible for the impaired baroreflex and that the interruption of renal afferent nerves restores the impaired baroreflex control of RSNA and modulates kidney function. The transient receptor potential cation channel subfamily V member 1 (TRPV1) plays a central role in the signalling pathway within renal afferent nerve endings (15). *In vitro* studies have shown that the basal activity of

TRPV1 is heightened and their responsiveness to activation is augmented during hypoxia (172). Therefore, we targeted intra-renal TRPV1 using capsaizepine followed by re-assessment of high-pressure (in cohort 2) and low-pressure baroreflex along with kidney function (in cohort 1). Blockade of TRPV1 channels caused potentiation in diuresis and natriuresis in CIH-exposed and sham groups. Renal excretory functions that were impaired in CIH-exposed rats were enhanced following TRPV1 blockade to comparable levels of sham rats. Therefore, we suggest that TRPV1 is involved in the impaired kidney functional responses to VE in CIH-exposed rats. However, since the RSNA inhibitory response to VE was not impaired in CIH-exposed rats and was not modulated by TRPV1 antagonism, we suggest that TRPV1 blockade increased diuresis and natriuresis in response to VE through a mechanism independent of RSNA. It is worth mentioning that stimulation of renal afferent nerves modulates the activity of neurons in the supraoptic nucleus (SON), the brain region that controls ADH release (50). However, we could not be conclusive about the effect of TRPV1 blockade on high-pressure baroreflex control of RSNA as it was not modulated in the second cohort, where rats exposed to CIH had modest hypertension without any modulation of the baroreflex gain curve. However, since the activation of TRPV1 in cohort 3 induced an equivalent sympatho-excitatory response in RSNA, it is likely that altered high-pressure baroreflex control is related to a mechanism that is independent of TRPV1, and the enhanced diuresis during TRPV1 antagonism is related to a mechanism independent of neural control of the kidney and/or the reno-renal reflex. This is further supported by the observation of no changes in the protein expression of TRPV1 in the kidney and the renal pelvic wall of CIH-exposed rats.

Kidney inflammation and oxidative stress were not evident in CIH-exposed rats in this study indicating that the CIH paradigm used herein mimics a moderate stage of OSA. This notion is supported by studies in humans showing that OSA is associated with chronic kidney disease (CKD) (215). Similarly, rodent models of CIH showed proteinuria and renal structural changes (380). Interestingly, our results revealed that the development of hypertension in CIH-exposed rats was not associated with evident kidney inflammation or oxidative stress. However, the lack of pathological changes in the kidney does not exclude the possibility of early pathophysiological changes as indicated by decreased renal blood flow and cortical PO₂, using the same model in another study from our laboratory (258). Moreover, the present study showed impaired

kidney function in CIH-exposed rats during fluid overload, indicating the emergence of renal dysfunction before the development of renal injury. In addition, it was shown previously that endothelial injury biomarkers such as intercellular adhesion molecule 1 (ICAM) are upregulated within three days of CIH exposure (342, 380). Nevertheless, our findings propose that kidney injury occurs at a later stage after the development of hypertension in CIH (and perhaps OSA), suggesting that renal pathological changes are secondary to hypertension itself, or hypertension in combination with hypoxia. The lack of renal inflammation and oxidative stress despite sodium and water retention, supports our suggestion of the presence of an external defect that reveals impaired diuresis and natriuresis, such as suppressed humoral action. Therefore, there is a time lag between OSA and subsequent detrimental changes in the kidney if the individual does not have additional kidney complications or confounding stressors. This suggests that the treatment of OSA at a moderate stage could delay kidney deterioration and could be preventive to the development of kidney injury in individuals who are compliant with OSA treatment. A previous study has shown a correlation between the rate of decline in kidney function and the compliance of individuals in the use of continuous positive airway pressure (CPAP) during a 2 year follow-up period (285).

Renal stenosis caused an increase in arterial blood pressure and peripheral vasoconstriction in cats, rats and rabbits, which were abolished by the denervation of the stenotic kidney (18, 44, 94, 295). Thus, the stimuli that cause activation of the SNA could be related to pressure and/or flow changes, hypoxaemia or hypercapnia (18). Rankin et al. (295) and Ashton et al. (18) have shown that the delivery of hypoxic blood into the kidney during constant pressure or flow causes an increase in the femoral perfusion pressure, which was not observed during the infusion of hypercapnic blood. Intra-renal infusion of aprotinin, an inhibitor of tissue kallikrein, during the infusion of hypoxic blood attenuated the increase in femoral perfusion pressure (18). In the same study, perfusion of the kidney with normoxaemic blood mixed with ischaemic mediators such as bradykinin resulted in ~ 19 mmHg increase in femoral perfusion pressure. This indicates that an acute decrease in renal PO₂ causes the production of ischaemic metabolites, and the latter promote sensory signals out of the kidney, leading to reflex increases in the sympathetic outflow and blood pressure. Of note, a decrease in renal cortical PO₂ was observed after exposure to CIH, similar to the protocol used in this study (258). Subsequently, we hypothesised that kallikrein-

kinin system is altered following CIH exposure and involved in exacerbated sympatho-excitatory outcome and blood pressure elevation. Our findings illustrated that CIH exposure is associated with alteration in the renal kallikrein-kinin system, in particular, in the renal pelvis where bradykinin receptors are involved in the reno-renal reflex. This is represented by impaired increase in the contralateral RSNA and heart rate during the intra-renal pelvic infusion of bradykinin and decreased expression of BK2R in the renal pelvic wall of CIH-exposed rats. The lack of changes in the expression of BK1R is consistent with no signs of renal inflammation or oxidative stress, which are known to be involved in the upregulation of BK1R. However, the absence of any significant changes in the cardiovascular parameters and RSNA in CIH-exposed rats during the inhibition of BK1R and BK2R indicate that they do not contribute to the tonic reno-renal reflex whether of mechano- or chemo-sensory type. This is similar to findings in SHR that showed apparent changes in the renal kinin system, but with no change in the afferent renal nerve activity (ARNA) during BK2R antagonism in the renal pelvic wall (45, 190). Nevertheless, decreased sympatho-excitatory response in CIH-exposed rats could be related to two mechanisms. First, the lack of increase in RSNA during the activation of bradykinin receptors may have been masked by the exacerbated sympatho-excitation in the resting state in CIH-exposed rats. Second, we suggest the presence of increased renal levels of bradykinin that caused the decreased expression of BK2R; thus, decreased responses to activation in CIH. Indeed, increased levels of bradykinin was shown in ischaemia and was involved in the pathogenesis of hypertension in SHR (18, 45), through decreased degradation of bradykinin in the latter. Bradykinin is a pro-inflammatory mediator that mediates a protective mechanism in hypertension and ischaemia-reperfusion injury through vasodilation (347, 352, 367). Bradykinin increases renal medullary and papillary perfusion pressure, and induces pressure diuresis and natriuresis to counteract ischaemia (353). However, the renal kinin system activates the chemo-sensory nerve endings and mediates a sympatho-excitatory effect (18, 29). While it was previously shown that the inhibition of BK2R restores the blunted baroreflex control of RSNA in rats with cisplatin-induced renal failure (3), the decreased sympatho-excitatory response to the activation of BK2R and no changes in the renal expression of BK1R in CIH, provide evidence that bradykinin receptors at a mild to moderate stage of the disease, do not contribute to RSNA sympatho-excitation and to the blunted baroreflex control of RSNA observed in cohort 1 of CIH exposure.

Moreover, it remains unresolved whether the presence of a blunted reno-renal reflex mechanism in CIH represents a protective physiological mechanism restraining sympatho-excitation and blood pressure elevation.

This is the first study that examined the kallikrein-kinin system after exposure to CIH and further studies are required to investigate plasma and renal levels of bradykinin and downstream signalling pathways of BK2R. We hypothesized that exacerbated excitatory reno-renal reflex contributes to sympathetic over-activity and hypertension in CIH. However, our results reveal opposite findings with attenuation in the sympatho-excitatory response in CIH. We expect that prolonged or severe protocols of CIH would be associated with progressive and different changes in the kallikrein-kinin system. It was shown that biomarkers of BK1R signalling pathway are overexpressed in the renal tissue of rats exposed to severe CIH such as MAPK and ERK (342, 380). Moreover, inflammatory mediators such as tumour necrosis factor- α (TNF- α) and interleukin-6 (IL-6) are highly expressed in kidneys after exposure to severe or prolonged CIH, known to increase the expression of BK1R (131, 224, 333, 335, 382). Therefore, the physiological consequences of changes in BK1R on the reno-renal reflex in CIH-exposed rats of other models are worth investigating. It was shown that increased expression of BK1R is associated with neuroinflammation, deleterious effects on kidney function and further elevation of blood pressure (286, 335, 367). Therefore, we propose that local pathological renal changes through BK1R might appear due to inflammation and apoptosis at an advanced stage of CIH driving an excitatory reno-renal reflex.

7.2. Limitations

As in other scientific studies, this study has several limitations. The animal model of CIH mimics arterial hypoxaemia, a feature of OSA in humans, without modelling other features such as hypercapnia and intra-thoracic pressure changes. Studies have shown that hypoxaemia is the primary stimulus responsible for enhanced chemoreflex drive and sympathetic over-activity (318, 324, 417). However, central and peripheral chemoreceptors are activated by hypercapnia, a feature of apnoea that can contribute to sympatho-excitation, but was not included in our model. Moreover, phenotypes studied in animals, as in rats of the current study, do not necessarily translate to human.

In this study, similar to other CIH studies, we referred to the expression of the hypertensive phenotype as a consequence of hypoxia cycles. However, other than hypoxaemia caused by hypoxia exposure, rats may have been exposed to other ancillary stressors such as sleep fragmentation and acoustic stimuli during the infusion of nitrogen and oxygen into the chambers to manipulate environmental oxygen, which may have contributed to anxiety and blood pressure elevation in CIH-exposed rats. However, separate work by our group reported no change in plasma corticosterone concentration in rats exposed to CIH (257), revealing the manifestation of hypertension without a requirement for a persistent elevation in a key stress hormone.

Furthermore, data were collected from anaesthetized rat preparations. As such, cardiovascular, renal, and autonomic-related outputs were altered compared with the conscious state. The use of anaesthesia such as urethane was shown to induce respiratory acidosis (404), which was observed in sham and CIH-exposed rats of cohorts 2 and 3. Nevertheless, respiratory acidosis was comparable between CIH-exposed and sham rats in both cohorts. Sodium pentobarbital anaesthetic, which has a fast action and which was only used as part of the induction phase in this study was shown to blunt the autonomic nervous system in earlier reports (322, 377). Urethane anaesthetic which was utilized for induction and maintenance of anaesthesia in the present study, was shown to preserve the autonomic baroreflex control of RSNA (322).

It is worth noting that I was not blinded to the identity of the experimental groups during surgical protocols. Furthermore, I was not blinded during ELISA, histopathological or immunofluorescence studies. However, I was fully blinded during the analysis of the *in vivo* data. I was also blinded during the capture and analysis of images for histology and immunofluorescence.

ELISA was conducted on full kidney tissue homogenates rather than isolated renal pelvic wall. This is because the amount of protein extracted from whole renal pelvic wall is 2 to 3 times less than the amount of protein extracted from a fraction of full kidney tissue. Therefore, it was difficult to carry out a wide range of analyses of inflammatory and oxidative stress biomarkers on homogenates of renal pelvic wall. Rather, we were homogenized the middle part of the kidney which includes the renal pelvic wall along with cortex and medulla. This is considered a significant limitation,

as shown in the analysis of bradykinin receptors, where renal pelvic wall homogenates showed different outcomes from the same analysis in kidney tissue homogenates (Figure 5.5). In addition, we quantified relative area occupied by the positive immunofluorescence labelling of TRPV1, calcitonin gene-related peptide (CGRP) and neurokinin 1 (NK1) receptor, which shows protein abundance in the renal pelvic wall. However, we did not quantify protein expression in terms of integrated density of immunofluorescence because each image with z-stacks has a different threshold that is set manually and is therefore subjective. Thus, in addition to immunofluorescence, we carried out ELISA to accurately quantify protein expression of TRPV1 and bradykinin receptors, but this was mostly in kidney homogenates.

Intra-renal administration of capsaizepine was unilateral, which might not reflect the full biological effect of TRPV1 antagonism. Unilateral infusion of drugs has been used effectively in other studies of baroreflex function (2, 3). In the present study, unilateral capsaizepine produced a decrease in basal blood pressure and produced changes in renal function suggesting efficacy; nevertheless, the effects of bilateral TPRV1 inhibition is worthy of further investigation.

Our study design involved the assessment of RSNA and renal excretory responses to VE in successive challenges, before and after intra-renal TRPV1 blockade. We acknowledge that restoration of renal excretory responses to VE in CIH-exposed rats, which was attributed to blockade of TRPV1 receptors, might relate to the performance of a second VE trial per se, independent of antagonism. Similarly, the attenuation in the RSNA response to 700 μ M bradykinin during BK1R antagonism and further during the second phase of combined BK1R and BK2R antagonism, could be related to the sequential infusion of bradykinin and desensitization of receptors. For the assessment of dose-response relationships, we randomized the order of infusion of different concentrations of bradykinin to minimize the possible effect of desensitization. Our data regarding kidney function responses to intra-renal pelvic infusion of bradykinin and capsaicin is limited due to the short duration of infusion. Longer duration of infusion would allow assessment of contralateral sodium and water excretion responses at steady-state, and would facilitate greater urine volumes to be collected from a single kidney for the analysis of other parameters. In support of this, it was shown that renal stenosis induces peripheral vasoconstriction that displayed

onset latency of 28 seconds in rabbits and 38 seconds in rats (295, 298). We also acknowledge that sample size for the analysis of bradykinin receptors in the renal pelvic wall is small and therefore the data needs to be interpreted with caution.

Our data on glomerular filtration rate (GFR) during VE should be viewed cautiously given that blood sampling was limited as we did not wish to interfere with blood pressure, and hence reflex control of RSNA, during VE challenges. As described in the methods, plasma samples were collected immediately before the start of VE (P2) and immediately at the end of VE (P3, when Uve5 was collected, 30 minutes of VE). Inulin concentration in the two blood samples were averaged and used to estimate GFR during the 30-minute challenge of VE. We did not collect plasma samples in the middle of urine collection phase i.e. during VE, although we acknowledge that it would be more accurate to do so. Altogether, we determined that it was more important to avoid manipulating blood pressure during VE challenge. On another hand, repetitive collection of blood samples during VE was associated with decreased haematocrit in CIH-exposed and sham rats before the start of the second VE phase (capsaizepine phase) (Table 8.4). We suggest that the decrease in haematocrit did not interfere with our results as the VE-induced haemodilution was comparable between the first and second VE challenges in CIH-exposed and sham rats, as shown in Figure 8.4.

Meanwhile, there are other limitations to the conclusions drawn from the study. We used a CIH paradigm that mimics mild-to-moderate OSA in humans to examine if baroreflex control of RSNA and heart rate, and kidney impairment contribute to the manifestation of hypertension. We were able to conclude that modulation of high- and low-pressure baroreflex control of RSNA are secondary to hypertension and are not associated with the development of hypertension in CIH. Moreover, renal function was altered in response to fluid overload despite no signs of oxidative stress or inflammation. This indicates that the kidney has an early response to hypoxia, but renal stress is not a major player in the development of hypertension in this model. However, since our model was associated with hypertension, the use of a shorter duration of CIH protocol to avoid the development of hypertension in rats, could be a useful model to test our hypothesis if renal impairment contributes to the manifestation of hypertension. Similar to other studies, studying the cardiorespiratory and autonomic

outputs after exposure to CIH at one time point shows only a snapshot of the whole spectrum of changes that manifest in response to exposure to CIH. As such, the lack of evidence of oxidative stress and inflammatory markers observed in this model illustrates an outcome after exposure to CIH for 14 days. However, the levels of these biomarkers could be oscillating at different time points before their measurement at day 15. In addition, we did not measure all oxidative stress markers and inflammatory cytokines; therefore, other markers could be altered within two weeks of exposure, as reported in other studies that showed elevation of endothelial dysfunction biomarkers within three days of exposure to severe CIH (30 cycles/hr) (277, 342).

7.3. Future studies and knowledge gaps

We studied baroreflex control in CIH-induced hypertension and concluded that baroreflex impairment does not contribute to the onset of hypertension. Moreover, we have seen that the activation of renal afferent nerves through bradykinin receptors reveals blunted sympatho-excitatory response in CIH and similar sympatho-excitation to sham rats in response to capsaicin. Therefore, it is less likely that renal afferent nerves increase sympathetic over-activity at the mild to moderate stage of CIH contributing to the onset of hypertension. However, it remains open to investigation if renal afferent nerves augment sympathetic over-activity in severe CIH and thus contribute to the exacerbation of hypertension. It would be interesting to determine if the excitatory reno-renal reflex contributes to the progression of hypertension in CIH-exposed rats. One potential approach is the use of selective renal deafferentation using the capsaicin gauze technique (101) before CIH exposure. Following exposure to severe CIH, the measurement of cardiovascular, autonomic and renal parameters in denervated and non-denervated rats would illustrate if renal pelvic chemosensory mechanisms contribute to hypertension at a later stage of OSA in cooperation with the enhanced chemosensory activity of the carotid bodies. It would also be very interesting to use the same experimental design to study the cardiovascular, autonomic and renal outcomes in guinea pigs which are known to have insensitive carotid bodies to hypoxia, yet they develop hypertension in response to severe CIH. The latter experiment would determine if there are peripheral sensory inputs from the kidney and/or from other peripheral sites that contribute to the autonomic disruption observed

in CIH. Of note, exposure of guinea pigs to a mild protocol of CIH caused decreased bradycardic response to phenylephrine (225). Moreover, guinea-pigs-exposed to 30 cycles/hr for 30 days was associated with hypertension and an increase in heart rate (84). These findings reveal a role for other peripheral sensory inputs or perhaps aberrant CNS plasticity that contributes to disrupted autonomic control of blood pressure and vascular tone despite the insensitivity of the guinea pig carotid bodies to hypoxia and evidence that there was no sensitization of the carotid bodies following CIH exposure (84). Therefore, renal deafferentation in guinea pigs prior to CIH exposure would determine if afferent sensory signals from the kidney are responsible for the disrupted autonomic control observed after CIH exposure.

We found that the RSNA sympatho-inhibitory response to VE was not changed following exposure to CIH, showing preserved low-pressure baroreflex control. However, left ventricular hypertrophy and structural cardiac changes were evident in humans with OSA (21) and in animals exposed to severe or prolonged CIH protocols (396, 398). Therefore, low-pressure baroreflex might exacerbate hypertension at a later stage of disease progression. Ours is the first study to examine the low-pressure baroreflex in CIH model and it would be of value to conduct baroreflex assessment in other protocols of CIH that mimic severe OSA. It would be of interest to measure ADH and aldosterone during the assessment of the low-pressure baroreflex. Moreover, antagonism of renal TRPV1 enhanced diuresis and natriuresis in CIH-exposed and sham rats. Therefore, we suggested that TRPV1 might be involved in the impaired renal excretory response to VE in CIH-exposed rats and we recommended that this suggestion should be considered with caution because the antagonism of TRPV1 also enhanced diuresis and natriuresis in sham rats, and the activation of TRPV1 by capsaicin induced a similar excitatory RSNA response in CIH-exposed and sham rats. Therefore, it could be that TRPV1 caused diuresis and natriuresis through a local renal effect independent of the reno-renal reflex. To confirm the role of TRPV1 in CIH-induced renal dysfunction, it would be interesting to use transgenic animals with a conditional knockout of renal TRPV1 channels to examine kidney functional responses to VE following exposure to CIH.

Previous studies have shown that bradykinin receptors, as a part of the reno-renal reflex mechanism, modulate baroreflex control of RSNA and mediate a sympatho-

excitatory effect (3, 18, 29). Bradykinin and bradykinin receptors were not previously studied in the CIH model. We showed that protein expression of bradykinin receptors in the kidney is not changed following CIH exposure. However, BK2R tends to be down-regulated in the renal pelvic wall of CIH-exposed rats along with suppressed increase in RSNA during the activation of bradykinin receptors. Further testing of a bigger sample size is required to confirm down-regulation of BK2R in the renal pelvic wall. Moreover, it would be interesting to determine whether the impaired RSNA response is physiologically related to suppressed sensory signalling or to other parts of the reno-renal reflex loop, such as modulation in the efferent sympathetic pathway. This can be investigated by direct recording of ARNA during bradykinin infusion to determine whether the afferent arm of the reno-renal reflex is compromised. In addition, an ex-vivo study of the renal pelvic wall to measure substance P release before and after the infusion of NK1 receptor blocker, BK2R agonist and phosphokinase C activator would illustrate if the sensory signalling pathway of BK2R is responsible for the impaired RSNA response to bradykinin infusion. It would also be interesting to further explore the putative role of BKR1. Following exposure to severe and prolonged CIH, it was shown that oxidative stress biomarkers and inflammatory cytokines accumulate in the kidney which are known to activate and up-regulate BK1R (15, 131, 224, 333, 335, 382). Since BK1R are involved in pathological signalling at the level of renal tissue in hypertension, one expects exacerbated sympatho-excitation through BK1R in renal sensory nerve endings. Therefore, a study of the reno-renal reflex through BK1R is worthy of investigation to explore OSA-related altered autonomic and cardiovascular outputs at a severe stage of the disease.

7.4. Conclusions

Moderate exposure to CIH resulted in hypertension and increased sympathetic outflow, with changes in kidney excretory function. CIH exposure, which caused renal sympatho-excitation in rats, was associated with enhanced basal diuresis and natriuresis. This suggests the presence of a compensatory mechanism that maintains basal sodium and water excretion at comparable levels to shams despite increased basal RSNA. Meanwhile, water and sodium retention were revealed in CIH-exposed rats in response to fluid overload, despite preserved RSNA sympatho-inhibitory

response to VE, associated with suppressed plasma [ANP]. This suggests altered humoral control of body fluid homeostasis contributing to renal excretory dysfunction during VE. Impaired diuresis and natriuresis in response to VE was alleviated following the inhibition of renal TRPV1 channels, suggesting that renal TRPV1 receptors might contribute to sodium and water retention during fluid overload in CIH-exposed rats, which requires further investigation. Mimicking an early stage of OSA, using a moderate protocol of CIH in this study, we showed that the high-pressure baroreflex control of RSNA and heart rate do not contribute to the onset of hypertension; rather, impaired baroreflex control of RSNA is secondary to hypertension. Moreover, renal histology and the analysis of biomarkers showed that kidney inflammation and oxidative stress were not essential for the development of hypertension in CIH, which is neurogenically-driven. Interestingly, the responsiveness of RSNA and heart rate to renal afferent nerve excitation, using the ischaemic metabolite, bradykinin, were blunted following CIH exposure. This was associated with decreased expression of BK2R in the renal pelvic wall with no change in the expression of BK1R. This suggests an attenuated excitatory reno-renal reflex at mild to moderate stage of the disease, suggesting a compensatory protective mechanism restraining the heightened efferent RSNA. Therefore, our findings indicate no pathological contribution of the reno-renal reflex at mild to moderate stage of CIH, suggesting it does not likely contribute to the onset of hypertension. Overall, sensory and local pathophysiological changes in the kidney are not obligatory for the development of hypertension in CIH, while further studies are required to examine the role of reno-renal reflex mechanisms in the progression of hypertension at later stages of the disease. This may have clinical implications in the consideration of OSA and CKD, indicating that early intervention to alleviate upper airway obstruction during sleep in hypertensive individuals with OSA might be required to prevent renal pathophysiological changes and progression to CKD, in the absence of other kidney-related comorbidities.

Appendix I

Table 8. 1. Oxidative stress and inflammatory biomarkers (↑, an increase; ↓, a decrease) in animals exposed to different protocols of CIH.

Biomarker	Level	Sample	Duration of exposure to IH (days, hr/day)	Species	Frequency of exposure (cycles/hr)	Intensity of hypoxia (% of O₂)	References
8-hydroxyl deoxy-guanosine	↑	Urine	28 days, 8 hr/day	Mice	12	10%	(164, 330)
Apoptotic cells	↑	Kidney tissue	56 days, 12 hr/day	Mice	30	8%	(80, 223, 224, 342, 382, 408, 409)
	↑	Kidney tissue	21 days, 8 hr/day	Rats	40	5%	
	↑	Kidney tissue	28 days, 8 hr/day	Rats	30	5-6%	
	↑	Kidney tissue	112 days, 8 hr/day	Rats	60	6-7%	
Bax/Bcl-2	↑	Kidney tissue	42 days, 8 hr/day	Mice	30	6-8%	(9, 382, 409)
	↑	Kidney tissue	84 days, 8 hr/day	Rats	60	5-7%	
	↑	Kidney tissue	35 days, 8 hr/day	Mice	60	6-7%	
	↑	Kidney tissue	60 days, 12 hr/day	Mice	30	8%	
Caspase 3	↑	Kidney tissue	42 days, 8 hr/day	Mice	30	6-8%	(408, 409)
	↑	Kidney tissue	84 days, 8 hr/day	Mice	40	5-7%	
Catalase	↓	Kidney tissue	28 days, 8 hr/day	Rats	40	5%	(224)

—

Collagen 1	↑	Kidney tissue	56 days, 12 hr/day	Mice	30	8%	(380, 409)
Collagen IV	↑	Kidney tissue	42 days, 8 hr/day	Mice	30	6-8%	(409)
			42 days, 8 hr/day	Mice	30	6-8%	
Connective tissue growth factor (CTGF)	↑	Kidney tissue	56 days, 12 hr/day	Mice	30	8%	(9, 224, 342, 380)
	↑	Kidney tissue	28 days, 8 hr/day	Rats	40	5%	
	↑	Kidney tissue	21 days, 12 hr/day	MT knockout mice	30	8%	
	↑	Kidney tissue	60 days, 12 hr/day	Mice	60	8%	
ERK1/2 phosphorylation	↑	Kidney tissue	3 days, 14 days and 56 days, 12 hr/day	Mice	30	8%	(342, 382)
	↑	Kidney tissue	35 days, 8 hr/day	Rats	60	6-7%	
HIF-1 α	↑	Kidney tissue	56 days, 12 hr/day	Mice	30	8%	(9, 224, 277, 342)
	↑	Kidney tissue	28 days, 8 hr/day	Rats	40	5%	
	↑	Kidney tissue	14 and 28 days, 7.5 hr/day	Rats	40	9%	
	↑	Kidney tissue	56 days, 12 hr/day	Mice	60	8%	

ICAM-1	↑	Kidney tissue	3 days, 7 days and 56 days, 12 hr/day	Mice	30	8%	(342, 380)
IL-1β	↑	Kidney tissue	NA, 10 hr/day	Mice	60	7%	(381)
IL-6	↑	Kidney tissue	28 days, 8 hr/day	Rats	40	5%	(224, 330, 382, 409)
	↑	Kidney tissue	42 days, 8 hr/day	Mice	30	6-8%	
JNK phosphorylation and P38 phosphorylation	↑	Kidney tissue	35 days, 8 hr/day	Rats	60	6-7%	(382)
Liver-type fatty acid-binding protein (L-FABP)	↑	Urine	28 days, 8 hr/day	Mice	12	10%	(150, 164)
Malondialdehyde	↓	Kidney tissue	3 days and 14 days, 12 hr/day	Mice	30	8%	(342, 380, 384)
	↑	Kidney tissue	56 days, 12 hr/day	Mice	30	8%	(381)
	↑	Kidney tissue	7 days, 12 hr/day	Mice and methionine (MT) knockout mice	30	8%	
	↑	Serum	42 days, 7 hr/day	Rats	20	6-8%	
	↑	Kidney tissue	NA, 10 hr/day	Mice	60	7%	
MCP-1	↑	Kidney tissue	42 days, 8 hr/day	Mice	30	6-8%	(409)

Metallothionen	↑	Kidney tissue	3 days and 7 days, 12 hr/day	Mice	30	8%	(380)
	↓	Kidney tissue	14 and 56 days, 12 hr/day	Mice	30	8%	(342, 380)
Mn SOD and Cu/Zn SOD	↓	Kidney tissue	14 days and 28 days, 7.5 hr/day	Rats	40	9%	(277)
NADPH dehydrogenase	↑	Kidney tissue	3 days and 7 days, 12 hr/day	Mice	30	8%	(380)
	↓		56 days, 12 hr/day	Mice			
Nitrotyrosine and caspases	↑	Kidney tissue	28 days, 8 hr/day	Rats	40	5%	(224)
Nrf2 and HO-1	↑	Kidney tissue	3 days, 12 hr/day	Mice			(342, 380)
	Normal	Kidney tissue	56 days, 12 hr/day	Mice			
	↑	Kidney tissue	3 days, 7 days and 21 days, 12 hr/day	Mice			
				MT knockout mice	30	8%	
	↓	Kidney tissue	56 days, 12 hr/day	Mice			
Oxidized cysteine (CysSSP)	↑	Kidney tissue	14 days, 10.5 hr/day	Rats	5.6	5%	(61)
	↑	Kidney tissue	3 days, 7 days and 56 days, 12 hr/day	Mice			(342, 380)
Plasminogen activator inhibitor-1 (PAI-1)	↑	Kidney tissue	7 days, 12 hr/day	MT knockout mice	30	8%	

Reduced cysteine (CysSH)/CysSSP	↓	Kidney tissue (medulla)	14 days, 10.5 hr/day	Rats	5.6	5%	(61)
		Kidney tissue (cortex)	21 days, 10.5 hr/day				
Renal fibrosis (Sirius red stain)	↑	Kidney tissue	14 days, 8 hr/day	Rats	40	5%	(224)
ROS	↑	Kidney tissue	56 days, 12 hr/day	Mice	30	8%	(342, 380)
	↑	Kidney tissue	112 days, 8 hr/day	Rats	30	5-6%	(80)
SOD	↑	Kidney tissue	21 days, 8 hr/day	Rats	40	5%	(223, 224, 277, 381)
	↓	Kidney tissue	28 days, 8 hr/day	Rats	40	5%	
	↓	Serum	14 and 28 days, 7.5 hr/day	Rats	40	9%	
	↓	Kidney tissue	NA, 10 hr/day	Mice	60	7%	
TGF-α	↑	Kidney tissue	28 days, 8 hr/day	Rats	40	5%	(224)
TGF-β	↑	Kidney tissue	28 days, 8 hr/day	Rats	40	5%	(9, 224, 380)
	↑	Kidney tissue	56 days, 12 hr/day	Mice	30	8%	
	↑	Kidney tissue	21 days, 12 hr/day	MT knockout mice	30	8%	

TNF- α	↑	Kidney tissue, plasma	28 days, 8 hr/day	Rats	40	5%	(224, 330, 382, 409)
	↑	Serum	35 days, 8 hr/day	Rats	60	6-7%	
	↓	RV/LM	7 days, 8 hr/day	Mice	10	10%	
	↑	Kidney tissue	42 days, 8 hr/day	Mice	30	6-8%	
Vascular cell adhesion protein 1 (VCAM-1)	↑	Kidney tissue	7 and 56 days, 12 hr/day	Mice			(342, 380)
	↑	Kidney tissue	7 days, 12 hr/day	MT knockout mice	30	8%	
VEGF	↑	Kidney tissue	60 days, 12 hr/day	Mice	60	8%	(9)

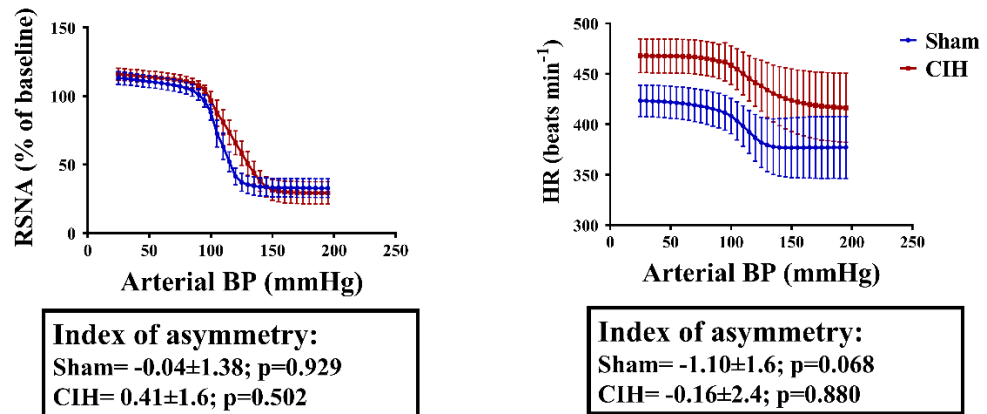


Figure 8.1. High-pressure baroreflex control of RSNA and HR using the five-parameter model. Data (mean \pm SE) are shown for RSNA (% of baseline, sham, n=9; CIH, n=9) or HR (sham, n=9; CIH, n=6) as a function of arterial blood pressure using the five-parameter model in the first cohort. Index of asymmetry was calculated using baroreflex parameters obtained from the five-parameter logistic equation and is expressed as mean \pm SD. A simple one-sample t-test was used to analyse if the index of asymmetry was not different from zero in CIH-exposed and sham rats. Data for baroreflex parameters are shown below in table 8.2. RSNA, renal sympathetic nerve activity; HR, heart rate; BP, blood pressure.

Table 8.2. High-pressure baroreflex parameters of RSNA and HR in sham and CIH-exposed rats of cohort 1.

Parameter	Sham	CIH	p-value	Sham	CIH	p-value
<i>RSNA baroreflex</i>				<i>HR baroreflex</i>		
<i>A1 (% or beats min⁻¹)</i>	85±33	103±36	0.317	85±33	103±36	1.000
<i>A2 (mmHg⁻¹)</i>	-0.18±0.14	-0.14±0.10	0.550	-0.18±0.14	-0.14±0.10	0.157
<i>A5 (mmHg⁻¹)</i>	-0.16±0.13	-0.26±0.55	0.442	-0.16±0.13	-0.26±0.55	0.077
<i>A3 (mmHg)</i>	106±5	113±13	0.188	106±5	113±13	0.480
<i>A4 (% or beats min⁻¹)</i>	34±21	29±23	0.656	34±21	29±23	0.239
<i>Max. gain (%.mmHg⁻¹ or beats min⁻¹. mmHg⁻¹)</i>	-3.2±2.1	-4.2±5.4	0.798	-3.2±2.1	-4.2±5.4	0.239

Data are expressed as mean±SD and represent baroreflex parameters of RSNA (sham, n=9; CIH, n=9) and HR (sham, n=9; CIH, n=6) of cohort 1 obtained from the five-parameter equation. Data were analysed using independent samples *t*-test or Mann-Whitney test. CIH, chronic intermittent hypoxia; RSNA, renal sympathetic nerve activity; HR, heart rate; A1, response range of RSNA; A2 and A5, gain (curvature) coefficients; A3, midpoint pressure of input; A4, the minimum response. Maximum gain was obtained by the calculation of the average of the two curvature parameters (A2 and A5) multiplied with the response range (A1) and divided by 4.562 (214).

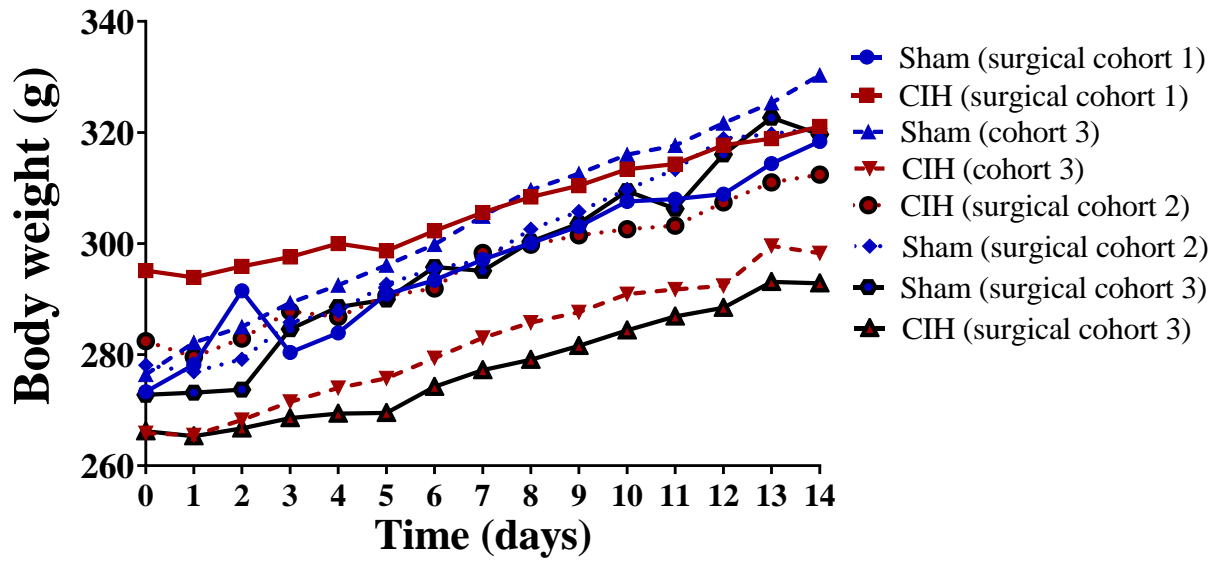


Figure 8. 2. Body weights recorded during 14 days of CIH and normoxia (sham) exposure. Data are presented as mean in grams (g) of rats' body weights on each day of cohort 1 (sham, n=10; CIH, n=10), cohort 2 (sham, n=12; CIH, n=10), cohort 3 (sham, n=15; CIH, n=14) and cohort 4 (sham, n=12; CIH, n=8).

Table 8. 3. Body weight gain parameters during 14 days of CIH and normoxia (sham) exposure.

	<u>Surgical cohort 1</u>			<u>Surgical cohort 2</u>		
	Sham (n=10)	CIH (n=10)	p-value	Sham (n=12)	CIH (n=10)	p-value
Slope (g/day)	2.9±0.8	2.1±0.5*	0.021	3.3±0.4	2.4±0.6***	<0.0001
% weight gain	15.8±3.2	8.61±2.2***	<0.0001	15.6±2.1	12.3±2.2**	0.003
Body weight after day 14 of exposure (g)	319±32	320±17	0.805	321±19	312±28	0.419
	<u>Surgical cohort 3</u>			<u>Cohort 4</u>		
	Sham (n=15)	CIH (n=14)	p-value	Sham (n=12)	CIH (n=8)	p-value
Slope (g/day)	3.5±1.1	2.1±0.9	0.001	3.7±0.7	2.5±0.5**	0.002
% weight gain	17.8±6.5	10.1±5.8	0.002	12.2±2.6	19.4±3.1***	<0.0001
Body weight after day 14 of exposure (g)	320±30	293±32	0.028	330±29	298±18*	0.010

Data are presented as mean±SD. Weight gain parameters are expressed as slope of body weight increase per day and percentage of weight gain after 14 days of exposure from basal body weight (day 0). Parameters were compared between sham and CIH groups using independent samples *t*-tests. (% weight gain= (weight day₁₄ – weight day₀)/weight day₀*100).

Table 8. 4. Haematocrit and blood gases analysis of surgical cohort 1 and cohort 2.

Cohort 1						
	Saline			CPZ		
	Sham	CIH	p-value	Sham	CIH	p-value
pH	7.34±0.03	7.35±0.03	0.442	7.32±0.04	7.33±0.04	0.745
PO ₂ (mmHg)	62.8±7.9	67.0±7.8	0.296	71.0±7.0	71.6±10.0	0.878
PCO ₂ (mmHg)	35.6±5.7	36.8±6.2	0.699	33.9±2.8	35.4±4.6	0.405
[HCO ₃ ⁻] (mmol L ⁻¹)	19.3±3.4	20.3±2.5	0.531	17.5±1.7	18.4±1.9	0.290
Base excess (mEq L ⁻¹)	-6.5±3.6	-5.4±2.3	0.500	-8.5±2.2	-7.6±2.1	0.405
Haematocrit (%PCV)	40.6±5.0	42.6±2.8	0.239	36.5±4.8	37.1±3.2	0.757
Cohort 2						
	Saline			CPZ		
	Sham	CIH	p-value	Sham	CIH	p-value
O ₂ supply (%)	29.3±1.1	27.8±0.3*	0.002	29.2±1.5	28.0±0.5*	0.013
pH	7.27±0.01	7.30±0.03	0.021	7.29±0.03	7.30±0.04	0.482
PO ₂ (mmHg)	91.1±8.6	95.4±6.9	0.252	90.5±7.1	94.0±10	0.586
PCO ₂ (mmHg)	55.6±6.7	50.1±4.8	0.103	54.1±4.1	47.3±5.0*	0.003
[HCO ₃ ⁻] (mmol L ⁻¹)	25.7±2.4	24.6±1.8	0.350	26.4±1.9	23.2±2.0*	0.003
Base excess (mEq L ⁻¹)	-1.3±2.3	-1.6±2.3	0.802	-0.3±2.1	-3.2±2.3*	0.013
Haematocrit (%PCV)	43.6±1.4	44.3±2.6	0.360	42.7±2.6	42.1±3.1	0.762

Data are presented as mean±SD and were compared using independent samples *t*-test. In cohort 1, blood samples were taken before the beginning of the saline and CPZ volume expansion challenges. In cohort 2, blood samples were taken before the injection of phenylephrine after the intra-renal infusion of saline and the intra-renal infusion of CPZ. In cohort 2, sham rats (n=10) were provided with a higher percentage of oxygen to reach an oxygen tension (PO₂) above 80 mmHg compared with CIH-exposed rats (n=10). O₂ supply represents % of pure oxygen gas mixed with pure nitrogen gas. PO₂, partial pressure of oxygen in arterial blood; PCO₂, partial pressure of carbon dioxide in arterial blood; [HCO₃⁻], bicarbonate concentration in arterial blood; PCV, packed cell volume; CPZ, capsiazepine. * p<0.05 compared with corresponding value of sham group.

Table 8. 5. Haematocrit and blood gases analysis of surgical cohort 3.

Cohort 3						
Before infusion of bradykinin			Before infusion of capsaicin			
	Sham	CIH	p-value	Sham	CIH	p-value
O ₂ supply (%)	27.2±1.6	25.8±2.1	0.082	27.3±1.6	24.4±2.5	0.289
pH	7.31±0.04	7.35±0.04*	0.021	7.32±0.03	7.34±0.05	0.178
PO ₂ (mmHg)	101±10	101.5±11.9	0.296	101±9	98±9	0.412
PCO ₂ (mmHg)	52.8±5.7	48.6±4.3	0.059	49.0±5.9	47.7±7.8	0.673
[HCO ₃ ⁻] (mmol L ⁻¹)	26.8±2.6	26.8±1.5	0.986	25.0±2.4	25.8±1.9	0.445
Base excess (mEq L ⁻¹)	0.5±2.8	1.2±1.9	0.513	-1.2±2.6	0.0±1.9	0.269
Haematocrit (%PCV)	43.3±3.8	45.8±2.3*	0.044	39.8±3.3	44.1±2.8*	0.006

Data are presented as mean±SD and were compared using independent samples *t*-test or Mann-Whitney test. Blood gases were analysed before the infusion of bradykinin and another blood sample was analysed before the infusion of capsaicin. CIH-exposed rats (n=11) were less acidotic with elevated haematocrit compared with sham rats (n=12). O₂ supply represents % of pure oxygen gas mixed with pure nitrogen gas. PO₂, partial pressure of oxygen in arterial blood; PCO₂, partial pressure of carbon dioxide in arterial blood; [HCO₃⁻], bicarbonate concentration in arterial blood; PCV, packed cell volume. * p<0.05 compared with corresponding value of sham group.

Table 8. 6. A comparison of basal cardiovascular parameters and RSNA between sham and CIH-exposed rats of cohort 1 and 2.

After arterial cannulation (before renal surgical instrumentation)				
	MAP (mmHg)	HR (beats min ⁻¹)		
Cohort 1				
<i>Sham</i>	124±13	432±28		
<i>CIH</i>	143±7 [‡]	461±39		
Cohort 2				
<i>Sham</i>	115±11 ^{‡*}	411±29*		
<i>CIH</i>	127±9 ^{‡*}	425±41*		
2x2 ANOVA				
<i>Cohort</i>	P<0.001	P=0.010		
<i>Exposure</i>	P<0.001	P=0.087		
<i>Exposure x cohort</i>	P=0.222	P=0.630		
After stabilization (after renal surgical instrumentation)				
	MAP (mmHg)	HR (beats min ⁻¹)	RSNA(% of max)	RSNA (μV.s)
Cohort 1				
<i>Sham</i>	84±9	400±52	17±7	0.66±0.30
<i>CIH</i>	97±11	445±47 [‡]	36±15 [‡]	1.34±0.73
Cohort 2				
<i>Sham</i>	103±12*	436±19	24±10	1.39±0.84
<i>CIH</i>	107±18*	450±34 [‡]	32±18 [‡]	1.67±0.65
2x2 ANOVA				
<i>Cohort</i>	P=0.002	P=0.121	P=0.789	P=0.486
<i>Exposure</i>	P=0.097	P=0.024	P=0.003	P=0.064
<i>Exposure x cohort</i>	P=0.437	P=0.276	P=0.204	P=0.163

Data are presented as mean±SD and were collected from the first (sham, n=10; CIH-exposed, n=9) and second cohorts (sham, n=13; CIH-exposed, n=10). Baseline cardiovascular parameters were recorded for 2 minutes after ~4-5 minutes of arterial cannulation i.e. before retroperitoneal incisions were performed to expose the kidneys. Cardiovascular parameters and RSNA were also recorded for 2 minutes after the stabilization period, 1 hour following renal surgical instrumentation. Parameters of sham and CIH-exposed rats were compared between the first and the second cohort using two-way ANOVA. [‡] p<0.05 compared with sham rats of the same cohort. * p<0.05 compared with the same exposure group of cohort 1. CIH, chronic intermittent hypoxia; MAP, mean arterial blood pressure; HR, heart rate; RSNA (% of max), renal sympathetic nerve activity normalized to maximum activity recorded during baroreflex activation during euthanasia.

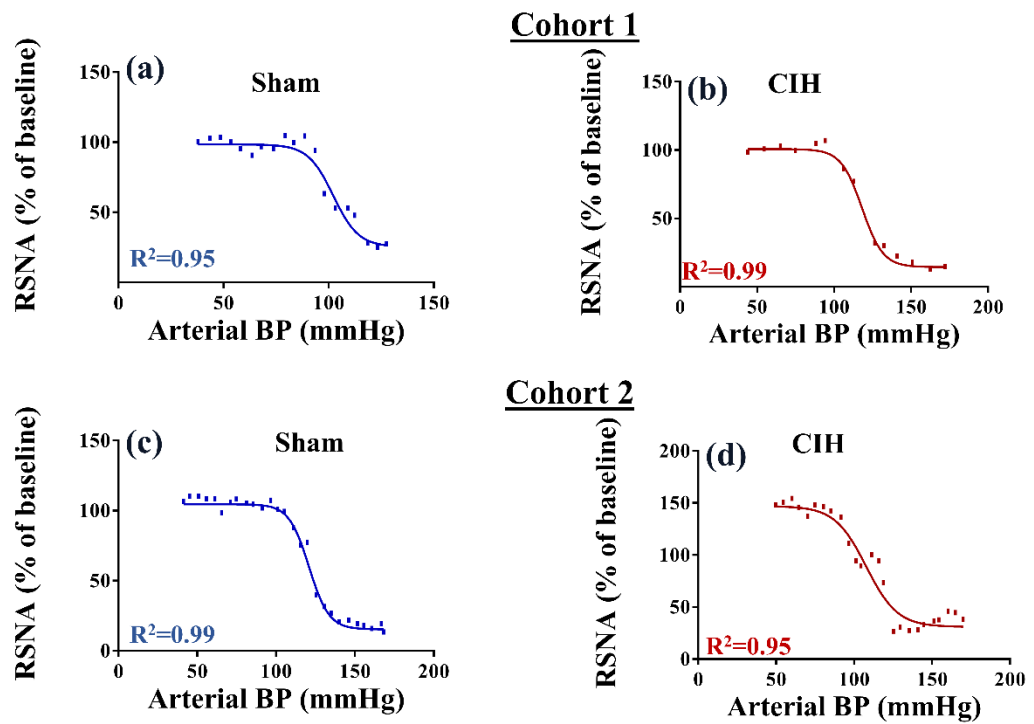


Figure 8.3. RSNA-MAP baroreflex curves of a sham and a CIH-exposed rat from cohort 1 and 2. Each figure shows RSNA (% of baseline) as a function of arterial blood pressure in a sham and a CIH-exposed rat of each cohort. RSNA (% of baseline) values were binned for every 5 mmHg change in mean arterial blood pressure. Therefore, each individual point represents the average of RSNA (% of baseline) during a 5 mmHg change in the mean arterial blood pressure. R-squared values show goodness of fit of data points around the sigmoidal regression line constructed by the four-parameter equation. Graphs (a) and (b) show the baroreflex curve of a sham and a CIH-exposed rat from the first cohort. Graphs (c) and (d) show the baroreflex curve of a sham and a CIH-exposed rat from the second cohort. RSNA, renal sympathetic nerve activity; BP, blood pressure; CIH, chronic intermittent hypoxia.

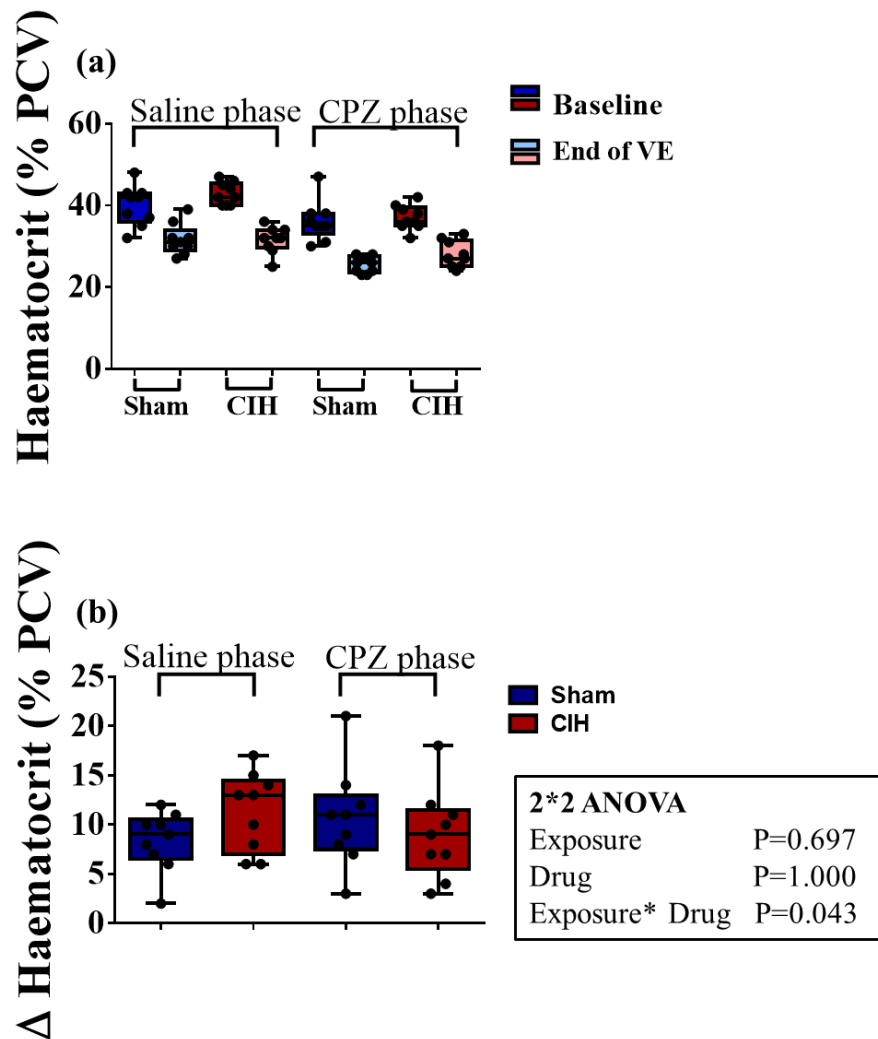


Figure 8. 4. Haematocrit changes during VE. Figure (a) shows box and whiskers plots where each individual point shows the haematocrit value of one rat either before (dark-coloured boxes) or at the end of VE (light-coloured boxes) during intra-renal infusion of saline and CPZ. Figure (b) shows box and whiskers plots representing the change in haematocrit during VE of sham (n=9) and CIH (n=9) groups during intra-renal infusion of saline and CPZ. Each individual point represents the value resulting from the subtraction of haematocrit at the end of VE from haematocrit prior to VE in each rat in the group. All box and whiskers plots display median, first quartile, third quartile, interquartile range, minimum and maximum values. PCV, packed cell volume; CPZ, capsazepine; VE, volume expansion; CIH, chronic intermittent hypoxia. Delta changes in haematocrit during VE were analysed using repeated-measures two-way ANOVA.

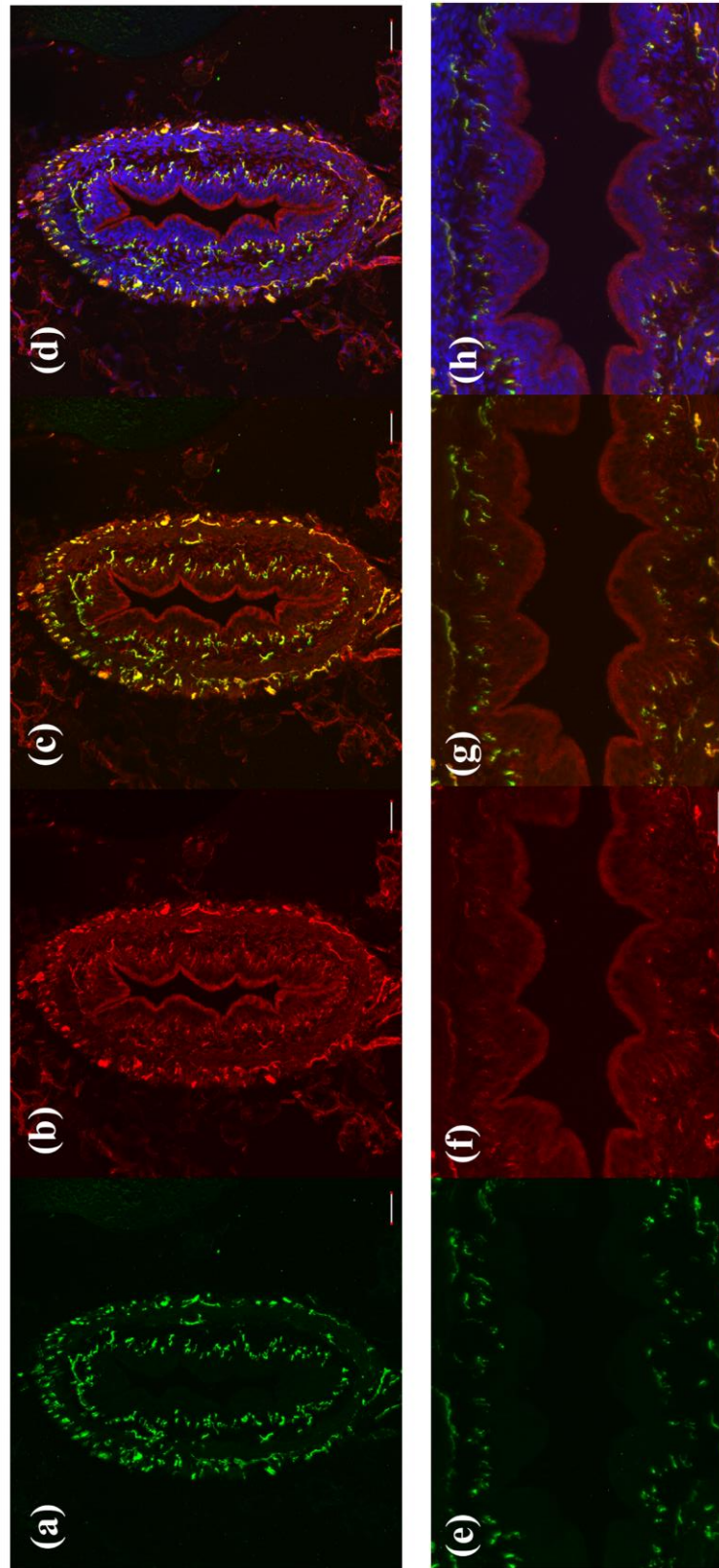


Figure 8. 5. Immunofluorescence of CGRP and NK1 in a cross section of ureter obtained from a sham rat. CGRP is FITC-labeled (a and e, green channel) and NK1 is AlexafLOUR 594-labeled (b and f, red channel). Similar to renal pelvic wall, co-localization (c and g) between CGRP and NK1 labelling appears in the outermost layers of the ureter while CGRP-positive labelling is more abundant than NK1 in the lamina propria layer. Blue labelling shows nuclei stained by DAPI in addition to co-localisation between CGRP and NK1 receptor (d and h). Images of the upper panel were captured using 20X magnification lens while lower panel images were taken under magnification of 40X. Scale bar 50 μ m. CGRP, calcitonin gene-related peptide; NK1, neurokinin-1 receptor.

List of publications, conference abstracts and awards

- **Peer-reviewed publications**

AlMarabeh S., Abdulla MH, and O'Halloran KD. Is Aberrant Reno-Renal Reflex Control of Blood Pressure a Contributor to Chronic Intermittent Hypoxia-Induced Hypertension? Front Physiol 10: 465, 2019.

AlMarabeh, S., O'Neill, J., Cavers, J., Lucking, E. F., O'Halloran, K. D., & Abdulla, M. H. Chronic intermittent hypoxia impairs diuretic and natriuretic responses to volume expansion in rats with preserved low-pressure baroreflex control of the kidney. Am. J. Physiol. Renal Physiol, 2020.

- **Publications outside PhD thesis**

Huang, C., AlMarabeh, S., Cavers, J., Abdulla, M. H., & Johns, E. J. (2020). Effects of intracerebroventricular leptin and orexin-A on the baroreflex control of renal sympathetic nerve activity in conscious rats fed a normal or high-fat diet. Clinical and Experimental Pharmacology and Physiology.

- **Conference abstracts**

AlMarabeh, S., Lucking, E. F., O'Halloran, K. D. & Abdulla, M. Low-pressure baroreflex control of renal sympathetic nerve activity in rats exposed to chronic intermittent hypoxia: Effect of TRPV1 channel blockade. Europhysiology 2018 (London, UK). **Poster presentation.**

AlMarabeh, S., O'Neill, J., Cavers, J., Lucking, E. F., Abdulla, M. & O'Halloran, K. D. Blunted diuretic and natriuretic responses to volume expansion following exposure to chronic intermittent hypoxia. APS/ASN Control of Renal Function in Health and Disease Conference, 2019 (Virginia, USA). **Poster presentation.**

AlMarabeh, S., O'Neill, J., Cavers, J., Lucking, E. F., Abdulla, M. & O'Halloran, K. D. Blunted diuretic response to volume expansion with preserved low-pressure baroreflex function in rats exposed to chronic intermittent hypoxia. 16th International Sleep and Breathing Conference, 2019 (Tampere, Finland). **Oral presentation.**

AlMarabeh, S., O'Neill, J., Cavers, J., Lucking, E. F., O'Halloran, K. D. & Abdulla, M. H. Baroreflex Control of Renal Sympathetic Nerve Activity and Renal Responses to Volume Expansion Following Intermittent Hypoxia in Rats. The FASEB Journal, 34: 1-1, 2020. **Accepted as oral presentation.**

AlMarabeh, S., O'Neill, J., Cavers, J., Lucking, E. F., O'Halloran, K. D. & Abdulla, M. H. Baroreflex control of RSNA and diuretic and natriuretic responses to saline overload in rats exposed to intermittent hypoxia with developed hypertension. New Horizons Research Conference, University College Cork, 2020. **Poster presentation.**

AlMarabeh, S., O'Neill, J., Cavers, J., Lucking, E. F., O'Halloran, K. D. & Abdulla, M. H. Baroreflex Control Of Renal Sympathetic Nerve Activity And Kidney Function Following Exposure To Intermittent Hypoxia In Rats. Section of Biomedical Sciences Annual Meeting of Royal Academy of Medicine in Ireland, 2021. **Short oral communication.**

AlMarabeh, S., Lucking, E. F., O'Halloran, K. D. & Abdulla, M. H. Chronic Intermittent Hypoxia Blunts Renal Sympathetic Nerve Activation By Intrapelvic Bradykinin In Rats. Section of Biomedical Sciences Annual Meeting of Royal Academy of Medicine in Ireland, 2021. **Short oral communication.**

AlMarabeh, S., Lucking, E. F., O'Halloran, K. D. & Abdulla, M. H. Renal Sympathetic Nerve Activity and Heart Rate Responses to Renal Pelvic Infusion of Bradykinin and Capsaicin in Rats Exposed to Intermittent Hypoxia. Experimental Biology 2021. **Poster presentation.**

- **Awards**

-Anne E. Suratt best oral presentation award at the 16th International Sleep and Breathing Conference in Tampere, Finland.

-Nominated to give an oral presentation at Experimental Biology, San Diego, 2020 during a special session of the APS Neural Control & Autonomic Regulation Section to compete for the Predoctoral NCARnation award. (Meeting cancelled due to COVID-19).

References

1. **Abdulla M, Duff M, and Johns E.** TRPV1 blockade restores the high-pressure baroreflex control of renal sympathetic nerve activity in cisplatin induced renal failure rats. In: *37th Congress of IUPS* Birmingham, UK: 2013.
2. **Abdulla MH, Brennan N, Ryan E, Sweeney L, Manning J, and Johns EJ.** Tacrolimus restores the high and low-pressure baroreflex control of renal sympathetic nerve activity in cisplatin-induced renal injury rats. *Exp Physiol* 104: 1726-1736, 2019.
3. **Abdulla MH, Duff M, Swanton H, and Johns EJ.** Bradykinin receptor blockade restores the baroreflex control of renal sympathetic nerve activity in cisplatin-induced renal failure rats. *Acta Physiol (Oxf)* 218: 212-224, 2016.
4. **Abdulla MH, and Johns EJ.** Nitric oxide impacts on angiotensin AT2 receptor modulation of high-pressure baroreflex control of renal sympathetic nerve activity in anaesthetized rats. *Acta Physiol (Oxf)* 210: 832-844, 2014.
5. **Abdulla MH, and Johns EJ.** Role of angiotensin AT2 receptors and nitric oxide in the cardiopulmonary baroreflex control of renal sympathetic nerve activity in rats. *J Hypertens* 31: 1837-1846, 2013.
6. **Abdulla MH, and Johns EJ.** The innervation of the kidney in renal injury and inflammation: a cause and consequence of deranged cardiovascular control. *Acta Physiol (Oxf)* 220: 404-416, 2017.
7. **Abdulla MH, and Johns EJ.** The role of brain angiotensin II (type 2) receptors and nitric oxide in the renal sympathoinhibitory response to acute volume expansion in conscious rats. *J Hypertens* 35: 338-347, 2017.
8. **Abumoawad A, Saad A, Ferguson CM, Eirin A, Woollard JR, Herrmann SM, Hickson LJ, Bendel EC, Misra S, Glockner J, Lerman LO, and Textor SC.** Tissue hypoxia, inflammation, and loss of glomerular filtration rate in human atherosclerotic renovascular disease. *Kidney Int* 95: 948-957, 2019.
9. **Abuyassin B, Badran M, Ayas NT, and Laher I.** Intermittent hypoxia causes histological kidney damage and increases growth factor expression in a mouse model of obstructive sleep apnea. *PLoS One* 13: e0192084, 2018.
10. **Accorsi-Mendonça D, and Machado BH.** Synaptic transmission of baro- and chemoreceptors afferents in the NTS second order neurons. *Auton Neurosci* 175: 3-8, 2013.
11. **Adeseun GA, and Rosas SE.** The impact of obstructive sleep apnea on chronic kidney disease. *Curr Hypertens Rep* 12: 378-383, 2010.
12. **Ahmad M, Makati D, and Akbar S.** Review of and Updates on Hypertension in Obstructive Sleep Apnea. *Int J Hypertens* 2017: 1848375, 2017.

13. **Ahmed SB.** Can Treatment of Obstructive Sleep Apnea with Continuous Positive Airway Pressure Still Improve Kidney Outcomes? *Am J Respir Crit Care Med* 196: 1370-1371, 2017.
14. **Ahmed SB, Ronksley PE, Hemmelgarn BR, Tsai WH, Manns BJ, Tonelli M, Klarenbach SW, Chin R, Clement FM, and Hanly PJ.** Nocturnal hypoxia and loss of kidney function. *PLoS One* 6: e19029, 2011.
15. **AlMarabeh S, Abdulla MH, and O'Halloran KD.** Is Aberrant Reno-Renal Reflex Control of Blood Pressure a Contributor to Chronic Intermittent Hypoxia-Induced Hypertension? *Front Physiol* 10: 465, 2019.
16. **Arjamaa O, and Nikinmaa M.** Hypoxia regulates the natriuretic peptide system. *Int J Physiol Pathophysiol Pharmacol* 3: 191-201, 2011.
17. **Ashack R, Farber MO, Weinberger MH, Robertson GL, Fineberg NS, and Manfredi F.** Renal and hormonal responses to acute hypoxia in normal individuals. *J Lab Clin Med* 106: 12-16, 1985.
18. **Ashton N, Clarke CG, Eddy DE, and Swift FV.** Mechanisms involved in the activation of ischemically sensitive, afferent renal nerve mediated reflex increases in hind-limb vascular resistance in the anesthetized rabbit. *Can J Physiol Pharmacol* 72: 637-643, 1994.
19. **Atkins EL, and Pearce JW.** Mechanisms of the renal response to plasma volume expansion. *Can J Biochem Physiol* 37: 91-102, 1959.
20. **Augustyniak RA, Maliszewska-Scislo M, Chen H, Fallucca J, and Rossi NF.** Acute angiotensin-converting enzyme inhibition evokes bradykinin-induced sympathetic activation in diabetic rats. *Am J Physiol Regul Integr Comp Physiol* 293: R2260-2266, 2007.
21. **Aziz F, and Chaudhary K.** The Triad of Sleep Apnea, Hypertension, and Chronic Kidney Disease: A Spectrum of Common Pathology. *Cardiorenal Medicine* 7: 74-82, 2017.
22. **Badran M, Abuyassin B, Golbidi S, Ayas N, and Laher I.** Uncoupling of Vascular Nitric Oxide Synthase Caused by Intermittent Hypoxia. *Oxid Med Cell Longev* 2016: 2354870, 2016.
23. **Balaszczuk AM, and Fellet AL.** Renal effects of dopamine and ANP in high volume expanded rats. *Journal of Physiology and Biochemistry* 57: 81-87, 2001.
24. **Banek CT, Knuepfer MM, Foss JD, Fiege JK, Asirvatham-Jeyaraj N, Van Helden D, Shimizu Y, and Osborn JW.** Resting Afferent Renal Nerve Discharge and Renal Inflammation: Elucidating the Role of Afferent and Efferent Renal Nerves in Deoxycorticosterone Acetate Salt Hypertension. *Hypertension* 68: 1415-1423, 2016.
25. **Barbee RW, and Trippodo NC.** The contribution of atrial natriuretic factor to acute volume natriuresis in rats. *Am J Physiol* 253: F1129-1135, 1987.

26. **Barrett CJ, Ramchandra R, Guild SJ, Lala A, Budgett DM, and Malpas SC.** What sets the long-term level of renal sympathetic nerve activity: a role for angiotensin II and baroreflexes? *Circ Res* 92: 1330-1336, 2003.
27. **Barros CC, Schadock I, Sihh G, Rother F, Xu P, Popova E, Lapidus I, Plehm R, Heuser A, Todiras M, Bachmann S, Alenina N, Araujo RC, Pesquero JB, and Bader M.** Chronic Overexpression of Bradykinin in Kidney Causes Polyuria and Cardiac Hypertrophy. *Front Med (Lausanne)* 5: 338, 2018.
28. **Barry E, and Johns E.** Bradykinin and excitatory reno- renal reflexes. *FASEB* 2012.
29. **Barry EF, and Johns EJ.** Intrarenal bradykinin elicits reno-renal reflex sympatho-excitation and renal nerve-dependent fluid retention. *Acta Physiol (Oxf)* 213: 731-739, 2015.
30. **Barton LJ, Lackner LH, Rector FC, and Seldin DW.** The effect of volume expansion on sodium reabsorption in the diluting segment of the dog kidney. *Kidney Int* 1: 19-26, 1972.
31. **Behm R, Mewes H, DeMuinck Keizer WH, Unger T, and Rettig R.** Cardiovascular and renal effects of hypoxia in conscious carotid body-denervated rats. *J Appl Physiol (1985)* 74: 2795-2800, 1993.
32. **Bell LB, Wilson DJ, Quandt LM, and Kampine JP.** Renal sympathetic and heart rate baroreflex function in conscious and isoflurane anaesthetized normotensive and chronically hypertensive rabbits. *Clin Exp Pharmacol Physiol* 22: 701-710, 1995.
33. **BERGER EY, and GALDSTON M.** The effect of anoxic anoxia on the human kidney. *J Clin Invest* 28: 648-652, 1949.
34. **Boer WH, Braam B, Fransen R, Boer P, and Koomans HA.** Effects of reduced renal perfusion pressure and acute volume expansion on proximal tubule and whole kidney angiotensin II content in the rat. *Kidney Int* 51: 44-49, 1997.
35. **Bonsignore MR, Parati G, Insalaco G, Marrone O, Castiglioni P, Romano S, Di Rienzo M, Mancia G, and Bonsignore G.** Continuous positive airway pressure treatment improves baroreflex control of heart rate during sleep in severe obstructive sleep apnea syndrome. *Am J Respir Crit Care Med* 166: 279-286, 2002.
36. **Booth LC, May CN, and Yao ST.** The role of the renal afferent and efferent nerve fibers in heart failure. *Front Physiol* 6: 270, 2015.
37. **Booth LC, Nishi EE, Yao ST, Ramchandra R, Lambert GW, Schlaich MP, and May CN.** Reinnervation of renal afferent and efferent nerves at 5.5 and 11 months after catheter-based radiofrequency renal denervation in sheep. *Hypertension* 65: 393-400, 2015.
38. **Braun C, Ade M, Unger T, van der Woude FJ, and Rohmeiss P.** Effects of bradykinin and icatibant on renal hemodynamics in conscious spontaneously hypertensive and normotensive rats. *J Cardiovasc Pharmacol* 30: 446-454, 1997.

39. **Brenner BM, Troy JL, and Daugharty TM.** On the mechanism of inhibition in fluid reabsorption by the renal proximal tubule of the volume-expanded rat. *J Clin Invest* 50: 1596-1602, 1971.
40. **Bruns FJ.** Decrease in renal perfusion, glomerular filtration and sodium excretion by hypoxia in the dog. *Proc Soc Exp Biol Med* 159: 468-472, 1978.
41. **Buckley MM, and Johns EJ.** Impact of L-NAME on the cardiopulmonary reflex in cardiac hypertrophy. *Am J Physiol Regul Integr Comp Physiol* 301: R1549-1556, 2011.
42. **Burke SL, Lim K, Moretti JL, and Head GA.** Comparison of sympathetic nerve activity normalization procedures in conscious rabbits. *Am J Physiol Heart Circ Physiol* 310: H1222-1232, 2016.
43. **Calaresu FR, and Ciriello J.** Renal afferent nerves affect discharge rate of medullary and hypothalamic single units in the cat. *J Auton Nerv Syst* 3: 311-320, 1981.
44. **Calaresu FR, Stella A, and Zanchetti A.** Haemodynamic responses and renin release during stimulation of afferent renal nerves in the cat. *J Physiol* 255: 687-700, 1976.
45. **Campbell DJ, Duncan AM, Kladis A, and Harrap SB.** Increased levels of bradykinin and its metabolites in tissues of young spontaneously hypertensive rats. *J Hypertens* 13: 739-746, 1995.
46. **Campese VM, and Kogosov E.** Renal afferent denervation prevents hypertension in rats with chronic renal failure. *Hypertension* 25: 878-882, 1995.
47. **Cao W, Li A, Li J, Wu C, Cui S, Zhou Z, Liu Y, Wilcox CS, and Hou FF.** Reno-Cerebral Reflex Activates the Renin-Angiotensin System, Promoting Oxidative Stress and Renal Damage After Ischemia-Reperfusion Injury. *Antioxid Redox Signal* 27: 415-432, 2017.
48. **Cao W, Li A, Wang L, Zhou Z, Su Z, Bin W, Wilcox CS, and Hou FF.** A Salt-Induced Reno-Cerebral Reflex Activates Renin-Angiotensin Systems and Promotes CKD Progression. *J Am Soc Nephrol* 26: 1619-1633, 2015.
49. **Carlson JT, Hedner JA, Sellgren J, Elam M, and Wallin BG.** Depressed baroreflex sensitivity in patients with obstructive sleep apnea. *Am J Respir Crit Care Med* 154: 1490-1496, 1996.
50. **Caverson MM, and Ciriello J.** Effect of stimulation of afferent renal nerves on plasma levels of vasopressin. *Am J Physiol* 252: R801-807, 1987.
51. **Cesare P, and McNaughton P.** A novel heat-activated current in nociceptive neurons and its sensitization by bradykinin. *Proc Natl Acad Sci U S A* 93: 15435-15439, 1996.

52. **Chaimovitz C, Spierer A, Leibowitz H, Tuma S, and Better OS.** Exaggerated phosphaturic response to volume expansion in patients with essential hypertension. *Clin Sci Mol Med* 49: 207-211, 1975.
53. **Chapleau MW, Hajduczuk G, and Abboud FM.** Peripheral and central mechanisms of baroreflex resetting. *Clin Exp Pharmacol Physiol Suppl* 15: 31-43, 1989.
54. **Chen HH, Cheng PW, Ho WY, Lu PJ, Lai CC, Tseng YM, Fang HC, Sun GC, Hsiao M, Liu CP, and Tseng CJ.** Renal Denervation Improves the Baroreflex and GABA System in Chronic Kidney Disease-induced Hypertension. *Sci Rep* 6: 38447, 2016.
55. **Chen HI, and Chang KC.** Assessment of threshold and saturation pressure in the baroreflex function curve: a new mathematical analysis. *Jpn J Physiol* 41: 861-877, 1991.
56. **Chen L, Einbinder E, Zhang Q, Hasday J, Balke CW, and Scharf SM.** Oxidative stress and left ventricular function with chronic intermittent hypoxia in rats. *Am J Respir Crit Care Med* 172: 915-920, 2005.
57. **Chen L, Markó L, Kaßmann M, Zhu Y, Wu K, and Gollasch M.** Role of TRPV1 channels in ischemia/reperfusion-induced acute kidney injury. *PLoS One* 9: e109842, 2014.
58. **Chhabra V, Anand AS, Baidya AK, Malik SM, Kohli E, and Reddy MPK.** Hypobaric hypoxia induced renal damage is mediated by altering redox pathway. *PLoS One* 13: e0195701, 2018.
59. **Chien CT, Chien HF, Cheng YJ, Chen CF, and Hsu SM.** Renal afferent signaling diuretic response is impaired in streptozotocin-induced diabetic rats. *Kidney Int* 57: 203-214, 2000.
60. **Chien CT, Fu TC, Wu MS, and Chen CF.** Attenuated response of renal mechanoreceptors to volume expansion in chronically hypoxic rats. *Am J Physiol* 273: F712-717, 1997.
61. **Coelho NR, Dias CG, João Correia M, Grácio P, Serpa J, Monteiro EC, Diogo LN, and Pereira SA.** Cysteine Oxidative Dynamics Underlies Hypertension and Kidney Dysfunction Induced by Chronic Intermittent Hypoxia. *Adv Exp Med Biol* 1071: 83-88, 2018.
62. **Cooper VL, Pearson SB, Bowker CM, Elliott MW, and Hainsworth R.** Interaction of chemoreceptor and baroreceptor reflexes by hypoxia and hypercapnia - a mechanism for promoting hypertension in obstructive sleep apnoea. *J Physiol* 568: 677-687, 2005.
63. **Coote JH.** A role for the paraventricular nucleus of the hypothalamus in the autonomic control of heart and kidney. *Exp Physiol* 90: 169-173, 2005.

64. **Cortelli P, Lombardi C, Montagna P, and Parati G.** Baroreflex modulation during sleep and in obstructive sleep apnea syndrome. *Auton Neurosci* 169: 7-11, 2012.
65. **Cortelli P, Parchi P, Sforza E, Contin M, Pierangeli G, Barletta G, and Lugaresi E.** Cardiovascular autonomic dysfunction in normotensive awake subjects with obstructive sleep apnoea syndrome. *Clin Auton Res* 4: 57-62, 1994.
66. **Cowley AW.** Renal medullary oxidative stress, pressure-natriuresis, and hypertension. *Hypertension* 52: 777-786, 2008.
67. **Cowley AW, Liard JF, and Guyton AC.** Role of baroreceptor reflex in daily control of arterial blood pressure and other variables in dogs. *Circ Res* 32: 564-576, 1973.
68. **CURRIE JC, and ULLMANN E.** Polyuria during experimental modifications of breathing. *J Physiol* 155: 438-455, 1961.
69. **Cutler MJ, Swift NM, Keller DM, Wasmund WL, and Smith ML.** Hypoxia-mediated prolonged elevation of sympathetic nerve activity after periods of intermittent hypoxic apnea. *J Appl Physiol* (1985) 96: 754-761, 2004.
70. **Dalmasso C, Ahmed NH, Leachman JR, and Loria AS.** Adipose Afferent Reflex Stimulation Increases The Activation Of The Organum Vasculosum Of The Lamina Terminalis (OVLT) In Obese Male Mice Exposed To Early Life Stress. *The FASEB* 34: 1-1, 2019.
71. **Dalmasso C, Jacqueline LR, Mounce S, Xu X, and Anglia LS.** Capsaicin-Induced Stimulation of Sensory Neurons in Adipose Tissue Promotes Increases in Blood Pressure in Mice Exposed to Early Life Stress. *FASEB* 574.11: 2019.
72. **Damy T, Paulino A, Margarit L, Drouot X, Stoica M, Vermes E, Gueret P, Adnot S, Rande JL, D'Ortho MP, and Hittinger L.** Left ventricle remodelling is associated with sleep-disordered breathing in non-ischaemic cardiopathy with systolic dysfunction. *J Sleep Res* 20: 101-109, 2011.
73. **de Paula PM, Tolstykh G, and Mifflin S.** Chronic intermittent hypoxia alters NMDA and AMPA-evoked currents in NTS neurons receiving carotid body chemoreceptor inputs. *Am J Physiol Regul Integr Comp Physiol* 292: R2259-2265, 2007.
74. **Del Rio R, Andrade DC, Lucero C, Arias P, and Iturriaga R.** Carotid Body Ablation Abrogates Hypertension and Autonomic Alterations Induced by Intermittent Hypoxia in Rats. *Hypertension* 68: 436-445, 2016.
75. **Del Rio R, Moya EA, and Iturriaga R.** Carotid body potentiation during chronic intermittent hypoxia: implication for hypertension. *Front Physiol* 5: 434, 2014.
76. **Del Rio R, Moya EA, Parga MJ, Madrid C, and Iturriaga R.** Carotid body inflammation and cardiorespiratory alterations in intermittent hypoxia. *Eur Respir J* 39: 1492-1500, 2012.

77. **Deres L, Eros K, Horvath O, Bencze N, Cseko C, Farkas S, Habon T, Toth K, and Halmosi R.** The Effects of Bradykinin B1 Receptor Antagonism on the Myocardial and Vascular Consequences of Hypertension in SHR Rats. *Front Physiol* 10: 624, 2019.
78. **Dias JP, Talbot S, Sénécal J, Carayon P, and Couture R.** Kinin B1 receptor enhances the oxidative stress in a rat model of insulin resistance: outcome in hypertension, allodynia and metabolic complications. *PLoS One* 5: e12622, 2010.
79. **Dickinson CJ.** Re: baroreceptors and the long-term control of blood pressure. *Exp Physiol* 89: 335-337; author reply 341, 2004.
80. **Ding W, Cai Y, Wang W, Ji L, Dong Y, Zhang X, Su M, Liu J, and Lu G.** Adiponectin protects the kidney against chronic intermittent hypoxia-induced injury through inhibiting endoplasmic reticulum stress. *Sleep Breath* 20: 1069-1074, 2016.
81. **Diogo LN, and Monteiro EC.** The efficacy of antihypertensive drugs in chronic intermittent hypoxia conditions. *Front Physiol* 5: 361, 2014.
82. **Ditting T, Freisinger W, Siegel K, Fiedler C, Small L, Neuhuber W, Heinlein S, Reeh PW, Schmieder RE, and Veelken R.** Tonic postganglionic sympathetic inhibition induced by afferent renal nerves? *Hypertension* 59: 467-476, 2012.
83. **Ditting T, Tiegs G, and Veelken R.** Autonomous innervation in renal inflammatory disease-innocent bystander or active modulator? *J Mol Med (Berl)* 87: 865-870, 2009.
84. **Docio I, Olea E, Prieto-Lloret J, Gallego-Martin T, Obeso A, Gomez-Niño A, and Rocher A.** Guinea Pig as a Model to Study the Carotid Body Mediated Chronic Intermittent Hypoxia Effects. *Front Physiol* 9: 694, 2018.
85. **Dopp JM, Philippi NR, Marcus NJ, Olson EB, Bird CE, Moran JJ, Mueller SW, and Morgan BJ.** Xanthine oxidase inhibition attenuates endothelial dysfunction caused by chronic intermittent hypoxia in rats. *Respiration* 82: 458-467, 2011.
86. **Drager LF, Bortolotto LA, Figueiredo AC, Silva BC, Krieger EM, and Lorenzi-Filho G.** Obstructive sleep apnea, hypertension, and their interaction on arterial stiffness and heart remodeling. *Chest* 131: 1379-1386, 2007.
87. **Duchen MR, and Biscoe TJ.** Mitochondrial function in type I cells isolated from rabbit arterial chemoreceptors. *J Physiol* 450: 13-31, 1992.
88. **Duka I, Kintsurashvili E, Gavras I, Johns C, Bresnahan M, and Gavras H.** Vasoactive potential of the b(1) bradykinin receptor in normotension and hypertension. *Circ Res* 88: 275-281, 2001.
89. **Dyavanapalli J, Jameson H, Dergacheva O, Jain V, Alhusayyen M, and Mendelowitz D.** Chronic intermittent hypoxia-hypercapnia blunts heart rate responses and alters neurotransmission to cardiac vagal neurons. *J Physiol* 592: 2799-2811, 2014.

90. **Emanuelli C, Chao J, Regoli D, Chao L, Ni A, and Madeddu P.** The bradykinin B1 receptor and the central regulation of blood pressure in spontaneously hypertensive rats. *Br J Pharmacol* 126: 1769-1776, 1999.
91. **Evans AM, Mahmoud AD, Moral-Sanz J, and Hartmann S.** The emerging role of AMPK in the regulation of breathing and oxygen supply. *Biochem J* 473: 2561-2572, 2016.
92. **Evans RG, Goddard D, Eppel GA, and O'Connor PM.** Stability of tissue PO₂ in the face of altered perfusion: a phenomenon specific to the renal cortex and independent of resting renal oxygen consumption. *Clin Exp Pharmacol Physiol* 38: 247-254, 2011.
93. **Faber JE.** Role of prostaglandins and kinins in the renal pressor reflex. *Hypertension* 10: 522-532, 1987.
94. **Faber JE, and Brody MJ.** Afferent renal nerve-dependent hypertension following acute renal artery stenosis in the conscious rat. *Circ Res* 57: 676-688, 1985.
95. **Fatouleh R, McKenzie DK, and Macefield VG.** Respiratory modulation of muscle sympathetic nerve activity in obstructive sleep apnoea. *Exp Physiol* 99: 1288-1298, 2014.
96. **Feng NH, Lee HH, Shiang JC, and Ma MC.** Transient receptor potential vanilloid type 1 channels act as mechanoreceptors and cause substance P release and sensory activation in rat kidneys. *Am J Physiol Renal Physiol* 294: F316-325, 2008.
97. **Fletcher EC.** Invited review: Physiological consequences of intermittent hypoxia: systemic blood pressure. *J Appl Physiol (1985)* 90: 1600-1605, 2001.
98. **Fletcher EC, Lesske J, Behm R, Miller CC, Stauss H, and Unger T.** Carotid chemoreceptors, systemic blood pressure, and chronic episodic hypoxia mimicking sleep apnea. *J Appl Physiol (1985)* 72: 1978-1984, 1992.
99. **Fletcher EC, Lesske J, Qian W, Miller CC, and Unger T.** Repetitive, episodic hypoxia causes diurnal elevation of blood pressure in rats. *Hypertension* 19: 555-561, 1992.
100. **Fogo A, and Ichikawa I.** Evidence for a pathogenic linkage between glomerular hypertrophy and sclerosis. *Am J Kidney Dis* 17: 666-669, 1991.
101. **Foss JD, Wainford RD, Engeland WC, Fink GD, and Osborn JW.** A novel method of selective ablation of afferent renal nerves by periaxonal application of capsaicin. *Am J Physiol Regul Integr Comp Physiol* 308: R112-122, 2015.
102. **Franchini KG.** Hemodilution mediates changes in renal hemodynamics after acute volume expansion in rats. *Am J Physiol* 274: R1670-1676, 1998.
103. **Friederich-Persson M, Persson P, Fasching A, Hansell P, Nordquist L, and Palm F.** Increased kidney metabolism as a pathway to kidney tissue hypoxia and damage: effects of triiodothyronine and dinitrophenol in normoglycemic rats. *Adv Exp Med Biol* 789: 9-14, 2013.

104. **Gao J, Kerut EK, Smart F, Katsurada A, Seth D, Navar LG, and Kapusta DR.** Sympathoinhibitory Effect of Radiofrequency Renal Denervation in Spontaneously Hypertensive Rats With Established Hypertension. *Am J Hypertens* 29: 1394-1401, 2016.
105. **Geppetti P.** Sensory neuropeptide release by bradykinin: mechanisms and pathophysiological implications. *Regul Pept* 47: 1-23, 1993.
106. **Ghahramani N, Ahmed F, Al-Laham A, and Lengerich EJ.** The epidemiological association of altitude with chronic kidney disease: Evidence of protective effect. *Nephrology (Carlton)* 16: 219-224, 2011.
107. **Giannattasio C, Seravalle GL, Bolla GB, Cattaneo B, Cléroux J, Cuspidi C, Sampieri L, Grassi G, and Mancina G.** Cardiopulmonary Receptor Reflexes in Normotensive Athletes With Cardiac Hypertrophy. *Circulation* 82: 1222–1229, 1990.
108. **Gloviczki ML, Glockner JF, Lerman LO, McKusick MA, Misra S, Grande JP, and Textor SC.** Preserved oxygenation despite reduced blood flow in poststenotic kidneys in human atherosclerotic renal artery stenosis. *Hypertension* 55: 961-966, 2010.
109. **Goetz KL.** Atrial receptors, natriuretic peptides, and the kidney--current understanding. *Mayo Clin Proc* 61: 600-603, 1986.
110. **Goetz KL, Bond GC, and Bloxham DD.** Atrial receptors and renal function. *Physiol Rev* 55: 157-205, 1975.
111. **Goetz KL, Wang BC, Geer PG, Leadley RJ, and Reinhardt HW.** Atrial stretch increases sodium excretion independently of release of atrial peptides. *Am J Physiol* 250: R946-950, 1986.
112. **Goldfarb-Rumyantzev AS, and Alper SL.** Short-term responses of the kidney to high altitude in mountain climbers. *Nephrol Dial Transplant* 29: 497-506, 2014.
113. **Golias C, Charalabopoulos A, Stagikas D, Charalabopoulos K, and Batistatou A.** The kinin system--bradykinin: biological effects and clinical implications. Multiple role of the kinin system--bradykinin. *Hippokratia* 11: 124-128, 2007.
114. **Gontijo JA, and Kopp UC.** Activation of renal pelvic chemoreceptors in rats: role of calcitonin gene-related peptide receptors. *Acta Physiol Scand* 166: 159-165, 1999.
115. **Gontijo JR, and Kopp UC.** Renal sensory receptor activation by calcitonin gene-related peptide. *Hypertension* 23: 1063-1067, 1994.
116. **Gontijo JR, Smith LA, and Kopp UC.** CGRP activates renal pelvic substance P receptors by retarding substance P metabolism. *Hypertension* 33: 493-498, 1999.
117. **Gonzalez CB, and Figueroa CD.** Vasopressin and bradykinin receptors in the kidney: implications for tubular function. *Biol Res* 32: 63-76, 1999.

118. **Goodwill VS, Terrill C, Hopewood I, Loewy AD, and Knuepfer MM.** CNS sites activated by renal pelvic epithelial sodium channels (ENaCs) in response to hypertonic saline in awake rats. *Auton Neurosci* 204: 35-47, 2017.
119. **Gottlieb DJ, Yenokyan G, Newman AB, O'Connor GT, Punjabi NM, Quan SF, Redline S, Resnick HE, Tong EK, Diener-West M, and Shahar E.** Prospective study of obstructive sleep apnea and incident coronary heart disease and heart failure: the sleep heart health study. *Circulation* 122: 352-360, 2010.
120. **Goulding NE, and Johns EJ.** Neural regulation of the kidney function in rats with cisplatin induced renal failure. *Front Physiol* 6: 192, 2015.
121. **Grassi G, Giannattasio C, Cl  roux J, Cuspidi C, Sampieri L, Bolla GB, and Mancia G.** Cardiopulmonary reflex before and after regression of left ventricular hypertrophy in essential hypertension. *Hypertension* 12: 227-237, 1988.
122. **Gu H, Lin M, Liu J, Gozal D, Scrogin KE, Wurster R, Chapleau MW, Ma X, and Cheng ZJ.** Selective impairment of central mediation of baroreflex in anesthetized young adult Fischer 344 rats after chronic intermittent hypoxia. *Am J Physiol Heart Circ Physiol* 293: H2809-2818, 2007.
123. **Guan P, Lin XM, Yang SC, Guo YJ, Li WY, Zhao YS, Yu FY, Sun ZM, An JR, and Ji ES.** Hydrogen gas reduces chronic intermittent hypoxia-induced hypertension by inhibiting sympathetic nerve activity and increasing vasodilator responses via the antioxidation. *J Cell Biochem* 120: 3998-4008, 2019.
124. **Guild SJ, McBryde FD, Malpas SC, and Barrett CJ.** High dietary salt and angiotensin II chronically increase renal sympathetic nerve activity: a direct telemetric study. *Hypertension* 59: 614-620, 2012.
125. **Guo QH, Tian YL, Wang Z, Li AY, Ma ZH, Guo YJ, Weiss JW, Ji ES, and Chu L.** Endothelin receptors in augmented vasoconstrictor responses to endothelin-1 in chronic intermittent hypoxia. *Clin Exp Pharmacol Physiol* 40: 449-457, 2013.
126. **Guyton A.** Role of the Kidney in Long Term Regulation of Blood Pressure. In: *Guyton and Hall Textbook of Medical Physiology* Saunders, 2010, p. 213-228.
127. **Habermann G, and Huckstorf C.** Cardiovascular and renal effects of systemic hypoxia in chronically instrumented conscious WKY and SHR rats. *Exp Clin Endocrinol Diabetes* 105 Suppl 2: 26-28, 1997.
128. **Haditsch B, Roessler A, and Hinghofer-Szalkay HG.** Renal adrenomedullin and high altitude diuresis. *Physiol Res* 56: 779-787, 2007.
129. **Hainsworth R.** Cardiovascular control from cardiac and pulmonary vascular receptors. *Exp Physiol* 99: 312-319, 2014.
130. **Hall JE.** Louis K. Dahl Memorial Lecture. Renal and cardiovascular mechanisms of hypertension in obesity. *Hypertension* 23: 381-394, 1994.

131. **Hall ME, do Carmo JM, da Silva AA, Juncos LA, Wang Z, and Hall JE.** Obesity, hypertension, and chronic kidney disease. *Int J Nephrol Renovasc Dis* 7: 75-88, 2014.
132. **Hart EC, and Charkoudian N.** Sympathetic neural regulation of blood pressure: influences of sex and aging. *Physiology (Bethesda)* 29: 8-15, 2014.
133. **Head GA, and Burke SL.** Renal and cardiac sympathetic baroreflexes in hypertensive rabbits. *Clin Exp Pharmacol Physiol* 28: 972-975, 2001.
134. **Hegde SS, Jadhav AL, and Lokhandwala MF.** Role of kidney dopamine in the natriuretic response to volume expansion in rats. *Hypertension* 13: 828-834, 1989.
135. **Hermansson K, Ojteg G, and Wolgast M.** The reno-renal reflex; evaluation from renal blood flow measurements. *Acta Physiol Scand* 120: 207-215, 1984.
136. **Hildebrandt W, Ottenbacher A, Schuster M, Swenson ER, and Bärtzsch P.** Diuretic effect of hypoxia, hypocapnia, and hyperpnea in humans: relation to hormones and O(2) chemosensitivity. *J Appl Physiol (1985)* 88: 599-610, 2000.
137. **Hindermann M, Martin T, Rodionova K, Loosen S, Ott C, Schmieder RE, Amann K, and Veelken R.** Effects of intrarenal afferent stimulation by Bradykinin on Renal Sympathetic Nerve Activity: Tonic Inhibition facilitating Sodium and Water Excretion. *FASEB J* 31: 1027.1022-1027.1022, 2017.
138. **Hinojosa-Laborde C, and Mifflin SW.** Sex differences in blood pressure response to intermittent hypoxia in rats. *Hypertension* 46: 1016-1021, 2005.
139. **Hoagland KM, Maddox DA, and Martin DS.** Intrarenal infusion of bradykinin elicits a pressor response in conscious rats via a B2-receptor mechanism. *Can J Physiol Pharmacol* 77: 563-570, 1999.
140. **Honig A.** Peripheral arterial chemoreceptors and reflex control of sodium and water homeostasis. *Am J Physiol* 257: R1282-1302, 1989.
141. **Huang C, AlMarabeh S, Cavers J, Abdulla MH, and Johns EJ.** Effects of intracerebroventricular leptin and orexin-A on the baroreflex control of renal sympathetic nerve activity in conscious rats fed a normal or high-fat diet. *Clin Exp Pharmacol Physiol* 48: 585-596, 2021.
142. **Huang J, Tamisier R, Ji E, Tong J, and Weiss WJ.** Chronic intermittent hypoxia modulates nNOS mRNA and protein expression in the rat hypothalamus. *Respir Physiol Neurobiol* 158: 30-38, 2007.
143. **Hughson MD, Puelles VG, Hoy WE, Douglas-Denton RN, Mott SA, and Bertram JF.** Hypertension, glomerular hypertrophy and nephrosclerosis: the effect of race. *Nephrol Dial Transplant* 29: 1399-1409, 2014.
144. **Hui K, Liu B, and Qin F.** Capsaicin activation of the pain receptor, VR1: multiple open states from both partial and full binding. *Biophys J* 84: 2957-2968, 2003.

145. **Ichikawa I, and Brenner BM.** Mechanism of inhibition of proximal tubule fluid reabsorption after exposure of the rat kidney to the physical effects of expansion of extracellular fluid volume. *J Clin Invest* 64: 1466-1474, 1979.
146. **Iturriaga R, Moya EA, and Del Rio R.** Inflammation and oxidative stress during intermittent hypoxia: the impact on chemoreception. *Exp Physiol* 100: 149-155, 2015.
147. **Jankov RP, Kantores C, Pan J, and Belik J.** Contribution of xanthine oxidase-derived superoxide to chronic hypoxic pulmonary hypertension in neonatal rats. *Am J Physiol Lung Cell Mol Physiol* 294: L233-245, 2008.
148. **Janssen BJ, van Essen H, Struyker Boudier HA, and Smits JF.** Hemodynamic effects of activation of renal and mesenteric sensory nerves in rats. *Am J Physiol* 257: R29-36, 1989.
149. **Janssen BJ, van Essen H, Vervoort-Peters LH, Struyker-Boudier HA, and Smits JF.** Role of afferent renal nerves in spontaneous hypertension in rats. *Hypertension* 13: 327-333, 1989.
150. **Javaheri S, and Dempsey JA.** Central sleep apnea. *Compr Physiol* 3: 141-163, 2013.
151. **Johns EJ, Kopp UC, and DiBona GF.** Neural control of renal function. *Compr Physiol* 1: 731-767, 2011.
152. **Joseph V, Laouafa S, Marcouiller F, Roussel D, Pialoux V, and Bairam A.** Progesterone decreases apnoea and reduces oxidative stress induced by chronic intermittent hypoxia in ovariectomized female rats. *Exp Physiol* 105: 1025-1034, 2020.
153. **Kakoki M, McGarrah RW, Kim HS, and Smithies O.** Bradykinin B1 and B2 receptors both have protective roles in renal ischemia/reperfusion injury. *Proc Natl Acad Sci U S A* 104: 7576-7581, 2007.
154. **Kang YM, Ma Y, Zheng JP, Elks C, Sriramula S, Yang ZM, and Francis J.** Brain nuclear factor-kappa B activation contributes to neurohumoral excitation in angiotensin II-induced hypertension. *Cardiovasc Res* 82: 503-512, 2009.
155. **Karim AS, Reese SR, Wilson NA, Jacobson LM, Zhong W, and Djamali A.** Nox2 is a mediator of ischemia reperfusion injury. *Am J Transplant* 15: 2888-2899, 2015.
156. **Karim F, Kidd C, Malpus CM, and Penna PE.** The effects of stimulation of the left atrial receptors on sympathetic efferent nerve activity. *J Physiol* 227: 243-260, 1972.
157. **Karim F, Poucher SM, and Summerill RA.** The effects of stimulating carotid chemoreceptors on renal haemodynamics and function in dogs. *J Physiol* 392: 451-462, 1987.

158. **Kario K, Bhatt DL, Kandzari DE, Brar S, Flack JM, Gilbert C, Oparil S, Robbins M, Townsend RR, and Bakris G.** Impact of Renal Denervation on Patients With Obstructive Sleep Apnea and Resistant Hypertension - Insights From the SYMPPLICITY HTN-3 Trial. *Circ J* 80: 1404-1412, 2016.
159. **Kario K, Ikemoto T, Kuwabara M, Ishiyama H, Saito K, and Hoshide S.** Catheter-Based Renal Denervation Reduces Hypoxia-Triggered Nocturnal Blood Pressure Peak in Obstructive Sleep Apnea Syndrome. *J Clin Hypertens (Greenwich)* 18: 707-709, 2016.
160. **Kassmann M, Harteneck C, Zhu Z, Nürnberg B, Tepel M, and Gollasch M.** Transient receptor potential vanilloid 1 (TRPV1), TRPV4, and the kidney. *Acta Physiol (Oxf)* 207: 546-564, 2013.
161. **Katholi RE, Hageman GR, Whitlow PL, and Woods WT.** Hemodynamic and afferent renal nerve responses to intrarenal adenosine in the dog. *Hypertension* 5: 1149-154, 1983.
162. **Kaur M, Chandran DS, Jaryal AK, Bhowmik D, Agarwal SK, and Deepak KK.** Baroreflex dysfunction in chronic kidney disease. *World J Nephrol* 5: 53-65, 2016.
163. **Kawada T, Shimizu S, Kamiya A, Sata Y, Uemura K, and Sugimachi M.** Dynamic characteristics of baroreflex neural and peripheral arcs are preserved in spontaneously hypertensive rats. *Am J Physiol Regul Integr Comp Physiol* 300: R155-165, 2011.
164. **Keiko T, Seiji U, Takashi K, Akira N, Takeshi S, and Yusuke S.** Renal sympathetic nerve denervation inhibits chronic intermittent hypoxia-induced hypertension by decreasing renin-angiotensin system and oxidative stress in a mouse model of sleep apnea syndrome. *Nephrology Dialysis Transplantation* 2017.
165. **KELLEY VC, and McDONALD RK.** Further observations on the effects of altitude anoxia on renal function. *Am J Physiol* 154: 201-206, 1948.
166. **Kent BB, Drane JW, Blumenstein B, and Manning JW.** A mathematical model to assess changes in the baroreceptor reflex. *Cardiology* 57: 295-310, 1972.
167. **Khan A, Abdul Sattar M, Rathore H, Ahmad A, Abdullah N, and John E.** Renal Denervation Restores the Baroreflex Regulation of Renal Sympathetic Nerve Activity in Rats Receiving Intrarenal Bradykinin. *FASEB* 31: 848.842-848.842, 2017.
168. **Khan SA, Sattar MA, Rathore HA, Abdulla MH, Ud Din Ahmad F, Ahmad A, Afzal S, Abdullah NA, and Johns EJ.** Renal denervation restores the baroreflex control of renal sympathetic nerve activity and heart rate in Wistar-Kyoto rats with cisplatin-induced renal failure. *Acta Physiol (Oxf)* 210: 690-700, 2014.
169. **Khan SA, Sattar MZ, Abdullah NA, Rathore HA, Abdulla MH, Ahmad A, and Johns EJ.** Obesity depresses baroreflex control of renal sympathetic nerve activity and heart rate in Sprague Dawley rats: role of the renal innervation. *Acta Physiol (Oxf)* 214: 390-401, 2015.

170. **Khan SA, Sattar MZA, Abdullah NA, Rathore HA, Ahmad A, Abdulla MH, and Johns EJ.** Improvement in baroreflex control of renal sympathetic nerve activity in obese Sprague Dawley rats following immunosuppression. *Acta Physiol (Oxf)* 221: 250-265, 2017.
171. **Kim DK, Natarajan N, Prabhakar NR, and Kumar GK.** Facilitation of dopamine and acetylcholine release by intermittent hypoxia in PC12 cells: involvement of calcium and reactive oxygen species. *J Appl Physiol (1985)* 96: 1206-1215; discussion 1196, 2004.
172. **Kim KS, Yoo HY, Park KS, Kim JK, Zhang YH, and Kim SJ.** Differential effects of acute hypoxia on the activation of TRPV1 by capsaicin and acidic pH. *J Physiol Sci* 62: 93-103, 2012.
173. **Kious KW, Twohey SCE, Keomanivong FE, Neidermann SE, Dirkman JJ, and Marcus NJ.** Chronic Intermittent Hypoxia Promotes Glomerular Hyperfiltration, Reductions in Renal Blood Flow, and Upregulation of Renal A2B Receptor Expression. *FASEB* 2019.
174. **Kline DD.** Chronic intermittent hypoxia affects integration of sensory input by neurons in the nucleus tractus solitarii. *Respir Physiol Neurobiol* 174: 29-36, 2010.
175. **Kline DD, Wang S, and Kunze DL.** TRPV1 channels contribute to spontaneous glutamate release in nucleus tractus solitarii following chronic intermittent hypoxia. *J Neurophysiol* 121: 881-892, 2019.
176. **Knuepfer MM, and Schramm LP.** The conduction velocities and spinal projections of single renal afferent fibers in the rat. *Brain Res* 435: 167-173, 1987.
177. **Konecny T, Kara T, and Somers VK.** Obstructive sleep apnea and hypertension: an update. *Hypertension* 63: 203-209, 2014.
178. **Kopp U.** Neural control of renal function. In: *Neural control of renal function* Morgan & Claypool life sciences, 2011.
179. **Kopp UC.** Endothelin in the control of renal sympathetic nerve activity. *Contrib Nephrol* 172: 107-119, 2011.
180. **Kopp UC.** Role of renal sensory nerves in physiological and pathophysiological conditions. *Am J Physiol Regul Integr Comp Physiol* 308: R79-95, 2015.
181. **Kopp UC, and Buckley-Bleiler RL.** Impaired renorenal reflexes in two-kidney, one clip hypertensive rats. *Hypertension* 14: 445-452, 1989.
182. **Kopp UC, Cicha MZ, Farley DM, Smith LA, and Dixon BS.** Renal substance P-containing neurons and substance P receptors impaired in hypertension. *Hypertension* 31: 815-822, 1998.
183. **Kopp UC, Cicha MZ, and Jones SY.** Activation of endothelin A receptors contributes to impaired responsiveness of renal mechanosensory nerves in congestive heart failure. *Can J Physiol Pharmacol* 88: 622-629, 2010.

184. **Kopp UC, Cicha MZ, and Smith LA.** Dietary sodium loading increases arterial pressure in afferent renal-denervated rats. *Hypertension* 42: 968-973, 2003.
185. **Kopp UC, Cicha MZ, and Smith LA.** PGE(2) increases release of substance P from renal sensory nerves by activating the cAMP-PKA transduction cascade. *Am J Physiol Regul Integr Comp Physiol* 282: R1618-1627, 2002.
186. **Kopp UC, Cicha MZ, Smith LA, Mulder J, and Hökfelt T.** Renal sympathetic nerve activity modulates afferent renal nerve activity by PGE2-dependent activation of alpha1- and alpha2-adrenoceptors on renal sensory nerve fibers. *Am J Physiol Regul Integr Comp Physiol* 293: R1561-1572, 2007.
187. **Kopp UC, Farley DM, Cicha MZ, and Smith LA.** Activation of renal mechanosensitive neurons involves bradykinin, protein kinase C, PGE(2), and substance P. *Am J Physiol Regul Integr Comp Physiol* 278: R937-946, 2000.
188. **Kopp UC, Grisk O, Cicha MZ, Smith LA, Steinbach A, Schlüter T, Mähler N, and Hökfelt T.** Dietary sodium modulates the interaction between efferent renal sympathetic nerve activity and afferent renal nerve activity: role of endothelin. *Am J Physiol Regul Integr Comp Physiol* 297: R337-351, 2009.
189. **Kopp UC, Matsushita K, Sigmund RD, Smith LA, Watanabe S, and Stokes JB.** Amiloride-sensitive Na⁺ channels in pelvic uroepithelium involved in renal sensory receptor activation. *Am J Physiol* 275: R1780-1792, 1998.
190. **Kopp UC, and Smith LA.** Bradykinin and protein kinase C activation fail to stimulate renal sensory neurons in hypertensive rats. *Hypertension* 27: 607-612, 1996.
191. **Kopp UC, and Smith LA.** Effects of the substance P receptor antagonist CP-96,345 on renal sensory receptor activation. *Am J Physiol* 264: R647-653, 1993.
192. **Kopp UC, and Smith LA.** Inhibitory renorenal reflexes: a role for substance P or other capsaicin-sensitive neurons. *Am J Physiol* 260: R232-239, 1991.
193. **Kopp UC, and Smith LA.** Renorenal reflex responses to renal sensory receptor stimulation in normotension and hypertension. *Clin Exp Hypertens A* 9 Suppl 1: 113-125, 1987.
194. **Kopp UC, and Smith LA.** Role of prostaglandins in renal sensory receptor activation by substance P and bradykinin. *Am J Physiol* 265: R544-551, 1993.
195. **Kopp UC, Smith LA, and DiBona GF.** Renorenal reflexes: neural components of ipsilateral and contralateral renal responses. *Am J Physiol* 249: F507-517, 1985.
196. **Krause BJ, Casanello P, Dias AC, Arias P, Velarde V, Arenas GA, Preite MD, and Iturriaga R.** Chronic Intermittent Hypoxia-Induced Vascular Dysfunction in Rats is Reverted by. *Front Physiol* 9: 901, 2018.
197. **Krum H, Schlaich M, Whitbourn R, Sobotka PA, Sadowski J, Bartus K, Kapelak B, Walton A, Sievert H, Thambar S, Abraham WT, and Esler M.**

Catheter-based renal sympathetic denervation for resistant hypertension: a multicentre safety and proof-of-principle cohort study. *Lancet* 373: 1275-1281, 2009.

198. **Kumagai H, Suzuki H, Ryuzaki M, Matsukawa S, and Saruta T.** Baroreflex control of renal sympathetic nerve activity is potentiated at early phase of two-kidney, one-clip Goldblatt hypertension in conscious rabbits. *Circ Res* 67: 1309-1322, 1990.

199. **Kumar GK, Rai V, Sharma SD, Ramakrishnan DP, Peng YJ, Souvannakitti D, and Prabhakar NR.** Chronic intermittent hypoxia induces hypoxia-evoked catecholamine efflux in adult rat adrenal medulla via oxidative stress. *J Physiol* 575: 229-239, 2006.

200. **Kumar P, and Prabhakar NR.** Peripheral chemoreceptors: function and plasticity of the carotid body. *Compr Physiol* 2: 141-219, 2012.

201. **Kuo TB, Yuan ZF, Lin YS, Lin YN, Li WS, Yang CC, and Lai CJ.** Reactive oxygen species are the cause of the enhanced cardiorespiratory response induced by intermittent hypoxia in conscious rats. *Respir Physiol Neurobiol* 175: 70-79, 2011.

202. **Lai CJ, Yang CC, Hsu YY, Lin YN, and Kuo TB.** Enhanced sympathetic outflow and decreased baroreflex sensitivity are associated with intermittent hypoxia-induced systemic hypertension in conscious rats. *J Appl Physiol (1985)* 100: 1974-1982, 2006.

203. **Leacy JK, Zouboules SM, Mann CR, Peltonen JDB, Saran G, Nysten CE, Nysten HE, Brutsaert TD, O'Halloran KD, Sherpa MT, and Day TA.** Neurovascular Coupling Remains Intact During Incremental Ascent to High Altitude (4240 m) in Acclimatized Healthy Volunteers. *Front Physiol* 9: 1691, 2018.

204. **Leonard BL, Navakatikyan MA, and Malpas SC.** Differential regulation of the oscillations in sympathetic nerve activity and renal blood flow following volume expansion. *Auton Neurosci* 83: 19-28, 2000.

205. **Leong CL, Anderson WP, O'Connor PM, and Evans RG.** Evidence that renal arterial-venous oxygen shunting contributes to dynamic regulation of renal oxygenation. *Am J Physiol Renal Physiol* 292: F1726-1733, 2007.

206. **Lessard A, Coleman CG, and Pickel VM.** Chronic intermittent hypoxia reduces neurokinin-1 (NK(1)) receptor density in small dendrites of non-catecholaminergic neurons in mouse nucleus tractus solitarius. *Exp Neurol* 223: 634-644, 2010.

207. **Leuenberger UA, Brubaker D, Quraishi SA, Quraishi S, Hogeman CS, Imadojemu VA, and Gray KS.** Effects of intermittent hypoxia on sympathetic activity and blood pressure in humans. *Auton Neurosci* 121: 87-93, 2005.

208. **Li HB, Huo CJ, Su Q, Li X, Bai J, Zhu GQ, and Kang YM.** Exercise Training Attenuates Proinflammatory Cytokines, Oxidative Stress and Modulates Neurotransmitters in the Rostral Ventrolateral Medulla of Salt-Induced Hypertensive Rats. *Cell Physiol Biochem* 48: 1369-1381, 2018.

209. **Li J, and Wang DH.** Differential mechanisms mediating depressor and diuretic effects of anandamide. *J Hypertens* 24: 2271-2276, 2006.
210. **Li J, and Wang DH.** Increased GFR and renal excretory function by activation of TRPV1 in the isolated perfused kidney. *Pharmacol Res* 57: 239-246, 2008.
211. **Liedtke WB, and Heller S.** TRP Ion Channel Function in Sensory Transduction and Cellular Signaling Cascades. 2007.
212. **Liem DA, Verdouw PD, Ploeg H, Kazim S, and Duncker DJ.** Sites of action of adenosine in interorgan preconditioning of the heart. *Am J Physiol Heart Circ Physiol* 283: H29-37, 2002.
213. **Lim K, Burke SL, Moretti JL, and Head GA.** Differential activation of renal sympathetic burst amplitude and frequency during hypoxia, stress and baroreflexes with chronic angiotensin treatment. *Exp Physiol* 100: 1132-1144, 2015.
214. **Lim K, van den Buuse M, and Head GA.** Effect of Endothelin-1 on Baroreflexes and the Cardiovascular Action of Clonidine in Conscious Rabbits. *Front Physiol* 7: 321, 2016.
215. **Lin CH, Lurie RC, and Lyons OD.** Sleep Apnea and Chronic Kidney Disease: A State-of-the-Art Review. *Chest* 157: 673-685, 2020.
216. **Lin CS, Lee SH, Huang HS, Chen YS, and Ma MC.** H₂O₂ generated by NADPH oxidase 4 contributes to transient receptor potential vanilloid 1 channel-mediated mechanosensation in the rat kidney. *Am J Physiol Renal Physiol* 309: F369-376, 2015.
217. **Lin M, Liu R, Gozal D, Wead WB, Chapleau MW, Wurster R, and Cheng ZJ.** Chronic intermittent hypoxia impairs baroreflex control of heart rate but enhances heart rate responses to vagal efferent stimulation in anesthetized mice. *Am J Physiol Heart Circ Physiol* 293: H997-1006, 2007.
218. **Linley JE, Ooi L, Pettinger L, Kirton H, Boyle JP, Peers C, and Gamper N.** Reactive oxygen species are second messengers of neurokinin signaling in peripheral sensory neurons. *Proc Natl Acad Sci U S A* 109: E1578-1586, 2012.
219. **Loeppky JA, Icenogle MV, Maes D, Riboni K, Hinghofer-Szalkay H, and Roach RC.** Early fluid retention and severe acute mountain sickness. *J Appl Physiol* (1985) 98: 591-597, 2005.
220. **Lohmeier TE, Lohmeier JR, Haque A, and Hildebrandt DA.** Baroreflexes prevent neurally induced sodium retention in angiotensin hypertension. *Am J Physiol Regul Integr Comp Physiol* 279: R1437-1448, 2000.
221. **Loredo JS, Clausen JL, Nelesen RA, Ancoli-Israel S, Ziegler MG, and Dimsdale JE.** Obstructive sleep apnea and hypertension: are peripheral chemoreceptors involved? *Med Hypotheses* 56: 17-19, 2001.

222. **Lu S, Mattson DL, and Cowley AW.** Renal medullary captopril delivery lowers blood pressure in spontaneously hypertensive rats. *Hypertension* 23: 337-345, 1994.
223. **Lu W, Kang J, Hu K, Tang S, Zhou X, Xu L, Li Y, and Yu S.** The role of the Nox4-derived ROS-mediated RhoA/Rho kinase pathway in rat hypertension induced by chronic intermittent hypoxia. *Sleep Breath* 21: 667-677, 2017.
224. **Lu W, Kang J, Hu K, Tang S, Zhou X, Yu S, and Xu L.** Angiotensin-(1-7) relieved renal injury induced by chronic intermittent hypoxia in rats by reducing inflammation, oxidative stress and fibrosis. *Braz J Med Biol Res* 50: e5594, 2017.
225. **Lucking EF, O'Connor KM, Strain CR, Fouhy F, Bastiaanssen TFS, Burns DP, Golubeva AV, Stanton C, Clarke G, Cryan JF, and O'Halloran KD.** Chronic intermittent hypoxia disrupts cardiorespiratory homeostasis and gut microbiota composition in adult male guinea-pigs. *EBioMedicine* 2018.
226. **Lucking EF, O'Halloran KD, and Jones JF.** Increased cardiac output contributes to the development of chronic intermittent hypoxia-induced hypertension. *Exp Physiol* 99: 1312-1324, 2014.
227. **Lundin S, Ricksten SE, and Thorén P.** Renal sympathetic activity in spontaneously hypertensive rats and normotensive controls, as studied by three different methods. *Acta Physiol Scand* 120: 265-272, 1984.
228. **Lyons OD, Inami T, Perger E, Yadollahi A, Chan CT, and Bradley TD.** The effect of fluid overload on sleep apnoea severity in haemodialysis patients. *Eur Respir J* 49: 1601789, 2017.
229. **Ma MC, Huang HS, Wu MS, Chien CT, and Chen CF.** Impaired renal sensory responses after renal ischemia in the rat. *J Am Soc Nephrol* 13: 1872-1883, 2002.
230. **Madeddu P, Salis MB, and Emanuelli C.** Altered baroreflex control of heart rate in bradykinin B2-receptor knockout mice. *Immunopharmacology* 45: 21-27, 1999.
231. **Mamenko M, Zaika O, and Pochynyuk O.** Direct regulation of ENaC by bradykinin in the distal nephron. Implications for renal sodium handling. *Curr Opin Nephrol Hypertens* 23: 122-129, 2014.
232. **Mancia G, Grassi G, and Giannattasio C.** Cardiopulmonary receptor reflex in hypertension. *Am J Hypertens* 1: 249-255, 1988.
233. **Mancia G, Grassi G, Parati G, Pomidossi G, Saino A, Malaspina D, Gregorini L, and Zanchetti A.** Control of circulation by arterial baroreceptors and cardiopulmonary receptors in hypertension. *J Cardiovasc Pharmacol* 8 Suppl 5: S82-88, 1986.
234. **Mandadi S, Numazaki M, Tominaga M, Bhat MB, Armati PJ, and Roufogalis BD.** Activation of protein kinase C reverses capsaicin-induced calcium-dependent desensitization of TRPV1 ion channels. *Cell Calcium* 35: 471-478, 2004.

235. **Marcus NJ, Li YL, Bird CE, Schultz HD, and Morgan BJ.** Chronic intermittent hypoxia augments chemoreflex control of sympathetic activity: role of the angiotensin II type 1 receptor. *Respir Physiol Neurobiol* 171: 36-45, 2010.
236. **Marcus NJ, Philippi NR, Bird CE, Li YL, Schultz HD, and Morgan BJ.** Effect of AT1 receptor blockade on intermittent hypoxia-induced endothelial dysfunction. *Respir Physiol Neurobiol* 183: 67-74, 2012.
237. **Marfurt CF, and Echtenkamp SF.** Sensory innervation of the rat kidney and ureter as revealed by the anterograde transport of wheat germ agglutinin-horseradish peroxidase (WGA-HRP) from dorsal root ganglia. *J Comp Neurol* 311: 389-404, 1991.
238. **Martinez-Maldonado M, Eknayan G, and Suki WN.** Influence of volume expansion on renal diluting capacity in the rat. *Clin Sci Mol Med* 46: 331-345, 1974.
239. **Mattson DL, and Cowley AW.** Kinin actions on renal papillary blood flow and sodium excretion. *Hypertension* 21: 961-965, 1993.
240. **Mayorov DN.** Brain superoxide as a key regulator of the cardiovascular response to emotional stress in rabbits. *Exp Physiol* 92: 471-479, 2007.
241. **McBryde FD, Liu B, Kasparov S, and Paton JF.** Chronic knockdown of nNOS in the paraventricular nucleus (PVN) produces persistent increases in arterial pressure and renal sympathetic nerve activity (RSNA) in the rat. *The FASEB Journal* 25: 1078.1078-1078.1078, 2011.
242. **McBryde FD, Malpas SC, Guild SJ, and Barrett CJ.** A high-salt diet does not influence renal sympathetic nerve activity: a direct telemetric investigation. *Am J Physiol Regul Integr Comp Physiol* 297: R396-402, 2009.
243. **Miki K, Yoshimoto M, and Tanimizu M.** Acute shifts of baroreflex control of renal sympathetic nerve activity induced by treadmill exercise in rats. *J Physiol* 548: 313-322, 2003.
244. **Milia AF, Gross V, Plehm R, De Silva JA, Bader M, and Luft FC.** Normal blood pressure and renal function in mice lacking the bradykinin B(2) receptor. *Hypertension* 37: 1473-1479, 2001.
245. **Minisi AJ.** Vagal cardiopulmonary reflexes after total cardiac deafferentation. *Circulation* 98: 2615-2620, 1998.
246. **Moraes DJ, Bonagamba LG, da Silva MP, Mecawi AS, Antunes-Rodrigues J, and Machado BH.** Respiratory Network Enhances the Sympathoinhibitory Component of Baroreflex of Rats Submitted to Chronic Intermittent Hypoxia. *Hypertension* 68: 1021-1030, 2016.
247. **Mulder J, Hökfelt T, Knuepfer MM, and Kopp UC.** Renal sensory and sympathetic nerves reinnervate the kidney in a similar time-dependent fashion after renal denervation in rats. *Am J Physiol Regul Integr Comp Physiol* 304: R675-682, 2013.

248. **Nagata K, Osada N, Shimazaki M, Kida K, Yoneyama K, Tsuchiya A, Yasuda T, and Kimura K.** Diurnal blood pressure variation in patients with sleep apnea syndrome. *Hypertens Res* 31: 185-191, 2008.
249. **Nanduri J, Vaddi DR, Khan SA, Wang N, Makerenko V, and Prabhakar NR.** Xanthine oxidase mediates hypoxia-inducible factor-2 α degradation by intermittent hypoxia. *PLoS One* 8: e75838, 2013.
250. **Narkiewicz K, Pesek CA, Kato M, Phillips BG, Davison DE, and Somers VK.** Baroreflex control of sympathetic nerve activity and heart rate in obstructive sleep apnea. *Hypertension* 32: 1039-1043, 1998.
251. **Narkiewicz K, van de Borne PJ, Montano N, Dyken ME, Phillips BG, and Somers VK.** Contribution of tonic chemoreflex activation to sympathetic activity and blood pressure in patients with obstructive sleep apnea. *Circulation* 97: 943-945, 1998.
252. **Neylon M, Marshall J, and Johns EJ.** The role of the renin-angiotensin system in the renal response to moderate hypoxia in the rat. *J Physiol* 491 (Pt 2): 479-488, 1996.
253. **Neylon M, Marshall JM, and Johns EJ.** The effects of chronic hypoxia on renal function in the rat. *J Physiol* 501 (Pt 1): 243-250, 1997.
254. **Neylon M, Marshall JM, and Johns EJ.** The effects of systemic hypoxia on renal function in the anaesthetized rat. *J Physiol* 487 (Pt 2): 497-511, 1995.
255. **Nisbet RE, Graves AS, Kleinhenz DJ, Rupnow HL, Reed AL, Fan TH, Mitchell PO, Sutliff RL, and Hart CM.** The role of NADPH oxidase in chronic intermittent hypoxia-induced pulmonary hypertension in mice. *Am J Respir Cell Mol Biol* 40: 601-609, 2009.
256. **Nishi EE, Bergamaschi CT, and Campos RR.** The crosstalk between the kidney and the central nervous system: the role of renal nerves in blood pressure regulation. *Exp Physiol* 100: 479-484, 2015.
257. **O'Connor KM, Lucking EF, Bastiaanssen TFS, Peterson VL, Crispie F, Cotter PD, Clarke G, Cryan JF, and O'Halloran KD.** Prebiotic administration modulates gut microbiota and faecal short-chain fatty acid concentrations but does not prevent chronic intermittent hypoxia-induced apnoea and hypertension in adult rats. *EBioMedicine* 59: 102968, 2020.
258. **O'Neill J, Jasione G, Drummond SE, Brett O, Lucking EF, Abdulla MA, and O'Halloran KD.** Renal cortical oxygen tension is decreased following exposure to long-term but not short-term intermittent hypoxia in the rat. *Am J Physiol Renal Physiol* 316: F635-F645, 2019.
259. **O'Sullivan JB, and Harrap SB.** Resetting blood pressure in spontaneously hypertensive rats. The role of bradykinin. *Hypertension* 25: 162-165, 1995.
260. **Oga Y, Saku K, Nishikawa T, Kishi T, Tobushi T, Hosokawa K, Tohyama T, Sakamoto T, Sunagawa K, and Tsutsui H.** The impact of volume loading-

induced low pressure baroreflex activation on arterial baroreflex-controlled sympathetic arterial pressure regulation in normal rats. *Physiol Rep* 6: e13887, 2018.

261. **Ong J, Kinsman BJ, Sved AF, Rush BM, Tan RJ, Carattino MD, and Stocker SD.** Renal sensory nerves increase sympathetic nerve activity and blood pressure in 2-kidney 1-clip hypertensive mice. *J Neurophysiol* 122: 358-367, 2019.

262. **Ow CPC, Ngo JP, Ullah MM, Hilliard LuM, and Evan RG.** Renal hypoxia in kidney disease: Cause or consequence? *Acta Physiologica* 222: e12999, 2017.

263. **Oyarce MP, and Iturriaga R.** Contribution of Oxidative Stress and Inflammation to the Neurogenic Hypertension Induced by Intermittent Hypoxia. *Front Physiol* 9: 893, 2018.

264. **Palm F, Cederberg J, Hansell P, Liss P, and Carlsson PO.** Reactive oxygen species cause diabetes-induced decrease in renal oxygen tension. *Diabetologia* 46: 1153-1160, 2003.

265. **Parikh NA, Katsetos CD, Ashraf QM, Haider SH, Legido A, Delivoria-Papadopoulos M, and Mishra OP.** Hypoxia-induced caspase-3 activation and DNA fragmentation in cortical neurons of newborn piglets: role of nitric oxide. *Neurochem Res* 28: 1351-1357, 2003.

266. **Parpaite T, Cardouat G, Mauroux M, Gillibert-Duplantier J, Robillard P, Quignard JF, Marthan R, Savineau JP, and Ducret T.** Effect of hypoxia on TRPV1 and TRPV4 channels in rat pulmonary arterial smooth muscle cells. *Pflugers Arch* 468: 111-130, 2016.

267. **Patel KP, Xu B, Liu X, Sharma NM, and Zheng H.** Renal Denervation Improves Exaggerated Sympathoexcitation in Rats With Heart Failure: A Role for Neuronal Nitric Oxide Synthase in the Paraventricular Nucleus. *Hypertension* 68: 175-184, 2016.

268. **Patinha D, Pijacka W, Paton JFR, and Koeners MP.** Cooperative Oxygen Sensing by the Kidney and Carotid Body in Blood Pressure Control. *Front Physiol* 8: 752, 2017.

269. **Peng Y, and Prabhakar N.** Role of carotid bodies in chronic intermittent hypoxia-evoked augmented LTF of phrenic nerve activity. 22: 960.967-960.967, 2008.

270. **Peng YJ, Nanduri J, Yuan G, Wang N, Deneris E, Pendyala S, Natarajan V, Kumar GK, and Prabhakar NR.** NADPH oxidase is required for the sensory plasticity of the carotid body by chronic intermittent hypoxia. *J Neurosci* 29: 4903-4910, 2009.

271. **Peng YJ, Overholt JL, Kline D, Kumar GK, and Prabhakar NR.** Induction of sensory long-term facilitation in the carotid body by intermittent hypoxia: implications for recurrent apneas. *Proc Natl Acad Sci U S A* 100: 10073-10078, 2003.

272. **Peng YJ, and Prabhakar NR.** Effect of two paradigms of chronic intermittent hypoxia on carotid body sensory activity. *J Appl Physiol* (1985) 96: 1236-1242; discussion 1196, 2004.
273. **Peng YJ, Yuan G, Khan S, Nanduri J, Makarenko VV, Reddy VD, Vasavda C, Kumar GK, Semenza GL, and Prabhakar NR.** Regulation of hypoxia-inducible factor- α isoforms and redox state by carotid body neural activity in rats. *J Physiol* 592: 3841-3858, 2014.
274. **Peng YJ, Yuan G, Ramakrishnan D, Sharma SD, Bosch-Marce M, Kumar GK, Semenza GL, and Prabhakar NR.** Heterozygous HIF-1 α deficiency impairs carotid body-mediated systemic responses and reactive oxygen species generation in mice exposed to intermittent hypoxia. *J Physiol* 577: 705-716, 2006.
275. **Penna C, Mancardi D, Rastaldo R, Losano G, and Pagliaro P.** Intermittent activation of bradykinin B2 receptors and mitochondrial KATP channels trigger cardiac postconditioning through redox signaling. *Cardiovascular Research* 75: 2007.
276. **Petho G, and Reeh PW.** Sensory and signaling mechanisms of bradykinin, eicosanoids, platelet-activating factor, and nitric oxide in peripheral nociceptors. *Physiol Rev* 92: 1699-1775, 2012.
277. **Poonit ND, Zhang YC, Ye CY, Cai HL, Yu CY, Li T, and Cai XH.** Chronic intermittent hypoxia exposure induces kidney injury in growing rats. *Sleep Breath* 22: 453-461, 2017.
278. **Prabha K, Balan KV, Martin RJ, Lamanna JC, Haxhiu MA, and Dick TE.** Chronic intermittent hypoxia-induced augmented cardiorespiratory outflow mediated by vasopressin-V_{1A} receptor signaling in the medulla. *Adv Exp Med Biol* 701: 319-325, 2011.
279. **Prabhakar NR.** Carotid body chemoreflex: a driver of autonomic abnormalities in sleep apnoea. *Exp Physiol* 101: 975-985, 2016.
280. **Prabhakar NR, Dick TE, Nanduri J, and Kumar GK.** Systemic, cellular and molecular analysis of chemoreflex-mediated sympathoexcitation by chronic intermittent hypoxia. *Exp Physiol* 92: 39-44, 2007.
281. **Prabhakar NR, and Kumar GK.** Mechanisms of sympathetic activation and blood pressure elevation by intermittent hypoxia. *Respir Physiol Neurobiol* 174: 156-161, 2010.
282. **Prabhakar NR, Kumar GK, Nanduri J, and Semenza GL.** ROS signaling in systemic and cellular responses to chronic intermittent hypoxia. *Antioxid Redox Signal* 9: 1397-1403, 2007.
283. **Prabhakar NR, Kumar GK, and Peng YJ.** Sympatho-adrenal activation by chronic intermittent hypoxia. *J Appl Physiol* (1985) 113: 1304-1310, 2012.
284. **Pratt-Ubunama MN, Nishizaka MK, Boedefeld RL, Cofield SS, Harding SM, and Calhoun DA.** Plasma aldosterone is related to severity of obstructive sleep apnea in subjects with resistant hypertension. *Chest* 131: 453-459, 2007.

285. **Puckrin R, Iqbal S, Zidulka A, Vasilevsky M, and Barre P.** Renoprotective effects of continuous positive airway pressure in chronic kidney disease patients with sleep apnea. *Int Urol Nephrol* 47: 1839-1845, 2015.
286. **Qin L, Du Y, Ding H, Haque A, Hicks J, Pedroza C, and Mohan C.** Bradykinin 1 receptor blockade subdues systemic autoimmunity, renal inflammation, and blood pressure in murine lupus nephritis. *Arthritis Res Ther* 21: 12, 2019.
287. **Qiu Y, Zheng F, Ye C, Chen AD, Wang JJ, Chen Q, Li YH, Kang YM, and Zhu GQ.** Angiotensin Type 1 Receptors and Superoxide Anion Production in Hypothalamic Paraventricular Nucleus Contribute to Capsaicin-Induced Excitatory Renal Reflex and Sympathetic Activation. *Neurosci Bull* 36: 463-474, 2020.
288. **Querido D, and Isaacson LC.** Blood-volume expansion in the rat: natriuresis accompanied by a fall in filtration fraction. *Clin Sci (Lond)* 60: 283-293, 1981.
289. **Raff H, Jankowski BM, Bruder ED, Engeland WC, and Oaks MK.** The effect of hypoxia from birth on the regulation of aldosterone in the 7-day-old rat: plasma hormones, steroidogenesis in vitro, and steroidogenic enzyme messenger ribonucleic acid. *Endocrinology* 140: 3147-3153, 1999.
290. **Ralevic V, Kendall DA, Randall MD, Zygmunt PM, Movahed P, and Högestätt ED.** Vanilloid receptors on capsaicin-sensitive sensory nerves mediate relaxation to methanandamide in the rat isolated mesenteric arterial bed and small mesenteric arteries. *Br J Pharmacol* 130: 1483-1488, 2000.
291. **Ramchandra R, and Barrett CJ.** Regulation of the renal sympathetic nerves in heart failure. *Front Physiol* 6: 238, 2015.
292. **Ramchandra R, Barrett CJ, Guild SJ, and Malpas SC.** Evidence of differential control of renal and lumbar sympathetic nerve activity in conscious rabbits. *Am J Physiol Regul Integr Comp Physiol* 290: R701-708, 2006.
293. **Ramchandra R, Hood SG, Frithiof R, and May CN.** Discharge properties of cardiac and renal sympathetic nerves and their impaired responses to changes in blood volume in heart failure. *Am J Physiol Regul Integr Comp Physiol* 297: R665-674, 2009.
294. **Ramchandra R, Hood SG, Frithiof R, McKinley MJ, and May CN.** The role of the paraventricular nucleus of the hypothalamus in the regulation of cardiac and renal sympathetic nerve activity in conscious normal and heart failure sheep. *J Physiol* 591: 93-107, 2013.
295. **Rankin AJ, Ashton N, and Swift FV.** The reflex effect of changes in renal perfusion on hindlimb vascular resistance in anaesthetized rabbits. *Pflugers Arch* 421: 585-590, 1992.
296. **Raven PB, Fadel PJ, and Ogoh S.** Arterial baroreflex resetting during exercise: a current perspective. *Exp Physiol* 91: 37-49, 2006.

297. **Recordati GM, Moss NG, Genovesi S, and Rogenes PR.** Renal receptors in the rat sensitive to chemical alterations of their environment. *Circ Res* 46: 395-405, 1980.
298. **Recordati GM, Moss NG, and Waselkov L.** Renal chemoreceptors in the rat. *Circ Res* 43: 534-543, 1978.
299. **Ren Y, Garvin J, and Carretero OA.** Mechanism involved in bradykinin-induced efferent arteriole dilation. *Kidney Int* 62: 544-549, 2002.
300. **Resta O, Guido P, Rana L, Procacci V, Scarpelli F, and Picca V.** Depressed baroreceptor reflex in patients with obstructive sleep apnea (OSA). *Boll Soc Ital Biol Sper* 72: 247-254, 1996.
301. **Ribon-Demars A, Pialoux V, Boreau A, Marcouiller F, Larivière R, Bairam A, and Joseph V.** Protective roles of estradiol against vascular oxidative stress in ovariectomized female rats exposed to normoxia or intermittent hypoxia. *Acta Physiol (Oxf)* 225: e13159, 2018.
302. **Ricketts JH, and Head GA.** A five-parameter logistic equation for investigating asymmetry of curvature in baroreflex studies. *Am J Physiol* 277: R441-454, 1999.
303. **Riggs JL, Pace CE, Ward HH, Gonzalez Bosc LV, Rios L, Barrera A, and Kanagy NL.** Intermittent hypoxia exacerbates increased blood pressure in rats with chronic kidney disease. *Am J Physiol Renal Physiol* 315: F927-F941, 2018.
304. **Ristoiu V, Shibasaki K, Uchida K, Zhou Y, Ton BH, Flonta ML, and Tominaga M.** Hypoxia-induced sensitization of transient receptor potential vanilloid 1 involves activation of hypoxia-inducible factor-1 alpha and PKC. *Pain* 152: 936-945, 2011.
305. **Rodriguez JA, Vio CP, Pedraza PL, McGiff JC, and Ferreri NR.** Bradykinin regulates cyclooxygenase-2 in rat renal thick ascending limb cells. *Hypertension* 44: 230-235, 2004.
306. **Roman RJ, Cowley AW, Garcia-Estañ J, and Lombard JH.** Pressure-diuresis in volume-expanded rats. Cortical and medullary hemodynamics. *Hypertension* 12: 168-176, 1988.
307. **Roy A, Farnham MMJ, Derakhshan F, Pilowsky PM, and Wilson RJA.** Acute intermittent hypoxia with concurrent hypercapnia evokes P2X and TRPV1 receptor-dependent sensory long-term facilitation in naïve carotid bodies. *J Physiol* 2017.
308. **Sakata M, Greenwald JE, and Needleman P.** Paradoxical relationship between atriopeptin plasma levels and diuresis-natriuresis induced by acute volume expansion. *Proc Natl Acad Sci U S A* 85: 3155-3159, 1988.
309. **Schanstra JP, Alric C, Marin-Castaño ME, Girolami JP, and Bascands JL.** Renal bradykinin receptors: localisation, transduction pathways and molecular basis for a possible pathological role (review). *Int J Mol Med* 3: 185-191, 1999.

310. **Schanstra JP, Neau E, Drogoz P, Arevalo Gomez MA, Lopez Novoa JM, Calise D, Pecher C, Bader M, Girolami JP, and Bascands JL.** In vivo bradykinin B2 receptor activation reduces renal fibrosis. *J Clin Invest* 110: 371-379, 2002.
311. **Schmidt M, Ledderhos C, and Honig A.** Kidney function during arterial chemoreceptor stimulation. I. Influence of unilateral renal nerve section, bilateral cervical vagotomy, constant artificial ventilation, and carotid body chemoreceptor inactivation. *Biomed Biochim Acta* 44: 695-709, 1985.
312. **Schmidt M, Wedler B, Zingler C, Ledderhos C, and Honig A.** Kidney function during arterial chemoreceptor stimulation. II. Suppression of plasma aldosterone concentration due to hypoxic-hypercapnic perfusion of the carotid bodies in anaesthetized cats. *Biomed Biochim Acta* 44: 711-722, 1985.
313. **Segawa Y, Hashimoto H, Maruyama S, Shintani M, Ohno H, Nakai Y, Osera T, and Kurihara N.** Dietary capsaicin-mediated attenuation of hypertension in a rat model of renovascular hypertension. *Clin Exp Hypertens* 42: 352-359, 2020.
314. **Selkurt EE.** Influence of hypoxia on renal circulation and on excretion of electrolytes and water. *American Journal of Physiology* 172: 700-708, 1953.
315. **SELKURT EE.** Sodium excretion by the mammalian kidney. *Physiol Rev* 34: 287-333, 1954.
316. **Semenza GL, and Prabhakar NR.** The role of hypoxia-inducible factors in oxygen sensing by the carotid body. *Adv Exp Med Biol* 758: 1-5, 2012.
317. **Shah NA, Yaggi HK, Concato J, and Mohsenin V.** Obstructive sleep apnea as a risk factor for coronary events or cardiovascular death. *Sleep Breath* 14: 131-136, 2010.
318. **Sharpe AL, Calderon AS, Andrade MA, Cunningham JT, Mifflin SW, and Toney GM.** Chronic intermittent hypoxia increases sympathetic control of blood pressure: role of neuronal activity in the hypothalamic paraventricular nucleus. *Am J Physiol Heart Circ Physiol* 305: H1772-1780, 2013.
319. **Shell B, Farmer GE, Nedungadi TP, Wang LA, Marciante AB, Snyder B, Cunningham RL, and Cunningham JT.** Angiotensin type 1a receptors in the median preoptic nucleus support intermittent hypoxia-induced hypertension. *Am J Physiol Regul Integr Comp Physiol* 316: R651-R665, 2019.
320. **Shell B, Faulk K, and Cunningham JT.** Neural Control of Blood Pressure in Chronic Intermittent Hypoxia. *Curr Hypertens Rep* 18: 19, 2016.
321. **Shi P, Diez-Freire C, Jun JY, Qi Y, Katovich MJ, Li Q, Sriramula S, Francis J, Sumners C, and Raizada MK.** Brain microglial cytokines in neurogenic hypertension. *Hypertension* 56: 297-303, 2010.
322. **Shimokawa A, Kunitake T, Takasaki M, and Kannan H.** Differential effects of anesthetics on sympathetic nerve activity and arterial baroreceptor reflex in chronically instrumented rats. *J Auton Nerv Syst* 72: 46-54, 1998.

323. **Shimoura CG, Andrade MA, and Toney GM.** Central AT1 receptor signaling by circulating angiotensin II is permissive to acute intermittent hypoxia-induced sympathetic neuroplasticity. *J Appl Physiol* (1985) 128: 1329-1337, 2020.
324. **Silva AQ, and Schreihöfer AM.** Altered sympathetic reflexes and vascular reactivity in rats after exposure to chronic intermittent hypoxia. *J Physiol* 589: 1463-1476, 2011.
325. **Simon JK, Kasting NW, and Ciriello J.** Afferent renal nerve effects on plasma vasopressin and oxytocin in conscious rats. *Am J Physiol* 256: R1240-1244, 1989.
326. **Simone S, Rascio F, Castellano G, Divella C, Chieti A, Ditunno P, Battaglia M, Crovace A, Staffieri F, Oortwijn B, Stallone G, Gesualdo L, Pertosa G, and Grandaliano G.** Complement-dependent NADPH oxidase enzyme activation in renal ischemia/reperfusion injury. *Free Radic Biol Med* 74: 263-273, 2014.
327. **Singh P, Ricksten SE, Bragadottir G, Redfors B, and Nordquist L.** Renal oxygenation and haemodynamics in acute kidney injury and chronic kidney disease. *Clin Exp Pharmacol Physiol* 40: 138-147, 2013.
328. **Sleight P.** Arterial baroreflexes can determine long-term blood pressure. Baroreceptors and hypertension: time for a re-think? *Exp Physiol* 89: 337-341, 2004.
329. **Smits JF, and Brody MJ.** Activation of afferent renal nerves by intrarenal bradykinin in conscious rats. *Am J Physiol* 247: R1003-1008, 1984.
330. **Snyder B, Shell B, Cunningham JT, and Cunningham RL.** Chronic intermittent hypoxia induces oxidative stress and inflammation in brain regions associated with early-stage neurodegeneration. *Physiol Rep* 5: 2017.
331. **Sonnenberg H.** The renal response to blood volume expansion in the rat: proximal tubular function and urinary excretion. *Can J Physiol Pharmacol* 49: 525-535, 1971.
332. **Soukhova-O'Hare GK, Roberts AM, and Gozal D.** Impaired control of renal sympathetic nerve activity following neonatal intermittent hypoxia in rats. *Neurosci Lett* 399: 181-185, 2006.
333. **Souza DG, Lomez ES, Pinho V, Pesquero JB, Bader M, Pesquero JL, and Teixeira MM.** Role of bradykinin B2 and B1 receptors in the local, remote, and systemic inflammatory responses that follow intestinal ischemia and reperfusion injury. *J Immunol* 172: 2542-2548, 2004.
334. **Spielman WS, and Thompson CI.** A proposed role for adenosine in the regulation of renal hemodynamics and renin release. *Am J Physiol* 242: F423-435, 1982.
335. **Sriramula S.** Kinin B1 receptor: A target for neuroinflammation in hypertension. *Pharmacol Res* 155: 104715, 2020.

336. **Sriramula S, Haque M, Majid DS, and Francis J.** Involvement of tumor necrosis factor- α in angiotensin II-mediated effects on salt appetite, hypertension, and cardiac hypertrophy. *Hypertension* 51: 1345-1351, 2008.
337. **Steinhoff MS, von Mentzer B, Geppetti P, Pothoulakis C, and Bunnett NW.** Tachykinins and their receptors: contributions to physiological control and the mechanisms of disease. *Physiol Rev* 94: 265-301, 2014.
338. **Stella A, and Zanchetti A.** Functional role of renal afferents. *Physiol Rev* 71: 659-682, 1991.
339. **Steranka LR, Manning DC, DeHaas CJ, Ferkany JW, Borosky SA, Connor JR, Vavrek RJ, Stewart JM, and Snyder SH.** Bradykinin as a pain mediator: receptors are localized to sensory neurons, and antagonists have analgesic actions. *Proc Natl Acad Sci U S A* 85: 3245-3249, 1988.
340. **Sugiura T, Tominaga M, Katsuya H, and Mizumura K.** Bradykinin lowers the threshold temperature for heat activation of vanilloid receptor 1. *J Neurophysiol* 88: 544-548, 2002.
341. **Sun H, Li DP, Chen SR, Hittelman WN, and Pan HL.** Sensing of blood pressure increase by transient receptor potential vanilloid 1 receptors on baroreceptors. *J Pharmacol Exp Ther* 331: 851-859, 2009.
342. **Sun W, Yin X, Wang Y, Tan Y, Cai L, Wang B, Cai J, and Fu Y.** Intermittent hypoxia-induced renal antioxidants and oxidative damage in male mice: hormetic dose response. *Dose Response* 11: 385-400, 2012.
343. **Sun Z, Han J, Zhao W, Zhang Y, Wang S, Ye L, Liu T, and Zheng L.** TRPV1 activation exacerbates hypoxia/reoxygenation-induced apoptosis in H9C2 cells via calcium overload and mitochondrial dysfunction. *Int J Mol Sci* 15: 18362-18380, 2014.
344. **Swenson ER, Duncan TB, Goldberg SV, Ramirez G, Ahmad S, and Schoene RB.** Diuretic effect of acute hypoxia in humans: relationship to hypoxic ventilatory responsiveness and renal hormones. *J Appl Physiol (1985)* 78: 377-383, 1995.
345. **Tahawi Z, Orolinova N, Joshua IG, Bader M, and Fletcher EC.** Altered vascular reactivity in arterioles of chronic intermittent hypoxic rats. *J Appl Physiol (1985)* 90: 2007-2013, 2001.
346. **Takahashi H, and Buñag RD.** Centrally induced cardiovascular and sympathetic nerve responses to bradykinin in rats. *J Pharmacol Exp Ther* 216: 192-197, 1981.
347. **Tang M, Li X, Liu P, Wang J, He F, and Zhu X.** Bradykinin B2 receptors play a neuroprotective role in Hypoxia/reoxygenation injury related to pyroptosis pathway. *Curr Neurovasc Res* 15: 138-144, 2018.
348. **Tang M, Liu P, Li X, Wang JW, Zhu XC, and He FP.** Protective action of B1R antagonist against cerebral ischemia-reperfusion injury through suppressing

miR-200c expression of Microglia-derived microvesicles. *Neurol Res* 39: 612-620, 2017.

349. **Taylor NE, Glocka P, Liang M, and Cowley AW.** NADPH oxidase in the renal medulla causes oxidative stress and contributes to salt-sensitive hypertension in Dahl S rats. *Hypertension* 47: 692-698, 2006.

350. **Thrasher TN.** Baroreceptors and the long-term control of blood pressure. *Exp Physiol* 89: 331-335, 2004.

351. **Thrasher TN.** Unloading arterial baroreceptors causes neurogenic hypertension. *Am J Physiol Regul Integr Comp Physiol* 282: R1044-1053, 2002.

352. **Tirapelli CR, Bonaventura D, Tirapelli LF, and de Oliveira AM.** Mechanisms underlying the vascular actions of endothelin 1, angiotensin II and bradykinin in the rat carotid. *Pharmacology* 84: 111-126, 2009.

353. **Tornel J, Madrid MI, García-Salom M, Wirth KJ, and Fenoy FJ.** Role of kinins in the control of renal papillary blood flow, pressure natriuresis, and arterial pressure. *Circ Res* 86: 589-595, 2000.

354. **Tromp TR, Mahesh D, Joles JA, and Ramchandra R.** Direct Recording of Cardiac and Renal Sympathetic Nerve Activity Shows Differential Control in Renovascular Hypertension. *Hypertension* 71: 1108-1116, 2018.

355. **Twohey SC, Kious KW, Keomanivong FE, Neidermann SE, Dirkman JJ, and Marcus NJ.** Chronic Intermittent Hypoxia is Associated with Sustained Reduction in Renal Blood Flow and Downregulation of Renal KLF2. *FASEB* 33: 2019.

356. **Ueda M, Nomura G, Shibata H, Nishida H, Moriyama A, Kumagai E, and Toshima H.** Assessment of cardiopulmonary baroreflex function in hypertensive and normotensive subjects with or without hypertensive relatives. *Clin Exp Pharmacol Physiol Suppl* 15: 89-92, 1989.

357. **Uggere TA, Abreu GR, Sampaio KN, Cabral AM, and Bissoli NS.** The cardiopulmonary reflexes of spontaneously hypertensive rats are normalized after regression of left ventricular hypertrophy and hypertension. *Braz J Med Biol Res* 33: 589-594, 2000.

358. **Veelken R, Hilgers KF, Porst M, Krause H, Hartner A, and Schmieder RE.** Effects of sympathetic nerves and angiotensin II on renal sodium and water handling in rats with common bile duct ligation. *Am J Physiol Renal Physiol* 288: F1267-1275, 2005.

359. **Velasquez MT.** Chronic Renal Disease. In: *Chronic Renal Disease*, edited by Kimmel PL, and Rosenberg ME Academic Press, 2015, p. 634-645.

360. **Vemula P, Gautam B, Abela GS, and Wang DH.** Myocardial ischemia/reperfusion injury: potential of TRPV1 agonists as cardioprotective agents. *Cardiovasc Hematol Disord Drug Targets* 14: 71-78, 2014.

361. **Veress AT, and Pearce JW.** Effect of vagotomy on the renal response to blood volume expansion in the rat. *Can J Physiol Pharmacol* 50: 463-466, 1972.
362. **Vio CP, Salas D, Cespedes C, Diaz-Elizondo J, Mendez N, Alcayaga J, and Iturriaga R.** Imbalance in Renal Vasoactive Enzymes Induced by Mild Hypoxia: Angiotensin-Converting Enzyme Increases While Neutral Endopeptidase Decreases. *Front Physiol* 9: 1791, 2018.
363. **Vitela M, Herrera-Rosales M, Haywood JR, and Mifflin SW.** Baroreflex regulation of renal sympathetic nerve activity and heart rate in renal wrap hypertensive rats. *Am J Physiol Regul Integr Comp Physiol* 288: R856-862, 2005.
364. **Wainford R, and Frame A.** The role of the mechanosensitive renal sensory afferent nerve sympathoinhibitory reno-renal reflex in sympathetic outflow, natriuresis, and blood pressure regulation. *FASEB J* 31: 718.718-718.718., 2017.
365. **Walker BR.** Diuretic response to acute hypoxia in the conscious dog. *Am J Physiol* 243: F440-446, 1982.
366. **Walker BR, and Brizzee BL.** Renal vascular response to combined hypoxia and hypercapnia in conscious rats. *Am J Physiol* 254: R552-558, 1988.
367. **Wang PH, Campanholle G, Cenedeze MA, Feitoza CQ, Gonçalves GM, Landgraf RG, Jancar S, Pesquero JB, Pacheco-Silva A, and Câmara NO.** Bradykinin [corrected] B1 receptor antagonism is beneficial in renal ischemia-reperfusion injury. *PLoS One* 3: e3050, 2008.
368. **Wang Y, Babánková D, Huang J, Swain GM, and Wang DH.** Deletion of transient receptor potential vanilloid type 1 receptors exaggerates renal damage in deoxycorticosterone acetate-salt hypertension. *Hypertension* 52: 264-270, 2008.
369. **Wang Y, and Wang DH.** A novel mechanism contributing to development of Dahl salt-sensitive hypertension: role of the transient receptor potential vanilloid type 1. *Hypertension* 47: 609-614, 2006.
370. **Wang Y, and Wang DH.** Role of substance P in renal injury during DOCA-salt hypertension. *Endocrinology* 153: 5972-5979, 2012.
371. **Watanabe Y, Dohi S, Iida H, and Ishiyama T.** The effects of bupivacaine and ropivacaine on baroreflex sensitivity with or without respiratory acidosis and alkalosis in rats. *Anesth Analg* 84: 398-404, 1997.
372. **Weiss ML, and Chowdhury SI.** The renal afferent pathways in the rat: a pseudorabies virus study. *Brain Res* 812: 227-241, 1998.
373. **Welch WJ.** Intrarenal oxygen and hypertension. *Clin Exp Pharmacol Physiol* 33: 1002-1005, 2006.
374. **Widdop RE, Verberne AJ, Jarrott B, and Louis WJ.** Impaired arterial baroreceptor reflex and cardiopulmonary vagal reflex in conscious spontaneously hypertensive rats. *J Hypertens* 8: 269-275, 1990.

375. **Williams R, Lemaire P, Lewis P, McDonald FB, Lucking E, Hogan S, Sheehan D, Healy V, and O'Halloran KD.** Chronic intermittent hypoxia increases rat sternohyoid muscle NADPH oxidase expression with attendant modest oxidative stress. *Front Physiol* 6: 15, 2015.
376. **Witkowski A, Prejbisz A, Florczak E, Kądziela J, Śliwiński P, Bieleń P, Michalowska I, Kabat M, Warchol E, Januszewicz M, Narkiewicz K, Somers VK, Sobotka PA, and Januszewicz A.** Effects of renal sympathetic denervation on blood pressure, sleep apnea course, and glycemic control in patients with resistant hypertension and sleep apnea. *Hypertension* 58: 559-565, 2011.
377. **Wixson SK, White WJ, Hughes HC, Lang CM, and Marshall WK.** The effects of pentobarbital, fentanyl-droperidol, ketamine-xylazine and ketamine-diazepam on arterial blood pH, blood gases, mean arterial blood pressure and heart rate in adult male rats. *Lab Anim Sci* 37: 736-742, 1987.
378. **Wong PC, Guo J, and Zhang A.** The renal and cardiovascular effects of natriuretic peptides. *Adv Physiol Educ* 41: 179-185, 2017.
379. **Wongmekiat O, and Johns E.** Contribution of endothelial nitric oxide synthase in the blunted renal responses to volume expansion in diabetic rats. *Exp Physiol* 86: 481-488, 2001.
380. **Wu H, Zhou S, Kong L, Chen J, Feng W, Cai J, Miao L, and Tan Y.** Metallothionein deletion exacerbates intermittent hypoxia-induced renal injury in mice. *Toxicol Lett* 232: 340-348, 2015.
381. **Wu X, Chang SC, Jin J, Gu W, and Li S.** NLRP3 inflammasome mediates chronic intermittent hypoxia-induced renal injury implication of the microRNA-155/FOXO3a signaling pathway. *J Cell Physiol* 233: 9404-9415, 2018.
382. **Wu X, Gu W, Lu H, Liu C, Yu B, Xu H, Tang Y, Li S, Zhou J, and Shao C.** Soluble Receptor for Advanced Glycation End Product Ameliorates Chronic Intermittent Hypoxia Induced Renal Injury, Inflammation, and Apoptosis via P38/JNK Signaling Pathways. *Oxid Med Cell Longev* 2016: 1015390, 2016.
383. **Wyss JM, Aboukarsh N, and Oparil S.** Sensory denervation of the kidney attenuates renovascular hypertension in the rat. *Am J Physiol* 250: H82-86, 1986.
384. **Xiang YH, Su XL, Hu CP, Luo YQ, and He RX.** [A study of the related pathways of oxidative stress in chronic intermittent hypoxia rats and the effect of N-acetylcysteine]. *Zhonghua Jie He He Hu Xi Za Zhi* 33: 912-916, 2010.
385. **Xie C, Sachs JR, and Wang DH.** Interdependent regulation of afferent renal nerve activity and renal function: role of transient receptor potential vanilloid type 1, neurokinin 1, and calcitonin gene-related peptide receptors. *J Pharmacol Exp Ther* 325: 751-757, 2008.
386. **Xie C, and Wang DH.** Ablation of transient receptor potential vanilloid 1 abolishes endothelin-induced increases in afferent renal nerve activity: mechanisms and functional significance. *Hypertension* 54: 1298-1305, 2009.

387. **Xie C, and Wang DH.** Effects of a high-salt diet on TRPV-1-dependent renal nerve activity in Dahl salt-sensitive rats. *Am J Nephrol* 32: 194-200, 2010.
388. **Xie S, Deng Y, Pan YY, Ren J, Jin M, Wang Y, Wang ZH, Zhu D, Guo XL, Yuan X, Shang J, and Liu HG.** Chronic intermittent hypoxia induces cardiac hypertrophy by impairing autophagy through the adenosine 5'-monophosphate-activated protein kinase pathway. *Arch Biochem Biophys* 606: 41-52, 2016.
389. **Xu B, Zheng H, Liu X, and Patel KP.** Activation of afferent renal nerves modulates RVLN-projecting PVN neurons. *Am J Physiol Heart Circ Physiol* 308: H1103-1111, 2015.
390. **Xu W, Chi L, Row BW, Xu R, Ke Y, Xu B, Luo C, Kheirandish L, Gozal D, and Liu R.** Increased oxidative stress is associated with chronic intermittent hypoxia-mediated brain cortical neuronal cell apoptosis in a mouse model of sleep apnea. *Neuroscience* 126: 313-323, 2004.
391. **Yamamoto A, Keil LC, and Reid IA.** Effect of intrarenal bradykinin infusion on vasopressin release in rabbits. *Hypertension* 19: 799-803, 1992.
392. **Yamamoto K, Eubank W, Franzke M, and Mifflin S.** Resetting of the sympathetic baroreflex is associated with the onset of hypertension during chronic intermittent hypoxia. *Auton Neurosci* 173: 22-27, 2013.
393. **Yamamoto K, Lalley P, and Mifflin S.** Acute intermittent optogenetic stimulation of nucleus tractus solitarius neurons induces sympathetic long-term facilitation. *Am J Physiol Regul Integr Comp Physiol* 308: R266-275, 2015.
394. **Yan B, Li L, Harden SW, Gozal D, Lin Y, Wead WB, Wurster RD, and Cheng ZJ.** Chronic intermittent hypoxia impairs heart rate responses to AMPA and NMDA and induces loss of glutamate receptor neurons in nucleus ambiguus of F344 rats. *Am J Physiol Regul Integr Comp Physiol* 296: R299-308, 2009.
395. **Yan B, Soukhova-O'Hare GK, Li L, Lin Y, Gozal D, Wead WB, Wurster RD, and Cheng ZJ.** Attenuation of heart rate control and neural degeneration in nucleus ambiguus following chronic intermittent hypoxia in young adult Fischer 344 rats. *Neuroscience* 153: 709-720, 2008.
396. **Yang X, Zhang L, Liu H, Shao Y, and Zhang S.** Cardiac Sympathetic Denervation Suppresses Atrial Fibrillation and Blood Pressure in a Chronic Intermittent Hypoxia Rat Model of Obstructive Sleep Apnea. *J Am Heart Assoc* 8: e010254, 2019.
397. **Ye C, Qiu Y, Zhang F, Chen AD, Zhou H, Wang JJ, Chen Q, Li YH, Kang YM, and Zhu GQ.** Chemical Stimulation of Renal Tissue Induces Sympathetic Activation and a Pressor Response via the Paraventricular Nucleus in Rats. *Neurosci Bull* 36: 143-152, 2020.
398. **Yin X, Zheng Y, Liu Q, Cai J, and Cai L.** Cardiac response to chronic intermittent hypoxia with a transition from adaptation to maladaptation: the role of hydrogen peroxide. *Oxid Med Cell Longev* 2012: 569520, 2012.

399. **Yoshida Y, Fogo A, and Ichikawa I.** Glomerular hemodynamic changes vs. hypertrophy in experimental glomerular sclerosis. *Kidney Int* 35: 654-660, 1989.
400. **Yu H, Carretero OA, Juncos LA, and Garvin JL.** Biphasic effect of bradykinin on rabbit afferent arterioles. *Hypertension* 32: 287-292, 1998.
401. **Yu SQ, Ma S, and Wang DH.** Activation of TRPV1 Prevents Salt-Induced Kidney Damage and Hypertension After Renal Ischemia-Reperfusion Injury in Rats. *Kidney Blood Press Res* 43: 1285-1296, 2018.
402. **Yu SQ, Ma S, and Wang DH.** TRPV1 activation prevents renal ischemia-reperfusion injury-induced increase in salt sensitivity by suppressing renal sympathetic nerve activity. *Curr Hypertens Rev* 2019.
403. **Zalucky AA, Nicholl DD, Hanly PJ, Poulin MJ, Turin TC, Walji S, Handley GB, Raneri JK, Sola DY, and Ahmed SB.** Nocturnal hypoxemia severity and renin-angiotensin system activity in obstructive sleep apnea. *Am J Respir Crit Care Med* 192: 873-880, 2015.
404. **Zehendner CM, Luhmann HJ, and Yang JW.** A simple and novel method to monitor breathing and heart rate in awake and urethane-anesthetized newborn rodents. *PLoS One* 8: e62628, 2013.
405. **Zenteno-Savin T, and Castellini MA.** Changes in the plasma levels of vasoactive hormones during apnea in seals. *Comp Biochem Physiol C Pharmacol Toxicol Endocrinol* 119: 7-12, 1998.
406. **Zhang J, Zheng L, Cao J, Chen B, and Jin D.** Inflammation induced by increased frequency of intermittent hypoxia is attenuated by tempol administration. *Braz J Med Biol Res* 48: 1115-1121, 2015.
407. **Zhang W, Carreño FR, Cunningham JT, and Mifflin SW.** Chronic sustained and intermittent hypoxia reduce function of ATP-sensitive potassium channels in nucleus of the solitary tract. *Am J Physiol Regul Integr Comp Physiol* 295: R1555-1562, 2008.
408. **Zhang XB, Cai JH, Yang YY, Zeng YM, Zeng HQ, Wang M, Cheng X, Luo X, and Ewurum HC.** Telmisartan attenuates kidney apoptosis and autophagy-related protein expression levels in an intermittent hypoxia mouse model. *Sleep Breath* 2018.
409. **Zhang Y, Su X, Zou F, Xu T, Pan P, and Hu C.** Toll-like receptor-4 deficiency alleviates chronic intermittent hypoxia-induced renal injury, inflammation, and fibrosis. *Sleep Breath* 23: 503-513, 2018.
410. **Zhao MM, Tan XX, Ding N, and Zhang XL.** [Comparison of efficacy between continuous positive airway pressure and renal artery sympathetic denervation by radiofrequency ablation in obstructive sleep apnea syndrome patients with hypertension]. *Zhonghua Yi Xue Za Zhi* 93: 1234-1237, 2013.

411. **Zhong B, and Wang DH.** N-oleoyldopamine, a novel endogenous capsaicin-like lipid, protects the heart against ischemia-reperfusion injury via activation of TRPV1. *Am J Physiol Heart Circ Physiol* 295: H728-735, 2008.
412. **Zhu Y, and Wang DH.** Segmental regulation of sodium and water excretion by TRPV1 activation in the kidney. *J Cardiovasc Pharmacol* 51: 437-442, 2008.
413. **Zhu Y, Wang Y, and Wang DH.** Diuresis and natriuresis caused by activation of VR1-positive sensory nerves in renal pelvis of rats. *Hypertension* 46: 992-997, 2005.
414. **Zhu Y, Xie C, and Wang DH.** TRPV1-mediated diuresis and natriuresis induced by hypertonic saline perfusion of the renal pelvis. *Am J Nephrol* 27: 530-537, 2007.
415. **Zoccal DB, Bonagamba LG, Oliveira FR, Antunes-Rodrigues J, and Machado BH.** Increased sympathetic activity in rats submitted to chronic intermittent hypoxia. *Exp Physiol* 92: 79-85, 2007.
416. **Zoccal DB, Bonagamba LG, Paton JF, and Machado BH.** Sympathetic-mediated hypertension of awake juvenile rats submitted to chronic intermittent hypoxia is not linked to baroreflex dysfunction. *Exp Physiol* 94: 972-983, 2009.
417. **Zoccal DB, Simms AE, Bonagamba LG, Braga VA, Pickering AE, Paton JF, and Machado BH.** Increased sympathetic outflow in juvenile rats submitted to chronic intermittent hypoxia correlates with enhanced expiratory activity. *J Physiol* 586: 3253-3265, 2008.
418. **Zygmunt PM, Petersson J, Andersson DA, Chuang H, Sörgård M, Di Marzo V, Julius D, and Högestätt ED.** Vanilloid receptors on sensory nerves mediate the vasodilator action of anandamide. *Nature* 400: 452-457, 1999.